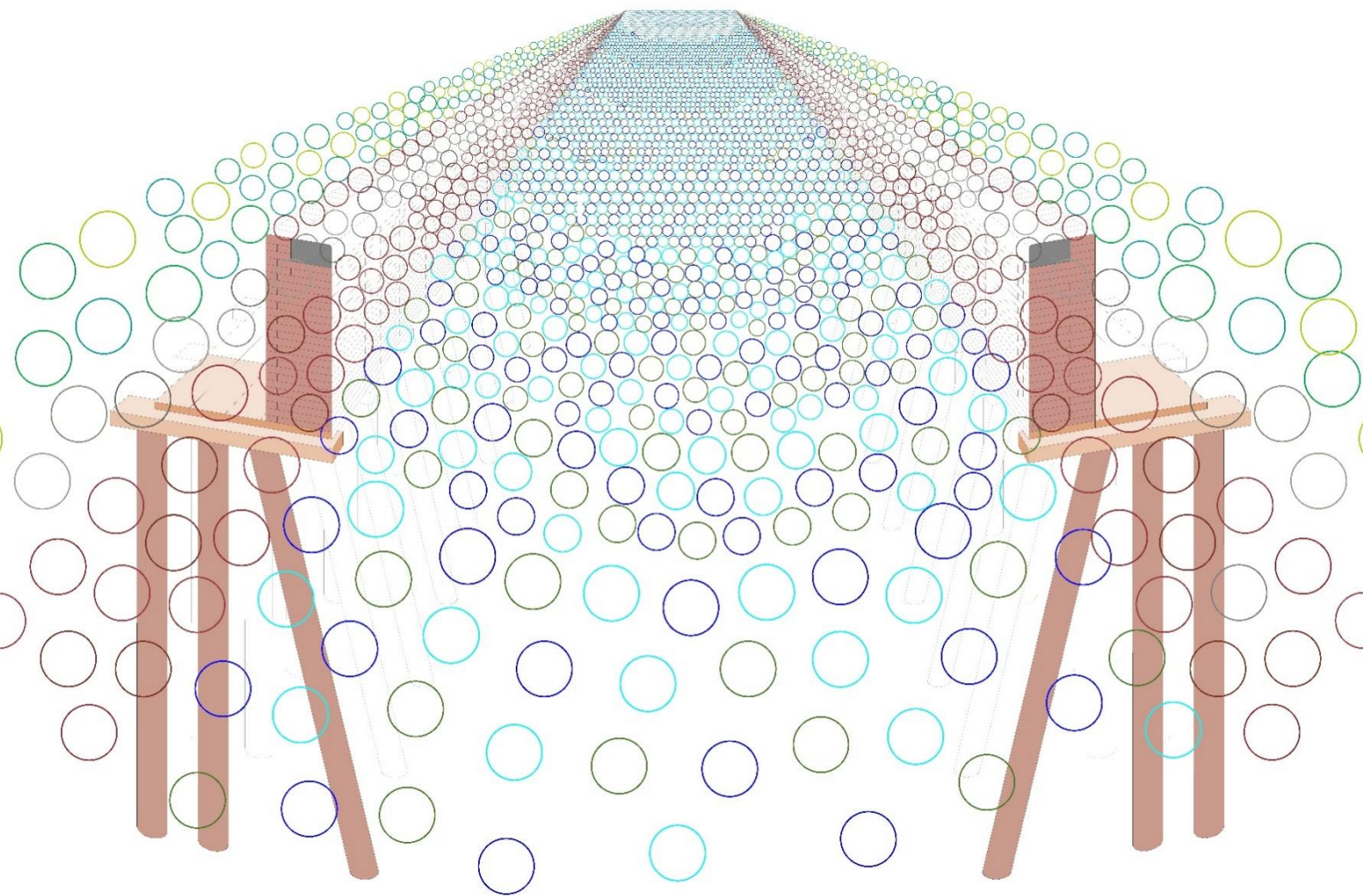


Influence of quay wall defects on the structural response



Martijn Haverkamp

Influence of quay wall defects on the structural response

By
M.J.A. (Martijn) Haverkamp

in partial fulfilment of the requirements for the degree of

Master of Science
in Structural Engineering

at Delft University of Technology
to be defended publicly on Monday, October 4th, 2021

Thesis committee:

Dr. ir. J.G. (Jarit) de Gijt	TU Delft
Dr. ir. M. (Mandy) Korff	TU Delft
Prof. dr. ir. J.W.G. (Jan-Willem) van der Kuilen	TU Delft
Ir. H.E. (Hans) Pacejka	Gemeente Rotterdam

An electronic version of this thesis is available at <http://repository.tudelft.nl/>

Abstract

Inner-city quay walls fulfil a number of very important functions where the retention of water is the most important one observed from a structural perspective. Despite their importance, not all of these structures are very well maintained, especially the older ones. Each municipality has their own maintenance regime, depending on the allocated budget. Deficient quay wall management of a few municipalities in the Netherlands resulted already in several quay wall failures, but there are also a lot of those structures still in a good condition. The differences in quay wall compositions and internal force transfer mechanisms could be one of the reasons why some structures do not show signs of deterioration where others are in a very deteriorated state. This hypothesis is the starting point for the following research question:

“What is the influence of structural deficiencies to the overall strength and stability of a wooden foundation system under a quay wall structure?”

To be able to answer this question, more insight is needed on quay wall compositions, wood degradation, and the design of a quay wall structure.

Quay wall structures were built since people started to transport goods over water. The quay wall compositions changed over many centuries by trial and error until a stable structure was created. Around the 15th century, the first quay walls were built consisting of retaining wall composed of brick or rubble stone on top of a timber framework. In the western part of the Netherlands, foundation piles were needed to stabilize the structure where the length of the piles were determined by the depth of the first bearing sand layer.

Wood was very commonly applied in older quay wall structures because it is a widely available material and it can easily be processed in the desired shape. Wood is an organic material, so it is prone to bacterial degradation besides the other common types of degradation. For a very long time it was believed that bacterial degradation is only present at buried archaeological sites of a few thousand years old, but later on bacterial wood degraders were also found at younger foundation piles. The late discovery resulted in a huge knowledge gap for bacterial degradation compared to degradation by fungi. From the year 2000 onwards, a few research projects were performed to retrieved samples from foundation piles. A few general trends were observed. All foundation piles with a lifetime of more than 100 years contain signs of bacterial decay where pine and alder piles are in general more severely degraded than spruce piles. A lot of variation in the degree of degradation was found at the investigated sites, so local circumstances in the subsoil also play a significant role. To assess the actual condition of a timber foundation pile that is still in service, a penetrometer can be used as a measurement device for a first indication of the residual timber strength. When information about the actual degradation patterns is required, a wood sample can be investigated in a laboratory by microscopic observations.

The timber elements in a pile foundation transfers the superstructure loads via internal force mechanisms to the subsoil. The foundation piles in a deep foundation are the most essential parts because they are the only load-bearing elements in direct contact with the soil. A pile can be loaded both in axial and lateral direction where the first one is split up into compressive and tensile piles. Piles in compression obtain their geotechnical bearing strength by pile tip and pile shaft resistance. When the layers above the bearing sand layers settles significantly, negative skin friction acts as an additional load along the pile shaft. The exact values of both friction forces depend on the location of the neutral plane which involves both pile displacements and soil settlements. The bearing strength of a tension pile

depends only on tensile resistance along the pile shaft. Laterally loaded piles obtain their resistance by the lateral soil reaction as a response on the lateral pile displacement. Besides geotechnical pile resistances, each foundation element has to withstand internal forces caused by the external loads. The resistance values between the elements differs a lot due to the anisotropic behaviour of timber.

The geotechnical and material resistances are used as a basis for the study to the influence of quay wall defects on the internal force transfer mechanisms. Five quay wall structures with different geometries in Rotterdam and The Hague are selected for the structural calculations. With the help of the assessment reports, a few common defects are chosen which are likely to occur for these kind of structures. First, the displacements and internal forces of the pile cap beam in the middle cross-section are calculated when the structure shows no signs of structural declination. The obtained results are then compared with the same base quantities at the middle pile cap beam in the model where one of the structural defects is applied. In this way, the effect of each defect can be determined.

Although there are large differences between the composition of the various quay wall structures, a general conclusion can be drawn from the performed calculations. A larger number of piles under a quay wall structure has a positive influence on the redistribution of internal forces from a weakened spot to an unaffected part of the structure.

List of figures

figure 1-1: example of an assessment framework for quay walls and bridges (Gemeente Amsterdam, 2019).....	2
figure 1-2: total closure of the Nieuwe Herengracht in Amsterdam (Bewonersraad Nieuwmarkt/Groot Waterloo, 2019).....	2
figure 1-3: report structure.....	5
figure 2-1: chart of the soil conditions in the Netherlands (Wageningen University & Research, 2006).....	7
figure 2-2: protection measures of timber piles to prevent damage during pile driving (Tomlinson & Woodward, 2008).....	8
figure 2-3: wrought iron barbed nails (De Vree, 2020).....	8
figure 2-4: development of inner-city quay walls in time (De Gijt et al., 2014).....	8
figure 2-5: composition of a historic quay wall with English and Dutch definitions for the quay wall parts accompanied by a global axis system.....	10
figure 3-1: components of a tree system with the definitions for the different sections (Blaß & Sandhaas, 2017).....	12
figure 3-2: typical load–deformation behaviour of timber for tension (t) and compression (c) with curves for loading parallel (0) and perpendicular (90) loading to the fibre direction.....	14
figure 3-3: relation between load and load duration for timber (Jorissen, 1995).....	15
figure 3-4: fungal species with an influence on the wood structure (Sutter, 1997).....	16
figure 3-5: required pile length for a stable foundation for different parts in the Netherlands (Veldhuyzen, 1963).....	18
figure 3-6: relation between the service life and the degree of degradation (Klaassen et al., 2000).....	21
figure 3-7: applied timber species in foundation elements in different cities in the Netherlands (BACPOLES, 2005).....	22
figure 3-8: relation between the density and the moisture content for pine, spruce, fir, and alder (BACPOLES, 2005).....	23
figure 3-9: extent of degradation for different wood species; left: influence of degree of degradation on moisture content and density for spruce and pine, right: mean degradation across the pile radius for 859 foundation piles (BACPOLES, 2005).....	23
figure 3-10: frequency diagrams for the degree of degradation; left: pine samples (n = 903), right: spruce samples (n = 789) (BACPOLES, 2005).....	24
figure 3-11: relation between the moisture content and specific gravity for pine, spruce, and alder (Klaassen, 2008).....	27
figure 3-12: comparison of the specific gravity and the moisture content with the compression strength for pine (Klaassen, 2008).....	27
figure 3-13: two types of penetrometers, left: Pilodyn (Istemi, n.d.), right: Specht (Profound, 2017).....	29
figure 3-14: Decision scheme for the need of sampling (NEN 8707 fig. 2, 2018).....	30
figure 4-1: failure mechanisms of a quay wall on a pile foundation (De Gijt et al., 2014).....	32
figure 4-2: load (S) and resistance (R) with their mean values and deviation from the mean (Jonkman et al., 2017).....	34
figure 4-3: lateral soil pressure coefficient as a function of the structural displacement (Verruijt, 2012).....	34
figure 4-4: schematisation of load model 1 (De Gijt et al., 2014).....	41
figure 4-5: schematisation of load model 2 (De Gijt et al., 2014).....	42
figure 4-6: deformed masonry structure by an adjacent tree (De Gijt et al., 2014).....	44
figure 4-7: results of wind tunnel test on conifer trees with average dimensions (diameter at breast height = 10–15 cm, tree height = 6–8 m) (Moore et al., 2018).....	45

figure 4-8: pile forces on a displacement pile.....	47
figure 4-9: shape of the failure mechanism around the pile tip (Koppejan & Van Mierlo, 1952).....	48
figure 4-10: infinitesimal element as the basis for Zeevaert–De Beer expression (Van Tol, 1994).....	50
figure 4-11: influence area around a pile (NEN–EN 1997–1 (NB) figure 7.m, 2019).....	51
figure 4-12: individual components of displacement for a single pile.....	52
figure 4-13: forces on a pile subjected to a tensile load.....	54
figure 4-14: stress distribution around a laterally loaded pile (Rocscience, 2018).....	55
figure 4-15: length to diameter ratio and the corresponding failure mechanisms (Budhu, 2011).....	56
figure 4-16: data flow diagram for the determination of the used calculation method.....	57
figure 4-17: soil model according to Winkler.....	58
figure 4-18: generic py-curve for an arbitrary soil (Rocscience, 2018).....	59
figure 4-19: model of a laterally loaded pile according to the subgrade reaction approach Reese, 1997).....	59
figure 4-20: soil modelled as a continuous elastic medium (Budhu, 2011).....	60
figure 4-21: relation between the pile support area and compressive resistance perpendicular to the fibre direction (F3O/SBRCURnet, 2016).....	63
figure 5-1: map of the Boompjeskade (Geostart, n.d.) accompanied by two photos of the structure (Google, n.d.).....	65
figure 5-2: cross-section of the Boompjeskade (BK–001) (Gemeente Rotterdam, personal communications, 2013).....	66
figure 5-3: map of the Haringvliet (GeoStart, n.d.) accompanied by two photos of the structure (Google, n.d.).....	67
figure 5-4: cross-section of the Haringvliet (HV–001) (Gemeente Rotterdam, personal communications, 2012).....	68
figure 5-5: map of the Noordwal (ArcGIS, n.d.) accompanied by two photos of the structure (Google, n.d.).....	68
figure 5-6: cross-section of the Noordwal (NW–001) (Ingenieursbureau Den Haag, 2020).....	69
figure 5-7: map of the Stieltjeskade (GeoStart, n.d.) accompanied by two photos of the structure (Google, n.d.).....	70
figure 5-8: cross-section of the Stieltjeskade (SK–001) (Gemeente Rotterdam, personal communications, 2013).....	71
figure 5-9: map of the Toussaintkade (ArcGIS, n.d.) accompanied by two photos of the structure (Google, n.d.).....	71
figure 5-10: cross-section of the Toussaintkade (TK–001) (Ingenieursbureau Amsterdam, 2016).....	72
figure 5-11: scheme for the quay wall calculations.....	73
figure 5-12: location and type of applied structural changes per modification.....	78
figure 5-13: extreme values related to displacement and internal forces.....	80
figure 5-14: comparison of the quay walls for the maximum value of the horizontal displacement; left: number of pile rows, right: pile distances in longitudinal direction.....	89

List of tables

table 3-1: approximative values for some practical cases (Blaß & Sandhaas, 2017).....	13
table 3-2: required pile lengths and the most common wood species in a few cities in the Netherlands.....	19
table 3-3: degree of degradation of pine piles in several Dutch cities (Klaassen et al., 2000).....	21
table 3-4: degree of degradation of spruce piles in several Dutch cities (Klaassen et al., 2000).....	21
table 3-5: mean depth of degradation for piles consisting of different wood species (Klaassen, 2008).....	25
table 3-6: pile characteristics for the investigation to local differences in degradation (Klaassen, 2008).....	26
table 3-7: indicative values for the degree of bacterial decay by spring-loaded penetrometer measurements (Klaassen et al., 2000).....	29
table 4-1: partial load factors for soil retaining structures (NEN 8707 table N.1, 2018).....	35
table 4-2: factors for the calculation of soil retaining structures (NEN 8707 table A.1, 2018).....	35
table 4-3: geotechnical parameters for driven foundation piles according to CC1 (NEN-EN 1997-1 (NB) table A.6 and par. 7.3.2.2 (b), 2019).....	36
table 4-4: geotechnical parameters for a soil retaining structure according to CC1 (NEN 8707 table N.2, 2018).....	37
table 4-5: different values for the modification factor of sawn timber (NEN-EN 1995-1-1 table 3.1, 2011).....	37
table 4-6: examples of load duration classes (NEN-EN 1995-1-1 (NB) table 2.1 and table 2.2, 2013)....	37
table 4-7: specific weight of commonly used quay wall materials.....	38
table 4-8: required displacement for active or passive soil pressure (NEN-EN 1997-1 (NB) table 9.c, 2019).....	40
table 4-9: load values for the model presented above (De Gijt et al., 2014).....	42
table 4-10: reduction factor for the number of truck passages (De Gijt et al., 2014).....	42
table 4-11: mooring forces of several vessels for inland shipping (Rijkswaterstaat, 2020).....	43
table 4-12: important parameters of tree species for structural calculations (De Gijt et al., 2014).....	44
table 4-13: Load combination factors for variable loads.....	46
table 4-14: values for the friction angle and the soil pressure coefficient (Van Tol, 1994).....	49
table 4-15: rheological factors according to Ménard (1971).....	60
table 5-1: colour scheme with values in percent.....	80
table 5-2: calculation results of the pile cap beam in the Boompjeskade at the middle section (y = 9.75 m).....	81
table 5-3: calculation results of the pile in the first pile row in the Boompjeskade at the middle section (x = 0.40 m, y = 9.75 m).....	81
table 5-4: calculation results of the pile cap beam in the Haringvliet at the middle section (y = 10.20 m).....	82
table 5-5: calculation results of the pile in the first pile row in the Haringvliet at the middle section (x = 0.18 m, y = 10.20 m).....	83
table 5-6: calculation results of the pile cap beam in the Noordwal located at the middle section (y = 10.44 m).....	84
table 5-7: calculation results of the pile in the first pile row in the Noordwal at the middle section (x = 0.12 m, y = 10.44 m).....	84
table 5-8: calculation results of the pile cap beam in the Stieltjeskade at the middle section (y = 9.90 m).....	85
table 5-9: calculation results of the pile in the first pile row in the Stieltjeskade at the middle section (x = 0.33 m, y = 9.90 m).....	86

table 5-10: calculation results of the pile cap beam in the Toussaintkade at the middle section ($y = 10.00$ m).....	87
table 5-11: calculation results of the pile in the first pile row in the Toussaintkade at the middle section ($x = 0.29$ m, $y = 10.00$ m).....	87

List of symbols

Latin symbols

A	=	area [m ²], cross-sectional area [m ²]
a	=	distance [m]
C	=	circumference [m ²], coefficient [-], consolidation factor [-]
c'	=	cohesion [kPa]
c' _a	=	adhesion [kPa]
d	=	diameter [m]
E	=	Young's modulus [N/mm ²] [kN/m ²], load effect [-]
F	=	force [kN]
f	=	function [-], strength [N/mm ²]
G	=	static load [kN] [kN/m ¹] [kN/m ²]
H	=	height [m]
I	=	second moment of area [m ⁴]
i	=	index number [-]
j	=	index number [-]
K	=	soil pressure coefficient [-]
k	=	effect factor [-], spring stiffness [kN/m] [kNm/rad]
k _{mod}	=	modification factor [-]
k _s	=	modulus of subgrade reaction [kN/m ²]
L	=	length [m]
l	=	length of friction zone [m]
m	=	simplification factor [m ⁻¹], index number [-]
m _H	=	Terzaghi's constant [-]
N _q	=	normal force [kN]
n	=	number of elements [-]
n _H	=	Terzaghi's constant [-]
P	=	prestressing load [kN]
p	=	groundwater pressure [kPa]
p _m	=	penetrometer measurement [mm]
Q	=	variable load [kN] [kN/m ¹] [kN/m ²]
q	=	distributed line load [kN/m ¹], distributed reaction force [kN/m ²]
R	=	resistance factor [-], resistance [kN], distance in a 3D-plane [m], ratio [-]
r	=	rise [m], radius [m], distance in a 2D-plane [m], root in a general solution [-]
S	=	load factor [-], spacing [m], first moment of area [m ³]
s	=	settlement [mm] [m], pile tip factor [-]
t	=	soil layer thickness [m], element thickness [mm], time [days]
u	=	speed [m/s], displacement [m]
V	=	volume [m ³], shear force [kN]
W	=	element width [mm]
w	=	transversal displacement [m]
X	=	material parameter [-]
x	=	transversal or crosswise direction [m]
y	=	longitudinal or lengthwise direction [m]
z	=	soil depth [m NAP]
{F}	=	force vector [-]
[K]	=	stiffness matrix [-]
{u}	=	displacement vector [-]

Greek symbols

α	=	angle [°] [rad], rheological factor [-]
α_Q	=	truck load factor [-]
β	=	reliability index [-], rheological factor [-], relative rotation [-]
β_1	=	tree taper constant [-]
γ	=	partial factor [-], specific weight [kN/m ³]
Δa	=	supplement factor [m]
ΔM_y	=	difference in bending moment [kNm]
ΔN	=	difference in normal force [kN]
Δu_x	=	difference in horizontal displacement [m]
Δu_z	=	difference in vertical displacement [m]
Δx	=	bar width [m], horizontal displacement [m]
$\Delta \sigma'_v$	=	change in effective soil stress [kPa]
δ	=	pile friction angle [°]
ε	=	strain [-]
θ	=	rotation [°] [rad]
μ	=	mean value [-]
ν	=	Poisson's ratio [-]
ξ	=	load reduction factor [-]
$\xi_{,3}$	=	correlation factor for the mean value of the pile bearing strength [-]
$\xi_{,4}$	=	correlation factor for the minimum value of the pile bearing strength [-]
ρ	=	density [kg/m ³]
σ	=	standard deviation [-], pressure [kN/m ²], total soil stress [kPa], internal stress [N/mm ²]
σ'	=	effective soil stress [kPa]
τ	=	shear stress [N/mm ²]
φ'	=	angle of internal friction [°]
ω	=	moisture content [%], skewness [mm/m]
ψ_0	=	load combination factor for variable loads [-]

Table of contents

1. Introduction.....	1
1.1 Problem statement.....	3
1.2 Research question.....	4
1.3 Report outline.....	4
2. Identification of the inner-city quay wall.....	6
2.1 Development of inner-city quay walls.....	6
2.2 Inner-city quay wall characteristics.....	9
3. Degradation of foundation elements.....	11
3.1 Wood as a construction material.....	11
3.2 Types of degradation.....	14
3.2.1 Chemical degradation.....	14
3.2.2 Mechanical degradation.....	15
3.2.3 Biological degradation.....	15
3.2.3.1 Fungi.....	15
3.2.3.2 Bacteria.....	17
3.2.3.3 Insects.....	17
3.3 Conducted research of degraded pile foundations.....	18
3.3.1 Applied wood species.....	18
3.3.2 Inventory of wood degradation studies.....	19
3.3.2.1 Van Etten et al. (2000).....	19
3.3.2.2 Klaassen, et al. (2000).....	20
3.3.2.3 BACPOLES (2005).....	22
3.3.2.4 Klaassen (2008).....	25
3.3.2.5 Findings.....	28
3.4 Assessment of foundation elements.....	28
4. Structural quay wall design.....	31
4.1 Failure mechanisms.....	31
4.2 Design and characteristic values.....	33
4.2.1 Partial load factors.....	35
4.2.2 Geotechnical resistance.....	36
4.2.3 Material resistance.....	36
4.3 Loads on the structure.....	37
4.3.1 Self-weight quay wall elements.....	38
4.3.2 Soil pressures at the backfill.....	38
4.3.3 Surface water pressure.....	40
4.3.4 Terrain loads.....	41
4.3.5 Mooring forces.....	43
4.3.6 Tree loads.....	43
4.3.7 Load combinations.....	46
4.4 Geotechnical loads and resistances.....	47
4.4.1 Piles loaded in compression.....	47
4.4.1.1 Base resistance.....	48
4.4.1.2 Shaft resistance.....	49
4.4.1.3 Negative skin friction.....	49
4.4.1.4 Pile settlement.....	51

4.4.1.5	Neutral plane location.....	52
4.4.2	Piles loaded in tension.....	53
4.4.2.1	Tensile resistance.....	54
4.4.2.2	Pile rise.....	54
4.4.3	Piles loaded in lateral direction.....	55
4.4.3.1	Calculation models.....	55
4.4.3.2	Quay wall model.....	58
4.4.3.2.1	Subgrade reaction.....	60
4.4.3.2.2	Continuum approach.....	60
4.5	Material resistance.....	61
4.5.1	Foundation piles.....	61
4.5.2	Horizontal orientated foundation elements.....	62
5.	Quay wall calculations.....	64
5.1	Case study.....	64
5.1.1	Boompjeskade, Rotterdam.....	65
5.1.2	Haringvliet, Rotterdam.....	67
5.1.3	Noordwal, The Hague.....	68
5.1.4	Stieltjeskade, Rotterdam.....	70
5.1.5	Toussaintkade, The Hague.....	71
5.2	Calculation approach.....	73
5.2.1	Collection of data.....	73
5.2.2	Superstructure loads.....	74
5.2.3	Lateral soil resistance.....	75
5.2.4	Joint stiffness.....	75
5.2.5	Axial pile head forces.....	76
5.2.6	Axial pile forces and resistances.....	76
5.2.7	Pile tip settlement and force.....	77
5.2.8	Neutral plane.....	77
5.2.9	Calculation model.....	77
5.2.10	Structural deficiencies.....	78
5.3	Model output.....	79
5.4	Interpretation of results.....	88
6.	Conclusions.....	91
6.1	Conclusions.....	91
6.2	Recommendations.....	92
	<u>Bibliography.....</u>	94
	<u>Appendices</u>	

“Many historic inner city quay walls are in a bad condition due to the continuous ongoing deterioration processes. Municipalities have implemented several different maintenance regimes adjusted to the urge of required interventions and the available budget. In this way, structural failure risks are kept as low as possible both at this moment and in the future.

1

Introduction

The Netherlands possesses a few remarkable features that makes it a unique country in relation to other West European nations. One of them is the relative long seashore along the west side of the country. At this shore, estuaries of relatively large rivers like the Rhine, Meuse and the Scheldt are situated. During the Middle Ages, many settlements were established near rivers and estuaries for the benefits of nautical transport possibilities. Their locations became prominent during the Golden Age where trading was the most important factor for flourishment and economic growth of the Netherlands. This period was the offspring for the modern civilization that has led to the country in its well-developed state.

The development of the country during many ages resulted in the accumulation of a few large cities near the west coast and in proximity of river estuaries. Well known cities are Amsterdam, Rotterdam and The Hague and together with a large amount of less significant venues this region has developed into the conurbation which is called “de Randstad”. It can be characterized as the aorta of the Dutch economy and welfare with indispensable key locations as the booming tourist sector in the capital city Amsterdam, the international harbour in Rotterdam and the governmental seat in The Hague.

One of the endangers to the west part of the Netherlands is the decreasing difference between the land and seawater levels. Sea level rise on the one hand and soil subsidence on the other hand has increased the complexity to keep the seawater outside along the years because a large part of the Netherlands is located below sea level. Water retention belongs to the main areas of concern for many centuries already in the Netherlands. To keep the water outside, various kinds of structures were built during the past years with water retention as their main or side function. All these water retaining structures forms together the water defence system to ensure that the Dutch feet stay dry.

Inner-city quay walls are one of the structures dealing with the retention of water. This type of structure is found in many cities across the Netherlands that were established along a river. Around the 19th century the improvement of the network of inland waterways and the opinion to use the space as efficient as possible gave the urge for the construction of vertical walls along canals and other water entities. In many inner-cities, the street image is nowadays still characterized by those historic quay walls. The retaining walls are usually very distinctive because the majority possesses a high cultural and historical value. To preserve the structures in their original state for the coming years, they are often designated as national heritage.

Despite the valuable appearance in a lot of city centres, there are large differences in the structural health of all kinds of historic quay walls. Each municipality decides the stringency of their own maintenance regime to keep those structures in function. In the Netherlands, the municipality of Amsterdam

manages the largest amount of quay walls with a total length of 600 km. The executive committee of the municipality of Amsterdam declared that the policy of decision-making was based on reactive management in the past (Gemeente Amsterdam, 2019). With this type of policy it was almost impossible to notice the deterioration in time and take appropriate measures when they were required. The last years a few incidents were reported where a small part or even an entire quay wall collapsed because of this policy. The municipality decided to alter the mindset into proactive management where decisions are based on the trade-off between the risks and the costs of a particular intervention (Gemeente Amsterdam, 2019). A simplified scheme of this strategy can be observed in *figure 1-1*.

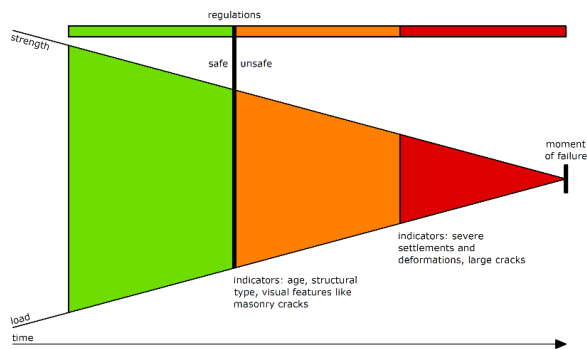


figure 1-1: example of an assessment framework for quay walls and bridges (Gemeente Amsterdam, 2019)

With the above assessment diagram, proactive management can be carried out for several different hydraulic structures. It is applicable only when the state of each hydraulic structure is mapped by visual observations and/or lab research of specimens on a regular basis. With this strategy it can be prevented that sudden drops in the structural strength remain unnoticed and adequate measures are taken in time. Structures in the green part of *figure 1-1* still perform as intended and therefore no measures are required at this moment. When a structure has an orange indication, it has deteriorated quite heavily and does not fulfil the requirements according to the Dutch building codes anymore. The structure still functions decently enough but monitoring on a more frequent basis is recommended because there might be a risk of propagating deterioration. A structure located in the red zone could result in acute danger for the environment and immediate action (or at least on a very short term) is unavoidable. Until the moment of renovation or rebuilt, it can be decided to decrease the loads on the structure by closing off the surroundings. In this way, casualties may be avoided at the structure. One example is the placement of traffic barriers as depicted in *figure 1-2*.



figure 1-2: total closure of the Nieuwe Herengracht in Amsterdam (Bewonersraad Nieuwmarkt/Groot Waterloo, 2019)

To limit the deterioration of foundation elements, they must be situated below the groundwater table as much as possible. Many municipalities in the Netherlands put a lot of effort in maintaining the

groundwater level at a constant height, but it becomes more and more complicated in recent years. The inundation of timber elements is endangered by the ongoing subsidence of the ground level, especially near the Dutch coast where the soil composition is mainly composed of layers that are sensitive to settlements. To retain dry feet near the water, the urge arises of lowering the surface water level. A possible consequence of this action is lowering of the groundwater level that is succeeded by an additional settlement of the soil layers. The continuous decrease of the band width in ground level variations increases the risk on exposed foundation elements. It is therefore important to propagate a proper water level policy for the protection of timber foundation elements against biological attacks. Groundwater fluctuations can be measured by a network of monitoring wells with small mutual spacings. Unforeseen local perturbations to the groundwater level are then detected, so measures to counteract the cause of this alteration can be set up on time.

Proper decision-making on quay walls and other older structures is very important for preservation in the long term. The municipality Amsterdam expects that all historic quay walls are renewed or replaced in a period of 20 years (Gemeente Amsterdam, 2019). By application of proactive management, the structural state of each quay wall can be determined. Consecutively, a planning is made where the quay walls in the worst condition have the highest priority for renovation or replacement. With this approach the situation is avoided where a lot of quay walls are replaced simultaneously with the risk of an unexpected economic loss as a possible consequence. This situation has to be prevented at all costs and therefore a systematic approach is recommended where construction activities are spread over a sufficiently long period of time.

1.1 PROBLEM STATEMENT

In the last few years, problems arise for a lot of quay walls in several city centres across the Netherlands. A few examples can be found in newspaper articles like the collapse of Bemuurde Weerd in Utrecht (Algemeen Dagblad, 2013), Nassaukade in Amsterdam (NOS, 2018) and recently of Grimborgwal (NOS, 2020). All of these quay walls are more than 100 years old and therefore the degree of deterioration of the quay wall elements can be quite serious. Especially for wooden foundation elements, problems are found because wood as a natural material is subjected to several biological processes. Various organisms are able to attack the wood which can result in a reduction of the timber strength.

The deterioration of the quay wall structure can induce various failure mechanisms that could lead to the collapse of the structure. Due to the large variation in failure mechanisms, the weak link could almost be any foundation element. Deficiencies in the masonry wall are often interfered in time by visual inspections because excessive deformations often appear in the form of cracks and the loosening of bricks. Information about the underlying foundation system is more complicated to obtain because it is often below the water table and the structure itself. Additionally, the foundation system consists of a very dense pile grid, so it is almost impossible to determine the weak links in the system only by observations. Schreurs (2017) also confirms in his master thesis report that the degree of degradation of wooden foundation piles is very location specific. From his conclusions it can be hypothesized that a foundation system can fail in a lot of different ways.

The location of the foundation piles in close proximity with each other also opens up the idea that failure of a single element does not directly result in failure of the total system. This viewpoint is confirmed by many examples of old quay walls showing excessive deformations and visible deficiencies that are still standing. The structure is probably able to redistribute forces over remaining foundation elements when one structural element fails or does not function as intended. A prerequisite for this adapted structural behaviour can be found in the presence of sufficient deformation capacity, otherwise the structure

would fail already at the moment the structure shows only limited deformations. A large question mark arises how the system is able to keep resisting all load impacts during the very long ongoing loading history.

As already mentioned, each municipality has its own maintenance regime and therefore large differences can be expected in the structural health at different locations. The municipality of Rotterdam is responsible for the maintenance of around 29 km of quay walls across the city (Gemeente Rotterdam, 2018). All structures are monitored on a regular basis by visual inspections and measurements to the deformations and overall structural condition. A good example can be found by the large database of ‘Funderingsloket’ that captures the structural health of many properties in Rotterdam and is also publicly accessible (<https://www.duikinjefundering.nl/>).

1.2 RESEARCH QUESTION

The extensive documentation of the quay walls in Rotterdam could help in a better understanding why quay wall structures with wooden foundations are still standing even when signs of excessive structural degradation are visible. From this exploration the following research question arises:

“What is the influence of structural deficiencies to the overall strength and stability of a wooden foundation system under a quay wall structure?”

This question is quite abstract, so the question is subdivided into a number of sub questions. These questions are listed below:

1. What are the characteristics of a historic quay wall in the Netherlands?
2. Which conditions/factors influence the degradation of wooden foundation elements?
3. What are the force transfer mechanisms in a timber pile foundation from the ground level to the subsoil?
4. How can deficiencies be incorporated in a structural model?
5. Which conclusions can be drawn from the calculation results?

1.3 REPORT OUTLINE

The sub questions given above are used as a guideline for the setup of this report where each question is considered separately in each chapter. Chapter 2 ‘Identification of the inner-city quay wall’ is an elaboration on the available information about quay wall structures with a wooden pile foundation like the building method, the structural elements, and other characteristics. Subsequently, in chapter 3 ‘Degradation of foundation elements’ influences of wood degradation on the material properties are highlighted. Many quay wall foundations are affected by degradation of wooden foundation elements that could induce peculiar failure mechanisms in a quay wall structure. Wood degradation is not included in the European standards (Eurocode) but several researchers have made attempts to incorporate the influence of wood degradation on a structure. An overview of the required structural and geotechnical calculations for the structural assessment of a quay wall structure are given in chapter 4 ‘Structural quay wall design’. Various combinations of structural deficiencies are then incorporated into a structural model. The results of the calculations are presented in chapter 5 ‘Quay wall calculations’. Finally, the results of the computations are discussed in chapter 6 ‘Conclusions and recommendations’ with the inclusion of further recommendations.

The above text is converted into *figure 1-3* by a simplified schematisation of the report structure.

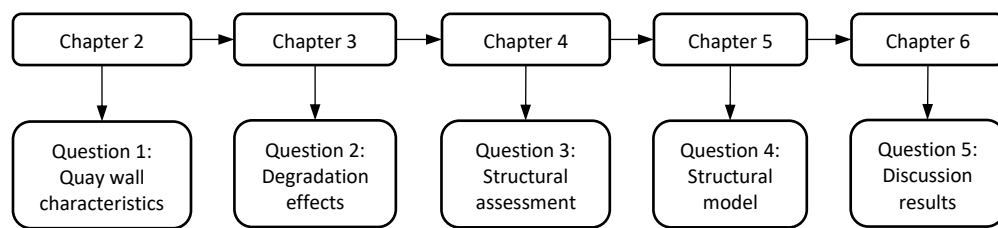


figure 1-3: report structure

“Quay wall structures have been used for thousands of years in various shapes and compositions all over the world. A lot of historic quay walls still characterise the street image in many cities in the Netherlands. Each structure has its own structural characteristics depending on the applied building method and local availability of resources.”

2

Identification of the inner-city quay wall

As long as civilization exists, people were inspired to explore the infinite and mysterious appearing oceans. Because of the possibility of economic gain and the search for new liveable places, exploring and trading became important motives for the extension of opportunities for many people. Living near the sea was the easiest way to meet these targets, so a lot of key places near the coast became inhabited. To facilitate shipping, several mooring places grew out from preliminary mooring facilities to ports or trading places.

2.1 DEVELOPMENT OF INNER-CITY QUAY WALLS

The offspring of quay wall structures goes back to the period where several civilizations started, a few thousand years ago. De Gijt (2010) described in his doctoral thesis that the first remains of such structures dated back to a period around 3000 BC. Local available materials like clay, natural stone and wood were used and due to the lack of knowledge, the composition of these structures was very basic. A frequent shape was a clay core for the water tightness surrounded by a framework made of wood and/or stone to obtain sufficient overall stability. The general shape of the first structures did not alter much until the invention of cast iron and brick stones around the 15th century. From this period onwards, more sophisticated structures were built on the obtained experience mainly based on trial and error of former structural shapes.

More advanced and heavy weighted quay wall structures also entailed foundation related problems, especially in the western part of the Netherlands due to the composition of the soil. At the start of the Holocene period (around 11.700 years ago), glaciers in the Alps started to melt due to a temperature rise. The melting water carried large amounts of peat and clay substances via the Rhine and Meuse in several river branches towards the North Sea. Near the coastline these sediments were deposited on top of the Pleistocene sand. The variability in deposition rate caused large differences in the composition of subsoils in the western part of the Netherlands. A global overview of the different soil types and their locations is given in figure 2-1.



figure 2-1: chart of the soil conditions in the Netherlands (Wageningen University & Research, 2006)

The unconsolidated clay and peat layers caused a lot of trouble for the stability of structures in the past. The first types of quay walls constructed at the beginning of the 17th century were founded on a wooden grillage. During the construction, the landside of the retaining wall was often elevated with dredged material from the waterside. Increased soil pressures were often the initiation of soil settlements where records showed that final settlements with a maximum value of 1.5 à 2 m were not uncommon (CUR211E, 2005).

To overcome stability problems of quay walls, wooden foundation piles were used. In the heyday of construction with wooden foundation piles, many improvements were made. At the beginning, a lot of workmen were needed to generate a blow with a sufficiently high magnitude such that the pile migrates into the subsoil. The impact was created by lifting a heavy falling block and releasing it on top of the pile head. To obtain the highest efficiency for each blow, a good cooperation between the staff members was required. According to Klaassen and Creemers (2012), several chants with a primarily obscene character were sung to maintain a strict pile driving rhythm. Later on, the intensive work was adopted by machine power in the form of driving equipment.

To prevent damage to the slender piles during the pile driving processes, both pile head and tip were protected. Around the pile head an iron or mild steel hoop (Dutch: mesband) was applied to prevent splitting of the pile as a result of hammer blow impacts. To be able to place the ring over the pile head, the diameter of the pile at the top was reduced. When the pile was driven into very dense and hard soil layers, it was often equipped with a cast steel point at the pile tip.

In many timber pile foundations, the piles were connected to the other foundation elements with a mortise and tenon joint (Dutch: pen-en-gat verbinding). The pile was placed inside a sawn recess of the pile cap beam (Dutch: kesp) and connected to the beam with wrought iron barbed nails (Dutch: hakkelbout). The various components related to pile driving and connection are shown in *figure 2-2* and *figure 2-3*.

2. Identification of the inner-city quay wall

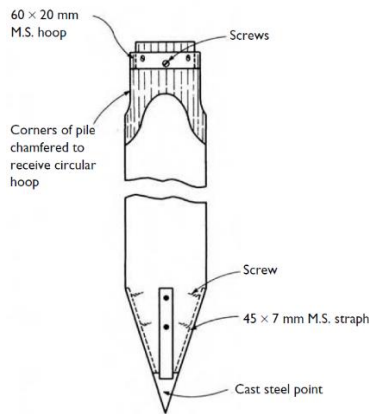


figure 2-2: protection measures of timber piles to prevent damage during pile driving (Tomlinson & Woodward, 2008)



figure 2-3: wrought iron barbed nails (De Vree, 2020)

Until the year 1950, wooden foundation piles were dimensioned according to an empirical method. No soil classification with CPTs was possible before this time, so the minimum required pile length into the sand bearing layer was done in another way. First, a number of very long test piles were driven into the ground. When these piles did not displace any further for a certain impact load, it was assumed that the pile has achieved sufficient bearing capacity. The obtained results about the soil resistance were then used for the determination of the required pile length and the minimum number of blows with an empirical expression, called the “Hollandse Heiformule”.

When the application of concrete and steel became normalised after the end of World War II, the possibilities in structural design became unlimited. Ship loading and unloading as a functional requirement faded into the background for inner city quay walls due to the transfer of these activities to harbour areas. The shape of the quay wall changed from a vertical partition design to a design based on more local demands related to the environment. In *figure 2-4*, a global overview is depicted about the application of generalised quay wall shapes in a chronological order

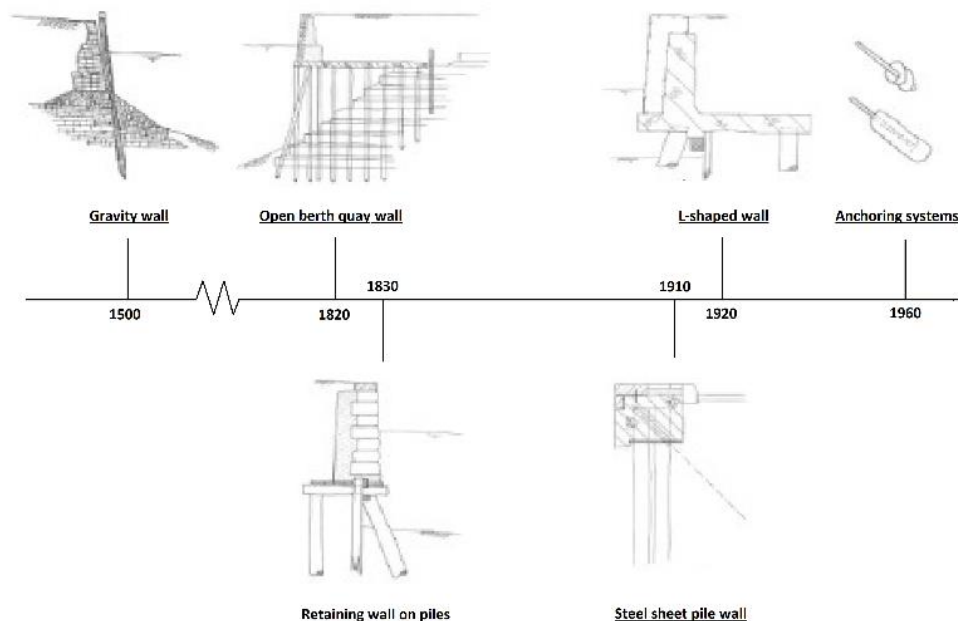


figure 2-4: development of inner-city quay walls in time (De Gijt et al., 2014)

2. Identification of the inner-city quay wall

Most inner-city quay walls with a wooden pile foundation were built about 150 years ago or more. This type of structures with a wooden floor are treated below in the next paragraph '2.2 Inner-city quay wall characteristics',

2.2 INNER-CITY QUAY WALL CHARACTERISTICS

A large quantity of quay walls in many Dutch inner cities are constructed around the 19th century. The retaining wall is often composed of brick stones founded on a wooden framework of vertically and horizontally oriented elements. Many historic quay walls were adapted a few times throughout the years to meet the applicable user requirements, so a lot of the structures are modernized with newer materials like concrete and steel. The overview below shows a description of components in a typical Dutch quay wall structure with a wooden foundation in its current state based on the report of Sas (2007) and the book written by De Gijt et al. (2014).

1. Retaining wall – vertical separation between the land and the water side. It is composed of brick, stones, or concrete dependent on the period of construction and the availability of materials. The quay wall is often equipped with a concrete coping to protect the upper side of the wall. When the quay wall has a significant retaining height, often grout anchors were applied to receive a certain share of the horizontal loads on the structure.
2. Foundation piles – element for the force transfer of superstructure loads to the subsoil. The piles are often positioned in pile rows along the length of the quay wall. The first pile row is identified as the front row of piles at the waterside. Often a combination of vertical piles and batter piles is present under the quay wall structure. Batter piles are used when the horizontal component of the total load is considerably large. The total pile bearing strength heavily depends on the driving depth of the pile tip into the stable bearing layer.
3. Foundation beams – wooden beams which were applied to obtain a certain degree of stability between the foundation piles during construction. Beams with a transverse orientation are called pile cap beams and connect the vertical piles with each other. When also batter piles are located under the quay wall, cross-beams were placed on top of the pile cap beams to connect those piles to the rest of the foundation structure.
4. Floor elements – plated elements positioned in the longitudinal direction for the distribution of superstructure loads and the soil weight over the pile cap beams.
5. Grating beam – longitudinal beam element located in the centre of the masonry wall are needed for the placement of the footing brick layer during construction. This element is not present at retaining walls composed of materials other than brick stones.
6. Soil retaining screen – vertical element in the soil, often positioned in front of the first pile row or behind the last pile row. The main function is the limitation of erosion processes when a groundwater flux is initiated by a level difference between the surface water and the groundwater. The screen is usually not a part of the original structure because erosion often becomes problematic when the structure is already in service for a few decades.
7. Quay wall furniture – most quay walls are equipped with various instruments like ladders, bollards, and handrails to facilitate activities on and around the water. Only bollards are part of the structural system because forces are generated on the quay wall when a ship is moored.

A simplified overview of the several elements with their particular location inside the element is presented in *figure 2-5*. In this drawing, the numbering corresponds to the enumeration given above.

Many historic quay wall concepts originate mostly from the Dutch etymology, so for each description a Dutch translation is added.

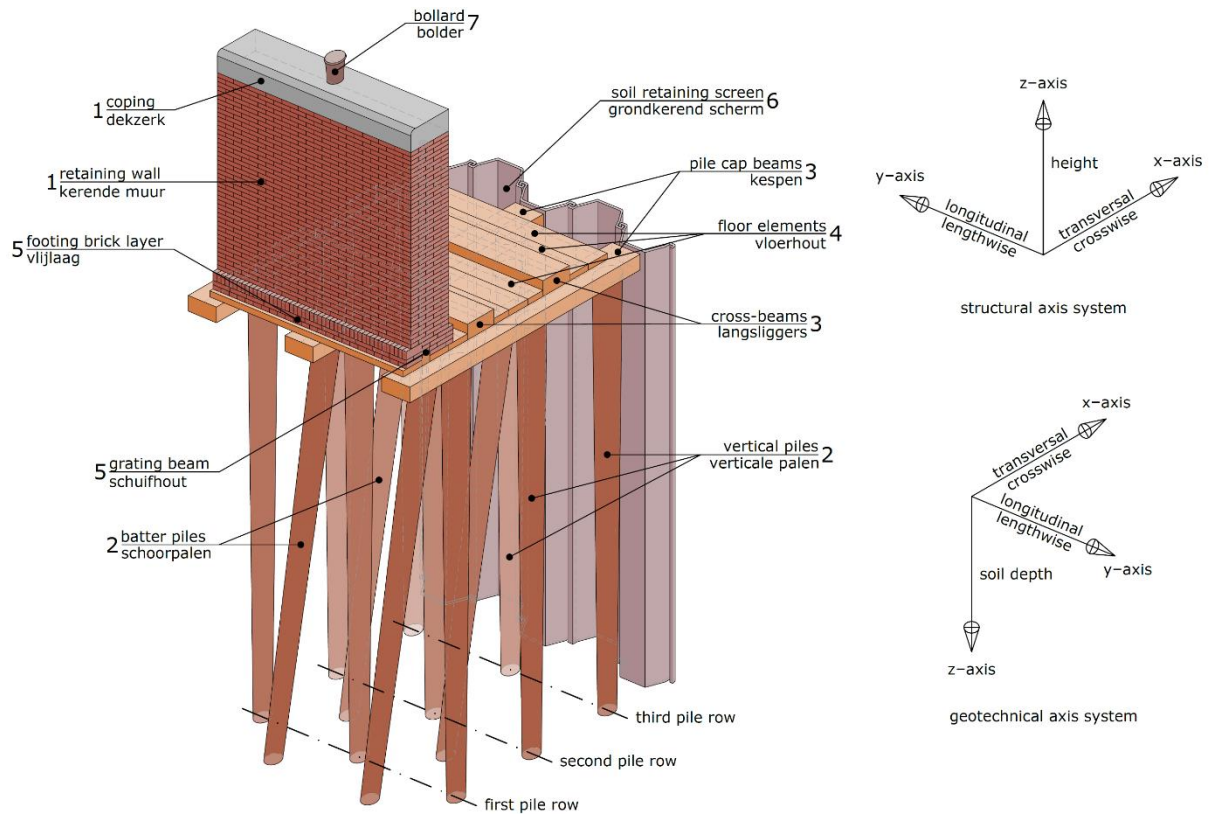


figure 2-5: composition of a historic quay wall with English and Dutch definitions for the quay wall parts accompanied by a global axis system

“A large part of the very old quay wall structures is composed of timber that is characterised by its organic composition and anisotropic behaviour. The material is susceptible to various organisms where foundation piles are mainly threatened by bacteria and fungi. Insights in the actual condition of timber elements can be obtained nowadays in various ways whereafter adequate measures could be taken if necessary.”

3

Degradation of foundation elements

Foundation elements of historic quay wall structures are often entirely made of timber. Various timber species are vulnerable to external influences due to the texture and composition of the material. Those influences could endanger the resistance of foundation elements when the time of exposure is equal to a few decades. This is the reason why many timber foundation structures of historic quay walls are deteriorated and currently in poor condition. From several observations and inspections, it was revealed that the structural condition differs a lot between the quay wall structures. In this chapter, it is shown why one structure is heavily deteriorated while others are still in a good state. A start is made with paragraph ‘3.1 Wood as a construction material’ where the characteristics of wood are given. The following paragraph ‘3.2 Types of degradation’ describes how timber is deteriorated by various external factors. In paragraph ‘3.3 Conducted research of degraded pile foundations’, several studies are presented that were related to the degradation of foundation piles. The chapter ends with an overview of the assessment of foundation elements in a timber foundation system in paragraph ‘3.4 Assessment of foundation elements’.

3.1 WOOD AS A CONSTRUCTION MATERIAL

At almost all places around the world where people live, trees are widely present. It is not surprising that wood from trees is used for many ages with several kinds of purposes. One of them is the construction of houses and other structural systems. It is a good construction material because it is cheap, has large dimensions, and is easy to modify into the desired shape. Nowadays, concrete and steel are often more preferable because wood has quite some limitations due to its very specific characteristics. Those peculiarities are described here.

Before going more in-depth, one extra note must be added. In above pieces of text, terms of wood and timber are alternated after each other. It is important to make a clear distinction between both terms because their definitions are not exactly the same. The term wood is used only in the cases when a link is made to the general features of the material. It is denoted as timber when the material is processed into structural components like the elements in a foundation structure. In the following chapters, the above given definitions are applied as accurate as possible to prevent ambiguous wordings.

The versatility of wood for different applications emerges from its particular composition. It is a natural and organic material which fulfils a lot of different functions inside a tree. The section between the roots and the crown is the most useful part in structural perspective due to its large volume and favourable properties. The most used definitions for this tree part are stem, trunk, or bole. The tree stem is

composed of different parts where each has their own function. Main functions of the trunk are the provision of strength to the tree and the transport of water and nutrients between the tree crown and the root system. When a tree section is cut into pieces, the components in *figure 3-1* can be distinguished where each component has its own function. They are described briefly in the enumeration given below.

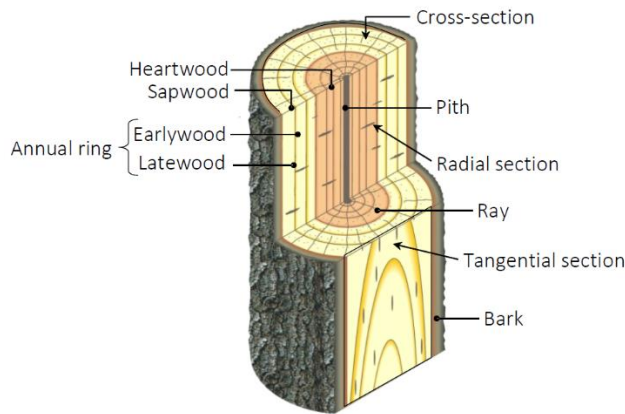


figure 3-1: components of a tree system with the definitions for the different sections (Blaß & Sandhaas, 2017)

- Bark: the outer rim of the stem which is the first boundary of the tree against intruders. It is split up into an inner bark and outer bark. The former consists of dead cells where the latter transfers nutrients from the crown to the cambium and storage cells deeper inside the trunk.
- Cambium (phloem): a very thin layer of cells located between the bark and the wood. In this layer, the growth of the tree in radial direction is secured by the division of wood cells. The trunk grows both from the inside out and from the outside in by the formation of annual rings. The formation of wood in one year during the spring and autumn is called earlywood and latewood, respectively. A tree prioritizes the formation of wood at the end of the year because the tree strength becomes more important than the transport of water when the outside temperature drops. The latewood is therefore thicker than the earlywood.
- Sapwood (xylem): the younger portion of the annual rings is used for the transport of and storage of water located at a close distance from the bark. The sapwood width depends on the wood species and bounds the region with physically active and dead cells.
- Heartwood: when a tree matures and grows primarily in radial direction, the inner part of the tree loses its transport function and provides only strength and stability to the tree. The transformation of sapwood to heartwood is called heartwood formation. The affected cells die and closes off their connections with neighbour cells. The heartwood has often a darker colour due to the storage of constituents.
- Pith: the midpoint of the stem which is only a few millimetres thick. It has the same function as the surrounding heartwood but is recognized by its dark colour.

The above given components are present in all kinds of trees but not in similar compositions and proportions. Every tree species can be assigned to one of the following two groups: softwoods and hardwoods. The term hardwood suggests that the material is harder than softwood, but this is not definitely true. Both terms are actually related to the composition of the wood tissue. Softwood or gymnosperm trees are characterized by its simple structure of only two cell types. All types of conifers belong to this group where cedar, Douglas fir, pine, and spruce are the most well-known species. Hardwood or angiosperm trees are built up from a higher variety of cell types, so its microscopical structure is more complex. Most deciduous trees are classified as hardwoods including species like oak,

maple, beech, and ash. The exact differences between softwoods and hardwoods are found on microscopic scale but are not of significant importance for this thesis report.

The physics of wood does not depend only on the applied wood species, but also on external factors. One very important parameter influenced by the surroundings is the moisture content. Wood is a porous material, so it tries to reach the same relative humidity as the surrounding air. The moisture content is defined by the proportion between the mass of dry wood (oven-dry state) and the mass with the actual level of moisture inside a timber element. A few examples of structural applications with typical values for this parameter are shown in *table 3-1*.

purpose of use	ω [%]
structural timber	8–20
external windows and doors	13–16
furniture, room doors, interior structure with permanent heating	6–9
plywood, LVL, musical instruments	5–7

table 3-1: approximative values for some practical cases (Blaß & Sandhaas, 2017)

A change in the moisture content has a large influence on the shrinkage and swelling behaviour of a timber element. The shrinkage and swelling are not the same in the tangential, radial and longitudinal sections of *figure 3-1* due to the alignment of the wood cells. Volume change in each direction becomes problematic when a timber element cannot move freely inside a structure which results in the generation of internal stresses. When the stresses become too high, severe distortions and cracks in the element could appear.

The moisture content also has an influence on the liveability of organisms in wood. In general, a minimum level of 20% is required for the modification of the wood structure by those organisms like decay or discolouration (Blaß & Sandhaas, 2017). Only the upper bound value for structural timber in *table 3-1* would be sufficient for decay processes, but the used definition in this table is quite broad. Foundation piles normally contain a higher percentage of moisture, especially when they are in direct contact with groundwater or surface water. In paragraph ‘3.2 Types of degradation’, an overview is given of the organisms which could affect the timber elements in quay wall structures.

There is a large variability of trees around the world where even single trees inside one species are not identical. Every tree tries to adapt itself to the environmental conditions in such a way that its survivability is as high as possible, so each one of them has therefore a unique fingerprint. When a tree is processed into a number of timber elements, properties must be assigned to the obtained pieces. A designer cannot guarantee a reliable timber structure when the strength and stiffness parameters of the structural elements are unknown. The specification of the structural parameters is done by strength grading. The quality of a piece of timber is determined by visual or machine grading. Visual grading techniques are primarily based on the knot area ratio where the number of knots over a certain area is marked and listed. The classification can be supplemented by observing pith presence, annual ring width, and crack patterns. The key parameter for machine grading is the modulus of elasticity. A distinction is made between destructive and non-destructive testing. The modulus of elasticity has a better correlation with the bending strength than the knot area ratio, so mechanical grading is more accurate than visual grading (Blaß & Sandhaas, 2017). For both hardwoods and softwoods, a list is made with strength classes where each class has a standardized set of strength and stiffness parameters. Those tables can be found in the building codes related to timber design.

Next to the variability of parameters, the wood structure also has an effect on the loading response of a timber element. Unlike steel, timber is an anisotropic material due to the orientation of the wood cells in the stem. Each type of loading results in a different response of a timber element. Often a simplified straw model is used to understand the load–deformation behaviour in different directions where each loading situation has its own particular failure mechanism. Two principal directions are distinguished which are parallel and perpendicular to the grain. Combining both directions with a compressive or tensile force, gives the stress–strain curve in *figure 3-2*.

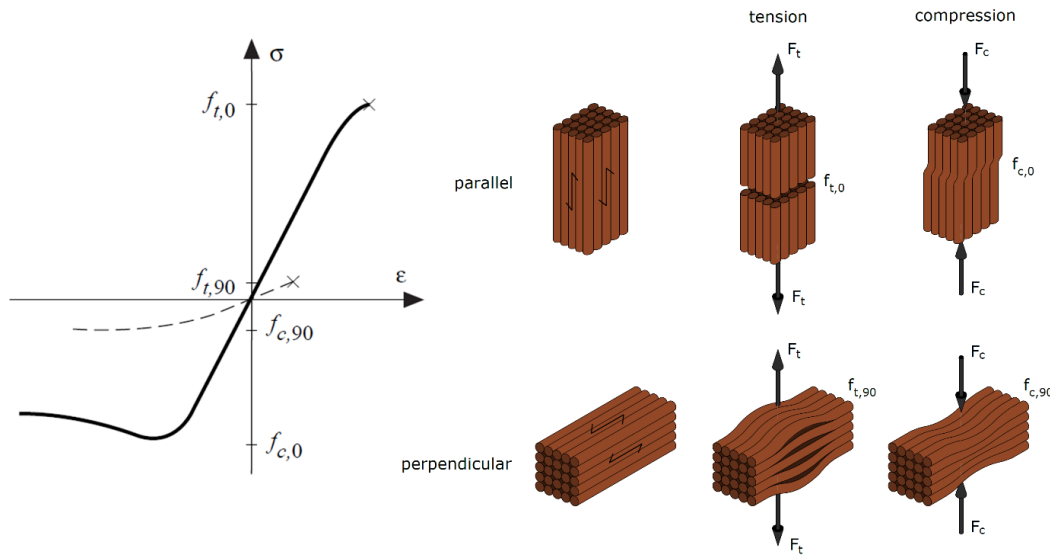


figure 3-2: typical load–deformation behaviour of timber for tension (t) and compression (c) with curves for loading parallel (0) and perpendicular (90) loading to the fibre direction

A timber element can resist a higher load parallel to the wood fibres compared to the perpendicular fibre direction. These differences will also appear in timber elements of a quay wall structure. Foundation piles are primarily loaded in axial direction where the beam elements are subjected to loads perpendicular to the element axis. The determination of the resistance of various foundation parts will be treated further in paragraph '4.5 Material resistance' for the various timber foundation elements.

3.2 TYPES OF DEGRADATION

A timber structure is subjected to several external influences which could endanger the structural integrity. One of them is material deterioration by ongoing processes over a long period of time. Three types of processes can be distinguished for timber elements which are chemical, mechanical, and biological degradation as mentioned by De Gijt et al. (2014). Each form of degradation is treated separately in the following paragraphs.

3.2.1 CHEMICAL DEGRADATION

Chemical degradation occurs when the molecules of a material are broken down into smaller parts. A very well-known example of this kind of deterioration is corrosion of steel. Most outdoor timber elements are subjected to weathering effects like sunlight exposure, hail impact, freeze/thawing effects and thermal loading. This set of degradation mechanisms are actually a combination of chemical and mechanical degradation because the impact of hail can result in local deformations of the material. Weathering effects have usually an influence depth of 6 mm/century (Kirker & Wynandy, 2014), so the influence of chemical degradation on the strength and stiffness properties of timber can be neglected.

3.2.2 MECHANICAL DEGRADATION

When a structural element is subjected to high stresses for a certain time period, a drop in the material resistance could occur. This is called mechanical degradation and becomes noticeable for materials that are sensitive to creep deformation and stress relaxation. Wood is also susceptible to mechanical degradation because it behaves as a viscoelastic material. Of these two types of deformation properties, creep deformation is the most critical one. In *figure 3-3*, a typical creep deformation curve for wood is shown.

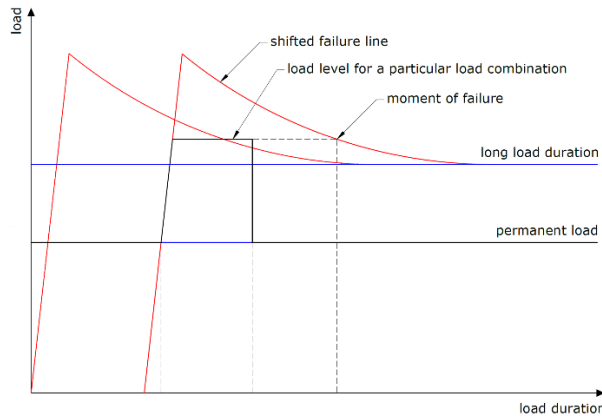


figure 3-3: relation between load and load duration for timber (Jorissen, 1995)

The resistance of a piece of timber decreases when the duration of the load is extended due to an increased creep deformation. Two different resistance values are given above by means of the blue lines. A permanent load lower than the resistance at long duration will not lead to failure. When the load is increased for a momentary period of time above the long duration strength but below the short duration strength, also no failure will occur. Only when the load duration is extended until a pre-set time instance, a failure mechanism appears and damage becomes visible. In the building codes, a number of reduction factors for load duration classes are given which are required for the design value of the timber strength. The exact values of these factors are given in paragraph '4.2.3 Material resistance'.

3.2.3 BIOLOGICAL DEGRADATION

Biological degradation of a material occurs when it is attacked by organisms. These living creatures degrade organic materials by decomposition as part of the carbon cycle in nature. Wood is one of those materials where complex molecule structures are gradually reduced to simpler molecules and finally into CO₂ and water (Blanchette et al., 1990). These molecules are composed of several chemical components where a few of them are preferred more than others for consumption due to the different levels of toxicity. Each type of organism has its own preferences for wood substances resulting in typical degradation patterns. In general, sapwood is more prone to biological decay than heartwood due to the closing mechanisms of heartwood cells (Blaß & Sandhaas, 2017), so the highest degree of degradation is often located in the outer part of a stem. Wood-inhabiting organisms can be classified into three groups: fungi, bacteria, and insects. Their characteristics and behaviour inside a piece of wood are treated below in separate paragraphs.

3.2.3.1 FUNGI

Degradation of wood by fungi emerges from the contact of spores in the air with the surface of the material. Under the right conditions, hyphae grow into the wood structure to extract nutrients and

substances. Unlike wood-degrading bacteria, fungi limit themselves primarily to sapwood decay because of toxic chemicals in the heartwood (Clausen, 1996). One of the main parameters is the moisture content which must be at least 20% for fungal growth. In *figure 3-4*, a classification system of fungi is shown with a relation to the degradation of wood.

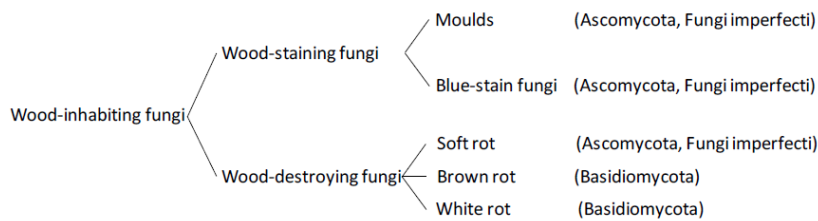


figure 3-4: fungal species with an influence on the wood structure (Sutter, 1997)

Above classification is based on the damage pattern caused by fungi. A first branch is made between wood-staining fungi and wood-destroying fungi. The former has primarily a visual effect where the latter is able to disassemble the inner wood structure. It does not matter if the foundation piles are discoloured by a fungal infection in terms of strength, so no detailed description is needed for the moulds and the blue-stain fungi any further.

The first wood-destroying fungal type is the soft rot fungi. It affects the part of the cell walls which provides a large portion of the bearing strength of timber. Even at the beginning stage of infestation, significant effects on the strength are observed. The name is derived from the dull and soft appearance of affected wood and becomes visible from the moment when the cross-section has already decayed heavily. Hardwood is in general more susceptible to soft rot attack than softwood. Soft rot flourishes particularly at the transition of air to soil (Blaß & Sandhaas, 2017), so foundation piles are primarily at risk by this fungal type.

Like soft rot, brown rot also breaks down the strength part of the woody tissue resulting in strength reduction and a loss of mass. The degradation pattern is characterized by the defragmentation of the surface into deep cubical pieces with a brownish shade. Brown rot fungi prefer high temperatures around 30 °C (Houtinfo.nl, 2013), so interior elements like furniture are degraded more likely than elements in non-heated environments. Brown rot in quay wall parts is therefore not expectable.

White rot is characterized by the degradation of the adhesive substances between the cell walls resulting in a loss of stiffness. It is often accompanied by a loss of strength, but only for certain occasions. As the name indicates, white rot gives a white colour. A spongy texture also belongs to the characteristics. White rot becomes prevalent when the wood moisture content remains high (20% or more) for a longer period (SHR, 2015). A persistent wet climate is quite common for quay wall foundations, so degradation by white rot fungi cannot be neglected.

The moist environment around the foundation elements is desirable for most fungal species. According to De Gijt et al. (2014), fungal decay of foundation elements can be quite devastating with maximum decay rates of 10 mm for soft rot fungi and even 100 mm for white rot fungi. The greatest limiting factor for these theoretical values is the availability of oxygen. Fungal processes are on hold when the supply chain of oxygen is cut-off, so inundated foundation elements are not threatened by fungal attacks. When an element is exposed to the air for short periods of time, fungal activity has to start up after each water level drop and its influence remains insignificant in this case. Only when a timber part is exposed for long persistent periods, fungal attack has a major influence on the timber properties like strength and

stiffness properties. As a result, especially pile heads of foundation piles in the front rows are susceptible to invasion by fungi because these elements are covered the least by surrounding soil.

3.2.3.2 BACTERIA

Bacteria play a very important role in the nitrogen cycle on Earth. Bacterial species are able to convert complex molecules into simpler compounds which can be used as building blocks for new chemical components. The decay of wood belongs to one of those bacterial processes. Only very recently (in the 1960s), a relation was found between wood degradation and the role of bacterial species (Clausen, 1996). Before this time it was believed that bacterial degradation was an extremely slow process that attacked only archaeological wood specimens buried very deep under the ground (Huisman et al., 2008). When the role of wood decay by bacteria was researched more intensively, it was found out that there a lot of different types of bacteria which colonize wooden objects and modify its structural properties. Bacterial species responsible for these changes are called wood-degrading bacteria. Unlike fungi, bacteria are less selective to environmental conditions. Bacterial degradation is also not limited by toxic substances in the wood (Clausen, 1996). From a large set of microscopical observations to wood samples, two different types of wood-degrading bacteria were distinguished based on the degradation patterns which are erosion and tunnelling bacteria. Both bacterial types are described briefly because the actual degrading mechanisms on microscopic level are not of interest for this report.

Erosion bacteria erode the face of a cell wall by alignment with the target. Released degrading enzymes create erosion channels or throughs in the cell wall. The name of tunnelling bacteria originates from the creation of tunnels during the degradation of cell walls. They penetrate through the cell wall by a change of its shape. The transformation helps with the regulation of the required amount of enzymes for the breakthrough of each wood cell wall layer. Both bacterial types are active in a wide range of different environments, but there is one striking difference between the two. Where tunnelling bacteria require a certain degree of oxygen, erosion bacteria thrive very well in both aerobic and anaerobic environments (Singh et al., 2016). Erosion bacteria are therefore the only degraders in oxygen-free places.

It is not surprising that timber foundation elements of quay wall structures are affected by bacterial decay. De Gijt et al. (2014) states in their book that the water flow around objects, permeability of the material, timber species, and timber qualities are the most important parameters for the severity of decay of foundation elements. Maximum values for the degradation rate of 1 mm/year are observed in case optimal conditions are provided for bacteria. This value is much lower than fungal decay but bacterial decay becomes governing for waterlogged and buried timber elements.

3.2.3.3 INSECTS

Insects damage the wood by the creation of burrows below the surface. For the vast majority of species, only the larvae inhabit and damage the wood. A distinction can be made between greenwood insects, dry-wood and decaying insects where the name relates to the preference for a certain condition of wood. Dry-wood insects are therefore the group that attacks timber in buildings and civil structures.

Foundation piles under quay walls are almost entirely embedded into the soil. Only the pile heads of the piles in the front rows are often exposed due to a descending slope of the ground towards the water. The high level of moisture around the structure prevents that most species lay eggs inside a timber element. The exceptions are pile worms and gribble which are notorious for the destruction of timber elements in hydraulic structures (De Gijt et al., 2014). Both creatures form drilling holes in the wood with possible large reductions in the timber bearing strength as a consequence. Luckily, no historic quay wall foundations are threatened by pile worms or gribble because those creatures are found only in

salty or brackish waters. Inner-city quay walls are normally located in freshwater regimes, so the decay by insects is not relevant here.

3.3 CONDUCTED RESEARCH OF DEGRADED PILE FOUNDATIONS

Through the years more and more problems of timber foundation structures emerge. The first observations of deteriorated timber elements were performed quite recently, around the 1950s (Klaassen, 2008), so no documentation about foundation deficiencies is available before this time. One of the reasons could be that risks of foundation failures are hidden into the ground which complicates proper assessment of the structural condition. From that period onwards, many investigations were performed on timber foundations. Of all foundation elements, the most attention is paid to foundation piles due to extra dimension with the surrounding soil, but most principles about foundation piles are also relatable to pile cap beams and floor elements.

3.3.1 APPLIED WOOD SPECIES

For the construction of quay walls, large bulks of wood material were needed for a pile foundation, especially in the western part of the Netherlands as mentioned in paragraph '3.3.1 Applied wood species'. To ensure sufficient stability for the structure, the foundation piles must reach a stable sand layer. The depth of this sand layer differs a lot between various Dutch cities. In Rotterdam much longer piles were needed compared to other cities like Haarlem and Amsterdam. According to Klaassen (2008), the thickness of the clay and peat layers varies along the coast from 6 m in Haarlem to 16 m in Rotterdam. A global overview of the required pile length in the Netherlands is depicted in *figure 3-5*.

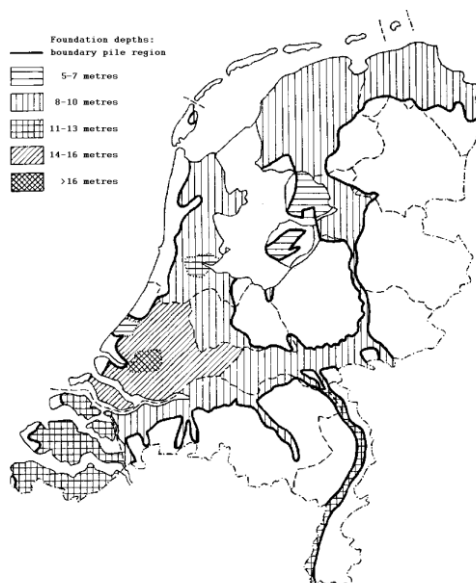


figure 3-5: required pile length for a stable foundation for different parts in the Netherlands (Veldhuijzen, 1963)

The required pile length and the availability of tree stem batches at the time of construction had an effect on the applied wood species. From several foundation inspections it followed that longer piles were mainly composed of spruce and fir where shorter piles often were made of pinewood (Klaassen & Creemers, 2012). To a lesser extent also Douglas fir, alder, and oak piles were found (De Gijt et al., 2014). The piles were placed under a quay wall in a very dense pile grid with diameters ranging from 200–350 mm. In exceptional cases even smaller pile diameters were found. In *table 3-2*, a brief overview is given

of the pile characteristics in a number of Dutch cities based on the reports from Veldhuyzen (1963), Klaassen et al. (2000), and Klaassen (2008).

municipality	pile length [m]	most prevalent wood species		
		primary	secondary	tertiary
Rotterdam	16 – 23	spruce	pine	–
Amsterdam	12 – 14	pine	spruce	alder
Gouda	10 – 15	spruce	pine	–
Zaanstad	7 – 9	pine	spruce	–
Haarlem	2 – 5	pine	spruce	–
The Hague	2 – 5	pine	spruce	–
Dordrecht	14 – 16	spruce	pine	fir
Descriptive names accompanied by the scientific plant names pine = Scots pine (<i>Pinus sylvestris</i>) spruce = Norway spruce (<i>Picea abies</i>) fir = silver fir (<i>Abies alba</i>) alder = alder (<i>Alnus spec.</i>)				

table 3-2: required pile lengths and the most common wood species in a few cities in the Netherlands

According to Klaassen and Creemers (2012), not all required pile diameters and lengths could be retrieved from forests in the Netherlands. The short piles made of pinewood were widely available from domestic tree plantations, but spruce and fir were mainly imported in large bulks from Scandinavian countries, Belgium, Poland, and Germany. The differences in supply and demand in several periods of time resulted in a large variety of applied wood species for foundation piles around the Netherlands.

3.3.2 INVENTORY OF WOOD DEGRADATION STUDIES

In the past few years, a number of studies were performed to the biological decay of foundation elements. They were initiated to obtain a general picture of the actual condition of the foundation elements and to gain more knowledge about the degradation mechanisms. Most investigations in the recent past aimed at bacterial decay in comparison with fungal decay because the latter is described very extensively in literature already. For a long time it was believed that bacterial decay was a very slow process that was harmful only to archaeological artifacts. When more and more problems with deteriorated foundation piles showed up, the attention was focused primarily on degradation in anoxic environments which is exclusively associated to bacteria.

3.3.2.1 VAN ETTEN ET AL. (2000)

Around the year of 1997, a few warnings arrived at the former ministry of housing, spatial planning, and the environment (Dutch: ministerie van VROM) about fungal decay of timber foundation piles in several Dutch cities. Authorities of several municipalities were worried about the actual state of the timber foundations and subsequent foundation deficiencies in the near future. In response to these alarming messages, the ministry decided to give a request to a consortium of research companies for a literature study about the size and impact of this problem. The provided report describes the relevant fungal species for wood degradation, parameters related to fungal growth, and the possible causes of fungal decay in Dutch foundation piles made of timber. The first two points are described already in paragraph '3.2.3 Biological degradation', so no more attention is paid to these subjects. Only the third point provides new matter about fungal decay of foundation piles.

Fungal species are only active in oxygenated environments which means that foundation elements are endangered by fungi when they are exposed to the air. Timber elements are free of fungal decay when

they are situated below the groundwater table. For the preservation of timber foundation elements, it is therefore important that municipalities implement a proper water management policy. The groundwater level is very sensitive to influences from the surroundings. They are induced by natural causes in the form of precipitation (supply) or drought (retention) and by human interference. Examples of the latter are adjustments to the pavement at street level, removal or placement of vegetation and changes to the subsoil. These are planned interventions, but also unforeseen changes to the groundwater table could take place. The most common problem is a leaking or draining sewer system located above or below the groundwater level. Uneven settlements along the sewer system are the main cause of groundwater disturbance by sewer water, especially for pipes consisting of short segments with lots of connections and thus weak spots.

To characterize the influence of fungal decay on a timber foundation, Esser and Buitenkamp (1996) decided to investigate wooden samples retrieved from horizontal oriented foundation elements in a laboratory. The following conclusions were drawn from the experiment:

- The degree of decay increases for a long cumulative period of exposure to the air. Piles in a tidal zone where wet and dry periods are alternated in succession on a daily basis, are free of fungal attacks.
- Horizontal oriented foundation elements are mainly composed of heartwood because the sapwood is often removed to adjust them to the desired rectangular or circular shape.
- Heartwood is in general more resistant against fungal decay than sapwood due to the large amount of additives.

The translation of above findings to timber elements is quite complicated because of the different compositions. Foundation piles contain a lot more sapwood than the other elements because tree stems were debarked before they were driven into the soil. Pile cap beams and floor elements are also situated at a higher level than foundation piles, so the exposure time of oxygen is longer for the horizontal orientated foundation elements.

The main subject of this literature study was focused on the geographic distribution of fungal decay in timber piles in the Netherlands. Companies in related work fields were asked to deliver reports about foundation inspections where a certain period of exposure was proven or fungal decay was revealed by microscopic analysis. The outcomes of this investigation did not lead to remarkable features. Fungal decay occurs on a local scale, so each pile foundation has a chance of a certain degradation by fungi during its lifetime.

3.3.2.2 KLAASSEN, ETAL. (2000)

In the same period of the investigation to fungal decay, the ministry of housing, spatial planning, and the environment wanted a literature study in 2000 about bacterial decay in timber foundation piles in the Netherlands. More and more messages showed up around the deteriorated state of timber piles, so more background knowledge about bacterial degradation was desired. The research to the current state of the foundation piles across several cities in the Netherlands was performed by a survey. Companies were asked to send results of old foundation investigations to the research group. All delivered information was analysed and captured in tables.

The first inventory was aimed towards the applied timber species for foundation piles in cities across the Netherlands. From the observed data, around 50% of the piles were made of pine, 20% were made of spruce and the remaining 30% were not identified. The spreading of those two species is mainly dependent on the required pile length as stated in the previous paragraph.

The next step in the research was focused on the degree of degradation across the cities. Only permanently saturated piles were considered, so elements with fungal patterns were excluded from the survey. From the remaining batch, spruce and pine piles were assessed separately because differences in bacterial decay between the species were expected on beforehand. The assessment was done with a penetrometer. More information about this measurement device is given in paragraph '3.4 Assessment of foundation elements'. In *table 3-3* and *table 3-4*, the ratios of bacterial degradation per municipality are given for pine and spruce, respectively.

municipality	decay magnitude					number
	total	severe	moderate	weak	none	
Amsterdam	44 %	13 %	44 %	0 %	0 %	16
Zaanstad	8 %	23 %	46 %	22 %	1 %	502
Haarlem	52 %	25 %	19 %	4 %	0 %	731
Gouda	31 %	37 %	28 %	4 %	0 %	126
Rotterdam	0 %	0 %	100 %	0 %	0 %	1
Dordrecht	25 %	25 %	50 %	0 %	0 %	4

table 3-3: degree of degradation of pine piles in several Dutch cities (Klaassen et al., 2000)

municipality	decay magnitude					number
	total	severe	moderate	weak	none	
Amsterdam	22 %	50 %	22 %	6 %	0 %	18
Zaanstad	0 %	4 %	14 %	63 %	20 %	56
Haarlem	13 %	25 %	43 %	17 %	2 %	107
The Hague	0 %	0 %	0 %	0 %	100 %	4
Gouda	12 %	19 %	34 %	31 %	4 %	139
Rotterdam	0 %	0 %	0 %	100 %	0 %	4
Dordrecht	9 %	27 %	41 %	23 %	0 %	22

table 3-4: degree of degradation of spruce piles in several Dutch cities (Klaassen et al., 2000)

From the tables given above, it follows that around 55% of the pine piles was degraded severely where only 30% of the spruce piles shows this level of decay. Another remarkable feature is the difference between the cities; for instance, foundation piles from Haarlem are much more degraded than piles from Zaandam.

The degree of degradation is also coupled to the estimated construction year of the pile foundation to see if older piles are degraded more severely than younger piles. In *figure 3-6*, the relation between the approximated age and the measured penetration depth is given for pine samples.

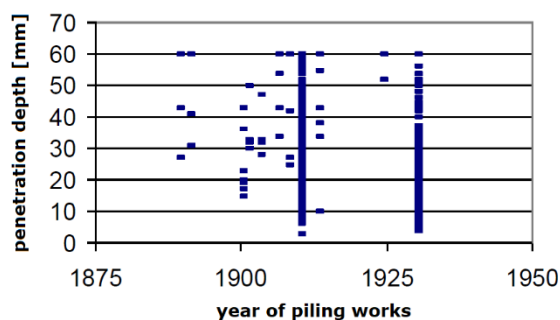


figure 3-6: relation between the service life and the degree of degradation (Klaassen et al., 2000)

Two vertical lines are shown that corresponds to the foundation piles in Haarlem and Zaanstad. The quantity of delivered reports by those two cities surpasses the numbers of other cities which results in a distorted image. The selective character of the obtained measurements results in a plot where no clear trend is visible. When the degradation between both municipalities is compared with each other, it follows that the older piles in Haarlem are degraded more than the younger piles in Zaanstad. It is not known if this differences depends exclusively on the age or other factors like local conditions also play a role.

3.3.2.3 BACPOLES (2005)

In contrast to fungal decay, bacterial decay of wooden objects possessed a lot of uncertainties in the last years. To acquire knowledge about the degradation processes under different circumstances, a large research project about deteriorated foundation elements was initiated. The project was called BACPOLES which is an abbreviation of bacterial wood decay in foundation poles. The project was funded by the European Commission where scientists of five European countries collaborated from 2002 to 2005. The main objectives of the project are listed below:

- Obtain basic knowledge of the impact of bacterial decay on wood buried into the ground (foundation piles and archaeological remains).
- Develop practical guidelines for the preservation of timber foundation elements against bacterial decay.
- Gain information about bacterial processes in wood by the isolation and identification of wood degrading bacteria.

Only the first bullet point is relevant for this report because it relates the influence of bacteria to foundation elements in a soil environment. The research was based on the available information about foundations from Great Britain, Sweden, Germany, Italy, and the Netherlands.

One of the studies used as input for the BACPOLES project was performed by SHR where more than 4000 samples were analysed in the laboratory from 1997 until 2004. The samples originated from foundation piles situated in the Dutch cities Haarlem, Amsterdam, and Dordrecht. Those cities were chosen because of the severe foundation problems related to biological degradation. The found timber species are given below in *figure 3-7*.

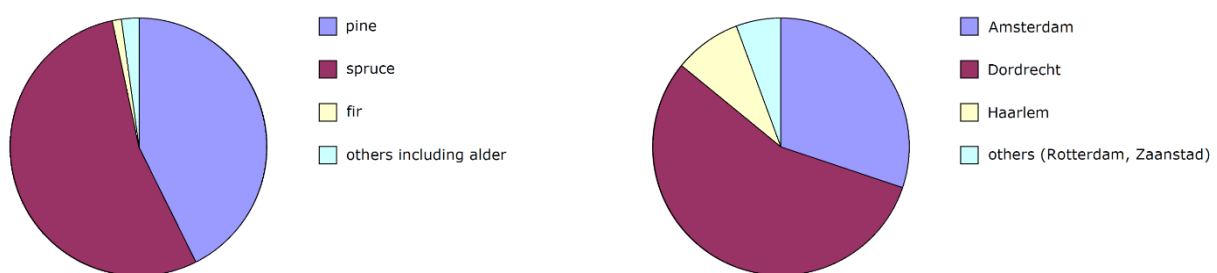


figure 3-7: applied timber species in foundation elements in different cities in the Netherlands (BACPOLES, 2005)

The database is supplemented with values for the moisture content and wood density for the species. In *figure 3-8*, the relation between the two parameters is plotted. For three timber species, a good correlation is found where a lower moisture content results in a higher density.

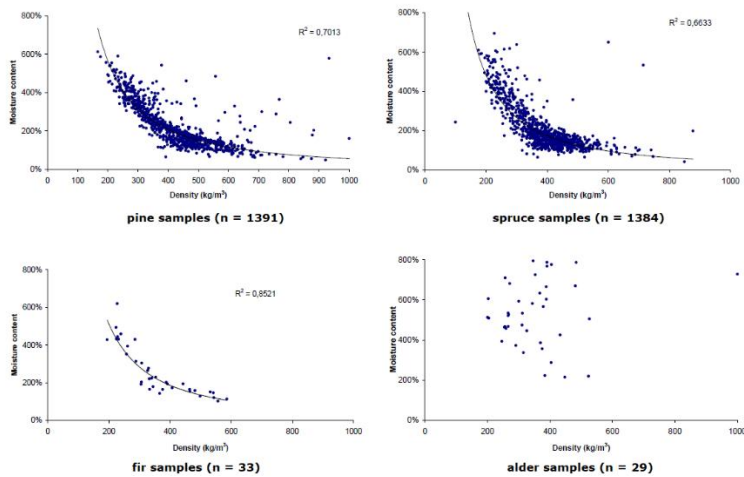


figure 3-8: relation between the density and the moisture content for pine, spruce, fir, and alder (BACPOLES, 2005)

The decay patterns in the wood samples were investigated by a light microscope. SHR defined six categories for the degree of decay ranging from sound timber to totally degraded timber. The relation between the decay and the two considered timber parameters is given in figure 3-9 for the two timber species with the largest set of samples. It is accompanied by a bar plot which includes the mean value for the degree of degradation across the pile radius.

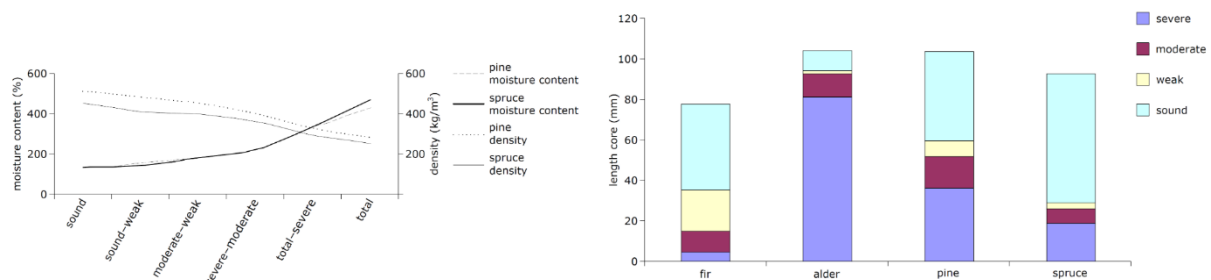


figure 3-9: extent of degradation for different wood species; left: influence of degree of degradation on moisture content and density for spruce and pine, right: mean degradation across the pile radius for 859 foundation piles (BACPOLES, 2005)

From the left graph it becomes visible that the severity of decay has a large influence on both moisture content and wood density. The moisture content increases with a higher level of degradation because a more open wood structure contains more voids where water can be accumulated. The same principle is valid for the density of the material; a heavily degraded piece of wood has lost a number of cell wall substances, so the weight becomes less than the weight for a piece of sound wood. The right graph shows a large distribution of wood qualities across the species. It seems that alder possesses the lowest resistance against bacteria and fungi, but this is not necessarily true. Alder piles are on average older than other timber piles which would partially clarify the large differences in degradation. The measurement data in the bar plot for fir piles implies a very sustainable wood species compared to the others, but the sample size is too small to approve this perception. In contrast to fir, more samples are available for pine and spruce. Spruce possesses overall a greater resistance against biological decay than pine. The degraded section is on average twice as thick in pine samples than in spruce samples.

A more detailed comparison between pine and spruce piles can be made with a frequency diagram. This mathematical tool visualizes how many times a certain result is found relative to the total number of samples. The frequency diagrams on basis of the degradation degree are depicted in figure 3-10. In

these diagrams, the cross-section of the pile is split up into segments with a length of 10 mm from the bark to the pith.

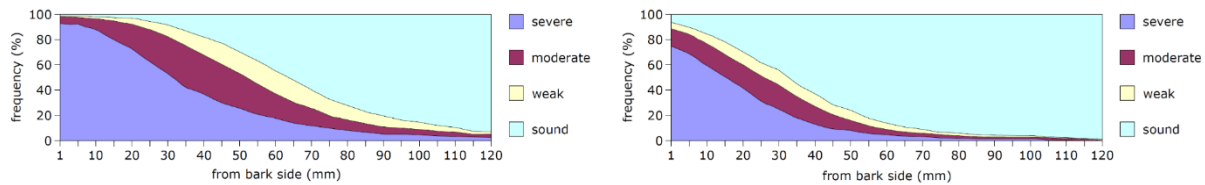


figure 3-10: frequency diagrams for the degree of degradation; left: pine samples (n = 903), right: spruce samples (n = 789) (BACPOLES, 2005)

The frequency diagrams for pinewood indicates that 5 % of the piles shows no signs of degradation where a portion of 90 % has a severely degraded outer skin. At a depth of 40 mm, half of the total number of piles is severely degraded. The degradation of the spruce piles at the outside is characterized by 10 % with a sound skin and 75 % with a heavily degraded surface. Around 50 % of the piles is severely degraded at a depth of 20 mm.

Another research approach described in the BACPOLES project was focused on the influence of peat on the degree of bacterial degradation. In the western part of the Netherlands, the soil contains large deposits of peaty soils. The origin of the groundwater flow has a large contribution on the exact composition of the peat. The peat layers in Amsterdam are poor in nutrients due to a main supply of rainwater and upwelling groundwater. In Haarlem, a higher concentration of nutrients is found as a result of groundwater flow through the dunes at the North Sea. At locations where the peat has a higher concentration of nutrients, more severe degradation in timber foundation piles was observed. The salinity of the groundwater also has an influence on the degradation. Piles located in freshwater reveals more signs of advanced decay than piles in salty or brackish water.

Besides the content of the groundwater, the groundwater flow could also play a role in bacterial decay of foundation piles. Bacteria are only motile when a medium transports them to their desired place, in this case a piece of buried wood. It was speculated that the differences in the degree of bacterial decay depends on the groundwater dynamics in combination with the composition of the soil and wood species (BACPOLES, 2005). This concept was endorsed by archaeological field observations where submerged wood was more susceptible to degradation than wood in less permeable soils. The constructed hypothesis comprises the increase of wood degradation when the permeability of the material is higher than the surrounding soil. To test this hypothesis, an experiment was set up with sound tree stems of different wood species. The permeability was determined by the placement of a container with water on the top of the stem and measuring the outflow of water at the bottom side. Only the axial direction was considered because water cannot flow along the radial or tangential sections due to the microscopic structure of the wood. The following results were found:

- The permeability depends mainly on the applied wood species. Pine has the highest permeability followed by spruce and Douglas fir with an intermediate permeability. Alder is the least permeable of the tested species. The findings are only valid for the sapwood because heartwood is considered as impermeable.
- Water pressure on top of the stem has a positive correlation with the water flow through the wood.

The experiment was performed with non-degraded tree stems. In reality, foundation piles always show some signs of degradation, so the expected permeability is higher for these elements. Unfortunately, it

is not possible to perform flow experiments with a foundation pile in service, so the actual influence of the permeability of a degraded pile and the surroundings on water flow is still unknown.

Although, the simulation of water transport through a foundation pile is only possible to a limited extent, the observed differences between pine and spruce are in line with the water flow experiment. Together with the observations about the influence of nutrients in peaty soils, it is clear that biological degradation highly depends on the local circumstances around the foundation piles.

3.3.2.4 KLAASSEN (2008)

To acquire relations between bacterial decay and relevant parameters, wood researcher Klaassen performed quantitative research to measurement data related to degraded foundation piles. In his study, three topics were examined more in depth. The retrieved data for this study comes from the BACPOLES project and foundation inspections of timber foundations.

- Determination of the differences of bacterial degradation between wood species which were used for the construction of timber foundations.
- Investigation to the bacterial degradation in different sections of a foundation pile.
- Finding relations between the degree of degradation and some wood properties.

The first subject about differences in degradation between wood species is based on a total of approximately 2000 samples of foundations under historical buildings with an age of around 100 years. Most samples originated from foundation piles in Amsterdam, but also other cities in the Netherlands were represented with smaller batch sizes. The wood specimens were retrieved with an increment borer at a height of 50 cm below the pile head from the outside towards the pith. The cores were investigated in a laboratory on the degree of degradation. Each sample is classified into one of the three degradation classes; severe, moderate, or weak decay. For each class, the mean degradation depth is determined. The investigation results of the wood samples are shown in *table 3-5*.

municipality	wood species	sample size n [-]	mean depth of decay from bark towards pith [mm]		
			severe	moderate	weak
Amsterdam (n = 1692)	pine	827	36	17	10
	spruce	826	21	9	14
	fir	12	3	19	27
	alder	27	81	11	1
Haarlem (n = 77)	pine	59	25	17	7
	spruce	18	14	16	3
Zaandam (n = 76)	pine	57	27	19	8
	spruce	19	7	6	3
Dordrecht (n = 56)	pine	13	32	11	11
	spruce	38	11	9	4
	fir	5	7	7	4
Rotterdam (n = 44)	pine	5	15	2	7
	spruce	39	8	4	6
Wilnis (n = 22)	pine	1	5	5	20
	spruce	21	5	9	7
The Hague (n = 9)	pine	8	7	45	10
	spruce	1	0	30	5

table 3-5: mean depth of degradation for piles consisting of different wood species (Klaassen, 2008)

From all samples it was observed that the degree of degradation decreases from the outside towards the pith. In the table above, a large variability in degradation is present between species, but also

between different cities. Despite the large variation in the degree of degradation, the following tendencies were noticed:

- Pine is degraded more severely than spruce in each city.
- Fir shows the same degradation patterns as spruce.
- Foundation piles of alder are completely degraded.
- The heartwood of foundation piles is unaffected in contrast to the sapwood.

The differences between the degradation in a single species could also be declared by the sapwood width. Trees from Dutch plantations has matured earlier than the trees in neighbouring countries, so the amount of sapwood in Dutch stems is greater than the sapwood size in logs cut from other regions. Younger trees were often shorter in length than their older versions, so the Dutch trees were mainly applied in Haarlem, Zaandam, and Amsterdam with a shallower location of the first sand layer. In Rotterdam and The Hague, the stable layer is situated much deeper into the ground, so the piles from longer and full-grown trees were used in these cities.

Secondly, Klaassen looked at the differences of degradation inside a single pile. He distinguished two directions in the investigation; across the pile diameter (radial) and along the pile length (longitudinal). A total number of 26 foundation piles were extracted from the soil and sawn into disks with thicknesses of 20 cm. From the total batch, piles originated from 100 year-old buildings in Haarlem, Dordrecht, and Amsterdam and archaeological sites in the Netherlands, Germany, and Sweden. The origin, diameter, length, and building period for each pile are given in *table 3-6*.

municipality	wood species	n [-]	d [cm]	L [m]	Construction period
Amsterdam (NL)	pine	2	23	11	1926
	spruce	2	23	11	1 st century
Borselle (NL)	oak	2	18	2	1895
Haarlem I (NL)	poplar	3	13.5	4	1895
Haarlem II (NL)	pine	6	12	1	1900
Rotterdam (NL)	fir	1	25	14.5	1903
	spruce	2	25	14.5	1903
Zaandam (NL)	pine	3	11	7	1937
Stockholm (SE)	pine	2	25	6	1895
Travenhorst (DE)	oak	3	27	1.5	late medieval

table 3-6: pile characteristics for the investigation to local differences in degradation (Klaassen, 2008)

Oak is barely used for foundation piles, so the results from observations and experiments with this species are not considered in this thesis report. The same decision is made for very short piles (6 m or less).

From the measurements of the degree of degradation along the pile length, no remarkable differences were found. The degradation increased slightly towards the pile tip for a few piles, but for the majority it remained constant along the pile length. Piles from Rotterdam showed the least degree of decay; only the outermost layer with a thickness of 1–2 mm was affected. Similar patterns were recognized for piles from Haarlem and Zaandam. The outer parts of the piles were severely degraded over the entire pile length. Only heartwood remained unaffected in the investigated piles. Although a limited gradient of bacterial decay was observed along the pile length, it cannot be ruled out immediately for timber piles. The batch size is simply too small to exclude the influence of the gradient on the affected pile properties.

The last research topic comprises the relation between the degree of degradation on the properties of a foundation pile. To determine the compression strength of the degraded wood, small test blocks were compressed that were obtained from the same piles given in *table 3-6*. Before each block was compressed on a test bank until failure, the specific gravity and moisture content were determined. The blocks with signs of fungal decay were omitted from this research. The obtained results were plotted in several graphs per wood species. The graphs for oak are not presented in this thesis report because oak piles are usually not found under quay wall structures. Firstly, the relation between the moisture content and the specific gravity is given in *figure 3-11*.

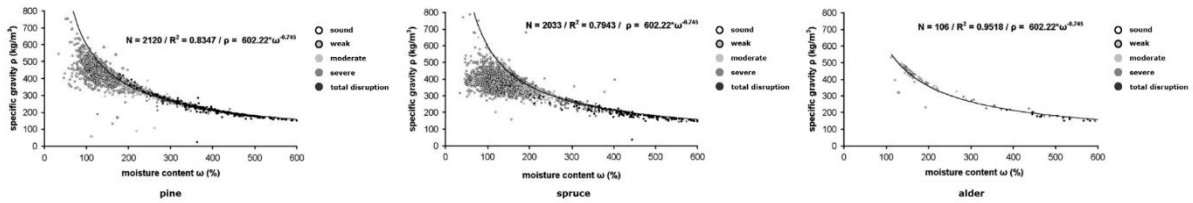


figure 3-11: relation between the moisture content and specific gravity for pine, spruce, and alder (Klaassen, 2008)

For all three species, a similar relation is found with a strong correlation. Especially for the region with a moisture content higher than 200%, the test results follow more or less the same curve.

$$\rho = 602.22 \times \omega^{-0.745} \quad 3.1$$

Mostly weak or non-degraded test blocks with low levels of moisture content deviated from this line due to the significant influence of trapped air inside the samples.

Subsequently, the test results for the moisture content with the compression strength and the specific gravity with the compression strength are visualised in separate graphs. The plots of *figure 3-12* are given only for pine because the entire range of degradation is not covered by the subsets of other species.

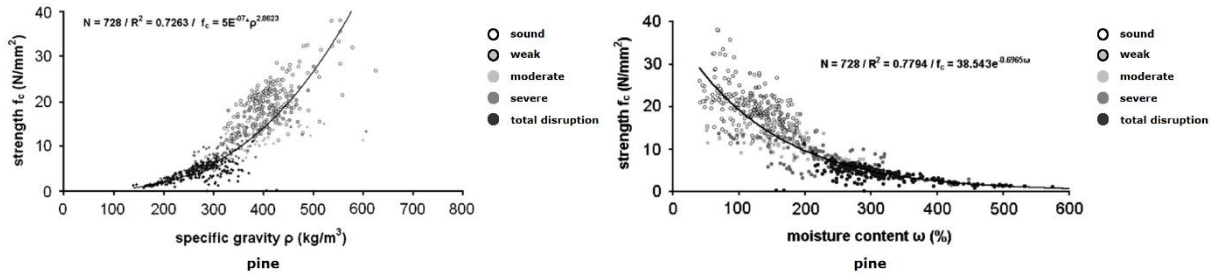


figure 3-12: comparison of the specific gravity and the moisture content with the compression strength for pine (Klaassen, 2008)

As expected, severely degraded wood samples possess a lower compression strength value than less degraded samples. In the left graph, almost all degraded samples are situated in the regions with a low specific gravity, so bacterial decay has a large influence on both the specific gravity and the compression strength. A similar pattern is visible in the right graph. Destroyed wood structures contains a lot of voids where water can be accumulated that results in a high moisture content. A degraded piece of wood is disorganized by a large number of openings between the cell walls and therefore retains a low compression strength. In both plots a curve is drawn for the detection of a trend between the observed parameters. The relation in the right graph can be used to estimate the compressive strength in a wood specimen with a mathematical expression (NEN 8707 app. D, 2018).

$$f_c = 38.543 \times e^{-0.6965 \times \omega}$$

3.2

The expression is applicable in the following conditions:

- For cases where the timber specimen is fully saturated.
- Valid for sound or timber degraded only by bacteria, so pieces with fungal spores are not suitable for this calculation method.
- A reliable estimate is obtained when the sample size is sufficiently large.

The formula can be used for all segments along a retrieved drill core from a foundation element. It is important to be cautious with the transport of the samples to the investigation site, so exposure to exterior influences and contaminations remains to a limited extent.

3.3.2.5 FINDINGS

After the examination of all the documents and measurement results from these countries, the following generalized conclusions can be drawn:

- Fungal decay is more likely present in horizontal orientated foundation elements than foundation piles due to the location of each part relative to the groundwater table. Fully saturated foundation piles only show decay patterns related to bacterial attacks.
- A tendency towards a higher level of degradation when a combination of bacterial and fungal decay is observed.
- All timber foundations older than 100 years and situated below the groundwater level show signs of bacterial decay. The severity of decay is the highest in the outermost layer of a foundation pile and decreases towards the centre of the element.
- Spruce wood has a higher resistance against bacterial decay than pine and alder, although some observations revealed the opposite result where the pinewood was degraded less than spruce piles.
- The degree of bacterial degradation is location-specific; measurement results between Dutch cities shows a large variety in degradation for the same timber species. Large fluctuations in the groundwater level seems to be a trigger for a high degradation rate caused by bacteria and fungi.
- Biological degradation can have a significant influence on the strength and stiffness properties of the timber material.

3.4 ASSESSMENT OF FOUNDATION ELEMENTS

In the previous section, several studies were performed to obtain a global overview of the biological degradation of timber foundation piles. Despite the detection of a few clear trends, biological degradation depends heavily on local circumstances. It is therefore highly recommended to observe each foundation structure individually to acquire an accurate overview of the structural state. A brief overview of the required activities for a foundation inspection is given below (VROM, 2003):

1. Excavation of a trial pit (Dutch: inspectieput) to access a selected part of the foundation structure.
2. Classification of the subsoil where the ground level, soil composition, level of the soil layer transitions, and the groundwater table are determined. In the Netherlands, the Amsterdam Ordnance Datum (Dutch: Normaal Amsterdams Peil (NAP)) is used for the notation of geographic altitudes.

3. Measurements at the foundation structure to obtain a global overview of the structural condition. Relevant information consists of the description of location and dimensions of the foundation elements, measurements of structural deformations, and descriptions of the actual state of the foundation elements.
4. Visual assessment of the condition of the brick or concrete retaining wall on deficiencies like cracks, loosened brick stones, and local deformations
5. Assembly of measurement data by a penetrometer. It is a measurement device that determines the actual indentation hardness of a material. A penetrometer for wood measures the thickness of the soft skin where the obtained results are an indication for the degree of degradation by bacteria and fungi. The instrument is placed against the assigned element whereafter a steel pin is released with a constant force on the surface. The created dent is an indication for the actual condition of the wood. There are two types of penetrometers accepted in the Netherlands for the measurement of wood hardness: Pylodyn and De Specht. Pictures of both devices are given in figure 3-13.



figure 3-13: two types of penetrometers, left: Pylodyn (Istemi, n.d.), right: Specht (Profound, 2017)

Both instruments give quite accurate results when they are calibrated on a regular basis. A number of impacts must be performed at predefined spots on a timber element to achieve a representative measurement. The obtained results give a good impression of degree of degradation in a timber foundation element. An indication for the degree of degradation can be given for certain values of the measurements. They are mentioned in table 3-7.

p_m [mm]	decay magnitude
$p_m > 35$	totally disintegrated
$20 < p_m < 35$	severe
$10 < p_m < 20$	moderate
$5 < p_m < 10$	weak
$p_m < 5$	none

table 3-7: indicative values for the degree of bacterial decay by spring-loaded penetrometer measurements (Klaassen et al., 2000)

6. Collection of photographs of the structure. To capture the structural condition in a proper way, a number of overview and detail photos is needed.
7. Retrieval of samples from the timber foundation for the investigation in a laboratory. Samples are collected by the use of an increment borer and submerged immediately after extraction in cooled water to prevent pollution with external substances. The necessity for sampling can be determined with the assessment scheme in figure 3-14 which is based on the penetration values and the dimensions of the tested element from step 5.

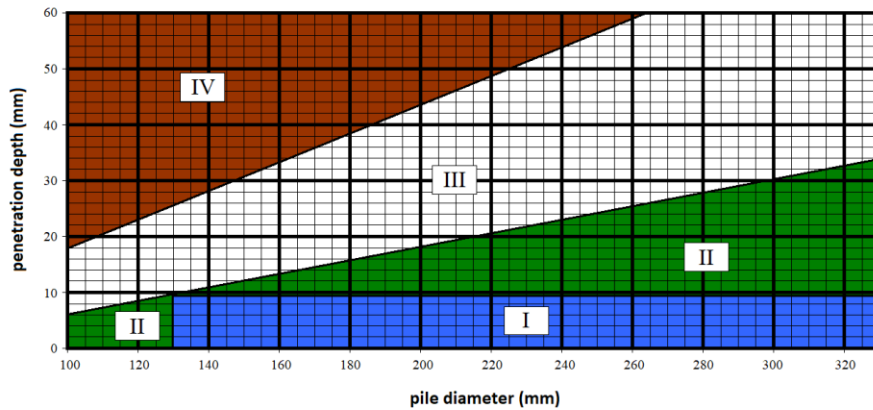


figure 3-14: Decision scheme for the need of sampling (NEN 8707 fig. 2, 2018)

In this diagram, four different regions can be distinguished:

- Region I – With the combination of the diameter and the penetration depth it can be concluded that the decay does not influence the structural integrity. Retrieving wood samples from the foundation parts is not necessary.
- Region II – The foundation parts are slightly affected. The degree of degradation is limited so it has no detrimental effects on the strength of the element. Samples are required only to investigate the cause of the degradation and the development of the degradation rate over time.
- Region III – Retrieving samples from foundation parts is necessary to get sufficient amount of data for determination of the actual strength of the element.
- Region IV – The pile is severely degraded in relation to the pile diameter where it already can be concluded that the actual strength of the foundation pile is insufficient. A wood sample in these situations is required only when the cause of degradation has to be found.

Sample investigations in a laboratory are performed to find out the timber species, type of degradation, severity of degradation along the specimen length, and additional parameters like the density and the moisture content. The same classes as given in *table 3-7* are used to classify the severity by biological degradation via a microscope. Additionally, the residual timber strength can be estimated with the help of *equation (3.2)*.

With above steps, a good review of the structural condition can be given in the form of a report. For a more detailed analysis, additional calculations can be made with the inclusion of certain calculation rules based on the results of penetrometer tests. Those mathematical expressions for both foundation piles and horizontal oriented elements are given in section '4.5 Material resistance'.

“A quay wall structure is subjected to several types of loads. They are introduced at the retaining wall, floor elements, and pile cap beams and transferred via the foundation piles to the subsoil. Each element has to resist those forces by their own material resistance where foundation piles are also accompanied by geotechnical resistance emerging from the soil–structure interaction. The load values for every possible failure mechanism must be smaller than the resistances to ensure structural integrity.”

Structural quay wall design

Many historic quay wall structures are still in service despite the ongoing degradation of structural elements. The overall strength and stability depend on the resistance factor delivered by the soil–structure interaction and the load factor in the form of load combinations acting on the quay wall. A quay wall element is loaded both in horizontal and vertical directions, so a lot of load transfer mechanisms between the foundation elements can be distinguished.

In this chapter, the various design rules are presented for the structural assessment of an existing quay wall structure according to the current building codes. In general, the current design rules are proposed for newly built structures where the structural elements are in perfect synergy with each other. The rules do not allow strains in the plastic regime, so only elastic strains are allowed that do not result in permanent deformations. Fortunately, a major part of the quay wall assessment follows more or less elastic theories and those are presented in the following paragraphs.

A quay wall structure can fail in various ways. The accompanying failure mechanisms are presented in paragraph ‘4.1 Failure mechanisms’. Structural failure must be avoided at almost all costs, so structural design is based nowadays on the calculation of load and resistance values with partial factors as described in paragraph ‘4.2 Design and characteristic values’. In paragraph ‘4.3 Loads on the structure’, the set of possible quay wall loads is given. The resistance part can be split up into geotechnical and material resistance. The former is denoted in paragraph ‘4.4 Geotechnical loads and resistances’ where the latter is outlined in paragraph ‘4.5 Material resistance’.

4.1 FAILURE MECHANISMS

There are many conceivable ways possible where a structure fails and loses its intended functions. The moment of failure depends on the acting loads on a structure and the resistance of the structural elements. For each possible failure mechanism, a limit state check can be written where the load factor may not be higher than the resistance factor. For structural designs, the limit state factors always follow a linear relation.

$$Z = R - S \quad 4.1$$

Failure occurs when the limit state gets below zero, so:

$$R < S \quad 4.2$$

Losing the overview of all potential structural dangers can be prevented by the assignment of each mechanism in a certain category. In the Eurocode standards, the following classification system is proposed:

- GEO (geotechnical failure): failure or very large deformations in the subsoil where the soil strength delivers a significant force to the total resistance (bearing strength of foundations and retaining walls, soil failure and structures loaded by soil forces).
- STR (structural failure): internal failure or excessive deformations of the structure or individual elements; examples are shallow foundations, deep foundations or soil retaining walls. The strength of the structural elements has a large contribution to the resistance.
- EQU (loss of equilibrium): movement of the structure or subsoil considered as a stiff entity. The strength of the materials and the subsoil do not have a noteworthy contribution to the resistance.
- UPL (uplifting): loss of equilibrium of the structure or the subsoil as a result of uplift by water pressure or other vertical loads (uplift structure, failure of tension elements).
- HYD (hydraulic failure): hydraulic heave, internal erosion, and erosion by centred groundwater flow in the subsoil as the result of hydraulic gradients (piping, bursting of the topsoil).

For each type of foundation an overview can be made of all possible failure mechanisms that could occur. In *figure 4-1*, eight different ways of partial or full collapse are depicted for this type of structure.

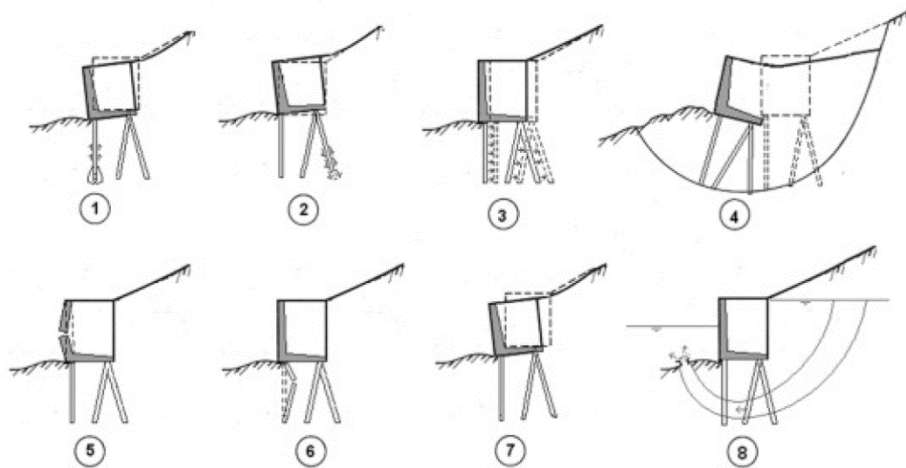


figure 4-1: failure mechanisms of a quay wall on a pile foundation (De Gijt et al., 2014)

Each failure mechanism can be subdivided into the above given limit states.

1. Exceedance of the vertical bearing strength (GEO)
2. Exceedance of the vertical tensile strength (GEO)
 - single pile
 - pile group with inclusion of the clump criterion
3. Soil failure by a horizontal load on a pile foundation (GEO)
4. Exceedance of the overall stability (GEO)
5. Structural failure of the retaining wall (STR)
6. Structural failure of the piles by compression, tension, buckling, and shearing (STR)
7. Structural failure by excessive displacement of the foundation structure (STR)
8. Failure by internal erosion (piping) (HYD)

Only mechanisms directly related to the research question will be treated in the following paragraphs. Important cases are 1, 2, 4, 6, and 7. The other ones (3, 5, and 8) are not considered any further because they are not directly influenced by the degradation of wooden foundation elements.

Each element in a quay wall structure can be assigned to a one or more failure mechanisms. Geotechnical failure is solely relatable to foundation piles because they are the only elements in direct contact with the soil. The geotechnical resistance of a foundation pile is treated in paragraph '4.4 Geotechnical loads and resistances'. Horizontal orientated foundation elements like pile cap beams, floor elements, and cross-beams are not influenced by geotechnical processes, so their resistances are exclusively determined by material parameters. The resistance against structural failure of all timber components is described in paragraph '4.5 Material resistance'.

Elements like grating beams and soil retaining screens are usually also composed of timber, but they are not considered any further in this report. According to Sas (2007), grating beams were used to align the masonry wall in horizontal direction during the construction stage, so the contribution of these elements to the structural behaviour is very marginal. A soil retaining screen is also not a structural element because its main function is the prevention of soil erosion behind the structure.

Before going into detail about the loads on the structures and the resistances of the foundation elements, more attention is given first to how the design and characteristic values are calculated for the different limit states.

4.2 DESIGN AND CHARACTERISTIC VALUES

To perform a structural assessment, several checks have to be performed to verify if the structure is able to resist the loads acting on the structure. As already stated in the previous paragraph '4.1 Failure mechanisms', each check can be written in the form of a generic limit state function given as *equation (4.1)*. The more specified input follows then from one of the five classes (STR, GEO, EQU, UPL, and HYD). Each variable factor in the limit state function has a mean value and a standard deviation. The standard deviation defines the spread or uncertainty of a factor around a mean value. The characteristic values of the resistance and load factors are dependent on these parameters.

$$\begin{cases} R_k = \mu_R + k_R \times \sigma_R \\ S_k = \mu_S + k_S \times \sigma_S \end{cases} \quad 4.3$$

The load factor comprises all kinds of external loads and actions caused inside a structure. Examples of resistance factors are material properties, stiffness characteristics, or geometrical properties. In the material sections of the Eurocode, a material property of a structural element is defined as the 5-quantile of a strength parameter where a stiffness parameter corresponds to a mean value. In these expressions, also a factor is included that depends on the effect of the load on the structure. When the factor is positive, the action of the load is unfavourable for the structure. In other words, the load has an unstable effect on the structure. The opposite result is reached for a negative value of the effect factor. In this case, the load has a favourable effect on the total resistance, so it stabilizes the structure. A simple representation of the load and resistance factors with their descriptive parameters is given in *figure 4-2*.

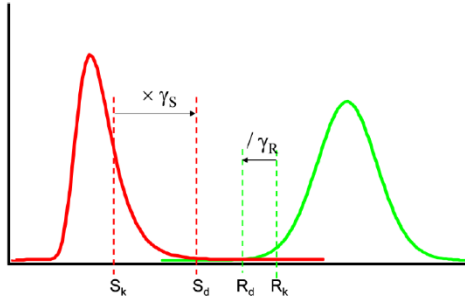


figure 4-2: load (S) and resistance (R) with their mean values and deviation from the mean (Jonkman et al., 2017)

For several load types and structures, probabilistic calculations were made in the past that resulted in predefined partial safety factors. To limit the computation time for various kinds of structures, predefined partial factors can be used instead of making an extensive probabilistic computation each time a structure is assessed. The representative values are translated to design values with the following mathematical operations:

$$\begin{cases} R_d = \frac{R_k}{\gamma_R} \\ S_d = \gamma_S \times S_k \end{cases} \quad 4.4$$

Substitution of *equation (4.4)* into *equation (4.2)* leads to a generalised verification of a resistance factor with its counteracting load part:

$$\frac{R_k}{\gamma_R} < \gamma_S \times S_k \quad 4.5$$

The above limit state function is used for a calculation in the ultimate limit state (ULS). ULS requirements are related to extreme events that causes loss of bearing strength of a structure. The reduction could have several reasons such as material fracture, excessive displacements, loss of equilibrium or geotechnical failure. They are connected to the more specific failure mechanisms as were treated already in paragraph '4.1 Failure mechanisms'.

Another important limit state is acquired from *equation (4.5)* by setting the partial factors equal to one or using *equation (4.2)*.

$$R_k < S_k \quad 4.6$$

This is the serviceability limit state (SLS) and is used to checks the structural responses to loads appearing on a daily basis. They are needed to prevent hindrance and feelings of discomfort by for instance structural vibrations or unaesthetic appearance in the environment in the form of cracks. Such events do not threaten the structural behaviour but are still not acceptable on behalf of user's preferences.

When a quay wall structure is loaded, responses follow from the foundation structure and the surrounding subsoil. A structural assessment in ULS is then accompanied by design load values and resistance factors in the form of geotechnical (GEO) and strength (STR) parameters according to *equation (4.4)*. All three contributions are treated separately in paragraph '4.2.1 Partial load factors', paragraph '4.2.2 Geotechnical resistance', and paragraph '4.2.3 Material resistance'. For verifications based on SLS, no design values are needed.

4.2.1 PARTIAL LOAD FACTORS

The magnitude of the partial factors in ULS is defined by a load group for the load factors and a consequence class for the resistance factors. For quay wall structures built around the 19th century, the following decisions are made:

- A verification of a pile foundation on normal stresses and the geotechnical pile bearing strength is classified as load group B (NEN-EN 1990 (NB) par. A.2.3.1 (5), 2011).
- The consequence classes (CC1, CC2, CC3) indicate the degree of social disruption at the moment of quay wall failure. For inner-city quay walls with a retaining height smaller than 5 m, consequence class 1 is recommended (CUR 166, 2014). This suggestion seems acceptable because failure of a quay wall section accounts for a limited loss of life probability.

In addition, consequence class 1 is split into the subparts CC1a and CC1b with a difference in the disapproval period. When the demolition or renovation of a quay wall is planned within one year, CC1a is used. In all other cases CC1b has to be applied. In this report only non-depreciated quay walls are treated and therefore consequence class CC1b is adopted. The classification comprises a set of partial factors as can be seen in *table 4-1*.

symbol	value ^a
$\gamma_{G,dst}$ [-]	1.00
$\gamma_{G,stab}$ [-]	1.00
$\gamma_{Q,dst}$ [-]	1.10
$\gamma_{Q,stab}$ [-]	0
^a renovation, construction before 2003 ($\beta = 2.8$)	

table 4-1: partial load factors for soil retaining structures (NEN 8707 table N.1, 2018)

Above values can be applied in *equation (4.4)* to obtain the design value of the load. The only exceptions are the design values for soil and water pressures because they are determined in a different way. The magnitude of those pressures depends on water and ground levels with respect to a certain reference system, so multiplication with a factor does not result in representative answers. There are two methods available to obtain the design of the soil and water pressures. One is by the addition of a certain supplement and the other by the multiplication of the standard deviation with a partial geotechnical factor. In *table 4-2*, values are given for both options together with the calculation of the design value.

parameter	Δa and γ for $X_{k,a}$		X_d [-]
	γ_{GEO} [-]	Δa [m]	
retaining height	1.80	0.24	$\max\{\mu_s + \gamma \times \sigma_s; \mu_s + \Delta a\}$
(ground)water level at lower side	1.45	0.17	$\max\{\mu_s + \gamma \times \sigma_s; \mu_s + \Delta a\}$
(ground)water level at higher side	0.74	0.05	$\max\{\mu_s + \gamma \times \sigma_s; \mu_s + \Delta a\}$
^a renovation, construction before 2003 ($\beta = 2.8$)			

table 4-2: factors for the calculation of soil retaining structures (NEN 8707 table A.1, 2018)

The standard deviation is only known when a full probabilistic calculation is performed which is not the case in this report. Therefore, the water level is then corrected by a supplement value. In the table of the Eurocode, also a minimum bound value is given for the lower water level. This level is governing

only when the turning stability or internal stresses of an element have to be verified. Both checks are superfluous to answer the research question, so the minimum value is omitted here.

4.2.2 GEOTECHNICAL RESISTANCE

Loads on the superstructure are transferred to the subsoil via soil–structure interaction. Several checks must be performed with a variety of geotechnical parameters. Two different parameters can be distinguished. Resistance factors for the pile bearing strength and load factors for soil pressures. The design values of the resistance factors and the load factors are determined with *equation (4.4)*. The pile bearing capacity will be derived from soil probing diagrams. The corresponding resistance factors for the calculation of the pile bearing capacity are given in *table 4-3*. Load factors from the subsoil are shown in *table 4-4*.

symbol	value
γ_b [–]	1.20
γ_{nsf} [–]	var. ^a
γ_s [–]	1.20
γ_{st} [–]	1.35
γ_t [–]	1.20
^a $\gamma_{nsf} = 1.0$ for single piles, $\gamma_{nsf} = 1.2$ for pile groups	

table 4-3: geotechnical parameters for driven foundation piles according to CC1 (NEN–EN 1997–1 (NB) table A.6 and par. 7.3.2.2 (b), 2019)

symbol	value [–] ^a
$\gamma_{\psi'}$ [–]	1.15
$\gamma_{c'}$ [–]	1.15
γ_{γ} [–]	1.00
^a renovation, construction before 2003 ($\beta = 2.8$)	

table 4-4: geotechnical parameters for a soil retaining structure according to CC1 (NEN 8707 table N.2, 2018)

The partial factor for effective cohesion is applied only in the case when cohesive soils have an unfavourable effect on the structure, otherwise it is equal to 1.00.

4.2.3 MATERIAL RESISTANCE

Timber elements are composed of a natural material, so they behave differently compared to fabricated materials like steel or concrete. As stated in paragraph ‘3.2.2 Mechanical degradation’, the strength and stiffness properties of timber are influenced by creep deformation and the humidity level of the surroundings. Both factors are incorporated in a modification factor (NEN–EN 1995–1–1 par. 2.4.1 (1), 2011).

$$R_d = k_{mod} \times \frac{R_k}{\gamma_M} \quad 4.7$$

Values for this modification factor are given in *table 4-5*.

climate class	k_{mod} [-]				
	permanent	long	medium	short	very short
1	0.60	0.70	0.80	0.90	1.10
2	0.60	0.70	0.80	0.90	1.10
3	0.50	0.55	0.65	0.70	0.90

table 4-5: different values for the modification factor of sawn timber (NEN-EN 1995-1-1 table 3.1, 2011)

Furthermore, a material factor is included. For sawn timber, the following value is proposed (NEN-EN 1995-1-1 table 2.3, 2011).

$$\gamma_M = 1.3$$

When the timber resistance is assessed, both the duration and climate class are needed. In *table 4-6*, magnitudes of cumulative durations of characteristic loads are given with specific examples.

load duration class	cumulative load duration	load examples
permanent	longer than 10 years	self-weight
long	6 months – 10 years	storage
medium	1 week – 6 months	imposed floor loads
short	less than 1 week	snow, wind
very short	–	exceptional loads

table 4-6: examples of load duration classes (NEN-EN 1995-1-1 (NB) table 2.1 and table 2.2, 2013)

The decision for the climate class is based on the moisture content in the timber in relation to temperature and the relative humidity of the environment.

- climate class 1: moisture content corresponding to a temperature of 20 °C of the surrounding air which is only a few weeks higher than 65% per year. For most coniferous timber species (Dutch: naaldhout) the mean value of the moisture content will not be higher than 12%.
- climate class 2: moisture content corresponding to a temperature of 20 °C of the surrounding air which is only a few weeks higher than 85% per year. For most coniferous timber species, the mean value of the moisture content will not be higher than 20%.
- climate class 3: climate conditions that results in a higher moisture content than climate class 2.

A well-reasoned decision has to be made for the climate and the load duration class because the modification factor from *table 4-5* has a large influence on the strength and stiffness values for timber elements.

4.3 LOADS ON THE STRUCTURE

When you think for a while, numerous cases are conceivable for external factors that could endanger the structural integrity of a quay wall. Most obvious examples are soil pressures, mooring forces, and vehicle loads. Less common but not impossible events are the occurrence of ship collisions, explosions, earthquakes, and many others. Especially ship collisions are certainly possible during the structural lifetime of a quay wall, but it is still an exceptional load case. The possible consequences of the impact of a ship with a quay wall are considerably large such that unavoidable restoration measures are needed immediately after the occurrence of such event. To limit the number of possible load combinations, only loads are selected with a regular presence and a non-negligible magnitude. The following external loads are used for the assessment of the foundation structure:

- self-weight of quay wall elements (paragraph ‘4.3.1 Self-weight of the quay wall elements’)
- soil pressures of the backfill (paragraph ‘4.3.2 Soil pressures at the backfill’)
- surface water pressure (paragraph ‘4.3.3 Surface water pressure’)
- terrain loads (paragraph ‘4.3.4 Terrain loads’)
- mooring forces (paragraph ‘4.3.5 Mooring forces’)
- tree loads (paragraph ‘4.3.6 Tree loads’)

These components are treated below in the following paragraphs. All load cases can be classified as variable or permanent loads. The first type shows up on a regular basis where the static type is present during the entire lifetime of a structure. Only characteristic values are presented in above paragraphs which are translated to design values in paragraph ‘4.2 Design and characteristic values’. Load combinations are needed due to the fact that not all loads are present simultaneously on the structure. Those are presented in paragraph ‘4.3.7 Load combinations’.

4.3.1 SELF-WEIGHT QUAY WALL ELEMENTS

Each quay element itself contributes for a certain part to the total load. These gravitational forces are by definition no external loads, but they definitely contribute to the total load on the system. The self-weight of a structural component is defined by the specific weight of the material and its dimensions.

$$\begin{cases} F_g = \gamma_g \times V \\ q_g = \gamma_g \times A \end{cases} \quad 4.8$$

In *table 4-7*, an overview is given of the specific weight of materials that could be present inside a historic quay wall.

material	γ [kN/m ³]	reference
brick (fired clay)	16.0	Daily Civil, 2018
rubble stone (not specified)	28.0	NEN-EN 1991-1-1 table A.2, 2019
wood (strength class C24)	4.2	NEN-EN 1991-1-1 table A.3, 2019
concrete (reinforced)	25.0	NEN-EN 1991-1-1 table A.1, 2019

table 4-7: specific weight of commonly used quay wall materials

A retaining wall is often equipped with a coping composed of a deviant material. It does not have a large influence on the total self-weight, so the retaining wall is assumed to be homogeneous in terms of self-weight.

4.3.2 SOIL PRESSURES AT THE BACKFILL

The soil package located behind the retaining wall exerts both horizontal and vertical pressures onto the structure. A horizontal component is subjected to the retaining wall and a vertical contribution is resisted by the horizontally oriented foundation elements. The total vertical soil stress in a uniform soil follows from the dry or saturated soil weight, the phreatic surface, and the elevation of interest.

$$\begin{cases} \sigma_v z = \gamma_{dry} \times z & \text{when } z_{gw} \geq z \\ \sigma_v z = \gamma_{sat} \times z & \text{when } z_{gw} = z_{gr} \end{cases} \quad 4.9$$

At the phreatic surface, the groundwater pressure is equal to the atmospheric pressure. The exact groundwater level is often not known, so it has to be corrected with a supplement factor according to *table 4-2*. In the Netherlands, the ground and groundwater elevations are measured from a certain reference height called Amsterdam Ordnance Datum with its Dutch abbreviation NAP (Normaal Amsterdams Peil). In the case of a stratified soil or when the groundwater level is not equal to the

ground level, above equations are not valid. More sophisticated expressions are required in these situations that are elaborated further in appendix 'A.1 Soil pressures'.

The hydrostatic pressure caused by the groundwater level varies linearly over the soil depth by the specific weight of water with its reference at the phreatic surface level.

$$p_z = \gamma_w \times (z - z_{gw}) \quad 4.10$$

This level is equal to the groundwater level when no capillary rise is considered. It appears usually in very fine soils by suction forces originating from surface tension between particles. This additional pressure is neglected in this report because it has in almost all cases a nonsignificant influence on the pressure distribution.

The effective soil pressure is obtained by the extraction of the groundwater pressure from the vertical soil pressure.

$$\sigma'_v z = \sigma_v z - p_z \quad 4.11$$

Above expressions are used for the translation of vertical soil stresses to horizontal stresses. The generic method for the determination of lateral soil stresses on structures was invented by Rankine (1857). He based his theory on the failure criterion by Mohr–Coulomb (Verruijt, 2012). This theory describes the shear stress response of brittle materials loaded by normal stresses. It can be visualized by Mohr's circle inside the failure envelope of Coulomb. Rankine found the following two expressions for soils including a relation between the lateral earth pressure and the vertical pressure in the effective state.

$$\begin{cases} \sigma'_h z = K_a \times \sigma'_v z - 2c' \times \sqrt{K_a} & \text{where } K_a = \frac{1 - \sin \varphi'}{1 + \sin \varphi'} \\ \sigma'_h z = K_p \times \sigma'_v z + 2c' \times \sqrt{K_p} & \text{where } K_p = \frac{1 + \sin \varphi'}{1 - \sin \varphi'} \end{cases} \quad 4.12$$

The active and passive soil pressure coefficients are related to the movement of the structure and the direction of the horizontal soil pressure. When the structure is pushed away by the soil, the active soil pressure coefficient is used. For a structural translation opposed to the soil stress, the passive soil pressure coefficient has to be applied. In reality, the actual coefficient is somewhere in between those extreme cases. For a usual value of the internal friction angle, the actual coefficient is in between the following bounds:

$$\frac{1}{3} < K < 3 \quad \text{when } \varphi' = 30^\circ$$

A difference of a factor nine is found for this specific friction angle. Verruijt (2012) says that large uncertainties are typical for most soil parameters. It is recommended to use soil pressure coefficients with great caution to prevent large mistakes in the magnitudes of the horizontal soil pressures.

Another soil state was distinguished by the Hungarian Engineer Jáký (1936). When the structure doesn't move at all under influence of geotechnical loads, a neutral soil condition is obtained.

$$K_0 = 1 - \sin \varphi' \quad 4.13$$

The neutral soil pressure coefficient ranges from 0.35 for densely compacted sands to 0.75 for loose peaty soils. The possible values for the lateral soil coefficient are schematised in figure 4-3.

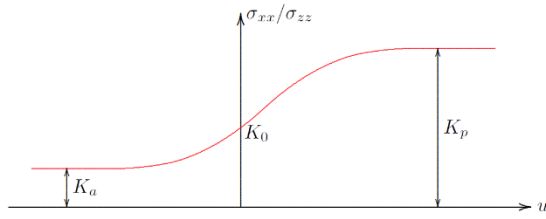


figure 4-3: lateral soil pressure coefficient as a function of the structural displacement (Verruijt, 2012)

In the Eurocode specific requirements are mentioned for the structural displacements and the correct choice for the soil coefficient. An overview is given in table 4-8 of boundary values related to structural translations and rotations.

active soil pressure	
translation ^a [m]	rotation [-]
0.001×H _{wall}	arctan(0.002) ^b
	arctan(0.005) ^c
^a displacements with the exclusion of rotations ^b rotation around a fixed point at the bottom ^c rotation around a fixed point at the top	

table 4-8: required displacement for active or passive soil pressure (NEN-EN 1997-1 (NB) table 9.c, 2019)

Some rigid geotechnical structures do not fulfil any of the above given requirements because they are more or less immovable. For these structures, the use of a neutral soil pressure coefficient is recommended in the calculation of the horizontal pressures.

To translate these requirements to a historic quay wall, it is important to figure out how the structure displaces. During the entire lifetime, the structural movement in the direction of the surface water is expected due to a higher value of the soil pressure than the hydrostatic surface water pressure on the long run. Given the very low values for achieving an active soil pressure state, it is expected that all quay wall structures satisfy this soil condition.

The total horizontal soil pressure on a structural element is finally calculated by the addition of the groundwater pressure to the effective soil pressure.

$$\sigma_h z = \sigma'_h z + p z \quad 4.14$$

4.3.3 SURFACE WATER PRESSURE

The hydraulic pressure from the outer surface water is a variable load factor where its magnitude is defined by the water level and the specific weight of water. The horizontal hydrostatic water pressure has a triangular shape over the water height.

$$\sigma_w z = \gamma_w \times z \quad 4.15$$

Track records of the water level over a long period are needed to determine different water tables where each has its own use. The water level variation is usually covered with two different water tables when structural calculations are made. These are the mean high water level (MHW) and the mean low water level (MLW). Like the elevations of the groundwater and soil levels in paragraph '4.3.2 Soil pressures at the backfill', the water level in the Netherlands is defined by the NAP-level. To apply the water pressure in structural calculations, a correction factor of table 4-2 is needed.

4.3.4 TERRAIN LOADS

A quay wall has to resist several load cases at surface level adjacent to the structure. The terrain load usually consists of traffic loads when the quay wall is accommodated by a road. For quay walls, a uniformly distributed terrain load is recommended over the entire structural length with a width of 20 m next to the structural element (NEN-EN 1997-1 (NB) par. 2.4.2 (c), 2019).

$$Q_{sur} \geq 10 \text{ kN/m}^2$$

The uniform load has a lower bound because it is used only in general cases where the actual terrain load magnitude is uncertain (CUR 166, 2014). In all other cases, the traffic is usually represented by load models. The simulation is usually done by the placement of a so-called tandem system on each driving lane. The magnitude of each system decreases when it is further away from the structure, so the most unfavourable loading situation is at the closest distance from the quay wall. The two models, derived from a configuration for traffic on bridges, turns trucks and passenger cars into concentrated and distributed loads (De Gijt et al., 2014). Exceptional convoy is not included in both models because this particular class is not allowed on the road without restrictions. In addition, dynamic load effects like the influence of acceleration and deceleration by vehicles are also excluded.

In figure 4-4, a top and cross-sectional view of traffic model 1 is depicted. The concentrated wheel pressures at a small contact area of $0.4 \times 0.4 \text{ m}^2$ are in this schematisation converted to single point loads.

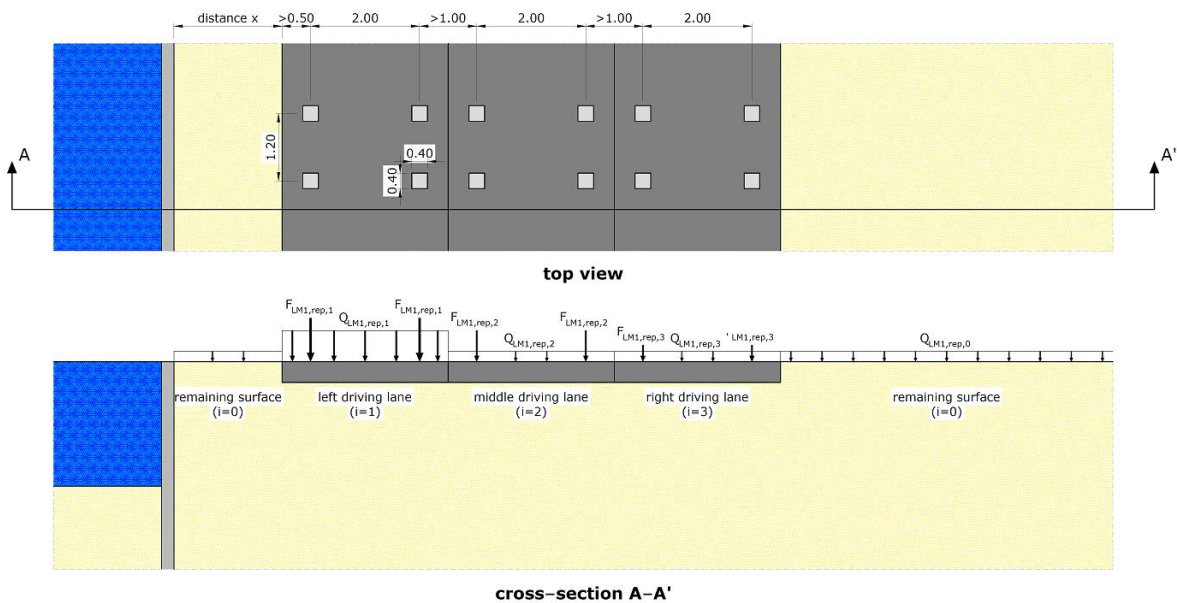


figure 4-4: schematisation of load model 1 (De Gijt et al., 2014)

In this model, both global and local load effects are included because it represents a regular arrangement of traffic along a quay wall. The image is accompanied by representative values in table 4-9 of the several traffic loads.

position	$F_{LM1,rep,i}$ [kN]	$Q_{LM1,rep,i}$ [kN/m ²]
first driving lane (i = 1)	150	9.0
second driving lane (i = 2)	100	2.5
third driving lane (i = 3)	50	2.5
other driving lanes (i > 3)	0	2.5
remaining surface (i = 0)	0	2.5

table 4-9: load values for the model presented above (De Gijt et al., 2014)

The representative values given above can be translated to characteristic values with a certain correction factor. It takes the number of trucks per traffic lane on a yearly basis into account because this specific group has the largest influence on the structural integrity of a quay wall.

$$\begin{cases} F_{LM1,i} = \alpha_Q \times F_{LM1,rep,i} \\ Q_{LM1,i} = \alpha_Q \times Q_{LM1,rep,i} \end{cases} \quad 4.16$$

Indicative values for the correction factor are given in table 4-10.

number of trucks per traffic lane per year [-]	α_Q [-]
> 2000.000	1.00
200.000	0.90
20.000	0.80
2.000	0.70
200	0.60

table 4-10: reduction factor for the number of truck passages (De Gijt et al., 2014)

A second load model consists of two wheel loads that stands for a single axle of a very heavy vehicle. The governing situation appears when one of the wheels is placed as close as possible to the structure. This model is depicted in figure 4-5. Also the prescribed contact area of 0.35×0.65 m² in this model is concentrated to one point.

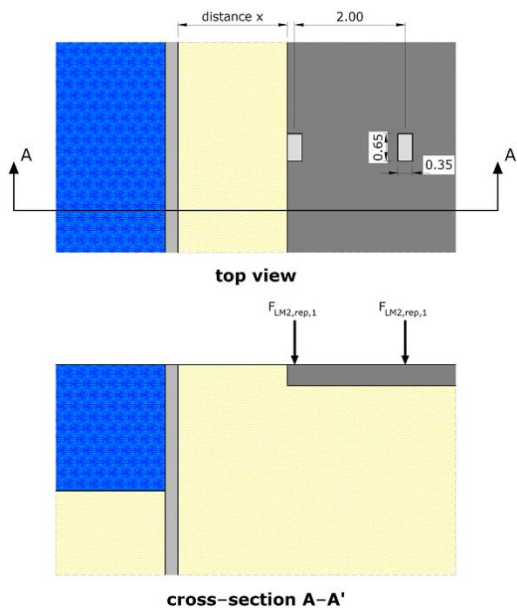


figure 4-5: schematisation of load model 2 (De Gijt et al., 2014)

This concept is used for the examination of local effects on rigid structural elements. The following magnitude of the load is used for the model:

$$F_{LM2,rep,1} = 200 \text{ kN}$$

The value in load model 2 can also be obtained by an expression similar to *equation (4.16)* because the same values of the truck correction factor in *table 4-10* can be used.

$$F_{LM2,i} = \alpha_Q \times F_{LM2,rep,i} \quad 4.17$$

Each load case depicted above has its own influence on the stress increase in the subsoil. A part of the load is uniformly distributed over the entire area next to the quay wall. This load type can be imported into Rankine's expressions to obtain the resulting horizontal and vertical soil stresses on the retaining wall and the foundation elements. The elaboration on this subject is given in appendix 'A.2 Load spreading models'. The soil in these models is assumed to behave as an elastic medium, so the influence of the surface load can be determined by the superposition principle. Therefore, the contribution of each load type is defined separately and summed up to obtain the total response.

4.3.5 MOORING FORCES

Not only variable loads from the landside act on the quay wall, but also ships could be part of the structural endangers. From paragraph '4.3 Loads on the structure', it was decided to omit exceptional circumstances from the set of load cases, so ship impacts are not considered. Mooring forces are then the only ship forces remaining active, provided that bollards or other mooring facilities are present on the structure. Otherwise, a ship is not taking part into the set of structural loads. Ship induced waves are in general too small to endanger the structure (De Gijt et al., 2014). Hence, they are not treated any further in this report.

The magnitude of the forces in the mooring ropes, also called hawser forces, depends on the movements of the ship, the mass of the ship, and the stiffness of the mooring cables (Molenaar & Voorendt, 2017). Several vessel sizes are found in the Dutch inner waters, so the bollards on a quay wall can be loaded by mooring forces of different values. The general guideline for waterways in the Netherlands recommends different numbers for the mooring force per barge size. Those values are listed in *table 4-11*.

ship sizes	F _{mr} [kN]
recreational	40
CEMT I	150
CEMT II	150
CEMT III	200
CEMT IV	200
CEMT V	250
CEMT VIa	300
CEMT VIb	350

table 4-11: mooring forces of several vessels for inland shipping (Rijkswaterstaat, 2020)

This force magnitude must be resisted both in parallel and perpendicular quay wall direction.

4.3.6 TREE LOADS

Many quay wall structures in the inner-cities are accompanied by a lawn of trees. The magnitude of the load generated by a tree can be quite significant, especially when the element is in close proximity to

the structure. Nowadays requirements are formed to prevent unnecessary large load influences on a structural object, so a tree is placed on a safe distance. The influence of a tree on a structure is split up into the following contributions (De Gijt et al., 2014):

- self-weight of the tree
- expansion load by the root system of the tree
- wind load on the crown transferred to the subsoil
- falling down of a tree

Several parameters are needed to treat a tree as a loading object. In *table 4-12*, a few specifications are given for common tree species along an inner-city quay wall.

tree species	H_{tree} [m]	d_{st} [m]	d_{cr} [m]	H_{cr} [m]	$F_{g,\text{tree}}$ [kN]
Oak	15	0.4	10	10	20
Tilia	15	0.4	10	10	15
Poplar	20	0.4	10	15	15

table 4-12: important parameters of tree species for structural calculations (De Gijt et al., 2014)

The most evident quantity to the total load share is the static weight defined by the volume of the wood material and its specific weight. It can be treated as a point load on surface level because the diameter of the tree stem is quite small relative to the total weight.

Another aspect is the influence of the root system to an adjacent structure. When a tree is located near a quay wall, the part of the root system at the quay wall side is blocked by this rigid boundary. The tree anchors itself in every possible direction and also tries to push through a vertical element. Many masonry walls are not able to resist root forces so often situations show up where the structure is pushed away in outward direction. An example of this phenomenon is captured in *figure 4-6*.



figure 4-6: deformed masonry structure by an adjacent tree (De Gijt et al., 2014)

These kind of deformations only occur very locally, so in most cases the masonry structure is damaged without further problems to the overall stability. The strength of the retaining wall is not of importance in this report. Hence, forces with its origin from the root system are not considered here.

An important function of the stability provided by the root system is the resistance against wind gusts around the crown of the tree. The magnitude of the wind load is characterized by the size, foliage, and crown height of the tree. There are no calculation rules provided in the European standards for wind induced forces on trees and therefore another approach has to be followed. Alternatively, the standard form of the drag equation of an object in a fully enclosing fluid can be used.

$$F_D = \frac{1}{2} \times C_D \times \rho_{air} \times A_{ref} \times u_{wind}^2 \quad 4.18$$

The first factor is the nondimensional drag coefficient. It is defined by the resistance of an object in an air flow and is often determined by practical experiments. For some tree species, this constant was obtained by wind tunnel tests. Analysis of the obtained data showed that the drag force is not proportional to the square of the wind speed. According to Moore et al. (2018), the value of the exponent lies in between 1.24 and 1.41 instead of 2. When a stream of wind goes around a tree, the branches move in the direction of the wind flow. The frontal area is then decreased compared to the situation when there is no wind. From several experiments conducted by Vollsinger et al. (2005), it was found that the frontal surface of the crown is decreased by 20 to 54% at a wind speed of 20 m/s depending on the tree species. The results of these experiments are depicted below in figure 4-7.

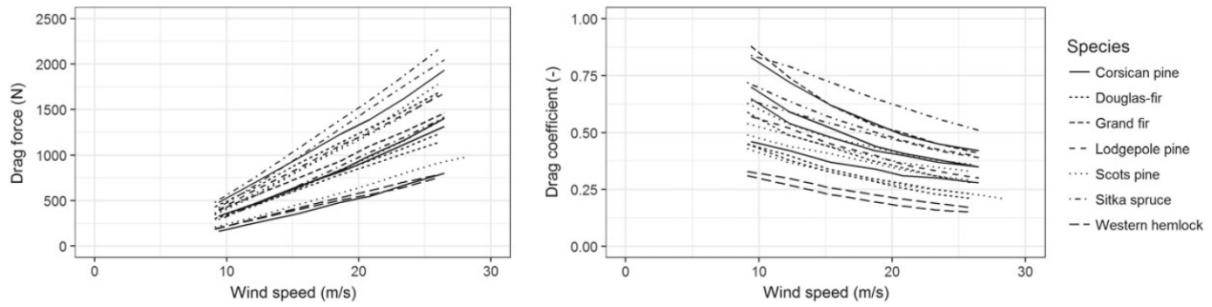


figure 4-7: results of wind tunnel test on conifer trees with average dimensions (diameter at breast height = 10–15 cm, tree height = 6–8 m) (Moore et al., 2018)

As already mentioned, the drag coefficient decreases for an increasing wind speed due to the alignment of branches in the direction of the wind flow. The resulting load increases, but it does not follow a parabolic relation as illustrated in the left graph. Based on earlier wind tunnel studies, Vogel (1994) composed a proportionality relation between the drag force and the wind speed.

$$F_D \propto u_{wind}^{1.35} \quad 4.19$$

At the moment of writing, no closed relations are known for the total wind load on a tree for a given wind speed. There are too many variables involved with an unknown significance to the total wind force. The sample results in the left graph of figure 4-7 also shows quite small force magnitudes. The influence of wind load transfer becomes even smaller due to the spreading in the subsoil. From this perception, it can be concluded that the influence of horizontal induced tree loads is negligible compared to other load magnitudes.

Another aspect with structural consequences for a retaining wall is failure of a tree. Extremely high wind speeds could result in the collapse of a tree leaving a large crater behind. The missing amount of soil endangers the stability of an adjacent structure, so immediate action is required to prevent irrecoverable damage. Tree toppling is an exceptional event, so it is not classified as a regularly occurring load case. As mentioned in paragraph '4.3 Loads on the structure', tree failure is irrelevant to provide an answer to the research question.

From all above considerations, only the self-weight of the tree cannot be ruled out as a load on a nearby structure, so it is included in structural calculations further on.

4.3.7 LOAD COMBINATIONS

Not all variable loads described in the preceding paragraphs will be active at the same moment or with the same magnitude. Each type of load can trigger a different failure mechanism and therefore several load combinations can be made. The possible combinations depends on the possible failure mechanisms as treated in paragraph '4.1 Failure mechanisms'. In the Eurocode standards, two generic functions of the load effects are given for the geotechnical and structural limit states (GEO and STR) (NEN-EN 1990 eq. 6.10a & 6.10b, 2011).

$$\begin{cases} E_d = \sum_{i \geq 1} \gamma_{G,i} \times G_{k,i} + \gamma_P \times P + \gamma_{Q,1} \times \psi_{0,1} \times Q_{k,1} + \sum_{i > 1} \gamma_{Q,i} \times \psi_{0,i} \times Q_{k,i} \\ E_d = \sum_{i \geq 1} \xi_i \times \gamma_{G,i} \times G_{k,i} + \gamma_P \times P + \gamma_{Q,1} \times Q_{k,1} + \sum_{i > 1} \gamma_{Q,i} \times \psi_{0,i} \times Q_{k,i} \end{cases} \quad 4.20$$

In both equations, factors are combined with each other when they are present at a structure. The expression with the highest outcome is more unfavourable in structural perspective, so this load combination is governing. The load combination factor accounts for the probability of occurrence of two or more variable loads acting simultaneously. There are two variable components which are the mooring force and the traffic loads. The load combination factors for these two loads are given in table 4-13.

parameter	ψ_0 [-]	reference
F_{LMi} [kN]	0.8	NEN-EN 1990 (NB) table NB.9-A2.1, 2011)
Q_{LMi} [kN/m ²]	0.8	NEN-EN 1990 (NB) table NB.9-A2.1, 2011
F_{mr} [kN]	0.7	Departement Mobiliteit & Openbare Werken, 2018

table 4-13: Load combination factors for variable loads

Another constant in equation (4.20) is a reduction factor for the permanent load. It is valid when the variable is declared as the governing component. For geotechnical structures like a quay wall, the following value of is applied (NEN-EN 1997-1 (NB) table A.3, 2019):

$$\xi_j = 0.89$$

With the partial factors from table 4-1 and table 4-2, a number of load combinations for the load effects can be composed. To limit the total time required for the calculations, only load combinations related to the governing situations for the structural strength and stability are considered. The following three combinations are chosen as the most relevant ones to use in structural calculations:

1. Load combination 1: Maximum loading situation (global): high surface water level (MHW) + traffic model 1 (LM1) + mooring force

$$E_d = \gamma_{G,dst} \times (F_g + F_{g,tree} + F_{w,MHW} + \sigma_v + \sigma_h) + \gamma_{Q,dst} \times (F_{LM1,i} + Q_{LM1,i}) + \gamma_{Q,dst} \times \psi_{0,1} \times F_{mr} \quad 4.21$$

2. Load combination 2: Maximum loading situation (local): high surface water level (MHW) + traffic model 2 (LM2) + mooring force

$$E_d = \gamma_{G,dst} \times (F_g + F_{g,tree} + F_{w,MHW} + \sigma_v + \sigma_h) + \gamma_{Q,dst} \times F_{LM2,i} + \gamma_{Q,dst} \times \psi_{0,1} \times F_{mr} \quad 4.22$$

3. Load combination 3: Minimum loading situation: low surface water level (MHW)

$$E_d = \gamma_{G,dst} \times (F_g + F_{g,tree} + F_{w,LHW} + \sigma_v + \sigma_h) \quad 4.23$$

For calculation in the SLS-state (serviceability limit state), no partial factors are required. However, the same expressions for the load combinations can still be used by setting the partial factors to a value equal to 1.00.

4.4 GEOTECHNICAL LOADS AND RESISTANCES

The soil–structure interaction of the quay wall is entirely related to the foundation piles because they are the only elements in direct contact with the soil. The soil and pile responses depend on how the structure is excited by external forces. An axial force in downward direction results in pile contraction and settlement as described in paragraph ‘4.4.1 Piles loaded in compression’. The opposite effect is obtained when the pile is subjected to an upward force. As a result, the pile elongates and rises from the subsoil. Both reactions are expressed in paragraph ‘4.4.2 Piles loaded in tension’. Another pile response becomes visible when the pile is loaded in lateral direction. The soil system along the pile axis determines how the element behaves. Due to the complex soil–structure interaction, several different models with their possibilities and limitations are used given in paragraph ‘4.4.3 Piles loaded in lateral direction’ to obtain the pile deformation and internal stresses. The lateral loading can act simultaneously with a compressive or tensile force, so two combinations are distinguished. Occurring stresses are then found by the superposition of the stresses from individual loading cases (Bowles, 1997).

4.4.1 PILES LOADED IN COMPRESSION

The interaction between the pile and the soil results in several forces on the foundation pile. The timber piles driven into the ground are called displacement piles because the application causes soil displacement and soil densification around the pile area. An overview of the possible forces loaded by an axial compression load with a few pile characteristics is given in *figure 4-8*.

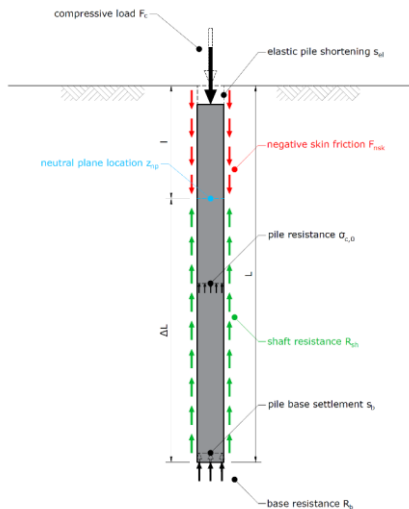


figure 4-8: pile forces on a displacement pile

The compression force on the pile head causes several force transfer components in the interface of the pile element and the surrounding soil. Each contribution is treated separately in a paragraph.

- Response of the pile tip (paragraph ‘4.4.1.1 Base resistance’)
- Friction along the pile surface (paragraph ‘4.4.1.2 Shaft resistance’)
- Weight of ‘hanging’ soil on the pile surface (paragraph ‘4.4.1.3 Negative skin friction’)
- Settlement of the pile into the soil (paragraph ‘4.4.1.4 Pile settlement’)

- Location of the change in friction force (paragraph '4.4.1.5 Neutral plane location)

4.4.1.1 BASE RESISTANCE

The resistance force at the pile tip follows from the prevention of pile deflection by the soil around the pile tip. There are several calculation methods available for the determination of this bearing force. A lot of calculation rules are based on the analogy of Terzaghi (1943) which was originally intended for the calculation of shallow footings.

$$R_b = N_q \times \sigma'_v(L_{pile}) \times A_b \quad 4.24$$

The bearing capacity coefficient in this standard expression is very difficult to determine due to the high uncertainty in the considered factors. In literature many different expressions for this parameter exists where differences are found greater than 900 % (Budhu, 2011).

The accepted calculation method in the Netherlands and some other countries is based on in-situ data. Required input is derived from measurements of the cone penetration tests (CPT). The cone of this soil penetration method is usually smaller than a foundation pile tip, so the tool is more sensitive for discontinuities in the soil layers (Hicks et al., 2014). Inaccuracy of the measurements is reduced by the introduction of an influence zone around the pile tip. In this zone discontinuities are smoothened over a certain pile length. The distance of the influence zone is based on a logarithmic spiral shape failure mechanism, which is called the Koppejan's method (Koppejan & Van Mierlo, 1952). The failure shape described above is visualised in figure 4-9.

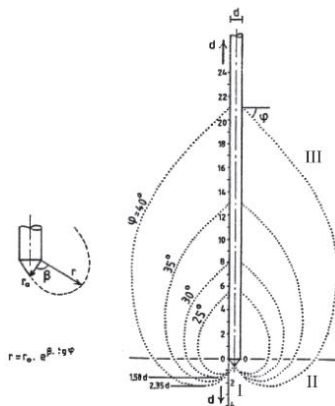


figure 4-9: shape of the failure mechanism around the pile tip (Koppejan & Van Mierlo, 1952)

A drawback of the Koppejan's method is that there is no scientific evidence for this failure mechanism (Van Baars et al., 2018). It was defined that the given failure mechanism is kinematically impossible and the failure zone is in contradiction with numerical calculations. Determination of the pile tip bearing capacity with this Dutch approach leads to an overestimation of 30 % (Van Tol et al., 2010). The calculation method for the pile base resistance according to the Eurocode is stated in appendix 'A.3 Pile taper function' and uses measured cone resistance values from CPT-diagrams.

Sas (2007) states in his report that the calculated stress can be delivered by sound spruce or pine foundation piles, but not by a reduced pile diameter as a result of degradation. The bearing strength depends in this case on the weakest link between the ground bearing strength and the pile resistance. For a dense sand layer the pile is the weakest link and the sand layer itself becomes the governing factor in case of loose soil.

4.4.1.2 SHAFT RESISTANCE

The positive contribution of shaft friction to the pile bearing capacity is called the shaft resistance. Pile settlement relative to the surrounding soil induces friction stresses at the interface of the pile and the surrounding soil. The stress has an upward direction when the pile has a greater displacement than the soil layers next to the pile. The friction force is based on Coulomb's friction law (1776) where the resisting component is activated by the average value of the lateral effective stress calculated with the neutral soil pressure coefficient.

$$R_s = \frac{1}{2} \times K_0 \times (Q_{sur} + \sigma'_v(L_{pile})) \times \tan \delta \times C_{pile,avg} \times L_{pile} \quad 4.25$$

The expression given above is not very reliable because it only takes the internal friction angle into account. A slightly different version of this expression is called the slip method (Van Tol, 1994).

$$\begin{cases} R_{s,max} = \sigma_{s,max} \times C_{pile,avg} \times L_{pile} \\ \sigma_{s,max} = \frac{1}{2} \times K_{slip} \times \sigma'_v(L_{pile}) \times \tan \delta \end{cases} \quad 4.26$$

The shaft friction stress can be derived from the effective vertical soil pressure and two soil parameters. For timber piles, the values in *table 4-14* can be used.

parameter	soil state	value
δ [-]	–	$2/3 \times \varphi'$
K_{slip} [-]	loose compaction	1.5
	dense compaction	40

table 4-14: values for the friction angle and the soil pressure coefficient (Van Tol, 1994)

Nowadays, a method based on cone penetration tests is used similar to the approach in paragraph '4.4.1.1 Base resistance'. At first, the shaft resistance was derived from the measured cone friction, but later on it was found that the obtained results were inaccurate compared to the derivation of values from the cone resistance (Van Tol, 1994). The current approach for the determination of the shaft friction is based on the cone resistance values over the region where an upward resisting force is expected as given in appendix 'A.5 Shaft resistance'. It is also compared with the slip method in a numerical example.

According to Sas (2007), the maximum occurring friction force is the highest in a dense sand layer, but still very low compared to the resistance of a timber pile. It is therefore quite certain that the degraded part is still able to transfer the stresses from the element to the surrounding soil.

4.4.1.3 NEGATIVE SKIN FRICTION

Negative skin friction is a load on the pile that is present over the soil layers which settles more than the pile deformation at the same soil depth. This skin friction is often present when the layers above the bearing sand layer are sensitive to consolidation processes. Especially clay and peat are soil types that could cause this additional loads on the piles. The friction force can be a quite considerable and there are even cases in which the magnitude of the skin friction is of the same order as the axial pile load (Backhausen & Van der Stoel, 2014).

Until the sixties of the previous century the load was not identified at all. In this period problems were observed which could not be derived with the actual geotechnical knowledge at that time. One of the famous examples of neglected skin friction is the Beurs van Berlage in Amsterdam (Klaassen & Creemers, 2012) which was constructed in 1898. It was supported by 4880 spruce and pine piles with an average length of 13 m. Around 8 years after the completion of the building, cracks became visible and

measures were necessary to ensure sufficient stability. A reason for the instability points to the location of the building because it was built on top of a sandy layer which was used to fill up the former riverbed of the Amstel river. The large amount of sand loaded the underlying peat and clay layers resulting in the consolidation of these weak layers. The appearing settlement led to the situation where a large part of the sand was kind of 'hanging' at the pile shaft due to interface friction. This additional loading was not foreseen and so the pile bearing capacity was overloaded that caused serious deformations in the structure.

Due to the late acknowledgment of this force, there is still not a generalized approach in the modelling available. The used calculation methods are therefore used as an approximation with a high level of uncertainty (Van Tol, 1994). At this moment there are two methods available for the determination of the negative skin friction where a distinction is made between a single pile and a pile in a pile group.

One of the methods is called the slip method which is often applied for single piles (Van Tol, 1994). The approach is similar to the slip method for positive shaft friction treated in paragraph '4.4.1.2 Shaft resistance' where the direction of the force and slightly different soil parameters are the only differences.

$$F_{nsf} = \frac{1}{2} \times K_0 \times \sigma'_v \times L \times \tan \delta \times C_{pile,avg} \times L_{pile} \quad 4.27$$

Above expression is derived from the approach of Coulomb friction in *equation (4.25)* for a homogeneous soil. The friction force is based on the mean value of the horizontal effective stress over the soil depth that follows from the conversion of the vertical effective stress with a neutral soil pressure coefficient according to *equation (4.13)*.

The other method specified for pile groups, invented by Zeevaert-De Beer (1962), follows from the vertical equilibrium of a very small amount of soil around a pile. In this method the vertical effective stress is reduced with the stress caused by skin friction. The skin friction expression is based on the mean vertical stress at the top and bottom side of a very thin slice of soil as depicted in *figure 4-10*.

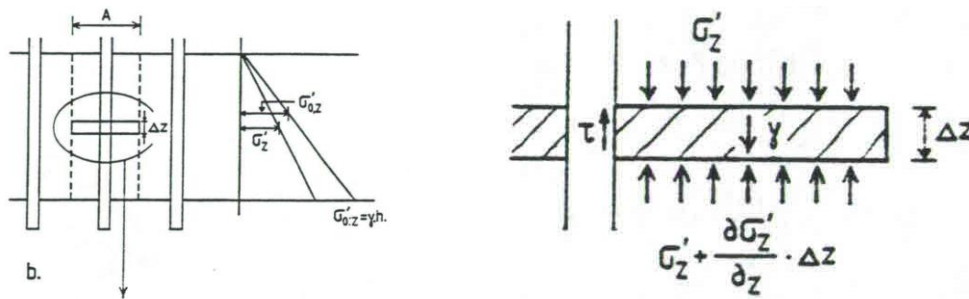


figure 4-10: infinitesimal element as the basis for Zeevaert-De Beer expression (Van Tol, 1994)

The simplest case is composed of a homogeneous soil composition with the groundwater level equal to the ground surface.

$$\begin{cases} \sigma_{nsf} = Q_{sur} + \gamma_{sat} \times L_{pile} - \frac{\gamma_{sat}}{m} \times (1 - e^{-m \times L_{pile}}) - Q_{sur} \times e^{-m \times L_{pile}} \\ F_{nsf} = A_{gr} \times \sigma_{nsf} \end{cases} \quad \text{where } m = \frac{C_{pile,avg} \times K_0 \times \tan \delta}{A_{gr}} \quad 4.28$$

The derivation of *equation (4.28)* is given in appendix 'A.13 Derivation of equation (4.28)'. The correct choice of one of the skin friction expressions depends on a criterium for the pile spacing (NEN-EN 1997-1 (NB) par. 7.3.2.2 (d), 2019).

$$S_{pile} = \sqrt{10 \times d_{head} \times L_{pile}} \quad 4.29$$

When the pile spacing is higher than above boundary value, *equation (4.27)* for single piles must be used. In all other cases, *equation (4.28)* for pile groups is needed. The calculation of negative skin friction along a pile in a pile group involves a certain pile group area. Each pile in a pile group has a certain soil clump 'attached' to the pile that depends on the pile spacing. The pile group area can be determined with *figure 4-11*.

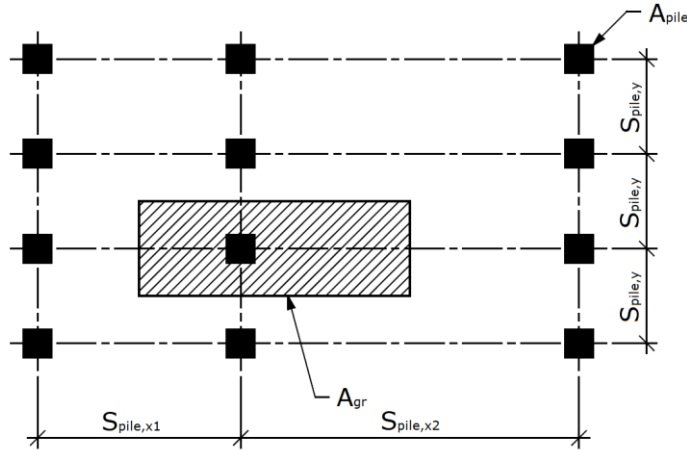


figure 4-11: influence area around a pile (NEN-EN 1997-1 (NB) figure 7.m, 2019)

$$A_{gr} = \left(\frac{1}{2} S_{pile,x1} + \frac{1}{2} S_{pile,x2} \right) \times S_{pile,y} - A_{pile} \quad 4.30$$

The calculated negative skin friction is reached only when the soil settlement attains a certain value. The soil settlement can be calculated with the expressions in appendix 'A.9.2 Soil settlement'. Three different situations can be distinguished (NEN-EN 1997-1 (NB) par. 7.3.2.2 (a), 2019):

- Soil settlement is higher than 0.1 m: apply the maximum possible negative skin friction as a load on the pile.
- Soil settlement is in between 0.02 and 0.1 m: negative skin friction depends on the interaction of the soil and pile settlements.
- Soil settlement is less than 0.02 m: negative skin friction is omitted due to its negligible influence

Where the reference height for the determination of the soil settlement is located at ground level. For the intermediate case, the values for the soil settlement and the pile displacement determine at which height the neutral plane is located. The exact procedure is given in paragraph '4.4.1.5 Neutral plane location'.

Both equations for the negative skin friction can be translated to situations with layered soil compositions and a groundwater table not equal to ground level. In appendix 'A.7 Negative skin friction', elaborative versions of these equations are given according to the Eurocode. It is accompanied by a numerical example to investigate the influence of the pile spacing on the total friction load.

4.4.1.4 PILE SETTLEMENT

Pile deflections under influence of several loads are inevitable, especially for the foundation piles under very old structures like the historic inner-city quay walls. As described in paragraph '2.1 Development of inner-city quay walls', the determination of the pile depth was determined with the 'Hollandse Heiformule'. The inadequate theoretical validation of the geotechnical pile bearing capacity resulted in large pile deflections of many old wooden piles over the years.

Minor pile deflections are not directly problematic for the stability of the structure. They actually help to redistribute forces from severely loaded parts to parts where only a fraction of the total load is present. Excessive pile deflections are not favourable because those could lead to pile failure and eventually to structural failure. In several standards, requirements are established both for SLS (serviceability limit state) and ULS (ultimate limit state). They are treated further in paragraph '4.6.3 Stability checks'.

The settlement of a pile foundation can be subdivided in the settlement of a single pile and settlement behaviour of a pile group as a result of the compaction of soil layers under the level of the pile tip (NEN-EN 1997-1 (NB) par. 7.6.4.2(a), 2019).

$$s_{pile,tot} = s_{pile} + s_{pile,gr} \quad 4.31$$

The single pile settlement is usually determined by test loads or test results from cone penetration tests. If this data source is absent, an alternative can be found with a theoretical formulation (NEN-EN 1997-1 (NB) par. 7.6.4.2(h), 2019).

$$s_{pile} = s_b + s_{el} \quad 4.32$$

A pile settlement according to this consideration consists of a pile tip settlement and elastic shortening of the element as a result of the load on the pile head and the negative skin friction stresses. The above described subdivision of the pile settlements is visualised in figure 4-12.

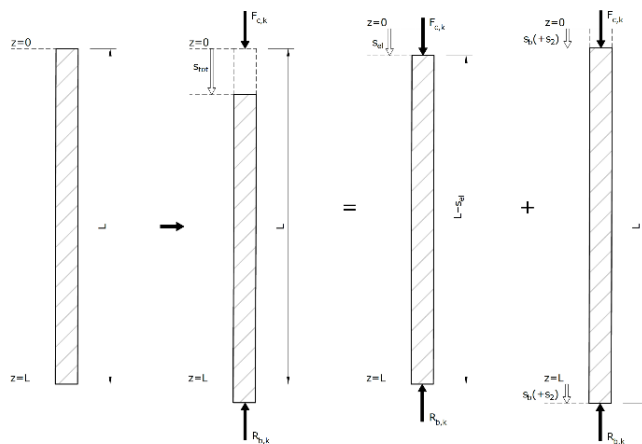


figure 4-12: individual components of displacement for a single pile

The settlement of the pile tip under the influence of the loading can be determined in two ways which depends on the extent of the available data. The first approach is based on measurements on a test pile at the project location. Monitoring stresses and displacements at several cross-sections over the pile length are in this case used to determine the normal force distribution. Those results then lead to the maximum allowable force on the pile head. When no test loads could be performed on a pile, the displacement is derived with load-displacement diagrams for the actual forces in the tip and at the shaft. Those diagrams and the corresponding calculation procedure are given in appendix 'A.8 Pile settlement'.

4.4.1.5 NEUTRAL PLANE LOCATION

The pile settlement has also an influence on the internal force distribution. From paragraphs '4.4.1.2 Shaft resistance' and '4.4.1.3 Negative skin friction', it follows that both force magnitudes act at different pile regions as a result of settlement differences between the pile and the soil. When the soil settles more

than the pile, a counteractive force in upward direction is generated which is called positive shaft friction. The opposite effect is reached when the pile displaces more than the surrounding soil. In this case a downward force develops inside the pile and so negative skin friction shows up. The soil depth where the positive shaft friction turns into negative skin friction is called the neutral plane. It is at a depth where the pile displacement is equal to the soil settlement.

$$u_{pile}(z_{np}) = s_{soil,tot}(z_{np}) \quad 4.33$$

The procedure for the determination of the neutral plane depth is given in appendix 'A.9 Neutral plane location'. In this appendix, also a numerical comparison for the pile displacement is made with a prismatic and non-prismatic shape of the foundation pile.

The determination of the neutral plane location is important because the stresses have a maximum value at this depth. It is often decided to have the neutral plane at the top of the first bearing sand layer which does not settle at all. In this way, no pile and soil settlements have to be computed, but this approach leads to very conservative results (Sas, 2007). For a higher allowable axial pile load it is favourable that the neutral plane is situated above the bearing sand layer because then the zone of negative skin friction is reduced.

The diameter for a tapered and degraded timber pile at the neutral plane can be determined when the taper rate is known and the degree of degradation is measured with penetrometer measurements. The exact degree of degradation is not known at pile tip level and is assumed to be half of the measured degradation at pile head level due to the absence of oxygen in the subsoil.

$$d_{pile,np} = f \cdot d_{head,z} - \frac{1}{2} \times (d_{head} - d_{head,eff}) \times \left(2 - \frac{l_{pile}}{L_{pile}}\right) \quad 4.34$$

Above formula is based on the expression of the branch organisation F3O/SBRCURnet (2016) for a pile with a linear taper rate. For most timber piles, a linear taper rate deviates from the actual cross-sectional variation along the length as stated in appendix 'A.3 Pile taper function', so a more generalized expression is presented in *equation (4.34)*. Both expressions assumes that the degradation at the pile tip is half of the measured degradation at the pile head with a linear relation between both levels.

4.4.2 PILES LOADED IN TENSION

A quay wall structure has to resist large external forces on the structure faced in downward direction. The majority of the piles will respond with an upward direction, but not all of them due to internal force transfer mechanisms. Resulting moments are then partly resisted by piles loaded in tension to achieve moment equilibrium in the structure. The occasional situation of a tension pile inside the pile grid means that only the tensile resistance of a single pile is required. The determination of the pile group resistance seems redundant, so it is not treated in this paragraph. The response of a pile loaded by an axial tensile force is depicted in *figure 4-13*.

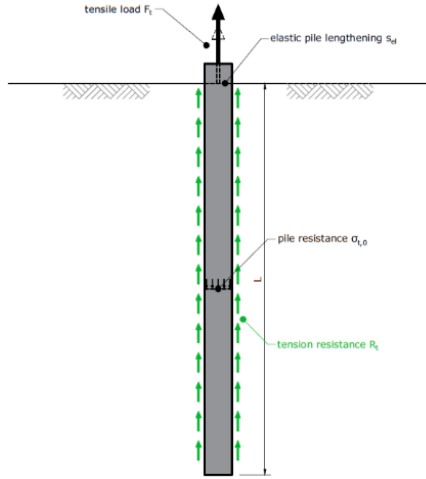


figure 4-13: forces on a pile subjected to a tensile load

A single pile loaded by a tensile force is resisted only by friction stresses along the pile shaft. Two components are related to this pile response:

- Friction along the pile surface (paragraph '4.4.2.1 Tensile resistance')
- Rise of the pile from the soil (paragraph '4.4.2.2 Pile rise')

4.4.2.1 TENSILE RESISTANCE

A single pile loaded in tension is resisted only from pulling out of the subsoil by friction stresses at the pile–soil interface. The expression for the pull–out capacity could be derived from Coulomb's friction law (1776) and is therefore similar to the expression for the shaft resistance of compressive piles in paragraph '4.4.1.2 Shaft resistance'. The only difference with *equation (4.25)* is the addition of a certain factor for the adhesion.

$$R_t = \left(c'_a + \frac{1}{2} \times K_0 \times (Q_{sur} + \sigma'_v(L_{pile})) \right) \times \tan \varphi' \times C_{pile,avg} \times L_{pile} \quad 4.35$$

A lot of uncertainties are incorporated into the formula given above. A more sophisticated approach is based on the soil parameters of CPT–results. The Eurocode expressions for this approach are given in appendix 'A.10 Tensile resistance'. For the derivation of these expressions with practical experiments, two requirements were composed to guarantee the validity of the calculation approach. The pile element must have a length–to–diameter ratio of 13.5 and a length with values in between 7 and 50 m.

4.4.2.2 PILE RISE

An axial tension force on the pile head results in an upward displacement of the element which is called pile rise. The total pile rise consists of the same components as the pile settlement of compression piles (NEN–EN 1997–1 (NB) par. 7.6.4.3 (a), 2019).

$$r_{pile,tot} = r_{pile} + r_{pile,gr} \quad 4.36$$

The contribution of the pile group rise is ignored because no pile groups under tension are considered in this report. The remaining parameter for the rise of a single pile is composed of two parts.

$$r_{pile} = r_{head} + r_{el} \quad 4.37$$

The rise of the pile head can be determined in two ways. It can be measured in–situ with a load on a test pile or approximated with a calculation. For this thesis report, the only possibility is the theoretical

consideration that consists of a load–displacement diagram for the shaft friction. The approach is presented in appendix ‘A.11 Pile rise’.

4.4.3 PILES LOADED IN LATERAL DIRECTION

Many foundation structures at quay walls have to resist large vertical forces, but they are also subjected to horizontal loading. A large share of the horizontal load is taken by the batter piles, but also vertical orientated piles receive a certain portion of the total load. A force perpendicular to the pile axis is called a lateral force. Lateral loading comprises all force contributions that act perpendicular to the pile axis or generate bending moments. Besides the arisen shear forces, the lateral loads could also induce bending moments when they have a certain eccentricity with respect to one of the pile ends. The combination of both components results in a horizontal pile deflection that is resisted by a reaction of the surrounding soil. In *figure 4-14*, a nonuniform stress distribution is given of a cross-section from a pile loaded by a combination of a bending moment and a horizontal load.

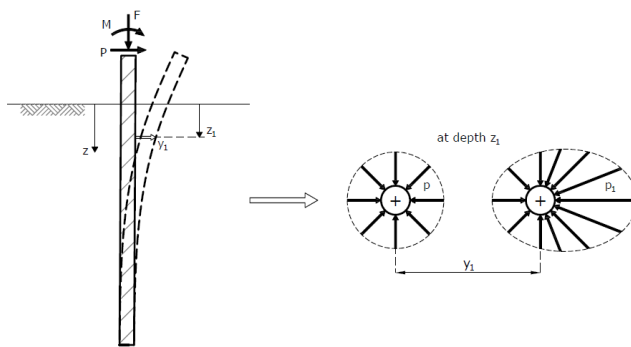


figure 4-14: stress distribution around a laterally loaded pile (Rocscience, 2018)

The soil is a nonlinear material and therefore the relationship between the soil reaction and the pile deflection is nonlinear. Several models were created in the past to calculate the response of a pile subjected to lateral loading. Due to the complicated pile–soil interaction, only computer models are able to generate reliable results. Hand calculations are exclusively useful in very simplified cases.

4.4.3.1 CALCULATION MODELS

For the calculation of the lateral pile displacement, quite some models are available that each have their strengths and weaknesses. Budhu (2011) states in his book that the choice of a computational model depends on the following characteristics:

- loading situation
- pile fixities
- pile slenderness ratio
- stress–strain behaviour of the soil
- soil stratification
- available computation time

A first distinction can be made based on the loading situation that can be translated to the driving mechanism of the lateral displacement (Backhausen & Van der Stoel, 2014).

1. Active lateral displacements from the soil around the foundation elements.
2. Lateral loads acting on the foundation system resulting in lateral soil responses around the foundation piles.

The first type of horizontal loading is based on horizontal soil deformations next to the foundation structure. It can be induced by the application of a ground elevation next to a deep foundation that leads to a horizontal stress increase and a subsequent horizontal soil displacement. The other possibility is the presence of lateral loads at the pile heads that are induced by internal force transfer mechanisms from the superstructure.

Pile fixities are the boundaries at each pile end and determines how the element is linked to its surroundings. The tip at the lower end of the pile is generally not able to rotate or translate due to the large soil resistance along the pile interface. If any movement is restricted, the tip can be modelled as a fixed support. At the top of the pile two extreme cases can be distinguished. Just like the pile tip, the pile head can also be modelled as fixed support when the foundation structure does not allow any displacements. The opposite situation is found for a pile head that functions as a hinge so no bending moments are taken. This is called a free support. In reality, the pile head connection is neither free nor fixed but lies somewhere in between those bounds. Despite the difficulty in the determination of the degree of joint rigidity, it has a large impact on the internal force distribution in the entire foundation structure, especially for deep foundations with short piles.

The next consideration for a legitimate pile model is the pile slenderness ratio. Short rigid piles have a different failure mechanism than long flexible piles. The pile classification depends on the ratio between the pile driving depth and the diameter (Budhu, 2011). Pile classifications in relation the corresponding failure mechanism are given in *figure 4-15*.

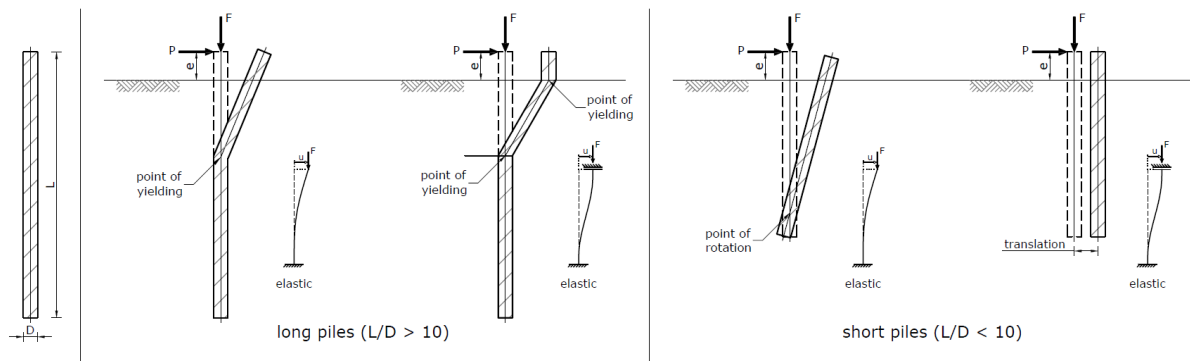


figure 4-15: length to diameter ratio and the corresponding failure mechanisms (Budhu, 2011)

It can be observed that plastic hinges will appear in long piles when the load causes internal stresses in the plastic regime. These hinges are absent in short piles because instability is usually the governing failure mechanism for this pile classification.

Another important aspect in obtaining the pile deflection is by a decision regarding the soil behaviour. In general, it can be stated that a sophisticated soil model requires various parameters that has to be obtained from literature study, valid estimates, and test results. A very extensive model is not better than simpler ones when proper input is lacking. It is therefore very important to base the decision making on the available data and model limitations to prevent outcomes full of errors.

The last two items can be combined because they are related to each other. In general, the more layers with different soil types are included in the model, the longer it takes to finish the calculation. Some of the methods can deal only with one soil type, so often they are used in the preliminary design stage to make global estimations.

All of the aspects mentioned above are more or less important for the choice of the calculation method. Moussa and Christou (2018) made a brief subdivision consisting of four calculation analogies where each method has their own characteristics:

- The ultimate limit state method (ULS) that is used for the maximum allowable lateral load on a pile.
- The subgrade reaction approach for the determination of the lateral pile deflection where the reaction of the soil is modelled as a series of linear or nonlinear springs.
- The continuum approach where the soil is characterized as a linear elastic continuous medium.
- The finite element method (FEM) is a special case of the continuum approach where partial differential equations are solved at discrete points (finite elements) that are implemented into a mesh grid at areas of interest.

In figure 4-16, a flow diagram is shown with a large set of calculation models based on the above introduction. Only the most prominent ones are selected, otherwise the diagram would not fit on one page. The flow diagram is deduced from the information of various sources in the form of master's theses (Ruigrok, 2010), (Cherqaoui, 2006) and a conference paper (Moussa & Christou, 2018).

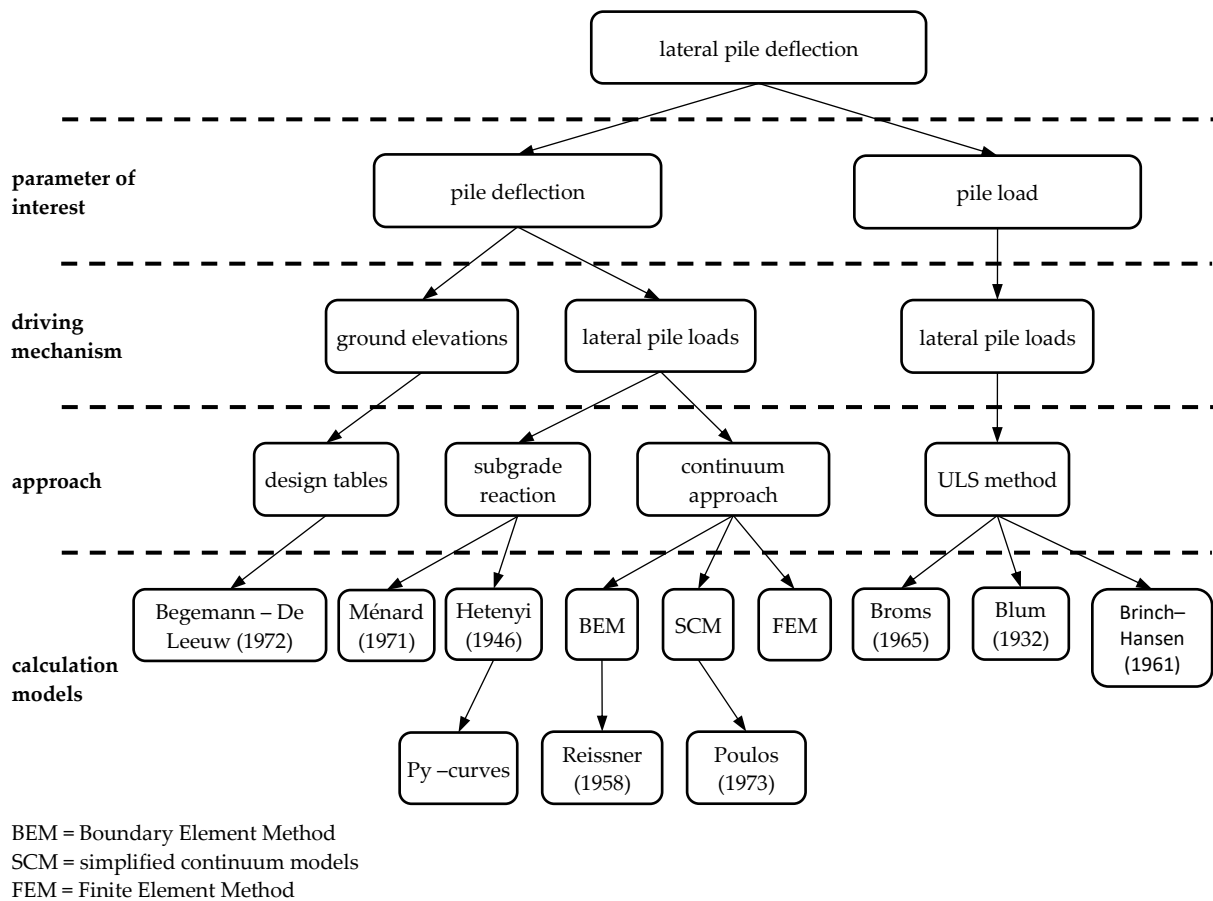


figure 4-16: data flow diagram for the determination of the used calculation method

From all above given possibilities dealing with lateral loading, an appropriate calculation model has to be chosen for quay wall structures. This is done in the following paragraph.

4.4.3.2 QUAY WALL MODEL

A suitable calculation method for the pile design under a quay wall structure has to fulfil a few prerequisites. Firstly, a choice has to be made on the parameter of interest. For a quay wall it is interesting to know the pile deflections because certain restrictions are assigned to this structural type in several design guidelines. Moreover, the models at the right side of the diagram are only handy for quick computations of single foundation piles in very specific conditions and therefore useless for pile grids in quay wall structures.

The second decision moment is based on how the structure is excited by an external influence. One of the options is a horizontal soil displacement next to the loaded object. An example is the elevation of the ground level nearby a structure that results in an increase of effective stresses in the subsoil. This scenario is not very likely to occur at a quay wall, so design methods based on this loading situation are not considered any further. The only choice left is a direct load application at the piles which is the standard case for lateral loading.

4.4.3.2.1 SUBGRADE REACTION

For the first approach, the pile is modelled as a beam supported by a series of elastic springs. Emil Winkler (1867) was the first person to find deflections and internal forces along the element according to this concept. His field of interest was the bedding response under railway tracks. He simplified the track to a continuous beam supported by a series of uncoupled and discrete translation springs with a linear-elastic behaviour according to Hooke's law. Winkler assumed proportionality between the soil bearing pressure and the soil settlement in such a way that the reaction in any point is influenced only by the deflection at the same point. A schematisation of this model is depicted in figure 4-17.

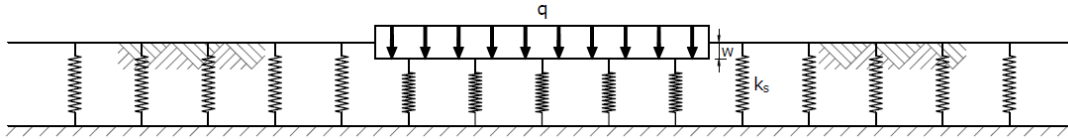


figure 4-17: soil model according to Winkler

The total load is split up into unit loads that are resisted by individual springs with a certain spring stiffness, also called modulus of subgrade reaction.

$$q = \sum_{i=1}^n q_i = \sum_{i=1}^n (k_{s,i} \times w_i) \quad 4.38$$

This method has large limitations such as spring uncoupling and the discontinuity in the soil medium (Moussa & Christou, 2018). Winkler's approach was improved and extended by Hetenyi (1946) in the form of a Euler-Bernoulli beam supported on an area with coupled springs. The resulting fourth order ordinary differential equation is translated to a laterally loaded pile with a prismatic shape by aligning the element with the vertical axis.

$$E_{pile} \times I_{pile} \times \frac{d^4 w_{pile}}{dz^4} + F_c \times \frac{d^2 w_{pile}}{dz^2} + k_s \times w_{pile} = 0 \quad 4.39$$

A distributed axial load is applied along the axis to include skin friction loads. The modulus of subgrade reaction deserves the most attention because it incorporates the soil-structure interaction. The most accurate concept still being used nowadays was invented by Matlock and Reese (1956). Both researchers made nondimensional charts for the calculation of the pile deflection and the internal forces along the pile length also known as py-curves (or pw-curves according to the used coordinate system in this report). These curves determine the lateral pile deflection by a certain soil response along the pile length.

$$p_{soil} = k_s \times w_{pile}$$

4.40

As already mentioned in paragraph '4.4.3 Piles loaded in lateral direction', soil particles in a volume behaves nonlinear when they are subjected to a load. Therefore, the modulus of subgrade reaction changes by the addition of a load increment. Especially when the load is close to the ultimate soil resistance. A generalised p_y -diagram is shown in figure 4-18.

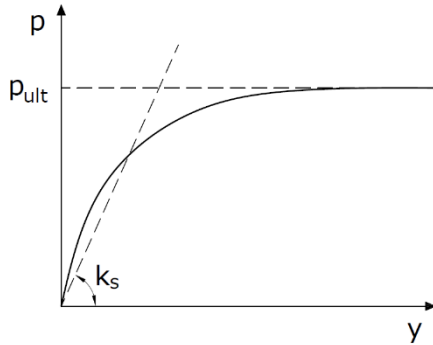


figure 4-18: generic p_y -curve for an arbitrary soil (Rocscience, 2018)

The modulus of subgrade reaction has a great influence on the pile deflection and it is therefore important to obtain a good estimation of this parameter (Bowles, 1997). A large set of full scale pile test were performed in the past with a variation in the soil type, pile depth, location of the groundwater table and pile properties. For each distinct change of conditions along the pile length, a node spring is created where a different p_y -diagram is applied. The nodal displacement follows then from equation (4.40). With a correct implementation of boundary conditions and interface conditions in between the ordinary differential equations, the lateral deflection as a function of the soil depth is obtained. In figure 4-19, an example of the pile schematised as nodal springs is depicted.

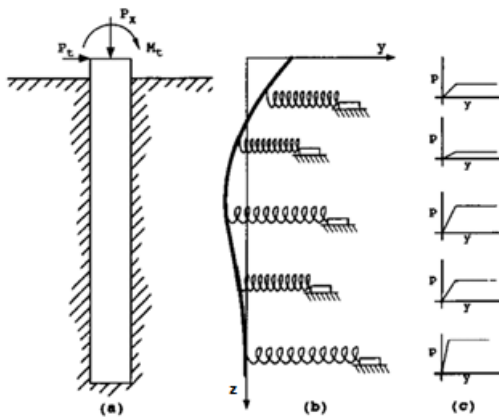


figure 4-19: model of a laterally loaded pile according to the subgrade reaction approach Reese, 1997)

Above method describes exclusively the lateral displacement of a single pile that does not correspond to deep foundations composed of grouped pile systems. The pile group deflection is then determined from a reduction of the individual pile displacement in correlation with the pile spacing and arrangement. Field tests have shown that piles in the front pile rows exhibit a higher pile resistance compared to the piles in the back. Also the piles in the centre of a row receive in general a smaller portion of the total load than the outer edges (Kempfert et al., 2002). The interaction of piles in a group is a very complicated principle and therefore computer programs are indispensable to acquire the correct pile group responses.

A simpler approach for the estimation of the subgrade of reaction moduli is the assignment of a constant value to a soil layer. Ménard et al. (1971) determined the subgrade reaction modulus for different soil types with a pressuremeter and found a relation between the measurement values and the subgrade of reaction modulus. A pressuremeter is not commonly used in the Netherlands, so the empirical relation was translated to a form where cone resistance values are used as input (GeoDelft, 2004).

$$\begin{cases} \frac{1}{k_s} = \frac{1}{3 \times E_{Ménard}} \times (0.39 \times (4.42 \times d_{pile})^\alpha + \alpha \times 0.5 \times d_{pile}) \\ E_{Ménard} = \beta \times q_{CPT} \end{cases} \quad 4.41$$

Above expression depends on rheological factors of the soil as given in *table 4-15*.

soil type	α [-]	β [-]
peat	1	3.0
clay	2/3	2.0
silt	1/2	1.0
sand	1/3	0.7
gravel	1/4	0.5

table 4-15: rheological factors according to Ménard (1971)

4.4.3.2.2 CONTINUUM APPROACH

The second method describes the soil as a continuous medium where the pile deflection is obtained along the vertical axis. A schematisation of this approach is given in *figure 4-20*.

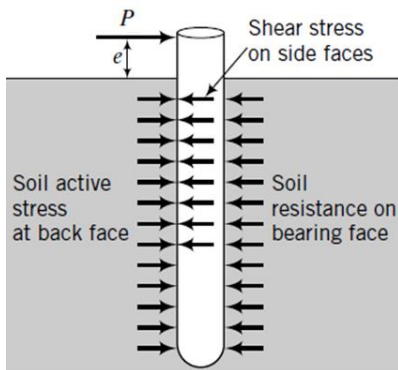


figure 4-20: soil modelled as a continuous elastic medium (Budhu, 2011)

Three different methods can be distinguished which are the Boundary Element Method (BEM), simplified continuum models (SCM), and the Finite Element Method (FEM).

In the boundary element method the pile is modelled as a thin vertical strip with boundary conditions at both pile ends. The soil acts here as an ideal linearly elastic medium. The approach comprises of two steps.

1. Integration of the Mindlin equation for a horizontal displacement caused by a lateral point load.
2. Calculation of the distributed normal stresses by a numerical calculation.

Application of the Mindlin theory is possible only when the pile is divided into equal segment lengths where each part is subjected individually to a uniformly distributed load. The shear stress between those segments is then neglected just as the adhesion of the pile with the soil. Horizontal soil displacements are calculated by the Mindlin equation where the pile deflection is determined by the differential equation of a Euler–Bernoulli beam similar to *equation (4.39)*. The correct value of the

horizontal displacement follows then by equating the displacements of the pile and the soil at the middle of each segment. Poulos (1973) introduced then nonlinear behaviour into the Boundary Element Method by consideration of the soil as an elastoplastic material.

Simplified continuum models do not make use of ordinary differential equations to describe the pile deflection and resulting internal forces, but instead are used to implement more alternative approaches. One of them is the Energy and Variational Calculus Method which is based on a minimum potential energy in the system with a homogeneous linear elastic soil. Another one was presented by Reissner (1958), also known as Reissner Simplified Continuum (RSC) model, where plane stresses are derived from a preloaded layer with a finite thickness and elastic soil properties. Both approaches described above are not very practical in use because complex mathematical formulations are involved (Moussa & Christou, 2018).

From all continuum approaches, the Finite Element Method (FEM) is the last one described more in detail. It is a mathematical tool to approximate the deflection and internal forces by partial differential equations based on the continuum theory. It divides the structure into a number of elements which are connected to each other by nodes. With the correct boundary conditions, the nodal displacements and nodal forces are solved in a matrix system with the help of a stiffness matrix. For a linear–elastic calculation, the following matrix equation is obtained:

$$[K]\{u\} = \{F\} \quad 4.42$$

Over the years, the mathematical descriptions were tuned numerous times, so better results could be obtained. It went from a one–dimensional beam element calculation with a linear–elastic homogeneous soil to very advanced models in a three–dimensional space with a stratified soil system that approximates towards full scale pile tests with a very high degree (Moussa & Christou, 2018). Also *py-curves* can be derived from the models which were already described in the subgrade reaction approach. A lot of programs nowadays use solving techniques based on finite element analysis like Plaxis, Abaqus, Diana and numerous others. Due to the model complexity and the large amount of required input, it is recommended to validate the obtained results with a simplified hand calculation.

4.5 MATERIAL RESISTANCE

When timber elements are assessed on strength, specific design rules in the ultimate limit state (ULS) are used. It is quite complicated to assess a foundation element because the cross–section consists of parts with different timber qualities. Nowadays, sawn timber elements are homogenised by removing weak spots in the material. Each timber piece is then assigned to a strength class with standard strength and stiffness values by a procedure called strength grading. To prevent excessive deformations, only strength values in the elastic regime are given in the building codes. It is not possible to assign a strength class to the old quay wall elements due to the large variation in wood species and the unknown quality.

In several guidelines, calculation rules are described that are valid for these elements with the inclusion of bacterial degradation. The branch organisation F3O/SBRCURnet (2016) focused on the implementation of calculation rules for degraded timber elements. A distinction is made between elements loaded parallel and perpendicular to the fibre direction. In a quay wall structure, exclusively foundation piles are loaded parallel to the fibre direction. The other foundation elements are all loaded perpendicular to the element axis. Calculation principles for both loading directions are described separately from each other in the following paragraphs.

4.5.1 FOUNDATION PILES

As stated in the previous sections, foundation piles under quay walls structures have to resist both horizontal and vertical loads. Depending on the loading situation, piles are loaded in compression, in tension, in lateral direction or by a combination of compression, tension and lateral loading. Unfortunately, only resistance values for compression parallel to the fibre direction are given for foundation piles (NEN 8707 par. 3.5 (2), 2018).

$$\begin{cases} f_{c,0,d} = 10.8 \text{ N/mm}^2 & \text{for } k_{mod} = 0.60 \\ f_{c,0,d} = 12.6 \text{ N/mm}^2 & \text{for } k_{mod} = 0.70 \end{cases} \quad 4.43$$

For both strength values, a modification factor and a system strength factor are incorporated. A distinction is made between a dominant permanent load (permanent, climate class 2) and the situation where the variable load is governing (long duration, climate class 2) with the values deduced from *table 4-5*.

The total pile resistance follows from the multiplication of the cross-sectional area with one of the strength values. The reduction by biological degradation can be calculated with an effective cross-sectional area based on the obtained penetration depths from a penetrometer (F3O/SBRCURnet, 2016).

$$\begin{cases} A_{pile,eff} = \frac{1}{4} \pi \times d_{pile,eff}^2 \\ d_{pile,eff} = d_{pile} - 2 \times (p_m + 5) \end{cases} \quad 4.44$$

A higher resistance is possible when the penetration values are supplied with results from a laboratory research. A slightly larger contributing area may be used when the depth of severe decay is less than the mean penetration depth.

$$d_{pile,eff} = d_{pile} - 2 \times p_m \quad 4.45$$

The pile resistance becomes even higher when the estimated compression strength is higher than a certain value.

$$d_{pile,eff} = d_{pile} - 2 \times (p_m - 5) \quad \text{when } f_{c,0,d} \geq 10 \text{ N/mm}^2 \quad 4.46$$

The compression strength of a timber pile is not the same along the length due to the pile tapering. As stated by Sas (2007) in his report, the axial compression has to be checked at two locations: at the pile head and at the neutral plane. Based on the acquired knowledge about biological degradation described in paragraph '3.3 Conducted research of degraded pile foundations', it is likely that the decay is less severe at the pile tip in comparison with the pile head due to the absence of fungi in soils. The branch organisation F3O/SBRCURnet (2016) assumes a degree of degradation at the pile tip which is twice as small as the measured decay at the pile head.

4.5.2 HORIZONTAL ORIENTATED FOUNDATION ELEMENTS

Both pile cap beams and cross-beams have to resist stresses perpendicular to the element axis only because no axial loading is present on these elements. Just like for foundation piles, only compressive stresses are given (NEN 8707 par. 3.5.2 (3), 2018). Those are not valid for the floor elements.

$$\begin{cases} f_{c,90,d} = 1.4 \text{ N/mm}^2 & \text{for } k_{mod} = 0.60 \\ f_{c,90,d} = 1.6 \text{ N/mm}^2 & \text{for } k_{mod} = 0.70 \end{cases} \quad 4.47$$

Above strength values are valid for spruce and pine with the same values for the modification factor as were given for the foundation piles. The values correspond with compression in the elastic regime, so they are quite low. When plastic deformations are allowed, the timber strength is increased. Timber

specimens were compressed in a laboratory experiment to obtain more realistic values for foundation elements. The following values were found for a compression of 30%:

$$\begin{cases} f_{c,90,d} = 2.0 \text{ N/mm}^2 & \text{for } k_{mod} = 0.60 \\ f_{c,90,d} = 2.3 \text{ N/mm}^2 & \text{for } k_{mod} = 0.70 \end{cases} \quad 4.48$$

The values below were found for a compression of 50%:

$$\begin{cases} f_{c,90,d} = 2.6 \text{ N/mm}^2 & \text{for } k_{mod} = 0.60 \\ f_{c,90,d} = 3.0 \text{ N/mm}^2 & \text{for } k_{mod} = 0.70 \end{cases} \quad 4.49$$

The use of these values in strength values is allowed only when the timber elements are situated directly above the foundation piles, so no bending will occur.

When the compression magnitude of the foundation elements is not relevant at all, the strength may be even higher. An additional requirement is the possibility for transferring a load between the entire pile cross-section and the upper beam element. With the penetrometer measurement of the beam element, the effective support area can be calculated (F3O/SBRCURnet, 2016).

$$W_{pcb,eff} = W_{pcb} - 2 \times (p_m - 10) \quad 4.50$$

The maximum allowable stress is higher when the support area is smaller. The exact relation between the pile contact area and the compressive stress is shown in *figure 4-21*.

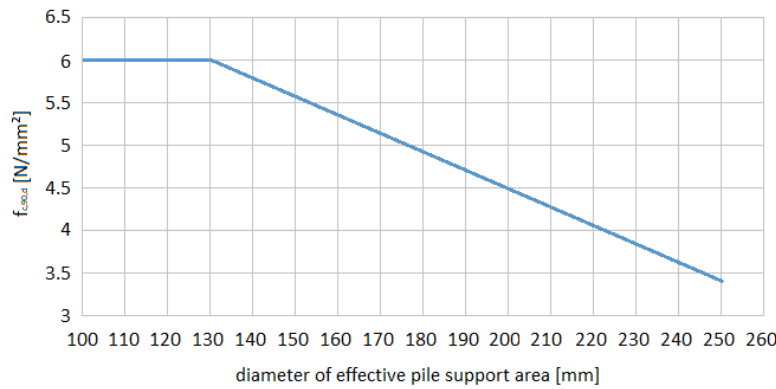


figure 4-21: relation between the pile support area and compressive resistance perpendicular to the fibre direction (F3O/SBRCURnet, 2016)

A stress value higher than 4.5 N/mm² may be used only when the following requirement is met or when the compression deformation of the horizontal element is less than 1/3 of the original thickness.

$$f_{c,90,d} \geq 4.5 \text{ N/mm}^2 \quad \text{when } H_{pcb} - 2 \times p_m - 10 \quad 4.51$$

Above relations are not valid for the floor elements because they are loaded primarily in bending.

“For the investigation to quay wall defects, a few quay wall structures in the Netherlands are selected according to predefined criteria. First, the response of a quay wall in perfect condition is determined whereafter its model is adjusted by the applications of structural debilitations. The results of both models are then compared with each other to find out the differences in structural responses and how the structure is still able to transfer the loads to the subsoil.”

Quay wall calculations

The historic quay walls found along the waterways in the Netherlands are able to withstand quite substantial loadings despite their age. When the foundation framework is still in a good condition, superstructure loads are transferred very efficiently to the foundation piles due to the dense pile grid and the resulting short spans of the beam elements. In this way, internal bending moments and shear forces do not get a chance to develop inside an element. Unfortunately, many foundation structures show several kinds of deficiencies that has a negative impact on the load transfer mechanisms. Each quay wall defect has its own influence on the structural behaviour ranging from almost negligible to enormous with a possible quay wall collapse as the worst case scenario.

To investigate the effect of foundation deficiencies on the structural behaviour of a quay wall, a few cases will be selected. The selection is succeeded by the description of the calculation strategy with the used calculation programs and the arrangement of the structural model. The selected quay walls are presented in paragraph ‘5.1 Case study’. With these considerations, a structural calculation is made for a quay wall in a perfect state, so with the absence of structural defects. The required steps in the calculation procedure are described in paragraph ‘5.2 Calculation approach’. After these computations, a selection is made in paragraph ‘5.3 Model output’ of common failure modes for timber foundation structures based on various quay wall inspections. Each factor is then applied one by one to the model to determine which deficiency has the greatest impact on the structural integrity. Finally, the calculation results of all quay wall defects are discussed in paragraph ‘5.4 Interpretation of results’.

5.1 CASE STUDY

Before performing calculations to historic quay wall structures, a few physical cases are chosen. All of those quay wall sections are located in Rotterdam or The Hague where the required quay wall data is provided by both municipalities. Not all types of quay wall structures are suitable for this thesis report, so a few points for the qualification of structures are needed. They are specified in the enumeration given below:

- A sufficient amount of data is available to be able to set up a proper structural model. The more information is known about the structure, the less assumptions have to be made. This viewpoint improves the quality of the performed analysis and more valuable conclusions follow from the obtained outcomes.
- Quay wall structures with a foundation entirely made of timber. There are also more recently built cases with a foundation consisting of concrete pile cap beams and timber foundation piles

to prevent exposure of the upper foundation elements, but those are not considered in this report.

- The quay wall section must have a length of at least 20 m with a homogeneous character along the select part. This requirement prevents the complexity of distinct alterations in the structural behaviour and the allowance for the implementation of justifiable boundary conditions in the computation model.

On basis of these considerations, the following quay wall structures are selected:

- Boompjeskade, Rotterdam
- Haringvliet, Rotterdam
- Noordwal, The Hague
- Stieltjeskade, Rotterdam
- Toussaintkade, The Hague

The selected quay wall structures are described separately with the main focus on the composition and the actual condition of the structure. The required information for each structure is disclosed by the municipality of Rotterdam by means of internal documents.

5.1.1 BOOMPJESKADE, ROTTERDAM

The Boompjeskade in Rotterdam is positioned along the Nieuwe Maas which is a bifurcation of the Meuse river. The location of the quay wall is given in *figure 5-1*.

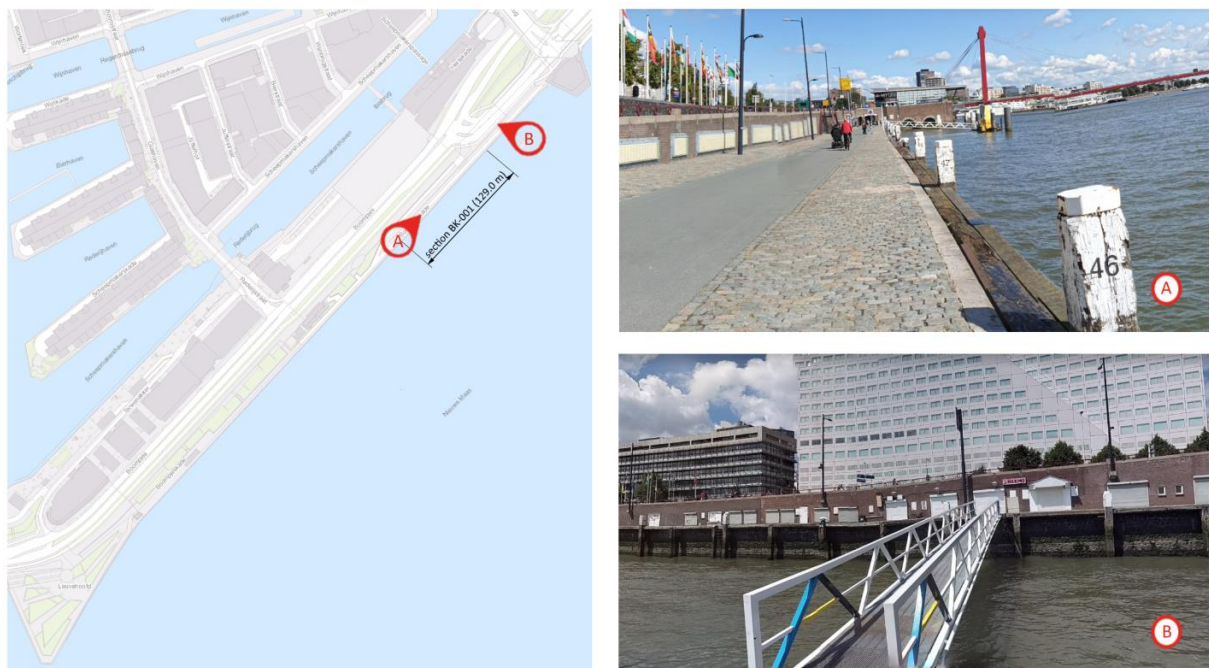


figure 5-1: map of the Boompjeskade (Geostart, n.d.) accompanied by two photos of the structure (Google, n.d.)

The quay wall has a total length of 770 m and comprises the land–water boundary from the Leuvehoofd in the left lower corner to the protruding building in the right upper corner of the map. Over a considerable length, remains of the former quay wall built in 1883 are still present in the subsoil (Gemeente Rotterdam, personal communications, 2013). Throughout the years, numerous compositions were built on top of the leftovers with a variation of timber and concrete foundations. The retaining wall is composed of brickwork with basalt columns. At the front part of the structure, timber fender

piles with a spacing of approximately 10 m are fixed to the wall by brackets just below the coping. No information about the maximum ship size is given, but from pictures of a moored ferry, CEMT class II is assumed. Between the quay wall and the elevated level of surrounding building, a paved strip is situated with a width of approximately 8.40 m. It is covered with a natural stone paving and asphalt for a one-way traffic road.

For this thesis report, the above section with a length of 129.0 m constructed in 1925/1926 is of interest because of the timber foundation framework where floor elements are placed in longitudinal direction on top of the pile cap beams. In 2012 a concrete floor was placed upon the timber floor elements which is not considered in this report. It is unknown how the beam elements are connected to the foundation piles, so the most prevailing connection type in old timber foundations are assumed which are mortise and tenon joints. In between the second and third pile row and the fourth and fifth pile row, batter piles are located that are connected to the pile cap beams with cross-beams.

From several inspections, a large variability in pile spacings is observed. The differences are equalized by taking the mean of the given range of values which simplifies the implementation into a structural model. In *figure 5-2*, a characteristic cross-section of the quay wall section is given in the situation before the concrete floor was placed. The dimensions in the figure are given in millimetres where the vertical datum is given in metres relative to the NAP-level.

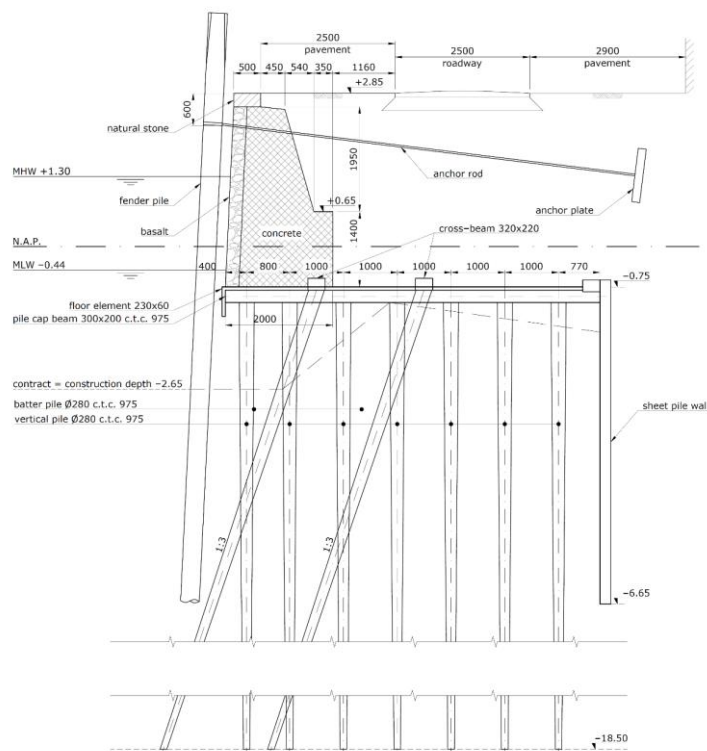


figure 5-2: cross-section of the Boompjeskade (BK-001) (Gemeente Rotterdam, personal communications, 2013)

The structural state of the Boompjeskade is checked in 2013 for the last time (Gemeente Rotterdam, personal communications, 2013). The assessment report contains measurements of the deformations, visual inspections, penetrometer measurements, and investigation of retrieved samples in the laboratory. The results of all investigations are described in appendix 'B.1 Boompjeskade, Rotterdam'.

5.1.2 HARINGVLIET, ROTTERDAM

The Haringvliet in Rotterdam is an inner harbour in the city centre of Rotterdam. It is sealed in by the Oude Haven in the west and the Boerengat in the east. An overview of the Haringvliet is given in *figure 5-3*.

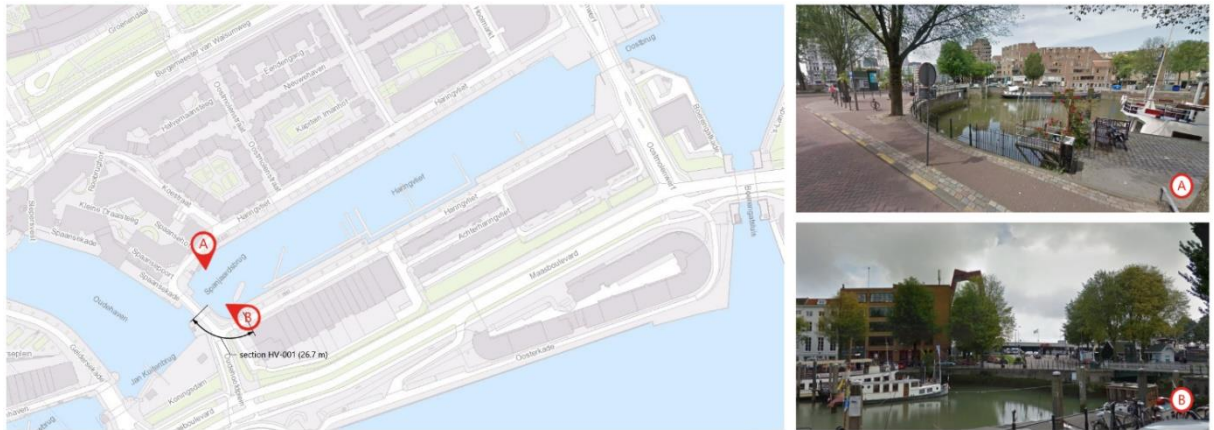


figure 5-3: map of the Haringvliet (GeoStart, n.d.) accompanied by two photos of the structure (Google, n.d.)

The Haringvliet is an enclosed basin with entrances at either side. The quay wall structure around the water body can be split up into more than twenty different compositions. The majority of the structures is completely made out of concrete with a L-wall supported by a deep foundation, but also smaller sections with timber foundations are still in service. All around the land–water boundary, ship mooring facilities are present where large jetty structures are situated along the south side of the harbour. Along both long linear sections of the Haringvliet, parking lots are located at a few metres away from the water.

The quay wall section of interest is situated at one of the sides of the Spanjaardsbrug. It has a total length of 26.7 m and a large part of the structure has a curved shape. This section was constructed in 1885 already but renovated in 2010 where the first layer of the brick wall was renewed from the upper side of the timber foundation till a level just below the coping (Gemeente Rotterdam, personal communications, 2012). The wall is founded on a timber framework with three rows of vertical piles. In between the second and third pile row a timber sheet pile wall is located. During inspections with a diving team, it could not be determined how the piles are connected to the pile cap beams. Inspections to the pile connections in adjacent sections revealed a mortise and tenon joint, so the same type of connection in the considered section is plausible. Another remarkable feature of the curved section is the large lime tree in proximity to the retaining wall as depicted in *figure 5-3*.

From the accurate description of the structure in the assessment report, the cross-section in *figure 5-4* could be drawn. It slightly differs from the original drawing in the report because the given range of values for a few elevations and structural element sizes is translated to a single value by taking the mean. The dimensions in the figure are given in millimetres where the vertical datum is given in metres relative to the NAP-level.

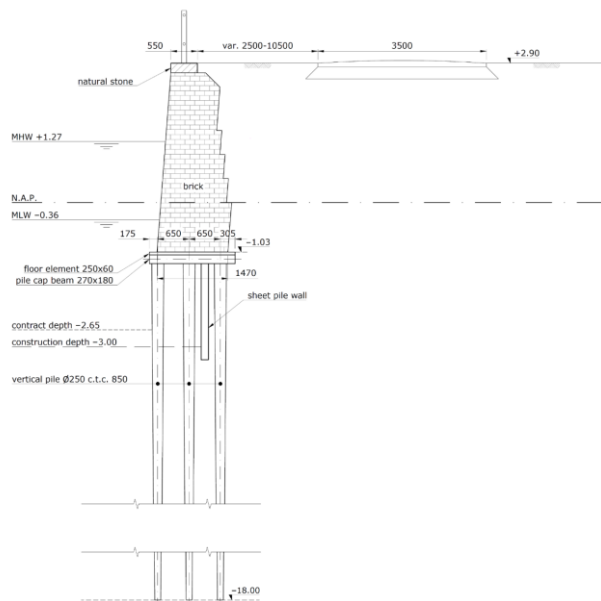


figure 5-4: cross-section of the Haringvliet (HV-001) (Gemeente Rotterdam, personal communications, 2012)

The structural conditions of the quay wall structures in the Haringvliet were determined for the last time in 2012 (Gemeente Rotterdam, personal communications, 2012). The assessment was comprised of measurement deformations, visual inspections, penetrometer tests, and determination of the residual quality of timber samples in the laboratory. Outcomes of these procedures can be found in appendix 'B.2 Haringvliet, Rotterdam'.

5.1.3 NOORDWAL, THE HAGUE

The Noordwal is situated along a canal in the inner city of The Hague. It is enclosed by the Bij de Westermolens bridge in the southwest and the junction with the Prinsessewal and the Prinssestraat in the northeast. The street is adjacent to the Veenkade at the other side of the canal. The exact location of the street is depicted in *figure 5-5*.

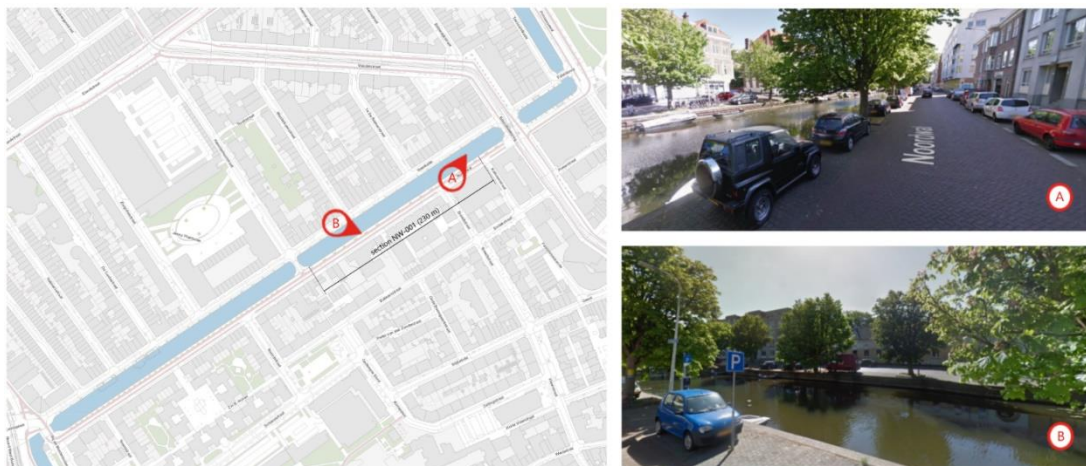


figure 5-5: map of the Noordwal (ArcGIS, n.d.) accompanied by two photos of the structure (Google, n.d.)

The total quay wall length along the Noordwal has a length of approximately 700 m. Several sections can be distinguished that are defined by the Hemsterhuisbrug halfway the Noordwal and the

Bibliotheekbrug close to the right end of the street. For the calculations in this report, the part between the wing walls of the Hemsterhuisbrug and the Kalkoenstraat with an estimated length of 230 m is considered. Along the quay wall length a parking lane is found that is interrupted every few metres by chestnut trees. The chestnuts are positioned at a distance of approximately 1.60 m from the quay wall with its reference at the centre of the tree.

The exact construction year of the quay wall is not known, but it is probably built around 1900 (Ingenieursbureau Den Haag, 2020). In 1954 a part of the brickwork above the waterline was substituted by a concrete slab finished off by a layer of bricks. Despite the renovation works in the past, the quay wall was strengthened in 2019 because of its poor condition. A sheet pile wall with jack posts was installed in front of the structure for quay wall strutting such that the tilting mechanism towards the water is counteracted. In the autumn of 2021, the construction activities for the replacement of the Noordwal are kicked-off where the current structure is replaced by a composition with a concrete pile foundation.

The structure without the propping system is composed of a retaining wall supported by a timber framework of pile cap beams, floor elements, and foundation piles. The wall consists of bricks with exclusion of the renewed upper part and becomes wider towards the foundation. In between the first two pile rows, a retaining wall of timber planks is located. No information is known about the connection between the pile and beam elements. A mortise and tenon joint is assumed because such connections were found in the Toussaintkade which is very similar in composition as the Noordwal. The structure is strengthened every 10 m with a thicker wall and a longer pile cap beam with an additional foundation pile. The buttress has a length of approximately 1 m.

A few dimensions in the drawings of the report were not clearly specified, so assumptions had to be made. A representative drawing of the considered section is given in *figure 5-6*. The dimensions in the figure are given in millimetres where the vertical datum is given in metres relative to the NAP-level.

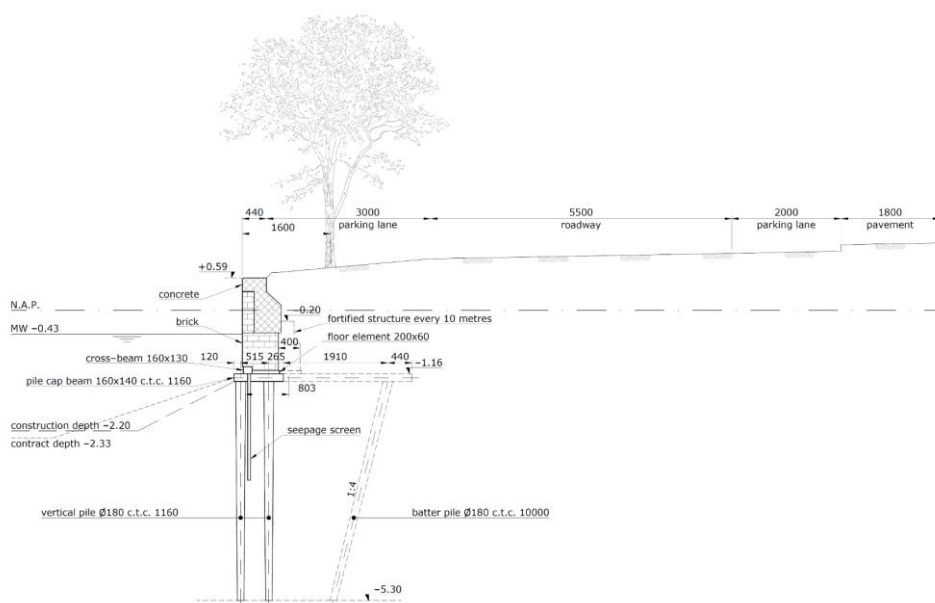


figure 5-6: cross-section of the Noordwal (NW-001) (Ingenieursbureau Den Haag, 2020)

The structural state of the quay wall at the Noordwal was assessed in 2016 and 2018 (Ingenieursbureau Den Haag, 2020). At both moments, deformations were measured, visual inspections and penetrometer

measurements were performed, and the residual parameters of timber samples were determined in the laboratory. Results of all these activities are presented in appendix 'B.3 Noordwal, The Hague'.

5.1.4 STIELTJESKADE, ROTTERDAM

The Stieltjeskade in Rotterdam is located in the Koningshaven near the Koninginnebrug. In figure 5-7, an overview of the quay wall is depicted.

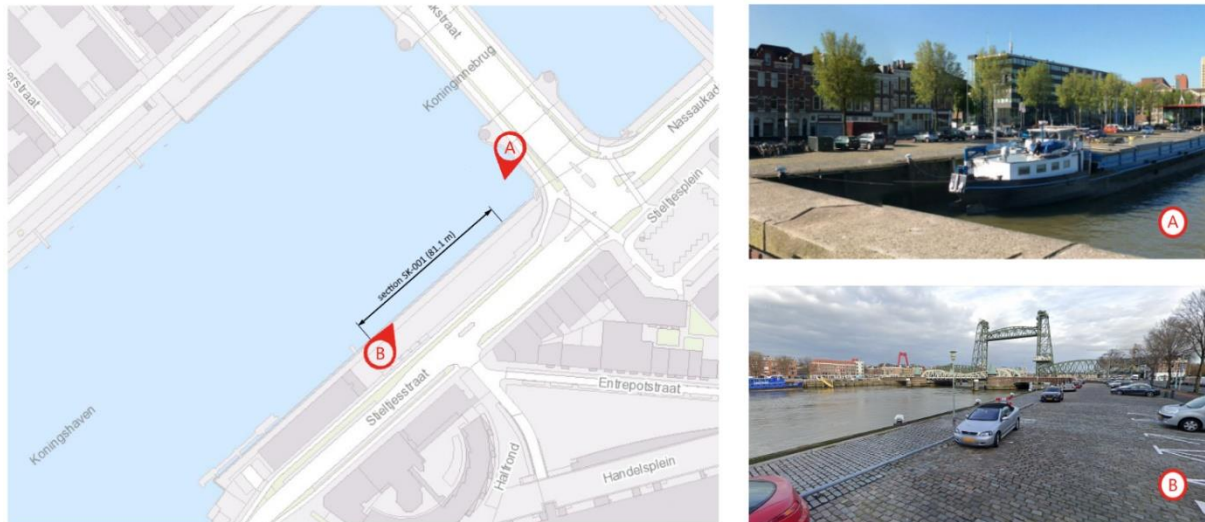


figure 5-7: map of the Stieltjeskade (GeoStart, n.d.) accompanied by two photos of the structure (Google, n.d.)

The quay wall constructed in 1929 actually consists of two sections. The part at the east side has a timber pile foundation where the foundation at the west part consists of concrete elements (Gemeente Rotterdam, personal communications, 2013). The superstructure is the same over the entire length; a concrete retaining wall covered by a layer of basalt stones. The part with the timber foundation is still in its original state where the other part is renewed in 1992. Along the entire length, mooring piles equipped with bollards with a spacing of approximately 10 m are attached to the structure to facilitate ship mooring activities. Each pile is resisted in horizontal direction by a ground anchor. The maximum ship size is not known, but from the observed ship above, CEMT class II is assumed. A parking lot is located behind the wall that is built up with cobble stones. The first 4 m are not accessible by cars due to the placement of a steel barrier.

The part with the timber foundation can be split up further into four parts with each a slightly different composition. The largest section has a length of 81.1 m. According to the assessment report, the timber foundation in this pile section consists of a framework where floor elements are placed in longitudinal direction on the pile cap beams. Those beam elements are connected to the foundation piles with a mortise and tenon joint. In between the first and second pile row and the third and fourth pile row, batter piles are located that are connected to the pile cap beams by cross-beams.

Despite the detailed description about the structural composition, many irregularities were still found along the quay wall length in terms of pile spacings and dimensions of the various elements. For a lot of parameters, minimum and maximum values are given in the report as an indication for the structural variations. To overcome difficulties with the implementation in a calculation program, a single value is used for each parameter by taken the mean of the range, so a regular pattern of structural elements is obtained. The cross-section in figure 5-8 is derived from the available data of the structure. It slightly differs from the drawing in the condition assessment report because not all required dimensions were

provided. The dimensions in the figure are given in millimetres where the vertical datum is given in metres relative to the NAP-level.

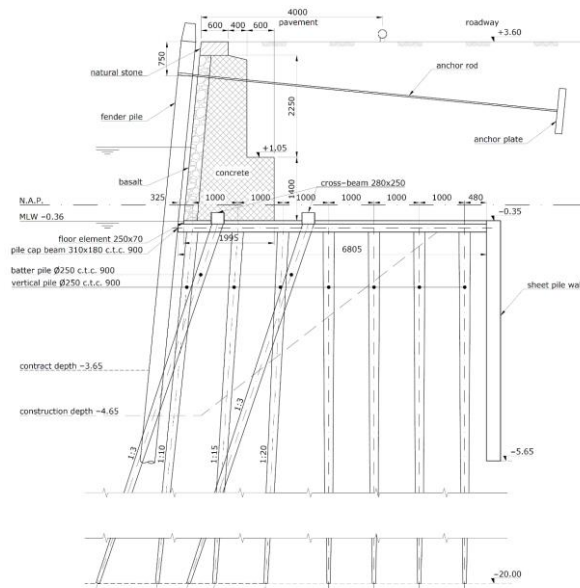


figure 5-8: cross-section of the Stieltjeskade (SK-001) (Gemeente Rotterdam, personal communications, 2013)

The actual condition of the structure is assessed in 2012 (Gemeente Rotterdam, personal communications, 2013). Four types of actions were performed: deformation measurements, visual inspections, penetrometer measurements, and investigation of retrieved samples in a laboratory. The results of all investigations are described in appendix 'B.4 Stieltjeskade, Rotterdam'.

5.1.5 TOUSSAINTKADE, THE HAGUE

The Toussaintkade is a street near the Noordeinde Palace in The Hague. In between the street and the palace, a canal is located that is shared with the Prinsessewal. The described situation is visualised in figure 5-9.



figure 5-9: map of the Toussaintkade (ArcGIS, n.d.) accompanied by two photos of the structure (Google, n.d.)

The quay wall of the Toussaintkade has an estimated length of 255 m with exclusion of the wing walls of the abutments at both outer ends of the canal. In between the parking lots at the quay wall, lime trees are aligned at a distance of approximately 1.50 m from the centre of the tree till the quay wall front.

The structure has undergone a few modifications to ensure sufficient bearing strength (Ingenieursbureau Amsterdam, 2016). Before the total renovation in 2018, the structure consisted of a brick wall supported by a deep foundation with timber elements. Technical documentation of this former structure could not be located, so the exact construction year is not known, but it is probably built around 1900. Around 1960, the upper side of the retaining wall was renewed by the replacement of a part of the brick wall by concrete. A lot of information could be obtained during the construction activities in the form of technical drawings. More recently, the structure showed large deformations that indicated a poor condition of the quay wall. The quay wall was temporarily stabilized in 2012 by the application of steel purlins at the front of the retaining wall and connecting the beam with a number of ground anchors. Later on, another emergency measure was needed by the closure of parking lots along the water's edge to gain a reduction of the total surface load. The risk of failure was eliminated by the replacement of the old structure with a new foundation plus concrete retaining wall.

The newest quay wall version present nowadays is not pertinent for this thesis report because the structure does not have a timber foundation structure anymore. Alternatively, a structural model is made in the situation before the application of the steel purlin in 2012. The superstructure consists of a brick wall where a part above the waterline is made of concrete covered by a brick layer. A few offsets are present in the wall, so the wall becomes wider towards the base. Along the quay wall length, 1.0 m thick buttresses are present every 10 m to increase the stiffness in longitudinal direction. The wall founded on a timber framework with floor elements, pile cap beams, and foundation piles where mortise and tenon joints are used to connect the piles with the beams. In between the first and second pile row, a timber seepage screen is located that is connected to the structure with a cross-beam.

From several measurements along the quay wall, many irregularities were found in terms of structural dimensions. The variation along the length is not considered in the structural model, so when a range of values is given for a single parameter, the mean value is taken. In *figure 5-10*, a representative cross-section of the Toussaintkade is drawn. The dimensions in the figure are given in millimetres where the vertical datum is given in metres relative to the NAP-level.

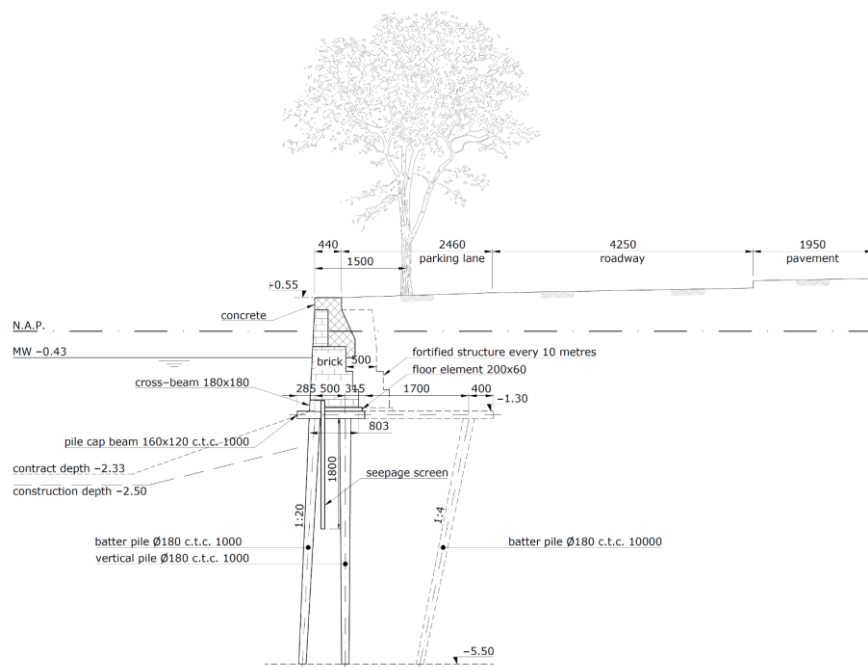


figure 5-10: cross-section of the Toussaintkade (TK-001) (Ingenieursbureau Amsterdam, 2016)

The structural assessment of the Toussaintkade was performed in 2009 (Gemeente Rotterdam, internal documents, 2009) and 2011 (Ingenieursbureau Amsterdam, 2016) in their original state. Both documents covered the aspects of deformation measurements, visual inspections, penetrometer measurements, and microscopic research to retrieved wood samples. In 2018, timber piles with their full length were retrieved from the subsoil that were left behind after the renovation of the quay wall (Gemeente Rotterdam, internal documents, 2018). Sections of those piles were loaded in a compression load machine until failure. The results of all these described investigations are presented in appendix ‘B.5 Toussaintkade, The Hague’.

5.2 CALCULATION APPROACH

Before the influence of the deficiencies on the quay wall structures in above paragraphs can be investigated, a few steps have to be taken first. A model is made where the structure functions as intended. To include structural deteriorations in this model, a number of defects are applied by adaptations to the structural composition. For each defect, a comparison is made between the results of the intact and the deteriorated structure. In this way, the influence on the structural behaviour can be determined. The above described calculation strategy is elaborated in *figure 5-11*.

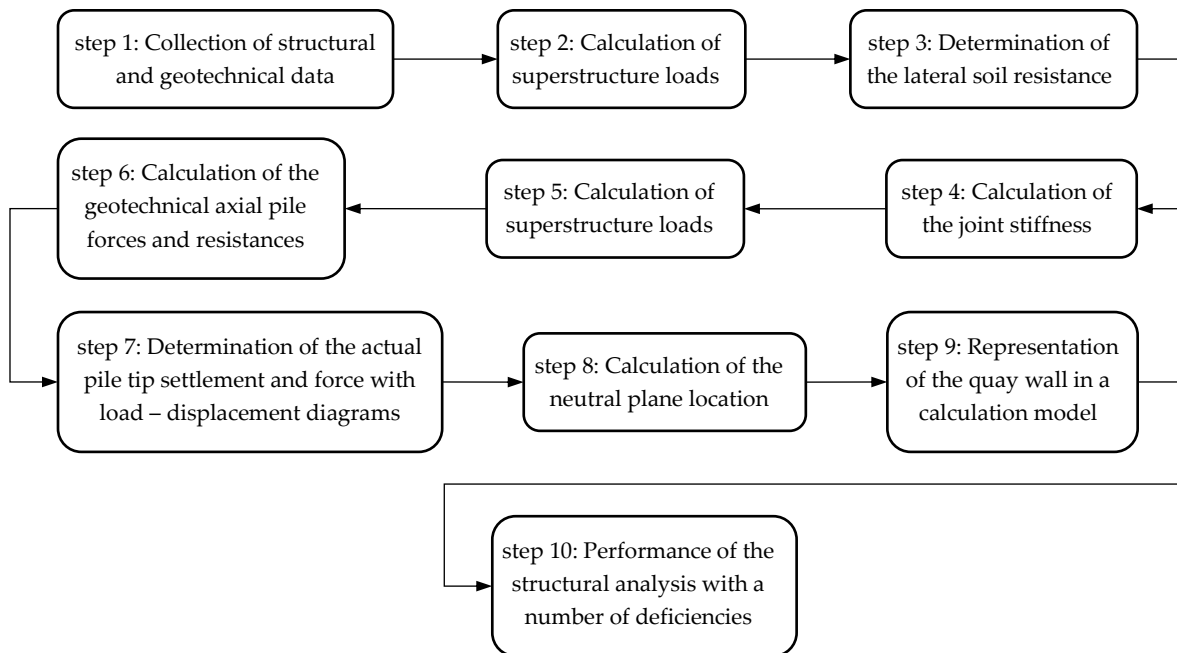


figure 5-11: scheme for the quay wall calculations

Each step is described more extensively in a separate paragraph. Those paragraphs are given below.

5.2.1 COLLECTION OF DATA

The first step towards quay wall calculations is the collection of the required specifications of the structure, surrounding soil, and external influences. During the construction of the old quay wall structures it was unlikely that the structural composition was depicted in a drawing, so other ways were needed to obtain a good description of the dimensions of the several quay wall parts. From paragraph ‘5.1 Case study’ and appendix ‘Appendix B: Assessment results of quay walls’ it followed that a lot of information was acquired by visual inspections and drawings of recent renovation works.

Soil parameters for the required geotechnical calculations are obtained by an open source on the internet. A very good tool is the website of DINOloket (www.dinoloket.nl) where soil probing data is made publicly for almost every location in the Netherlands. For this thesis report, the soil parameters for each quay wall structure are derived from a single soil probing at the closest distance from the project area. Soil data from more than one CPT–diagram improve the reliability in the used parameters, but also prolongs the total duration for the required calculations. More value is given to a shorter computation time because the increase in accuracy does not significantly contribute to the quality of the geotechnical calculations.

A third point related to the collection of the required data is the set of prescribed external factors on the quay wall structure. They follow from several guidelines, handbooks, building codes, and standards related to quay walls and similar geotechnical structures as presented in paragraph ‘4.3 Loads on the structure’.

With the collected data, the exact loads on the structure can be determined as described in the following paragraph.

5.2.2 SUPERSTRUCTURE LOADS

The loads on the superstructure from the previous paragraph can be used to determine the axial pile head forces on the foundation piles. As stated in paragraph ‘5.1 Case study’, a quay wall section with a minimal length of 20 m is used to exclude the influence of the model boundaries on the structural behaviour. Along this length, the variation of forces is nonuniformly distributed over the structure. To deal with this three–dimensional variety, the section is split up in a number of cross–sections with a spacing equal to the centre–to–centre distances of the pile cap beams. This procedure is done with a Python script (Calculation model – step 1) where the location and magnitude of each load contribution is used as input.

To determine the influence of distinct surface loads from the load models on the quay wall structure, load spreading models are needed. A distinction is made between the horizontal spreading forces on the quay wall and the vertical spreading forces on the pile cap beams.

The influence of the horizontal spreading forces on the structure is simplified by assuming the retaining wall as a rigid body. In this way, the deformation of this object does not have an influence on the internal force transfer in the foundation structure. With this simplification, the surface point load in the form of a distributed load according to *equation (A.10)* can be reduced to a distributed line load with a certain centre of gravity on the quay wall with *equation (A.11)* as a result of horizontal force spreading. The same procedure can be applied for the conversion of strip load from *equation (A.14)* to a single load according to *equation (A.15)*. The vertical force spreading for point and strip loads is characterized by *equation (A.7)*. In *equation (A.8)*, the distribution of the vertical force is evenly distributed over the influence area at a certain soil depth.

To put the forces and pressures from both load spreading models into the structural framework program Scia Engineer, the distributed loads on the structure has to be discretized. This is done by *equation (A.22)* for the horizontal force on the quay wall and *equation (A.20)* for the vertical forces on the pile cap beams.

The remaining loads on the structure are quite straightforward as input for the calculation model and therefore they are not further elaborated in this paragraph. An overview of the possible loads is given below.

- Uniform surface loads and soil loads
 - Total vertical soil pressure → *equation (A.1), equation (A.2), equation (A.3), and equation (A.4)*
 - Total horizontal soil pressure → *equation (4.14)*
- Surface water pressure → *equation (4.15)*
- Self-weight of the quay wall → *equation (4.8)*
- Mooring force (optional) → *table 4-11*
- Tree loads (optional) → *table 4-12*

The calculations in the Python script can be used as input in Scia Engineer to determine how the loads are transferred to the foundation piles.

5.2.3 LATERAL SOIL RESISTANCE

The response of a laterally loaded pile in quay wall structures can be calculated with a varying extensiveness where a more sophisticated model leads to results with a lower uncertainty level. For this thesis report, there is no need for an extensive model because the lateral deflection is not a key parameter to be able to answer the research question. Therefore, the decision is made to apply the empirical method by Ménard by making use of *equation (4.41)* and *table 4-15*.

The soil response is determined with *equation (4.40)* where the geotechnical program D-pile Group is used to obtain the pile displacements. The Poulos method is used for this purpose because it can deal with a large number of piles and takes pile-soil-pile interaction into account. Piles in very dense pile grids like the deep foundation of quay walls are not influenced only by horizontal loads, but also by the reaction of surrounding elements due to movements of the soil in between the piles.

An important choice in the Poulos method is the type of the connection of the pile cap beam with the piles. Only extreme cases of the joint rigidity are possible which are free or fixed. In appendix 'A.12.3 Numerical example of joint stiffness' a numerical example was made for the estimation of the rotational stiffness of a mortise and tenon joint. From the calculation results in *table A-18*, it is clear that the internal forces in this particular example are closer to the fixed case compared to the free case, so the fixed connection is used as input in the D-pile Group calculation. This decision is based on only one example, but for other quay wall compositions the same results are expected because of similar ratios between the dimensions of the pile cap beams and the foundation piles.

The load application in the program is only possible at the centre of gravity of the pile cap. This limitation in the input deviates from the actual force introduction into the structure, so the obtained results are just an approximation for the pile stiffness in lateral direction.

5.2.4 JOINT STIFFNESS

Before the first calculations of the quay wall models in Scia Engineer are done, first the rotational stiffness between the pile cap beam and the foundation pile has to be determined. The mortise and tenon joint is the most prevalent joint type for old timber structures where its rotational rigidity is approximated by *equation (A.74)* For the determination of this value, a few assumptions are made:

- The depth of the mortise hole is taken equal to half of the total height of the pile cap beam.
- The constriction of the part of the pile inside the pile cap beam is assumed to be 20% of the pile head diameter. This means that the width of the notch is equal to 10% of the pile head diameter at each side.

The values for the soil resistance can be used for the framework model in Scia Engineer which is treated in paragraph '5.2.5 Axial pile head forces'.

5.2.5 AXIAL PILE HEAD FORCES

When all forces are known, a framework with hinges is built in Scia Engineer that represents the timber pile foundation. For the calculations, a few considerations are made:

- For the calculation of the pile head forces, exclusively values in the ultimate limit state are used. Serviceability limit state requirements seems to be of no importance for older quay wall structures because no stability requirements are given in *table 4-15* related to the SLS. Another reason is that the partial factors in *table 4-1* are quite low, so the difference in the calculation results for both limit states will not be significantly large.
- Load model 1 is used to represent the maximum variable load at surface level along the quay wall. Load model 2 is useful when the bearing strength on a local scale has to be determined. Calculations accompanied by this load model does not grant valuable results on top of the calculations with load model 1, so load model 2 is not considered any further. This decision reduces the total calculation time enormously because only the load combination with the maximum loading situation on a global scale as given by *equation (4.21)* is applied.
- Floor elements are excluded from the calculation model because they do not have an important function in the internal force transfer mechanisms due to the simple supports in the system. This simplification requires the placement of the vertical loads directly on the beam elements.
- A few quay walls described in paragraph '5.1 Case study' are equipped with grout anchors to resist the horizontal forces from ship mooring. The anchor systems are connected with an anchor rod to the mooring facilities, so the ship forces are transferred directly to the quay wall structure. This direct force transfer between both elements leads to the possibility for omission of both entities because their behaviour does not result in internal forces in the structural system.
- The retaining wall has very large dimensions compared to the slender foundation elements, so the wall element behaves like a rigid body. The non-deformability of the element results in the substitution of the wall element by a beam element with a combined bending stiffness according to *equation (A.72)*.

Schematisation of the structure according to those bullet points determines the magnitudes of the pile head forces which are needed for the next step in the quay wall calculations.

5.2.6 AXIAL PILE FORCES AND RESISTANCES

With the results of the Scia Engineer calculations, the axial pile resistances can be calculated. These resistances are determined with a Python script (Calculation model – step 2). In this calculation sheet, the following resistances are calculated for compressive and tensile piles:

- Piles in compression ($F_{c,d} < 0$)
 - Pile tip resistance → *equation (A.28)*
 - Pile shaft resistance → *equation (A.29)*
 - Pile bearing capacity → *equation (A.35)*
 - Negative skin friction → *equation (A.38)*
 - Total pile force → *equation (A.36)*
- Piles in tension ($F_{c,d} > 0$)
 - Pile shaft resistance → *equation (A.61)*

The value of the negative skin friction depends on the value of the soil settlement at ground level calculated with *equation (A.58)*. According to paragraph '4.4.1.3 Negative skin friction', three situations can be distinguished. For two cases the negative skin is equal to either zero or the maximum value. For the other case the values of the friction forces are not yet known because their magnitudes depend on the depth of the neutral plane. A first estimation of the friction forces is made where the neutral plane is placed at the interface of the weak layers with the sand bearing layer. This assumption is needed to determine the total pile force and is used to determine the pile tip settlement with the load–displacement diagrams.

5.2.7 PILE TIP SETTLEMENT AND FORCE

The actual values of the pile tip force and settlement are found with the load–displacement diagrams from *figure A-23* and *figure A-24*. With the obtained value for the pile tip settlement, the pile tip can be schematised as a bi-axial spring according to *equation (A.56)*. This behaviour is favourable for the total bearing strength of the system because the settlements allow load redistributions till a certain degree.

The pile tip settlement values are used for the determination of the neutral plane described in the following paragraph.

5.2.8 NEUTRAL PLANE

The determination of the neutral plane location for piles under compression is required only when the settlement at ground level is in between the two bounds given in paragraph '4.4.1.3 Negative skin friction'. In this case the neutral plane is located at the soil depth where the soil settlement is equal to the pile displacement as given by *equation (4.33)*. An iterative process is required because the pile displacement depends on its turn on the friction zones which are determined by the depth of the neutral plane. The used procedure is elaborated in appendix 'A.9.4 Numerical example' where the graphical determination with the load–displacement diagrams is needed only at the start of the calculations because the obtained values are updated in each iteration step. This approach results in a fully automated calculation process in the form of another Python script (Calculation model – step 3).

At this point the axial pile behaviour is known and the next step is the determination of the pile response in lateral direction. The exact location of the neutral plane is then applied into a structural framework model in Scia Engineer which is treated in the upcoming paragraph '5.2.8 Calculation model'.

5.2.9 CALCULATION MODEL

With all considerations in the previous paragraphs, a structural model of the entire quay wall structure is built in Scia Engineer. The model resembles the one described in paragraph '5.2.5 Axial pile head forces', but now the supports are replaced by pile elements. The following adaptations related to the input are made:

- Subgrade of reaction modulus according to paragraph '5.2.3 Lateral soil resistance'.
- Rotational stiffness at the connection of the pile cap beam and the foundation pile determined with the procedure followed in appendix '5.2.4 Rotational joint stiffness'.
- Pile tip settlement according to the calculations in paragraph '4.4.1.4 Pile settlement'.

In this calculation the same considerations are used as given in paragraph '5.2.5 Axial pile head forces'. When the calculations are finished and the structural behaviour of the quay wall is determined, the next step is to investigate the influence of structural defects on the structure. This is done in paragraph '5.2.10 Structural deficiencies'.

5.2.10 STRUCTURAL DEFICIENCIES

To investigate the influence of structural deterioration on the integrity of a quay wall, the defects are applied to the model discussed in the previous paragraph one at a time. In this way, the influence of each defect on the structure can be determined by comparing the results from the intact and the altered model with each other. The selection of applied defects is based on the investigations of wood research in paragraph '3.3.2 Inventory of wood degradation studies' and quay wall reports in appendix 'Appendix B: Assessment B: Assessment results of quay walls', and literature. The following base quantities are used for this comparison:

- horizontal displacement
- vertical displacement
- internal normal force
- internal shear force
- internal bending moment

From the obtained output, only the displacements and force distributions in the pile cap beam and the foundation pile in the first pile row in the middle of the quay wall section are considered for the comparison between both structural states of a quay wall. In this way, the comparison remains concise but still clear for understanding how the structure behaves after a certain change.

The different modifications are given in *figure 5-12*. For each modification it is depicted how they are implemented in a calculation model. The figure is accompanied by a list with descriptions.

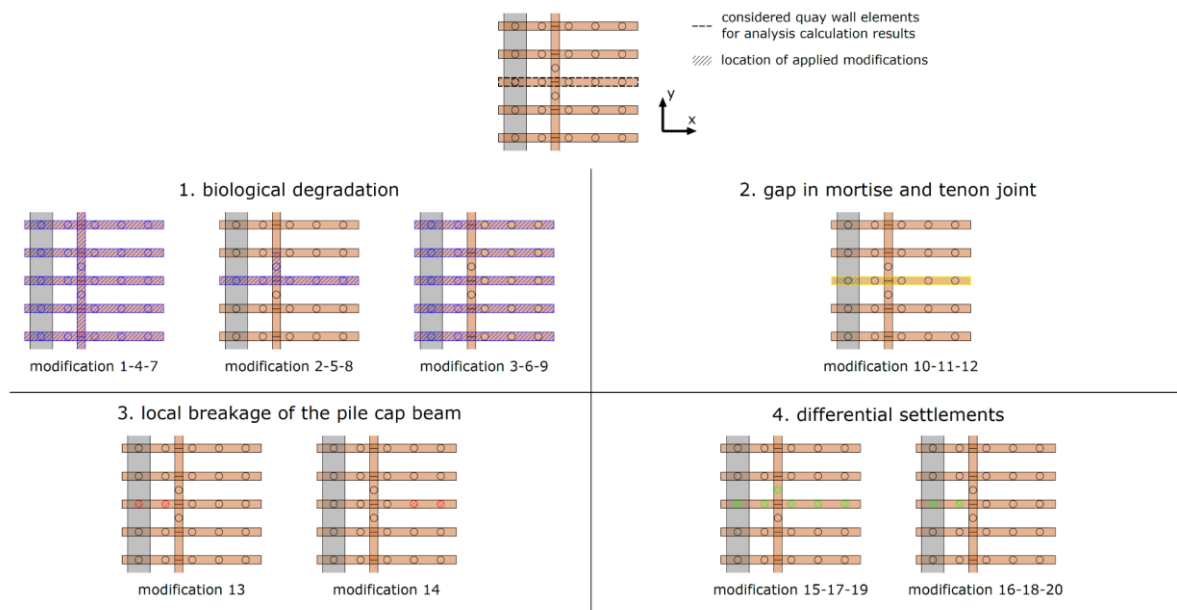


figure 5-12: location and type of applied structural changes per modification

1. biological degradation → application of *equation (4.44)* and *equation (4.50)*
 - 1.1 weak degradation ($p_m = 5 \text{ mm}$)
 - 1.1.1 entire structure **modification 1**
 - 1.1.2 crosswise (cross-section) **modification 2**
 - 1.1.3 lengthwise (first two pile rows) **modification 3**
 - 1.2 moderate degradation ($p_m = 15 \text{ mm}$)
 - 1.2.1 entire structure **modification 4**

1.2.2 crosswise (cross-section)	modification 5
1.2.3 lengthwise (first two pile rows)	modification 6
1.3 severe degradation ($p_m = 30$ mm)	
1.3.1 entire structure	modification 7
1.3.2 crosswise (cross-section)	modification 8
1.3.3 lengthwise (first two pile rows)	modification 9
2. gap in mortise and tenon joint → shift of pile cap beams in lengthwise direction	
2.1 small eccentricity ($e_y = 5$ mm)	modification 10
2.2 moderate eccentricity ($e_y = 25$ mm)	modification 11
2.3 large eccentricity ($e_y = 50$ mm)	modification 12
3. local breakage of the pile cap beam → pile loses its bearing function	
3.1 front part (first two pile rows)	modification 13
3.2 rear part (last two pile rows)	modification 14
4. differential settlements	
4.1 small settlement ($s_b = 5$ mm)	
4.1.1. crosswise (cross-section)	modification 15
4.1.2. lengthwise (first two pile rows)	modification 16
4.2 moderate settlement ($s_b = 10$ mm)	
4.2.1 crosswise (cross-section)	modification 17
4.2.2 lengthwise (first two pile rows)	modification 18
4.3 large settlement ($s_b = 20$ mm)	
4.3.1 crosswise (cross-section)	modification 19
4.3.2 lengthwise (first two pile rows)	modification 20

These adaptations are applied directly to the calculation models in Scia Engineer, so no recalculations in the Python scripts or D-Pile Group are performed. Some of the above described features could have significant impacts on the stiffnesses and resistance values of the structure, but these are not taken into account in this report to avoid very time-consuming operations. The results of the calculations are presented below in paragraph '5.3 Model output' according to the steps in *figure 5-11*. In appendix 'Appendix C: Calculation results', the intermediate results of the calculations for each quay wall structure are shown.

5.3 MODEL OUTPUT

The five quay wall structures are subjected to the described deficiencies in the previous paragraph whereafter the differences between the calculation results of the unscathed (initial) and the modified models are calculated. To get insight on the influence of the modification on the structure, a comparison is made between the maximum and minimum values of the selected base quantities. In this way, a clear overview is obtained on how the structural behaviour is changed by the application of a single modification. Those values are derived from the nodal displacements force and force diagrams supplied by the framework program Scia Engineer according to the axis system of *figure 2-5* and *figure 5-12*. In *figure 5-13*, a visualisation is given how these values are derived from the calculation results.

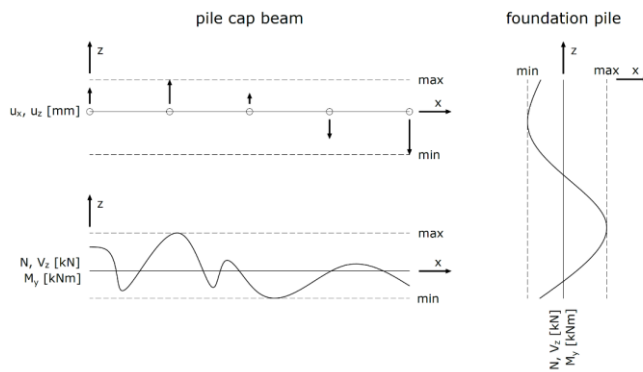


figure 5-13: extreme values related to displacement and internal forces

As described in paragraph '5.2.10 Structural deficiencies', the internal forces and displacements in the pile cap beam and the pile in the first pile row at the middle cross-section of the model are compared with each other. To quantify the influence of each adaptation to the model, the relative difference is calculated for each base quantity. For the horizontal displacement, the following expression is used:

$$\Delta u_x = \frac{u_{x,mod} - u_{x,int}}{u_{x,int}} \times 100 \quad 5.1$$

Similar expressions can be used for the other base quantities. Only the resulting outcomes per quay wall are shown in this paragraph. The exact values for the displacement and force results are denoted in appendix 'Appendix C: Calculation results'.

Colour indications are given to the base quantities for an indication of the magnitude of each adaptation on the structural behaviour of the model. A green cell means that the modification results in a reduction of the measured base quantity where a red colour is an indication for a relative increase. The colour intervals for each quantity are listed in table 5-1.

$\Delta u_x \geq 10 \%$	$\Delta u_z \geq 10 \%$	$\Delta N \geq 10 \%$	$\Delta V_z \geq 10 \%$	$\Delta M_y \geq 10 \%$
$5 \% \leq \Delta u_x < 10 \%$	$5 \% \leq \Delta u_z < 10 \%$	$5 \% \leq \Delta N < 10 \%$	$5 \% \leq \Delta V_z < 10 \%$	$5 \% \leq \Delta M_y < 10 \%$
$-5 \% < \Delta u_x \leq 5 \%$	$-5 \% < \Delta u_z \leq 5 \%$	$-5 \% < \Delta N \leq 5 \%$	$-5 \% < \Delta V_z \leq 5 \%$	$-5 \% < \Delta M_y \leq 5 \%$
$-10 \% < \Delta u_x \leq -5 \%$	$-10 \% < \Delta u_z \leq -5 \%$	$-10 \% < \Delta N \leq -5 \%$	$-10 \% < \Delta V_z \leq -5 \%$	$-10 \% < \Delta M_y \leq -5 \%$
$\Delta u_x \leq -10 \%$	$\Delta u_z \leq -10 \%$	$\Delta N \leq -10 \%$	$\Delta V_z \leq -10 \%$	$\Delta M_y \leq -10 \%$

table 5-1: colour scheme with values in percent

The calculation results per quay wall structure are given below in table 5-2, table 5-4, table 5-6, table 5-8, and table 5-10 for the pile cap beams and table 5-3, table 5-5, table 5-7, table 5-9, and table 5-11 for the foundation pile in the first pile row.

mod.	Δu_x		Δu_z		ΔN		ΔV_z		ΔM_y	
	min.	max.	min.	max.	min.	max.	min.	max.	min.	max.
1	2%	16%	4%	-4%	-7%	4%	0%	-2%	0%	-1%
2	1%	19%	4%	4%	-12%	2%	0%	-7%	0%	-5%
3	5%	-3%	0%	-4%	-7%	3%	0%	-2%	0%	-1%
4	5%	41%	11%	-7%	-12%	7%	-1%	-4%	0%	-1%
5	2%	44%	11%	7%	-23%	2%	0%	-15%	0%	-12%
6	12%	-3%	2%	-9%	-11%	5%	0%	-3%	0%	-1%
7	16%	103%	28%	-16%	-19%	12%	-1%	-6%	1%	-2%
8	2%	113%	28%	4%	-42%	0%	-1%	-30%	0%	-26%
9	31%	6%	10%	9%	-18%	8%	-1%	-6%	0%	-2%
10	0%	0%	0%	0%	-1%	0%	0%	0%	0%	0%

5. Quay wall calculations

11	0%	3%	0%	0%	-1%	0%	0%	0%	0%	0%
12	2%	19%	0%	-2%	-1%	0%	0%	-1%	0%	-1%
13	7%	-3%	67%	109%	-100%	1%	0%	-53%	0%	-91%
14	-9%	1319%	15039%	-7%	-3%	462%	658%	122%	1641%	0%
15	-1%	-6%	-3%	11%	7%	0%	2%	5%	0%	4%
16	-1%	0%	0%	56%	2%	-1%	0%	1%	0%	0%
17	0%	-6%	-1%	16%	2%	0%	2%	1%	0%	1%
18	1%	0%	0%	44%	0%	0%	0%	0%	0%	0%
19	0%	-3%	3%	16%	-8%	2%	2%	-5%	0%	-4%
20	5%	-3%	0%	104%	-6%	2%	0%	-3%	0%	-1%

table 5-2: calculation results of the pile cap beam in the Boompjeskade at the middle section ($y = 9.75 \text{ m}$)

mod.	ΔN		ΔV_z		ΔM_y	
	min.	max.	min.	max.	min.	max.
1	-2%	-2%	-7%	-13%	-6%	-8%
2	-6%	-6%	-12%	-17%	-6%	-13%
3	-2%	-2%	-7%	-13%	-3%	-7%
4	-3%	-3%	-12%	-27%	-6%	-14%
5	-12%	-12%	-23%	-33%	-11%	-25%
6	-3%	-3%	-11%	-27%	-3%	-13%
7	-5%	-5%	-19%	-23%	-8%	-22%
8	-25%	-25%	-42%	-37%	-25%	-45%
9	-5%	-5%	-18%	-17%	0%	-21%
10	0%	0%	-1%	0%	0%	0%
11	0%	0%	-1%	0%	0%	-1%
12	0%	0%	-1%	0%	0%	-1%
13	-	-	-	-	-	-
14	0%	0%	-3%	-7%	-11%	-1%
15	4%	4%	7%	3%	-3%	9%
16	1%	1%	2%	0%	-3%	2%
17	1%	1%	2%	0%	0%	2%
18	0%	0%	0%	0%	0%	0%
19	-4%	-4%	-8%	-3%	0%	-9%
20	-2%	-2%	-6%	-3%	6%	-9%

table 5-3: calculation results of the pile in the first pile row in the Boompjeskade at the middle section ($x = 0.40 \text{ m}$, $y = 9.75 \text{ m}$)

Biological degradation (modification 1 to 9) has a significant effect on the displacements and internal force transfer mechanisms of the pile cap beam and the foundation pile in the Boompjeskade. The maximum value of the vertical displacement increases a lot more than the minimal value when crosswise or global degradation occurs in the system. An exception is the lengthwise degradation where the minimum value has increased a lot more when a higher penetration is applied to the quay wall elements. It can be observed that the biological degradation even has a positive influence on the maximum value of the vertical displacement, but no clear relation can be found between the different degradation patterns. The internal force transfer in the pile cap beam is positively influenced or remains the same for different degradation magnitudes except for the maximum value of the normal force. The greatest decrease is found for the minimum value of the normal force which is directly related to the shear forces in the foundation pile. The largest effects on internal forces results from crosswise degradation.

The gap in the mortise and tenon joint (modification 10 to 12) and the subsequent pile cap beam shift on the foundation piles has no influence on the displacements and internal forces in one of the timber quay wall elements.

Breakage of the pile cap beam (modification 13 and 14) has a significant impact on the structural behaviour of the quay wall on that location. The influence of this failure mechanism is larger when it is located at the backside compared to the frontside, especially when the maximum vertical displacement is considered. Values indicate that the structure still functions but immediate measures are required to prevent structural failure. Internal forces in the pile situated in the front row are slightly reduced when the backside of the pile cap beam has failed.

Settlements of the foundation piles (modification 15 to 20) lead to a major increase of the maximum values of the vertical displacements where the influence of the lengthwise settlement is much larger than the crosswise settlement. The internal force transfer in both the pile cap beam and the foundation pile is almost not affected by differential settlement.

mod.	Δu_x		Δu_z		ΔN		ΔV_z		ΔM_y	
	min.	max.	min.	max.	min.	max.	min.	max.	min.	max.
1	5%	8%	23%	11%	-63%	3%	-11%	11%	13%	14%
2	0%	2%	21%	1%	-63%	-2%	-17%	-3%	0%	-11%
3	2%	2%	23%	10%	-63%	3%	-12%	13%	15%	14%
4	11%	13%	49%	23%	-100%	6%	-20%	18%	21%	25%
5	0%	2%	45%	2%	-100%	-5%	-29%	-7%	-6%	-22%
6	6%	5%	48%	20%	-100%	5%	-21%	24%	26%	25%
7	27%	23%	110%	45%	-100%	10%	-33%	27%	32%	39%
8	2%	0%	99%	5%	-100%	-13%	-45%	-18%	-19%	-47%
9	17%	5%	109%	39%	-100%	8%	-35%	39%	43%	39%
10	0%	-3%	0%	0%	0%	-2%	0%	0%	0%	0%
11	0%	-8%	0%	0%	0%	-6%	0%	-1%	0%	0%
12	1%	-23%	0%	0%	-13%	-18%	0%	-2%	0%	0%
13	0%	0%	2895%	0%	-100%	0%	-11%	3%	334%	-33%
14	5%	115%	1%	430%	0%	-100%	-98%	-98%	-98%	-78%
15	0%	0%	55%	4%	-50%	0%	-49%	-3%	0%	-19%
16	5%	5%	63%	7%	-13%	7%	-56%	42%	49%	89%
17	0%	2%	103%	5%	-100%	0%	-58%	-7%	-4%	-33%
18	10%	10%	124%	-26%	-25%	10%	-79%	52%	64%	139%
19	1%	2%	191%	5%	-100%	-12%	-57%	-14%	-11%	-19%
20	-45%	138%	252%	-48%	-38%	15%	-92%	49%	68%	178%

table 5-4: calculation results of the pile cap beam in the Haringvliet at the middle section ($y = 10.20$ m)

mod.	ΔN		ΔV_z		ΔM_y	
	min.	max.	min.	max.	min.	max.
1	-2%	-1%	-63%	-21%	-27%	0%
2	-4%	-3%	-63%	-28%	-32%	0%
3	-2%	-1%	-63%	-24%	-27%	0%
4	-4%	-2%	-75%	-45%	-45%	0%
5	-6%	-5%	-75%	-52%	-45%	0%
6	-4%	-2%	-75%	-45%	-45%	0%
7	-6%	-3%	-88%	-72%	-36%	0%
8	-12%	-9%	-88%	-76%	-32%	0%
9	-6%	-3%	-88%	-76%	-36%	0%
10	0%	0%	0%	0%	0%	0%

11	0%	0%	0%	0%	0%	0%
12	0%	0%	-13%	0%	0%	0%
13	-	-	-	-	-	-
14	2%	1%	0%	7%	9%	0%
15	-7%	-8%	-50%	-3%	-5%	0%
16	2%	2%	-13%	7%	5%	0%
17	-13%	-14%	-88%	-7%	-9%	0%
18	3%	3%	-25%	10%	9%	0%
19	-23%	-24%	-88%	-14%	32%	0%
20	1%	1%	-38%	10%	9%	0%

table 5-5: calculation results of the pile in the first pile row in the Haringvliet at the middle section ($x = 0.18$ m, $y = 10.20$ m)

For the Haringvliet, the effect of biological degradation (modification 1 to 9) is in general larger on the vertical displacement than on the horizontal displacement where the degradation over the entire structure has the largest impact. Besides the structural translations, the internal force transfer is also influenced by biological degradation but mainly in a positive way. This effect is visible for the minimum values of the normal force and shear force in the pile cap beam, both extreme values of the shear force in the foundation pile, and the minimum value of the bending moment in the foundation pile. Contrarily, the maximum values of the shear force and bending moment are increased significantly for degradation over the entire structure and along the lengthwise direction.

The gap in the mortise and tenon joints (modification 10 to 12) becomes only prevalent for large values. The maximum value of the vertical displacement and the normal force of the pile cap beam both gets positively influenced by this type of modification.

Loss of pile bearing resistance due to pile cap beam fracture (modification 13 and 14) contributes significantly to quay wall translations. Removal of the first two piles has the largest influence on the minimum value of the vertical displacement whereby missing of the two last two piles has a great contribution on the maximum value of the vertical displacement. Despite of those sharp increases, the structure still functions because the absolute value of the maximum vertical displacement is 30 mm downwards as given in appendix 'C.2.10 Structural deficiencies'. The displacement has resulted in redistribution of the forces over the remaining healthy part of the structure which appears in the reduction of internal forces in the pile cap beam.

Global and local pile settlements (15 to 20) have both a negative influence on the maximum value of the horizontal displacement and the minimum value of the vertical displacement of the pile cap beam. The internal forces in the pile cap beam remain more or less the same but this is not the case for the foundation pile in the first row. Large settlements have a positive effect on the normal force and the minimum value of the bending moment, but also result in quite large increases of the minimum value of the shear force and the maximum value of the bending moment.

mod.	Δu_x		Δu_z		ΔN		ΔV_z		ΔM_y	
	min.	max.	min.	max.	min.	max.	min.	max.	min.	max.
1	71%	0%	9%	6%	31%	16%	0%	0%	0%	0%
2	43%	20%	9%	6%	31%	16%	0%	0%	0%	0%
3	-7%	25%	9%	0%	12%	19%	0%	0%	-1%	0%
4	121%	55%	19%	14%	74%	42%	0%	0%	0%	0%
5	121%	55%	19%	14%	74%	42%	0%	0%	0%	0%
6	-7%	65%	19%	-3%	26%	47%	0%	0%	-1%	-1%
7	407%	180%	46%	43%	183%	104%	0%	0%	0%	0%

8	407%	185%	40%	44%	183%	115%	0%	0%	0%	0%
9	-14%	205%	42%	-19%	62%	124%	1%	-1%	1%	-2%
10	7%	15%	0%	0%	-33%	-7%	0%	0%	0%	0%
11	36%	40%	0%	1%	-100%	-22%	0%	0%	0%	0%
12	100%	80%	0%	2%	-100%	-12%	0%	0%	0%	0%
13	200%	-290%	9498%	118%	-90%	-100%	21%	-26%	44%	22%
14	-1450%	845%	1110984%	121%	-67%	-100%	-100%	179%	1015%	-100%
15	0%	5%	44%	-3%	2%	1%	0%	0%	-1%	0%
16	0%	5%	42%	0%	2%	3%	0%	0%	-1%	0%
17	-7%	15%	143%	-11%	7%	1%	0%	0%	-1%	0%
18	0%	15%	136%	2%	7%	4%	0%	0%	-1%	0%
19	-7%	25%	308%	-26%	14%	4%	0%	-1%	-1%	0%
20	0%	25%	292%	4%	14%	7%	1%	-1%	-1%	0%

table 5-6: calculation results of the pile cap beam in the Noordwal located at the middle section ($y = 10.44 \text{ m}$)

mod.	ΔN		ΔV_z		ΔM_y	
	min.	max.	min.	max.	min.	max.
1	1%	1%	-25%	16%	0%	-33%
2	2%	1%	-25%	16%	0%	-33%
3	1%	1%	-25%	19%	0%	-33%
4	-2%	-2%	25%	42%	10%	-33%
5	-1%	-1%	25%	42%	10%	-33%
6	1%	0%	25%	48%	0%	-33%
7	6%	5%	50%	104%	0%	-67%
8	-7%	-7%	100%	115%	30%	-33%
9	1%	-1%	75%	123%	10%	-33%
10	0%	0%	-25%	-8%	0%	-33%
11	0%	0%	-25%	-22%	0%	-33%
12	-2%	-1%	-25%	-32%	0%	-33%
13	-	-	-	-	-	-
14	-666%	-656%	27200%	-29%	310%	22700%
15	-9%	-9%	-25%	0%	-20%	0%
16	-15%	-15%	0%	1%	-10%	0%
17	-29%	-29%	50%	1%	-60%	0%
18	-39%	-39%	0%	4%	-50%	0%
19	-61%	-60%	175%	3%	-100%	200%
20	-76%	-74%	125%	7%	-100%	100%

table 5-7: calculation results of the pile in the first pile row in the Noordwal at the middle section ($x = 0.12 \text{ m}$, $y = 10.44 \text{ m}$)

Biological degradation (modification 1 to 9) at the Noordwal has a larger influence on the horizontal displacement than on the vertical displacement for different stages of biological degradation. The displacement values are higher for more advanced degradation except for the minimum value of the horizontal displacement and the maximum value of the vertical displacement. Looking at the internal forces in the pile cap beam, the normal force in the pile cap beam is the only internal force affected by this set of modifications. Increase of the normal force in the pile cap beam also has an effect on the increase of the shear force and a reduction of the bending moment in the foundation pile.

Gaps in the mortise and tenon joints (modification 10 to 12) results in a few minor changes in the displacement and internal forces of the pile cap beam and the foundation pile. Lateral movement of the pile cap beam leads to an increase of the horizontal displacement, but also to a reduction of the normal

force. Partial decoupling of the pile cap beam from the foundation pile also results in a lowering of the shear force and bending moment in the foundation pile in the first pile row.

The omission of two piles from the middle cross-section (modification 13 and 14) results in immediate failure of the structure as can be deduced from the values of the vertical displacement.

Differential pile settlements (modification 15 to 20) have a negative effect on the maximum value of the horizontal displacement and the minimum value of the vertical displacement. The increase of the latter is quite significant where crosswise and lengthwise settlement results do not show distinct differences. The internal forces in the pile cap beam are not influenced by this type of structural deterioration, but internal forces in the foundation pile are affected. The normal force and the minimum value of the bending moment in the foundation pile are both reduced for all settlement magnitudes where the minimum value of the shear force and the maximum value of the bending moment are increased only for severe settlements.

mod.	Δu_x		Δu_z		Δ		ΔV_z		ΔM_y	
	min.	max.	min.	max.	min.	max.	min.	max.	min.	max.
1	0%	-24%	17%	5%	-7%	52%	0%	-5%	-2%	1%
2	33%	-3%	18%	9%	-9%	14%	0%	-10%	-4%	-3%
3	0%	-4%	0%	20%	-1%	8%	0%	-2%	0%	0%
4	33%	-39%	39%	9%	-12%	92%	0%	-9%	-4%	2%
5	67%	-5%	39%	16%	-17%	29%	0%	-19%	-10%	-8%
6	0%	-3%	1%	45%	-2%	9%	0%	-2%	0%	0%
7	67%	-45%	96%	13%	-20%	151%	0%	-16%	-6%	3%
8	133%	-1%	97%	25%	-30%	57%	1%	-34%	-22%	-19%
9	0%	32%	13%	123%	1%	-14%	0%	-1%	0%	0%
10	0%	1%	0%	0%	0%	0%	0%	0%	0%	0%
11	0%	4%	0%	0%	0%	0%	0%	0%	0%	0%
12	0%	12%	0%	-1%	-2%	2%	0%	-1%	0%	0%
13	0%	-11%	577%	107%	-16%	-5%	0%	-40%	-37%	-20%
14	3533%	905%	47491%	-2%	-1%	2335%	352%	13%	700%	0%
15	0%	0%	7%	2%	-1%	3%	0%	-1%	-1%	0%
16	0%	-1%	0%	8%	0%	5%	0%	-1%	0%	0%
17	0%	-1%	16%	7%	-4%	8%	0%	-5%	-4%	-1%
18	0%	-8%	0%	25%	-2%	14%	0%	-2%	0%	0%
19	0%	-3%	34%	13%	-9%	35%	7%	-10%	-8%	-3%
20	0%	-18%	0%	53%	-4%	29%	0%	-4%	0%	0%

table 5-8: calculation results of the pile cap beam in the Stieltjeskade at the middle section ($y = 9.90 \text{ m}$)

mod.	ΔN		ΔV_z		ΔM_y	
	min.	max.	min.	max.	min.	max.
1	2%	3%	7%	3%	-1%	20%
2	-6%	-6%	-7%	-10%	-14%	0%
3	-5%	-5%	-7%	-10%	-13%	0%
4	4%	5%	7%	3%	-5%	40%
5	-13%	-13%	-21%	-23%	-28%	0%
6	-10%	-10%	-21%	-23%	-26%	0%
7	6%	7%	29%	-3%	-13%	53%
8	-28%	-28%	-36%	-50%	-54%	-27%
9	-23%	-22%	-29%	-43%	-48%	-13%
10	0%	0%	0%	0%	0%	0%
11	0%	0%	0%	0%	0%	0%

12	-1%	-1%	0%	0%	-1%	-7%
13	-	-	-	-	-	-
14	0%	0%	-7%	0%	0%	-7%
15	-2%	-2%	-7%	-3%	-5%	-7%
16	-2%	-2%	-7%	-3%	-4%	-7%
17	-5%	-5%	-14%	-10%	-10%	-13%
18	-4%	-4%	-7%	-7%	-9%	-13%
19	-10%	-10%	-21%	-20%	-19%	-27%
20	-7%	-7%	-21%	-17%	-19%	-20%

table 5-9: calculation results of the pile in the first pile row in the Stieltjeskade at the middle section ($x = 0.33$ m, $y = 9.90$ m)

The influence of biological degradation (modification 1 to 9) on the displacements of timber elements of the Stieltjeskade becomes prevalent in the minimum value of the horizontal displacement and the vertical displacement of the pile cap beam. This effect is absent for lengthwise degradation where exclusively the maximum value of the vertical displacement shows a considerable increase. This phenomenon also comes back in the maximum value of the normal force where the influence of entire and crosswise degradation is much larger than lengthwise degradation. The internal force transfer in the foundation pile in the first pile row is positively influenced by the crosswise and longitudinal biological degradation where degradation over the entire structure leads to an increase of the internal pile forces.

The translation of the pile cap beam in transverse direction due to gaps in the mortise and tenon joints (modification 10 to 12) has no influence on the displacements and internal force transfer mechanisms of the pile cap beam.

The quay wall has a different structural behaviour on the pile cap beam fracture (modification 13 and 14) at both ends. When the piles in the first two pile rows lose their bearing function, the structure is just barely able to function with a large absolute drop in the minimal vertical displacement of 400 mm as stated in appendix 'C.2.10 Structural deficiencies'. Bearing strength loss of the two piles results in a reduction of internal forces in the pile cap beam because of the decreased stiffness in the deteriorated section.

Differential settlements of the foundation piles (modification 15 to 20) have a negative effect on the vertical displacement when crosswise settlement occurs. Lengthwise settlement is detrimental only for the minimum value of the vertical displacement. The influence of this modification in the two quay wall elements is quite different. For the pile cap beam, only the maximum value of the normal force has changed in a negative way. When the foundation pile is considered, all internal forces are reduced for higher values of the settlements.

mod.	Δu_x		Δu_z		ΔN		ΔV_z		ΔM_y	
	min.	max.	min.	max.	min.	max.	min.	max.	min.	max.
1	2%	-6%	-7%	4%	-5%	4%	0%	-1%	-1%	0%
2	0%	-6%	-7%	4%	-8%	2%	0%	-3%	-1%	-2%
3	2%	-6%	21%	0%	-5%	5%	0%	-1%	0%	0%
4	5%	-19%	44%	10%	-8%	8%	0%	-1%	-1%	0%
5	2%	-25%	33%	10%	-16%	4%	0%	-10%	-1%	-5%
6	5%	-25%	44%	-2%	-8%	10%	0%	-1%	1%	0%
7	49%	-88%	102%	33%	-8%	17%	0%	-1%	-1%	0%
8	49%	-94%	49%	33%	-19%	9%	0%	-28%	-1%	-5%
9	5%	-106%	102%	-11%	-8%	22%	1%	-1%	2%	0%

10	0%	-19%	0%	0%	0%	-3%	0%	0%	0%	0%
11	2%	-56%	0%	1%	0%	-8%	0%	-1%	0%	0%
12	7%	-131%	-2%	2%	0%	-23%	0%	-2%	0%	-2%
13	37%	88%	3300%	26%	-100%	-90%	8%	-56%	14%	5%
14	49%	244%	1984574%	-84%	6%	-100%	-100%	37%	809%	-23%
15	2%	-6%	91%	-7%	-11%	1%	0%	-9%	0%	-5%
16	5%	-38%	93%	0%	-5%	3%	0%	-2%	0%	0%
17	2%	-6%	219%	-15%	-21%	3%	0%	-18%	0%	-5%
18	10%	6%	200%	1%	-10%	7%	0%	-4%	0%	1%
19	7%	-6%	474%	-31%	-37%	4%	0%	-32%	0%	-5%
20	20%	19%	398%	1%	-21%	13%	0%	-8%	0%	1%

table 5-10: calculation results of the pile cap beam in the Toussaintkade at the middle section ($y = 10.00$ m)

mod.	ΔN		ΔV_z		ΔM_y	
	min.	max.	min.	max.	min.	max.
1	-1%	0%	-5%	-15%	-18%	0%
2	-3%	-2%	-8%	-15%	-18%	-4%
3	-1%	0%	-5%	-15%	-18%	0%
4	-1%	-1%	-8%	-31%	-36%	-4%
5	-9%	-9%	-16%	-31%	-45%	-11%
6	-1%	-1%	-8%	-31%	-36%	-4%
7	-1%	-1%	-8%	-54%	-55%	-4%
8	-27%	-27%	-30%	-62%	-64%	-29%
9	-1%	-1%	-8%	-54%	-64%	-4%
10	0%	0%	0%	0%	0%	0%
11	-1%	-1%	0%	0%	0%	0%
12	-2%	-2%	0%	8%	9%	-4%
13	-	-	-	-	-	-
14	-19%	-19%	6%	31%	27%	-7%
15	-9%	-9%	-11%	0%	0%	-18%
16	-2%	-2%	-5%	0%	0%	-7%
17	-17%	-18%	-21%	0%	0%	-32%
18	-4%	-4%	-10%	8%	9%	-18%
19	-31%	-31%	-37%	8%	0%	-57%
20	-8%	-8%	-21%	15%	18%	-39%

table 5-11: calculation results of the pile in the first pile row in the Toussaintkade at the middle section ($x = 0.29$ m, $y = 10.00$ m)

Biological degradation (modification 1 to 9) at the Toussaintkade has the largest negative effect on the minimum value of the vertical displacement and the largest positive effect on maximum value of the horizontal displacement for all degradation patterns. The minimum value of the horizontal displacement and the maximum value of the vertical displacement are not affected significantly. Internal forces in the pile cap beam also remain more or less the same which is not the case for the foundation pile. The largest changes are the reduction of the maximum value of the shear force and the reduction of the minimum value of the bending moment for all different degradation patterns.

A horizontal shift of the pile cap beam on the foundation piles as a result of gaps in the mortise and tenon joints (modification 10 to 12) has only a small positive effect on the maximum value of the horizontal displacement.

Pile cap beam fracture (modification 13 and 14) results in very large values for the displacements, especially the minimum value of the vertical displacements. Removal of the pile bearing function of the piles in the first two rows does not lead immediately to quay wall failure, but it definitely results into stability problems. This follows from the absolute value of 150 mm for the vertical displacement as deduced from appendix 'C.2.10 Structural deficiencies'. The relative percentages given in the table above indicate that the structure is not able to function anymore when the piles in the last two rows are omitted from the model.

Differential pile settlements (modification 15 to 20) have the greatest influence on the pile cap beam by the vertical displacement. The table shows quite large negative changes of the minimum value for this base quantity. The other base quantities at the pile cap beam are not altered significantly. The impact of settlements on the internal forces in the foundation pile is in general favourable when the normal force, minimum value of the shear force, and the maximum value of the bending moment are considered.

5.4 INTERPRETATION OF RESULTS

In the previous paragraph, the calculation results are given for the effects of various quay wall defects on the structure where the most remarkable outcomes were highlighted in the text. From these results, a few general statements can be composed. They are given in the following enumeration:

1. Biological degradation has the greatest influence on the vertical displacement but its influence varies along the different quay wall compositions. Structures with a lot of pile rows (Boompjeskade and Stieltjeskade) are very susceptible to entire and crosswise degradation, but those structures seem to be insensitive to biological degradation in longitudinal quay wall direction because the stiffer components at the other pile rows take over a part of the load. The other quay wall structures (Haringvliet, Noordwal, and Toussaintkade) show a lower magnitude of vertical displacements, but this peculiarity can be assigned to the total number of piles that are possibly affected by biological degradation. Longitudinal degradation is more prevalent for those structures because relatively more piles are exposed to this pattern of degradation. Another base quantity clearly influenced by degradation is the shear force in the pile cap beams. For the Boompjeskade and Stieltjeskade, the large number of piles in combination with the short pile spacings results in the ability of force redistribution when some parts are becoming more flexible compared to others. This phenomenon is not visible for the other quay wall structures because they are supported by a smaller number of piles.
2. The shift of the pile cap beam has in a few cases only a minor influence on the base quantities of the pile cap beam and the foundation pile, but in general no major changes are observed for the quay wall structures.
3. Fracture of the pile cap beam results in significant changes of displacements and internal force distributions. The quay wall structures with a numerous amount of pile rows (Boompjeskade and Stieltjeskade) are still able to function after this local structural failure, but still are severely deteriorated by this occurrence. The quay wall structures with a limited amount of pile rows (Noordwal and Toussaintkade) are not able to resist this structural issue and so will fail immediately. In this case the structures lose their retaining function. The Haringvliet with its three pile rows is an exception to the above-mentioned cases because it is still able to function after a pile cap beam fracture. Probably the arch effect in combination with the dense pile grid are reasons for force redistributions after local disturbances showed up.
4. Differential settlements could result in problems related to the structural integrity, especially when vertical displacements are considered. The Boompjeskade and Stieltjeskade are not

affected a lot by a change in the axial pile stiffness because the neighbouring piles acquire a greater part of the total load share compared to the weakened piles. This capability cannot be activated in quay wall structures with a small number of pile rows (Haringvliet, Noordwal, and Toussaintkade), so large vertical displacements appear when the structures are subjected to differential settlements. Besides those differences between the two types of structural compositions, the Haringvliet shows a noteworthy reduction on the minimum values for the shear force. This remarkable feature is possibly caused by the arch effect in the quay wall structure in combination with a dense pile grid.

The general considerations given above can also be supplemented with a quantitative analysis of the calculation results. For the selected quay wall structures, a relation could be searched between the differences in structural properties and a certain base quantity. Examples of appropriate structural characteristics for the comparison of the structures with each other are the number of pile rows and the pile distances in longitudinal direction. Both properties are identifiable for all types of quay wall structures, so no assumptions have to be made in the structural analysis. To limit the amount of work, only one base quantity is selected. The minimum value of the horizontal displacement seems to be the most suitable parameter because its magnitude reveals the condition of the structure. A larger value for the horizontal outward deviation implies a worsened structural integrity. In figure 5-14, diagrams are made with the minimum horizontal displacements of the pile cap beam from table 5-2, table 5-4, table 5-6, table 5-8, and table 5-10. Absolute values higher than 150% for the relative differences are omitted from the graphs to keep a clear overview on the results.

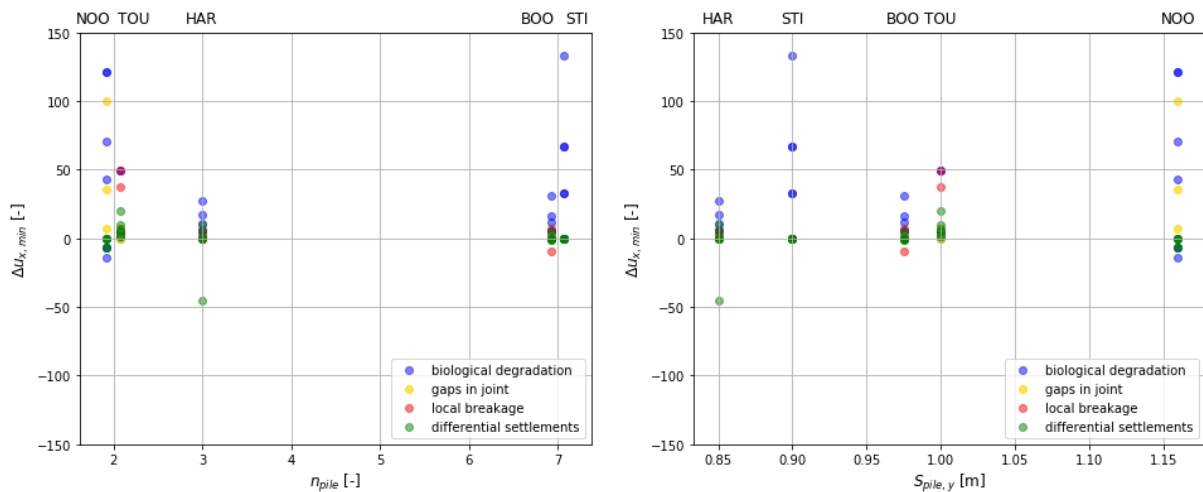


figure 5-14: comparison of the quay walls for the maximum value of the horizontal displacement; left: number of pile rows, right: pile distances in longitudinal direction

Analysis of the comparison between both plots does not lead to clear relations for the variable quay wall dimensions. Biological degradation has a large positive influence on the Noordwal and Stieltjeskade and is limited for the other quay wall structures. The two structures have a different number of pile rows and distances between the piles, so no correlation for biological degradation can be found. The same conclusion can be drawn for the gaps in the joint and the subsequent pile cap beam shift in longitudinal quay wall direction. This type of modification is prevalent for only one quay wall structure at the Noordwal, so no relation is possible here. The application of local pile cap beam fracture causes large changes of the internal force transfer mechanisms inside the quay wall elements with very large relative differences for the horizontal displacement as a result. Those values are not included in above graphs which leads to an incomplete set of datapoints for some of the quay wall structures. It prevents

the possibility for a relation between the base quantity and the chosen parameter. Differential settlement has no large influences on the horizontal displacement of the structures, so they remain more or less constant for a variable number of pile rows and pile distances in the direction along the quay wall structure.

“After the considerations in the previous chapters, finally the research question can be answered. A few simplifications were made during the composition of this report which also can be used as starting points for new master thesis topics or continuation of the study towards deterioration of historic quay walls.”



Conclusions and recommendations

In the final chapter of this report, the theoretical studies and calculations are discussed that were performed during the master thesis. In paragraph ‘6.1 Conclusions’, conclusions are drawn from the theoretical studies and calculations that were elaborated during the master thesis. Due to a limited amount of time to perform this research, a few simplifications were made to speed up the work. These limitations are mentioned in paragraph ‘6.2 Recommendations’ accompanied with opportunities for upcoming research projects which can contribute to a better understanding about the structural declination of quay walls.

6.1 CONCLUSIONS

In paragraph ‘1.2 Research question’ a few sub questions are composed which are needed to answer the main question. Each of them is answered briefly below.

1. What are the characteristics of a historic quay wall in the Netherlands?

Historic quay wall structures in the Netherlands have a similar setup. A retaining wall composed of brick or rubblestone is supported on a timber framework of floor elements, pile cap beams, and foundation piles. When the horizontal forces are substantially large, batter piles are needed to transfer these forces to the subsoil. These batter piles are often placed in between the main pile rows and connected to the pile cap beams with cross-beams. The foundation piles are commonly attached to the pile cap beams and cross-beams with mortise and tenon joints.

2. Which conditions/factors influence the degradation of wooden foundation elements?

The microscopical structure of wood can be influenced by chemical degradation, mechanical degradation, and biological degradation where the last two has the biggest impact. Degradation by mechanical factors is captured in a modification factor where also the influence of load duration and ambient conditions are incorporated. Biological degradation describes the deterioration of wood material by organisms like bacteria, fungi, and insects. For an inner-city quay wall, exclusively degradation by bacteria and fungi is relevant. The rate of bacterial degradation is quite slow, but the wood attacking micro-organisms excel in very extreme conditions far deep into the subsoil. Fungi are way more devastating for timber elements but they need sufficient amounts of oxygen to stay active. Fungal degradation becomes only detrimental in the situations where timber elements are exposed to the air in a humid environment for a long cumulative period. From several studies to retrieved samples of foundation piles, it was found out that bacterial decay is present in all foundation elements older

than 100 years old. Pine and alder are more prone to degradation than spruce, and large differences in the degree of degradation are found between the Dutch cities which implicates that local conditions play a role.

3. What are the force transfer mechanisms in a timber pile foundation from the ground level to the subsoil?

A timber structure is loaded by a variety of forces ranging from permanent loads to extreme loads. The structural composition and the applied loading cases determine the structural response. Piles in compression are resisted by tip and shaft resistances and subjected to an additional load in the form of negative skin friction. The depth of the neutral plane in the subsoil determines the magnitude of the friction forces. This depth of the neutral plane depends on the soil settlements and pile displacements. Piles loaded by a tensile force are resisted only by shaft friction. Besides axial resistances, foundation piles can also be loaded in lateral direction. The available computation time and the desired precision of the outcomes are the most decisive aspects in the decision for the most appropriate calculation model.

4. How can deficiencies be incorporated in a structural model?

Before quay wall defects can be applied, the quay wall must be captured as good as possible in a structural model to approach the actual behaviour of the structure. The set of applied deficiencies is based on the most common problems found by quay wall observations. Those are transformed into parametrical model adaptations, so the structural response to those deficiencies can be simulated.

5. Which conclusions can be drawn from the calculation results?

The influence of quay wall defects strongly depends on the composition of the quay wall. When the quay wall is equipped with a large number of pile rows, local effects like pile cap beam fracture and differential settlements have minor influence on the structural response than quay walls with two or three pile rows. A reason for this difference is a possible redistribution of forces when a part of the structure has declined. This degree of distribution increases when piles at the weakened spot are relieved by a larger number of piles. A more global effect like biological degradation has a bigger impact for quay walls with large numbers of piles because more piles are affected in this case. No relations could be found between the quay wall structures when the modification results were compared with each other on the number of pile rows and pile distances in the longitudinal quay wall direction. One of the reasons for this outcome is the limited number of investigated quay wall structures. A higher number of calculations gives a more complete dataset with results for the comparison of structures at a single parameter. Another explanation for the lack of relations is the high variety in different compositions, so the comparison is not always fair in terms of structural properties.

6.2 RECOMMENDATIONS

For the provision of an answer to the research question, not all aspects regarding this subject could be treated due to a limited amount of time. In the enumeration given below, simplifications in the used approach are highlighted. Those aspects could be used for the expansion towards a more sophisticated research project or used as a starting point for a new master thesis subject.

1. The used lateral soil model was quite simple. To increase the accuracy of the lateral pile behaviour calculation, more sophisticated models like Plaxis 3D that incorporate layered soil systems, rotational stiffness of the pile cap, and continuity in the horizontal soil movement of the separate layers.

2. A limited number of quay wall defects was used in the structural models. To gain more insight into deterioration of structures, more deficiencies like variations in element stiffness, rotational stiffness, and uneven loading in longitudinal quay wall direction can be applied. Also the mentioned defects in this report can be combined together in one model.
3. Only structural failure mechanisms are considered in this report, but a quay wall could fail in numerous other ways. Examples are geotechnical failure like piping or slope instability, structural instability like horizontal sliding or overturning of the retaining wall, and vertical uplift.
4. For the joints between the pile cap beam and the foundation piles, a linear relation for the rotational rigidity is considered. The joint rotation directly responds to an applied load and the ratio between both quantities remains constant for higher loads. In reality, the pile is not connected perfectly to the pile cap beam due to the presence of gaps and other imperfections in the joint. For a more realistic structural behaviour, a nonlinear relation for the joint stiffness is needed.
5. The external loads specified in this thesis report can be assigned to permanent or quasi-static load classes, but a quay wall structure is usually loaded by more different loads. Examples are dynamic loads like the acceleration or deceleration of traffic and wave loading or extreme loads like ship collisions. Incorporation of these loads in a structural model could lead to more realistic outcomes.

Bibliography

- Algemeen Dagblad. (2013, October 15). *Deel kademuur van Utrechtse gracht ingestort*. <https://www.ad.nl/utrecht/deel-kademuur-van-utrechtse-gracht-ingestort-aa5f82c7/>
- ArcGIS. (n.d.). [ArcGIS map of the Noordwal]. Retrieved March 27, 2021, from <https://arcg.is/1uPaOq>
- ArcGIS. (n.d.). [ArcGIS map of the Toussaintkade]. Retrieved March 27, 2021, from <https://arcg.is/04Lqfj>
- Backhausen, U., Van der Stoel, A.E.C. (2014). *Reader geotechniek voor het HBO*. KIVI.
- BACPOLES. (2005). *Preserving cultural heritage by preventing bacterial decay of wood in foundation piles and archaeological sites*. European Commission.
- Bewonersraad Nieuwmarkt Groot Waterloo. (2019, April 11). *Noodmaatregel*. <https://www.bewonersraad1011.amsterdam/noodmaatregel/>
- Blanchette, R.A., Nilsson, T., Daniel, G., Abad, A. (1990). Biological degradation of wood. In Rowell R.M., Barbour, R.J. (Eds.). *Archaeological wood: Properties, chemistry, and preservation*, 141–174. American Chemical Society.
- Blaß, H.J., Sandhaas, C. (2017). *Timber engineering: Principles for design*. KIT.
- Bowles, J.E. (1997). *Foundation Analysis and Design* (5th ed.). McGraw–Hill.
- Boussinesq, J. (1885). *Application des potentiels: À l'étude de l'équilibre et du mouvement des solides élastiques*. Gauthier–Villars.
- Budhu, M. (2011). *Soil mechanics and foundations*. John Wiley & Sons Inc.
- Caudullo, G., Tinner, W., De Rigo, D. (2016). *Picea abies* in Europe: Distribution, habitat, usage, and threats. In San–Miguel–Ayán, J., De Rigo, D., Caudullo, G., Houston Durrant, T., Mauri, A. (Eds.). *European atlas of forest tree species*, 114–116. Publications Office of the European Union.
- Cherqaoui, I. (2006). *Door grond horizontaal belaste palen* [Master thesis, Delft University of Technology]. Repository TU Delft. <http://resolver.tudelft.nl/uuid:91707307-f014-458e-88ce-2eecac1ab452>
- Clausen, C.A. (1996). Bacterial associations with decaying wood: A review. *International Biodeterioration & Biodegradation*, 101–107. [https://doi.org/10.1016/0964-8305\(95\)00109-3](https://doi.org/10.1016/0964-8305(95)00109-3)
- Coulomb, C.A. (1776). Essai sur une application des règles de maximis et minimis à quelques problèmes de statique: Relatifs à l'architecture. *Mémoires de Mathématique de l'Académie Royale de Science*, 7, 343–382.
- CUR 166. (2014). *Damwandconstructies (deel 1)*. SBRCURnet.
- CUR 211E. (2005). *CUR-report 211E: Handbook quay walls*. SBR.
- Daily Civil. (2018, October 27). *Unit weight of building materials*. <https://dailycivil.com/unit-weight-building-materials/>
- Das, B.M., Sobhan, K. (2014). *Principles of geotechnical Engineering* (8th ed.). Cengage Learning.

- De Gijt, J.G. (2010). *A history of quay walls: Techniques, types, costs and future* [Doctoral thesis, Delft University of Technology]. Repository TU Delft. <http://resolver.tudelft.nl/uuid:d62bbff8-e805-434a-893e-08940d58ae8c>
- De Gijt, J.G., Grotegoed, D., Roubos, A.A. (2014). *Binnenstedelijke kademuren*. SBRCURnet.
- De Vree, J. (2020, August 14). *Hakkelbout*. <https://www.joostdevree.nl/shtmls/hakkelbout.shtml>
- Descamps, T., Guerlement, G. (2009). Component method for the assessment of the axial, shear and rotational stiffness of connections in old timber frames. In Z. Zrikem et al. (Eds.), *Proceedings of the 9ème congrès national de mécanique Marrakech*, 268–270.
- Departement Mobiliteit & Openbare Werken. (2018). *Ontwerp, studie en berekeningsnota's*. Vlaamse overheid.
- DINOloket. (2017, January 14). [Cone penetration test at the Boompjeskade]. <https://www.dinoloket.nl/ondergrondgegevens>
- DINOloket. (2017, January 14). [Cone penetration test at the Haringvliet]. <https://www.dinoloket.nl/ondergrondgegevens>
- DINOloket. (2010, June 10). [Cone penetration test at the Noordwal]. <https://www.dinoloket.nl/ondergrondgegevens>
- DINOloket. (2017, January 13). [Cone penetration test at the Stieltjeskade]. <https://www.dinoloket.nl/ondergrondgegevens>
- DINOloket. (2010, June 11). [Cone penetration test at the Toussaintkade]. <https://www.dinoloket.nl/ondergrondgegevens>
- DINOloket. (1992, December 14). [Ground water well at the Boompjeskade]. <https://www.dinoloket.nl/ondergrondgegevens>
- DINOloket. (1992, December 14). [Ground water well at the Haringvliet]. <https://www.dinoloket.nl/ondergrondgegevens>
- DINOloket. (1969, December 14). [Ground water well at the Noordwal]. <https://www.dinoloket.nl/ondergrondgegevens>
- DINOloket. (1989, November 14). [Ground water well at the Stieltjeskade]. <https://www.dinoloket.nl/ondergrondgegevens>
- DINOloket. (1993, December 16). [Ground water well at the Toussaintkade]. <https://www.dinoloket.nl/ondergrondgegevens>
- Drdácký, M., Wald, F., Mareš, J. (1999). Modelling of real historic timber joints. *Transactions on the Built Environment*, 39, 169–178.
- Duan, A., Zhang, S., Zhang, X., Zhang, J. (2016). Development of a stem taper equation and modelling the effect of stand density on taper for Chinese fir plantations in Southern China. *PeerJ*, 4(4), 1–25. <https://doi.org/10.7717/peerj.1929>
- Esser, P.M., Buitenkamp, H.S. (1996). *Laboratoriumonderzoek naar de invloed van grondwaterstandverlaging op de conditie van houten horizontaal geplaatste elementen in funderingen*. TNO Research.

- F3O/SBRCURnet. (2016). *Richtlijn houten paalfunderingen onder gebouwen: Onderzoek en beoordeling* (3rd ed.). Author.
- Gemeente Amsterdam. (2019). *Actieplan bruggen en kademuuren*. Author.
- Gemeente Amsterdam. (2020). *Herstellen en verbinden: Bouwen aan het fundament van de stad*. Author.
- Gemeente Rotterdam. (2018). *Prioriteiten en indicatoren*.
<https://begroting2018.rotterdam.nl/p162912/prioriteiten-en-indicatoren>
- Geostart. (n.d.). [Geostart map of the Boompjeskade]. Retrieved March 27, 2021, from
<https://maps.rotterdam.nl/embed/rwkwfbt>
- Geostart. (n.d.). [Geostart map of the Haringvliet]. Retrieved March 27, 2021, from
<https://maps.rotterdam.nl/embed/vvggabg>
- Geostart. (n.d.). [Geostart map of the Stieltjeskade]. Retrieved March 27, 2021, from
<https://maps.rotterdam.nl/embed/icfvfmg>
- Google. (n.d.). [Google Maps Street View photos of the Boompjeskade]. Retrieved March 27, 2021, from
<https://goo.gl/maps/4d8vmdfq2XVxe2bv5>
- Google. (n.d.). [Google Maps Street View photos of the Haringvliet]. Retrieved March 27, 2021, from
<https://goo.gl/maps/gVw7qTcq1L3WthSr6>
- Google (n.d.). [Google Maps Street View photos of the Noordwal]. Retrieved March 27, 2021, from
<https://goo.gl/maps/t63nEB84yy9Bbm6p6>
- Google (n.d.). [Google Maps Street View photos of the Stieltjeskade]. Retrieved March 27, 2021, from
<https://goo.gl/maps/PyB5rGxYjghgbDGY6>
- Google (n.d.). [Google Maps Street View photos of the Toussaintkade]. Retrieved March 27, 2021, from
<https://goo.gl/maps/H3Ph7JXz66xs4D8s8>
- Hartsuiker, C., Welleman, J.W. (2016). *Engineering Mechanics: Volume: Stresses, strains, displacements*. Springer.
- Hetenyi, M. (1946). *Beams on elastic foundation: Theory with applications in the fields of civil and mechanical engineering*. University of Michigan Press.
- Hicks, M.A., Brinkgreve, R.B.J., Rohe, A. (2014). *Numerical methods in geotechnical engineering* (1st ed.). CRC Press.
- Houtinfo.nl. (2013). *Houtaantastingen: Deel 1*. Centrum Hout.
- Ingenieursbureau Amsterdam. (2016). *Vervanging kademuur Toussaintkade te Den Haag: VO ontwerpverantwoording*. Gemeente Amsterdam.
- Ingenieursbureau Den Haag. (2016). *Kademuur Noordwal (Torenstraat–Hemhuisterweg): Alternatieven vervangingsmethode van de kademuur aan de Noordwal*. Gemeente Den Haag.
- Istemi. (2014, February 11). *Valutazione del modulo elastico tramite Pilodyn*.
<http://www.istemi.it/prodotto/legno/valutazione-del-modulo-elastico-tramite-pilodyn/dde61838fc5560894d40fff6fc4d3037>

- Jáky, J. (1936). Stability of earth slopes. *Proceedings of the International Conference on Soil Mechanics*, 2, 125–129.
- Jarquio, R. (1981). Total lateral surcharge pressure due to strip load. *ASCE Journal of Geotechnical Engineering*, 107(10), 1424–1428. <https://doi-org.tudelft.idm.oclc.org/10.1061/AJGEB6.0001197>
- Jonkman, S.N.; Steenbergen, R.D.J.M.; Morales-Nápoles, O.; Vrouwenvelder, A.C.W.M.; Vrijling, J.K. (2017). *Probabilistic design: risk and reliability analysis in civil engineering*. Delft University of Technology.
- Jorissen, A. (1995). *Modificatie vochtgehalte en duurbelasting: Technische houtdocumentatie A 4/2–010210*. Centrum Hout.
- Kempfert, H.-G., Eigenbrod, K.D., Smoltczyk, U. (2002). Pile foundations. In Smoltczyk, U. (Ed.). *Geotechnical engineering handbook*, 83–227. Ernst & Sohn.
- Klaassen, R.K.W.M., Creemers, J.G.M. (2005). Wooden foundation piles and its underestimated relevance for cultural heritage. *Journal of Cultural Heritage*, 13, 123–128. <https://doi.org/10.1016/j.culher.2012.02.014>
- Klaassen, R.K.W.M. (2008). Bacterial decay in wooden foundation piles—Patterns and causes: A study of historical pile foundations in the Netherlands. *International Biodeterioration & Biodegradation*, 61, 45–60. <https://doi.org/10.1016/j.ibiod.2007.07.006>
- Klaassen, R.K.W.M., Den Nijs, P.J.M, Van Beusekom, G.W. (2000). *Bacteriële aantasting van houten paalfunderingen: Literatuurstudie en inventarisatie van de Nederlandse situatie* (2nd ed.). VROM.
- Kirker, G., Wynandy, J. (2014). Above ground deterioration of wood and wood-based materials. In Schultz, T.P., Goodell, B., Nicholas, D.D. (Eds.). *Deterioration and protection of sustainable biomaterials*, 113–129. American Chemical Society.
- Koppejan, A.W., Van Mierlo, J.C. (1952). *Lengte en draagvermogen van heipalen*. *Bouw*, 3.
- r, H. Reese, L.C. (1956). Non-dimensional Solutions for Laterally Loaded Piles with Soil Modulus Assumed Proportional to Depth. *Proceedings of 8th Texas conference on soil mechanics and foundation engineering*, 1–41.
- Meireman, P. (2016). *Basiscursus grondmechanica 2016* [Powerpoint slides]. Expertgroep Grondmechanica & Funderingstechniek. <https://docplayer.nl/47995818-Grondmechanica-draagvermogen-van-paalfunderingen-paul-meireman-7-december.html>
- Ménard, L., Bourbon, G., Gambin, M. (1971). Méthode générale de calcul d'un rideau ou d'un pieu sollicité horizontalement en fonction des résultats pressiométriques. *Sol-Soils*, 6, 357–377.
- Molenaar, W., Voorendt, M.Z. (2017). *Manual hydraulic structures*. Delft University of Technology.
- Moore, J., Gardiner, B., Sellier, D. (2018). Tree mechanics and wind loading. In Geitmann, A., Gril, J. (Eds.). *Plant biomechanics: from structure to function at multiple scales*, 79–106. Springer.
- Moussa, A., Christou, P. (2018). The evolution of analysis methods for laterally loaded piles through time. In M. Abu-Farsakh et al. (Eds.). *Proceedings of the 1st GeoMEast international congress and exhibition*, 65–94. https://doi.org/10.1007/978-3-319-61642-1_7

- NEN-EN 1990 (NB). (2011). *Nationale bijlage bij NEN-EN 1990+A1+A1/C2: Eurocode: Grondslagen van het constructief ontwerp*. Nederlands Normalisatie-instituut.
- NEN-EN 1991-1-1. (2019). *Eurocode 1: Belastingen op constructies – Deel 1-1: Algemene belastingen – Volumieke gewichten, eigen gewicht en gebruiksbelastingen voor gebouwen*. Nederlands Normalisatie-instituut.
- NEN-EN 1995-1-1. (2011). *Eurocode 5: Ontwerp en berekening van houtconstructies – Deel 1-1: Algemeen – Gemeenschappelijke regels en regels voor gebouwen*. Nederlands Normalisatie-instituut.
- NEN-EN 1995-1-1 (NB). (2013). *Nationale bijlage bij NEN-EN 1995-1-1+C1+A1 Eurocode 5: Ontwerp en berekening van houtconstructies – Deel 1-1: Algemeen - Gemeenschappelijke regels en regels voor gebouwen (inclusief NEN-EN 1995-1-1+C1+A1/C1:2012)*. Nederlands Normalisatie-instituut.
- NEN-EN 1997-1. (2016). *Geotechnisch ontwerp – Deel 1: Algemene regels*. Nederlands Normalisatie-instituut.
- NEN-EN 1997-1 (NB). (2019). *Nationale bijlage bij NEN-EN 1997-1 Eurocode 7: Geotechnisch ontwerp – Deel 1: Algemene regels*. Nederlands Normalisatie-instituut.
- NEN-EN 384. (2018). *Hout voor constructieve toepassingen: Bepaling van karakteristieke waarden van mechanische kenmerken en dichtheid*. Nederlands Normalisatie-instituut.
- NEN 8707. (2018). *Becoördeling van de constructieve veiligheid vaneen bestaand bouwwerk bij verbouw en afkeur: Geotechnische constructies*. Nederlands Normalisatie-instituut.
- Nichols, J., Totoev, Y.Z. (1997). Experimental determination of the dynamic modulus of elasticity of masonry units. In M. Wu et al. (Eds.). *Proceedings of the 11th international brick/block masonry conference*, 1, 1–6
- NOS. (2018, March 3). *Kademuur stort in, deel van Amsterdam uren zonder water*. <https://nos.nl/artikel/2220358-kademuur-stort-in-deel-van-amsterdam-uren-zonder-water.html>
- NOS. (2020, September 1). *Kademuur in centrum Amsterdam deels ingestort*. <https://nos.nl/artikel/2346286-kademuur-in-centrum-amsterdam-deels-ingestort.html>
- Ounekham, K. (2009). *Developing volume and taper equations for Styrax tonkinensis in Laos* [Master thesis, University of Canterbury New Zealand]. UC research repository. <http://hdl.handle.net/10092/3450>
- Poulos, H.G. (1973). *Analysis of piles in soil undergoing lateral movement*. *Journal of the soil mechanics and foundations division*, 99(5), 391–406. <https://doi-org.tudelft.idm.oclc.org/10.1061/JSFEAQ.0001879>
- Profound. (2018, February 24). *Houthardheidsmetingen de Specht*. <https://www.profound.nl/houthardheidsmetingen/?lang=nl>
- Rankine, W. (1857). On a stability of loose earth. *Philosophical Transactions of the Royal Society of London*, 147, 9–27.
- Reese, L.C. (1997). *Analysis of Laterally Loaded Piles in Weak Rock*. *Journal of geotechnical and geoenvironmental engineering*, 123(11), 1010–1017. [https://doi-org.tudelft.idm.oclc.org/10.1061/\(ASCE\)1090-0241\(1997\)123:11\(1010\)](https://doi-org.tudelft.idm.oclc.org/10.1061/(ASCE)1090-0241(1997)123:11(1010))

- Reissner, E. (1958). A note on deflections of plates on a viscoelastic foundation. *Journal of applied mechanics*, 25(1), 144–145.
- Rijkswaterstaat. (2020). *Richtlijnen vaarwegen 2020*. Author.
- Rocscience. (2018). *Laterally loaded piles*. Author.
- Ruigrok, J.A.T. (2010). *Laterally loaded piles: Models and measurements* [Master thesis, Delft University of Technology]. Repository TU Delft. <http://resolver.tudelft.nl/uuid:dbcf881e-9cdb-4689-9dbf-018b098d7481>
- Sas, F. (2007). *De houten paalfundering doorgezaagd: Rekenen aan een sterk verouderde houten paalfundering*. Gemeente Amsterdam stadsdeel Zuid.
- Schreurs, E. (2017). *Deterioration of timber pile foundations in Rotterdam* [Master thesis, Delft University of Technology]. Repository TU Delft. <http://resolver.tudelft.nl/uuid:10ae5bfb-cbb6-4544-a50f-ae76818784dd>
- Sharma, M., Oderwald, R.G. (2001). Dimensionally compatible volume and taper equations. *Canadian Journal of Forest Research*, 31(5), 797–803. <https://doi-org.tudelft.idm.oclc.org/10.1139/x01-005>
- Sharma, M., Zhang, S.Y. (2004). Variable–exponent taper equations for jack pine, black spruce, and balsam fir in Eastern Canada. *Forest Ecology and Management*, 198(1–3), 39–53. <https://doi.org/10.1016/j.foreco.2004.03.035>
- SHR. (2015, August 20). *Witrot*. <https://www.shr.nl/witrot>
- Simmons, E.A., Morgan, T.A., Berg, E.C., Hayes, S.W. Christensen, G.A. (2016). *Logging utilization in Oregon and Washington, 2011–2015*. United States Department of Agriculture.
- Singh, A.P., Kim Y.S., Singh, T. (2016). Bacterial degradation of wood. In Kim, Y.S., Funada R., Singh A.P. (Eds.). *Secondary Xylem Biology* (1st ed.), 169–190. Academic Press.
- Sutter, H.–P. (1997). *Holzschädlinge an kulturgütern erkennen und bekämpfen: Handbuch für denkmalpfleger, restauratoren, konservatoren, architekten und holzfachleute*. Haupt Verlag Ag.
- Terzaghi, K. (1943). *Theoretical soil mechanics*. John Wiley & Sons Inc.
- Tomlinson, M., Woodward, J. (2008). *Pile design and construction practice* (5th ed.). Taylor & Francis.
- USACE. (1994). *Design of sheet pile walls*. Author.
- Van Baars, S, Rica, S., De Nijs, G.A., De Nijs, G.J.J., Riemens, H.J. (2018). Dutch field tests validating the bearing capacity of Fundex piles. In Hicks, M.A., Pisanò, F., Peuchen, J. (Eds.). *Cone penetration testing 2018*, 101–107. CRC Press.
- Van Etten, B.D., Van de Kuilen, J.W.G., Den Nijs, P.J.M. (2000). *Schimmelaantasting in houten funderingspalen: Een literatuurstudie en inventarisatie van de Nederlandse situatie*. VROM.
- Van Tol, F. (1994). *Funderingstechnieken*. Delft University of Technology.
- Van Tol, F., Stoevelaar, R., Rietdijk, J. (2010). *Draagvermogen van geheide palen in internationale context*. *Geotechniek*, 14(5), 4–9.
- Veldhuyzen, C.J. (1963). *Het verbruik van houten heipalen in Nederland*. Landbouweconomisch Instituut.
- Verruijt, A. (2012). *Soil mechanics*. Vssd.

- Vogel, S. (1994). *Life in moving fluids: The physical biology of flow* (2nd ed.). Princeton University Press.
- Vollsinger, S., Mitchell, S.J., Byrne, K.E., Novak, M.D., Rudnicki, M. (2005). Wind tunnel measurements of crown streamlining and drag relationships for several hardwood species. *Canadian Journal of Forest Research*, 35, 1238–1249. <https://doi.org/10.1139/X05-051>
- VROM. (2003). *Protocol voor het uitvoeren van een funderingsinspectie aan houten paalfunderingen*. Author.
- Winkler, E. (1867). *Die lehre von der elastizität und festigkeit mit besonderer rücksicht auf ihre anwendung in der technik für polytechnische schulen, bauakademien, ingenieure, maschinenbauer, architecten, etc.* Dominicius.
- Zeevaert, L. (1962). Dynamic design and behaviour of friction piles: Compensated foundations. *De Ingenieur*, 25, 163–170.

Appendices

List of figures

figure A-1: example of the determination of soil stresses.....	A.2
figure A-2: stresses on a soil element (Verruijt, 2012).....	A.2
figure A-3: terms in the Boussinesq expressions (Bowles, 1997).....	A.3
figure A-4: vertical force spreading in the subsoil; left: circular loading pattern at a soil depth of 2 m, right: flattening of the stress curves for an increasing soil depth.....	A.4
figure A-5: theoretical model based on Terzaghi's expressions for a line load; left: elevation view, right: plan view (USACE, 1994).....	A.5
figure A-6: load spreading by a force application at a distance $a \leq 0.4H$ from the retaining wall.....	A.6
figure A-7: load spreading by a force application at a distance $a > 0.4H$ from the retaining wall.....	A.6
figure A-8: influence of the location of the point load on the horizontal soil response.....	A.7
figure A-9: radial stress as a result of a vertical strip load (Das & Sobhan, 2014).....	A.7
figure A-10: theoretical model based on Terzaghi's expressions for a strip load (USACE, 1994).....	A.8
figure A-11: load spreading under the influence of a strip load.....	A.8
figure A-12: approximation of the distributed vertical load by a Riemann sum.....	A.10
figure A-13: approximation of the distributed horizontal load by a Riemann sum.....	A.10
figure A-14: tree sections for processing to timber products (dbh = diameter at breast height, dob = diameter outside bark) (Simmons et al., 2016).....	A.12
figure A-15: varying diameter along the stem axis for different tree heights.....	A.12
figure A-16: comparison of taper functions.....	A.13
figure A-17: determination of the pile resistance with a CPT–diagram (Backhausen & Van der Stoel, 2014).....	A.14
figure A-18: numerical calculations of positive shaft friction force over the soil depth.....	A.16
figure A-19: negative skin friction for a single pile (NEN–EN 1997–1 (NB) figure 7.a, 2019).....	A.18
figure A-20: negative skin friction for a pile group (NEN–EN 1997–1 (NB) figure 7.b, 2019).....	A.19
figure A-21: comparison requirement with internal friction angle values for timber piles.....	A.20
figure A-22: comparison of slip method with Zeevaert–De Beer expression.....	A.20
figure A-23: relation between the ratio of the actual and the maximum pile tip bearing force with the pile tip settlement (NEN–EN 1997–1 (NB) figure 7.n, 2019).....	A.21
figure A-24: relation between the ratio or the actual and the maximum pile shaft friction force with the pile tip settlement (NEN–EN 1997–1 (NB) figure 7.o, 2019).....	A.21
figure A-25: group pile settlement.....	A.23
figure A-26: comparison of axial pile shortening for a pile with a prismatic shape and a tapered pile.....	A.24
figure A-27: diagram for a support modelled as a bilinear spring.....	A.25
figure A-28: case for research to influence of pile settlement change.....	A.27
figure A-29: load–displacement diagrams of the initial situation.....	A.29
figure A-30: determination of the neutral plane in the first iteration cycle.....	A.29
figure A-31: determination of the neutral plane in the second iteration cycle for both methods.....	A.30
figure A-32: influence of load variability on the load combination factor (NEN–EN 1997–1 (NB) figure 7.k, 2019).....	A.32
figure A-33: difference in bending stiffnesses along the pile cap beam.....	A.34
figure A-34: rotational stiffness of a beam–pile joint.....	A.35
figure A-35: equivalent spring model for a mortise and tenon joint for a positive bending moment (Descamps & Guerlement, 2009).....	A.36
figure A-36: load scheme for the determination of the rotational stiffness influence.....	A.37
figure A-37: rotational stiffness of a mortise and tenon joint.....	A.38
figure A-38: relations for the axial deformation of an element with an infinitesimal length.....	A.44

figure B-1: sample locations of the Boompjeskade (GeoStart, n.d.).....	B.2
figure B-2: sample locations of the Haringvliet (GeoStart, n.d.).....	B.4
figure B-3: sample locations of the Stieltjeskade (Geostart, n.d.).....	B.6
figure B-4: sample locations of the Toussaintkade (ArcGIS, n.d.).....	B.8
figure B-5: retrieved pile locations of the Toussaintkade (ArcGIS, n.d.).....	B.9

List of tables

table A-1: numerical values for the Riemann sum.....	A.10
table A-2: numerical values for the Riemann sum.....	A.10
table A-3: properties of several tree species.....	A.11
table A-4: recommended values for the calculation of the pile tip bearing strength.....	A.13
table A-5: parameters for the comparison of the slip method and the Eurocode expression.....	A.15
table A-6: correlation factors related to the structural rigidity and the number of soil probings (NEN–EN 1997–1 (NB) table A.10a and A.10b, 2019).....	A.17
table A-8: shape factor for different load areas (NEN–EN 1997–1 (NB) table 7.f, 2019).....	A.23
table A-9: used parameters.....	A.24
table A-10: parameters for each case in this numerical example.....	A.28
table A-11: results of the initial pile forces.....	A.28
table A-12: pile forces after one iteration.....	A.29
table A-13: pile reactions caused by different forces for the two calculation methods.....	A.30
table A-14: pile installation factor for different soil types (NEN–EN 1997–1 (NB) table 7.c and par. 7.6.3.3 (b), 2019).....	A.31
table A-15: Young's moduli for quay wall components (NEN–EN 1997–1 (NB) par. 7.6.4.2 (j), 2019).....	A.34
table A-16: used parameters.....	A.37
table A-17: used parameters.....	A.38
table A-18: calculation results from Scia Engineer.....	A.38
table B-1: penetration values of the Boompjeskade (Gemeente Rotterdam, personal communications, 2013).....	B.1
table B-2: microscopic results of the Boompjeskade (Gemeente Rotterdam, personal communications, 2013).....	B.2
table B-3: estimation residual strength of the foundation elements at the Boompjeskade (Gemeente Rotterdam, personal communications, 2013)	B.3
table B-4: penetration values of the Haringvliet (Gemeente Rotterdam, personal communications, 2012).....	B.4
table B-5: microscopic results of the Haringvliet (Gemeente Rotterdam, personal communications, 2012).....	B.5
table B-6: estimation residual strength of the foundation elements at the Haringvliet (Gemeente Rotterdam, personal communications, 2012).....	B.5
table B-7: penetration values of the Stieltjeskade (Gemeente Rotterdam, personal communications, 2013).....	B.6
table B-8: microscopic results of the Stieltjeskade (Gemeente Rotterdam, personal communications, 2013).....	B.7
table B-9: estimation residual strength of the foundation elements at the Stieltjeskade (Gemeente Rotterdam, personal communications, 2013).....	B.7
table B-10: penetration values for the piles at the Toussaintkade (Gemeente Rotterdam, internal documents, 2009).....	B.8
table B-11: microscopic results of the Toussaintkade (Gemeente Rotterdam, internal documents, 2009).....	B.9
table B-12: estimation residual strength of the foundation elements at the Toussaintkade (Gemeente Rotterdam, internal documents, 2009).....	B.9
table B-13: mechanical testing results from the timber foundation piles at the Toussaintkade (Gemeente Rotterdam, internal documents, 2009).....	B.10

Table of contents

A. Appendix A: Calculation principles.....	A.1
A.1 Soil pressures.....	A.1
A.2 Load spreading models.....	A.2
A.2.1 Vertical load spreading.....	A.3
A.2.2 Horizontal load spreading.....	A.4
A.2.2.1 Point load.....	A.5
A.2.2.2 Strip load.....	A.7
A.2.2.3 Discretization of load spreading.....	A.9
A.2.2.3.1 Vertical loads.....	A.9
A.2.2.3.2 Horizontal loads.....	A.10
A.3 Pile taper function.....	A.11
A.4 Base resistance.....	A.13
A.5 Shaft resistance.....	A.14
A.5.1 Eurocode expressions.....	A.15
A.5.2 Numerical comparison of the slip method with Eurocode 7.....	A.15
A.6 Total bearing capacity (compression).....	A.16
A.7 Negative skin friction.....	A.17
A.7.1 Eurocode expressions.....	A.17
A.7.2 Numerical comparison of slip method with Zeevaert–De Beer.....	A.20
A.8 Pile settlement.....	A.20
A.8.1 Eurocode expression.....	A.21
A.8.2 Numerical comparison of prismatic with tapered pile shape.....	A.23
A.9 Location of the neutral plane.....	A.24
A.9.1 Pile displacement.....	A.24
A.9.2 Soil settlement.....	A.25
A.9.3 Calculation approach.....	A.26
A.9.4 Numerical example.....	A.26
A.10 Tensile resistance.....	A.31
A.11 Pile rise.....	A.32
A.12 Stiffness properties.....	A.33
A.12.1 Element stiffness.....	A.33
A.12.2 Joint stiffness.....	A.34
A.12.3 Numerical example of joint stiffness.....	A.36
A.13 Derivation of equation 4.28	A.39
A.14 Derivation of equation A.10	A.41
A.15 Derivation of equation A.11	A.41
A.16 Derivation of equation A.51	A.44
B. Appendix B: Assessment results of quay walls.....	B.1
B.1 Boompjeskade, Rotterdam.....	B.1
B.2 Haringvliet, Rotterdam.....	B.3
B.3 Noordwal, The Hague.....	B.5
B.4 Stieltjeskade, Rotterdam.....	B.6
B.5 Toussaintkade, The Hague.....	B.7
C. Appendix C: Calculation results.....	C.1
C.1 Boompjeskade, Rotterdam.....	C.1

C.1.1	Collection of data.....	C.1
C.1.2	Superstructure loads.....	C.2
C.1.3	Lateral soil resistance.....	C.6
C.1.4	Joint stiffness.....	C.9
C.1.5	Axial pile head forces.....	C.9
C.1.6	Axial pile forces and resistances.....	C.11
C.1.7	Pile tip settlement and force.....	C.11
C.1.8	Neutral plane.....	C.13
C.1.9	Calculation model.....	C.14
C.1.10	Structural deficiencies.....	C.15
C.2	Haringvliet, Rotterdam.....	C.17
C.2.1	Collection of data.....	C.17
C.2.2	Superstructure loads.....	C.21
C.2.3	Lateral soil resistance.....	C.24
C.2.4	Joint stiffness.....	C.25
C.2.5	Axial pile head forces.....	C.26
C.2.6	Axial pile forces and resistances.....	C.27
C.2.7	Pile tip settlement and force.....	C.28
C.2.8	Neutral plane.....	C.29
C.2.9	Calculation model.....	C.29
C.2.10	Structural deficiencies.....	C.30
C.3	Noordwal, the Hague.....	C.32
C.3.1	Collection of data.....	C.32
C.3.2	Superstructure loads.....	C.35
C.3.3	Lateral soil resistance.....	C.38
C.3.4	Joint stiffness.....	C.39
C.3.5	Axial pile head forces.....	C.40
C.3.6	Axial pile forces and resistances.....	C.41
C.3.7	Pile tip settlement and force.....	C.42
C.3.8	Neutral plane.....	C.43
C.3.9	Calculation model.....	C.44
C.3.10	Structural deficiencies.....	C.45
C.4	Stieltjeskade, Rotterdam.....	C.48
C.4.1	Collection of data.....	C.48
C.4.2	Superstructure loads.....	C.51
C.4.3	Lateral soil resistance.....	C.53
C.4.4	Joint stiffness.....	C.55
C.4.5	Axial pile head forces.....	C.56
C.4.6	Axial pile forces and resistances.....	C.57
C.4.7	Pile tip settlement and force.....	C.59
C.4.8	Neutral plane.....	C.60
C.4.9	Calculation model.....	C.61
C.4.10	Structural deficiencies.....	C.62
C.5	Toussaintkade, the Hague.....	C.64
C.5.1	Collection of data.....	C.64
C.5.2	Superstructure loads.....	C.68
C.5.3	Lateral soil resistance.....	C.70
C.5.4	Joint stiffness.....	C.72
C.5.5	Axial pile head forces.....	C.72
C.5.6	Axial pile forces and resistances.....	C.73

C.5.7	Pile tip settlement and force.....	C.75
C.5.8	Neutral plane.....	C.76
C.5.9	Calculation model.....	C.76
C.5.10	Structural deficiencies.....	C.76

Appendix A: Calculation principles

For the calculation of a quay wall structure with a timber pile foundation, a few structural and geotechnical considerations must be elaborated. The following subjects are treated in this appendix:

- Soil pressures for stratified soil systems (appendix 'A.1 soil pressures')
- Spreading of surface loads through the subsoil (appendix 'A.2 Load spreading models')
- Comparison of different pile taper functions for timber piles (appendix 'A.3 Pile taper function')
- Pile base resistance of compressive piles according to the Eurocode (appendix 'A.4 Base resistance')
- Pile shaft resistance of compressive piles according to the Eurocode and the slip method accompanied by a numerical comparison(appendix 'A.5 Shaft resistance')
- Pile bearing capacity of compressive piles according to the Eurocode (appendix 'A.6 Total bearing capacity (compression)')
- Negative skin friction of compressive piles according to the Eurocode (appendix 'A.7 Negative skin friction')
- Pile settlement of compressive piles according to the Eurocode (appendix 'A.8 Pile settlement')
- Neutral plane depth for compressive piles (appendix 'A.9 Location of the neutral plane')
- Pile shaft resistance of tensile piles according to the Eurocode (appendix 'A.10 Tensile resistance')
- Pile rise of tensile piles according to the Eurocode (appendix 'A.11 Pile rise')
- Stiffnesses of the quay wall elements (appendix 'A.12 Stiffness properties')
- Derivation of equation (4.28) (appendix 'A.13 Derivation of equation (4.28)')
- Derivation of equation (A.10) (appendix 'A.14 Derivation of equation (A.10)')
- Derivation of equation (A.11) (appendix 'A.15 Derivation of equation (A.11)')
- Derivation of equation (A.50) (appendix 'A.16 Derivation of equation (A.50)')

A.1 SOIL PRESSURES

The pressure from the soil with a homogeneous composition and a groundwater table equal to ground level is easily computed with *equation (4.11)*. However, in practice no such conditions are found anywhere. A more sophisticated expression is needed to account for the groundwater level at a certain depth and a soil profile consisting of several layers. For a layered soil system, the vertical soil stress with a uniformly distributed surface load is defined by the groundwater table and the depth of interest for the value of the soil stress. Four situations can be distinguished.

1. The groundwater table is situated below the depth of interest in different soil layers $j < m$:

$$\sigma_v z = Q_{sur} + \sum_{i=1}^{j-1} (\gamma_{dry,i} \times t_i) + \gamma_{dry,j} \times \left(z - \sum_{i=1}^{j-1} t_i \right) \quad A.1$$

2. The groundwater table is situated above the depth of interest in the same soil layer $j = m$:

$$\sigma_v z = Q_{sur} + \sum_{i=1}^{j-1} (\gamma_{dry,i} \times t_i) + \gamma_{dry,j} \times (z_{gw} - z) \quad A.2$$

3. The groundwater table is situated below the depth of interest in the same soil layer $j = m$:

$$\sigma_v z = Q_{sur} + \sum_{i=1}^{j-1} (\gamma_{dry,i} \times t_i) + \gamma_{dry,j} \times (z_{gw} - z) + \gamma_{sat,j} \times (z - z_{gw}) \quad A.3$$

4. The groundwater table is situated below the depth of interest in different soil layers $j > m$:

$$\sigma_v z = Q_{sur} + \sum_{i=1}^{m-1} (\gamma_{dry,i} \times t_i) + \gamma_{dry,m} \times \left(z_{gw} - \sum_{i=1}^{m-1} t_i \right) + \gamma_{sat,m} \times \left(\sum_{i=1}^m t_i - z_{gw} \right) + \sum_{i=1}^{j-1} (\gamma_{sat,i} \times t_i) + \gamma_{sat,j} \times \left(z - \sum_{i=1}^{j-1} t_i \right) \quad A.4$$

The four situations as described with *equation (A.1)*, *equation (A.2)*, *equation (A.3)*, and *equation (A.4)* with their indices are depicted in *figure A-1*.

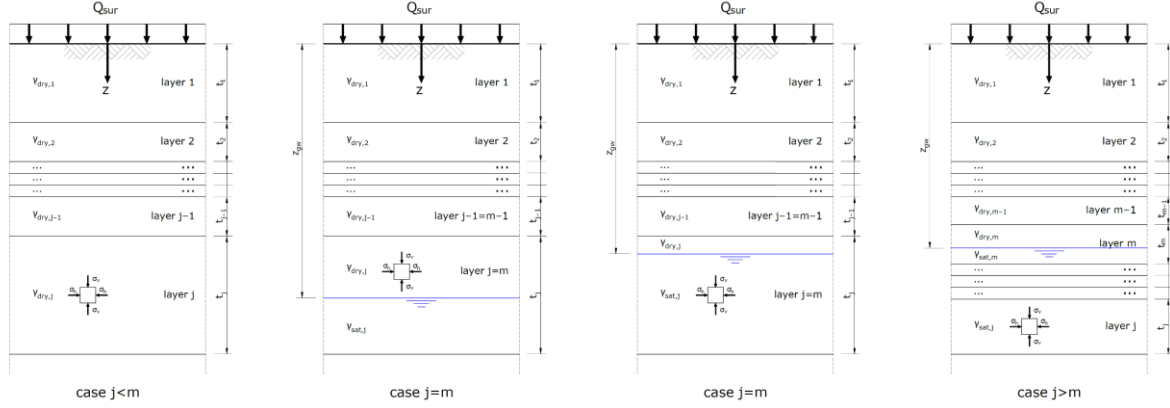


figure A-1: example of the determination of soil stresses

A.2 LOAD SPREADING MODELS

The influence of the loads located at surface level can be determined with force spreading models. A 3D-model is often required because the spreading takes place in all directions inside the subsoil. The soil particles act together as an anisotropic material when the substance is loaded in compression or shear. Advanced numerical methods are then required to include all soil characteristics for the acquisition of an accurate soil response under loading conditions.

In many cases, simplifications are possible in the stress-strain behaviour depending on the parameter of interest and the desired level of accuracy. Many comparisons were made in the past between different soil models according to linear elastic analysis and more advanced models with anisotropic behaviour. Verruijt (2012) states in his book that the difference in results for vertical normal stresses is very small. This cannot be said for the horizontal stresses and displacements because they are both very sensitive to the degree of extensiveness in the description of the soil parameters. Simplification to a homogeneous isotropic material implies the use of a linear relation between the stresses and the strains (constitutive relation). Coupling between both parameters is done with Hooke's law. An overview of the normal and shear stresses at an infinitesimal volume of soil is given in *figure A-2*.

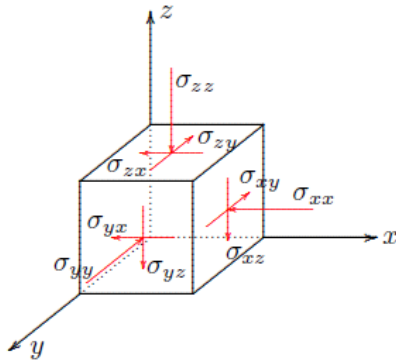


figure A-2: stresses on a soil element (Verruijt, 2012)

For each principal direction, a relation between the stresses and the strains is found:

$$\begin{cases} \varepsilon_{xx} = -\frac{1}{E} \times (\sigma_{xx} - \nu \times (\sigma_{yy} - \sigma_{zz})) \\ \varepsilon_{yy} = -\frac{1}{E} \times (\sigma_{yy} - \nu \times (\sigma_{xx} - \sigma_{zz})) \\ \varepsilon_{zz} = -\frac{1}{E} \times (\sigma_{zz} - \nu \times (\sigma_{xx} - \sigma_{yy})) \end{cases} \quad \text{A.5}$$

The Poisson's number defines the ratio between the lateral strain of an element and the strain in the direction of the applied load. A positive value for this ratio implies a lateral expansion when the element is compressed and a lateral contraction under influence of a tensile force.

The French scientist Joseph Boussinesq (1885) found a solution for the stresses and strains under the influence of a surcharge load in a homogeneous soil with linear elastic behaviour. The direction of stresses given with polar coordinates is depicted in *figure A-3*.

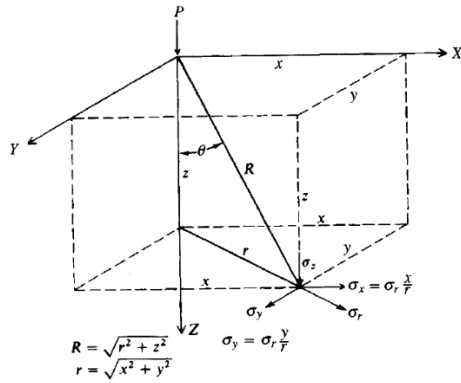


figure A-3: terms in the Boussinesq expressions (Bowles, 1997)

$$\begin{cases} \sigma_{zz} = \frac{3 \times F}{2 \times \pi} \times \frac{z^3}{R^5} \\ \sigma_{rr} = \frac{F}{2 \times \pi} \times \left(\frac{3 \times r^2 \times z}{R^5} - 1 - 2 \times \nu \times \frac{1}{R \times (R + z)} \right) \\ \sigma_{\theta\theta} = \frac{F}{2 \times \pi} \times \frac{1 - 2 \times \nu}{R^2} \times \left(\frac{R}{R + z} - \frac{z}{R} \right) \end{cases} \quad \text{where } \begin{cases} R = \sqrt{x^2 + y^2 + z^2} \\ r = \sqrt{x^2 + y^2} \end{cases} \quad \text{A.6}$$

With these expressions, several load models can be made for the determination of the vertical and horizontal load spreading on a quay wall structure. These representations are needed to implement the different terrain loads treated in paragraph '4.3.4 Terrain loads' into a structural program. First, a mathematical description is given in paragraph 'A.2.1 Vertical load spreading' for the vertical spreading of forces into the subsoil. Besides vertical load spreading also spreading in horizontal direction will occur as shown in paragraph 'A.2.2 Horizontal load spreading'. A distinction is made between point and strip loads because the required expressions for these load types are derived in different ways. Before the implementation of the acquired forces on the foundation elements into a structural framework program is possible, both loads must be discretized. This action is described in paragraph 'A.2.2.3 Discretization of load spreading'.

A.2.1 VERTICAL LOAD SPREADING

The vertical stress as a result of a point load is calculated with Boussinesq's expressions compiled in *equation (A.6)* for stresses in the z-direction. Here, the radial distance is set to zero to acquire the maximum stress value at a vertical distance below the point of application.

$$\sigma_{zz} \approx \frac{3F}{2\pi} \times \frac{z^3}{z^5} = \frac{3 \times F}{2\pi \times z^2} \quad \text{A.7}$$

A point load applied at ground level is spread in the subsoil in every possible direction and therefore a circular pattern is generated. A 3D-example of the load spreading is made visible in *figure A-4*. According to *equation (A.7)*, the maximum vertical soil stresses decrease over the soil depth with a quadratic term. In *figure A-4*, a plot is given of stress magnitudes at several locations along the vertical axis.

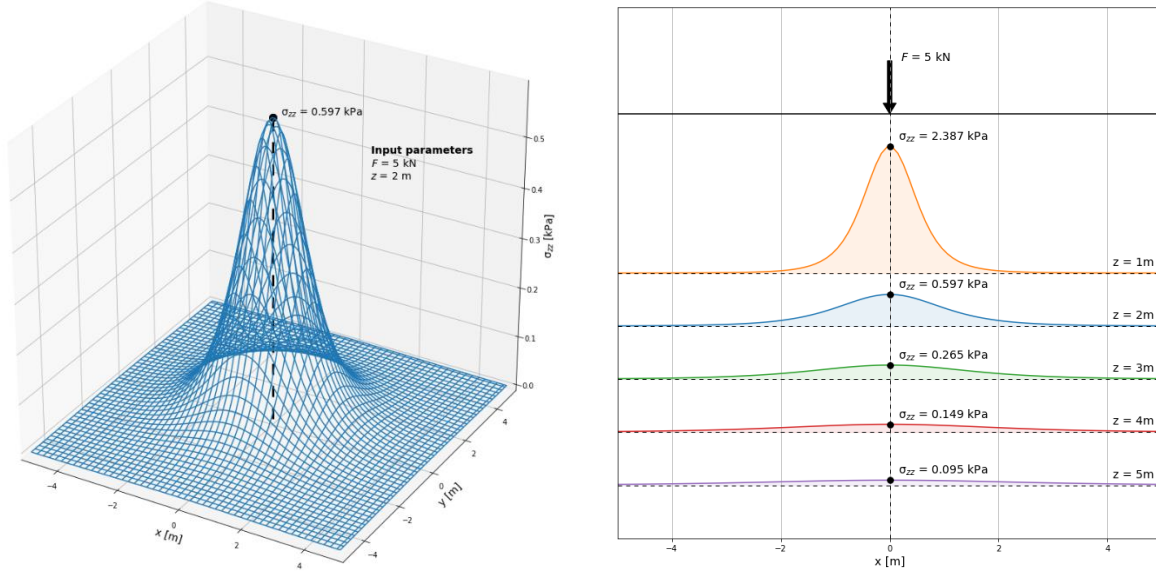


figure A-4: vertical force spreading in the subsoil; left: circular loading pattern at a soil depth of 2 m, right: flattening of the stress curves for an increasing soil depth

From the above graph it can be concluded that the point load is spread quite evenly at a few metres below the ground surface level. For a quay wall with a considerable retaining height (around 5 m), the assumption of a constant vertical stress at foundation level seems quite acceptable. The total spreading area is then derived from the linear relation between the area and the force. Substitution of *equation (A.7)* results in:

$$A = \frac{F}{\sigma_{zz}} = \frac{F}{\frac{3F}{2\pi \times z^2}} = \frac{2}{3} \pi \times z^2 \quad \text{A.8}$$

The strip loads given in *figure 4-4* and *figure 4-5* can also be translated to point loads just like the vertical load spreading calculation because the spreading principle for both types is similar. The contribution of each load type can be calculated separately and added up afterwards due to the superposition principle according to the theory of elasticity.

A.2.2 HORIZONTAL LOAD SPREADING

Besides the vertical spreading force on the foundation elements, also a horizontal component can be deduced from the surface load. The corresponding shape of horizontal stress over the height of the retaining wall depends on the horizontal distance of the surface load from the quay wall and its magnitude. With the assumptions of an elastic soil, Terzaghi (1943) invented a mathematical description for the horizontal stresses on the surface of a retaining wall for such kind of loading situations. He assumed incompressibility of the soil. This assumption is allowed when the occurring stresses are low compared to the stresses at the failure state, so an elastic stress state shows up. Terzaghi made use of

Boussinesq's equation (A.6) of the radial stress. It results in the location of the point load at the shortest distance from the element, so the highest value of the horizontal stress can be obtained. When the soil is incompressible, the horizontal component of equation (A.6) simplifies to:

$$\sigma_{xx} \ x, z = \frac{3F \times r^2 \times z}{2\pi \times R^5} \quad \text{where } \nu = 0.5 \quad \text{A.9}$$

A.2.2.1 POINT LOADS

In the following section a few abbreviations are made to clarify the used mathematical calculations:

- $\sigma_h \ y, z \rightarrow$ horizontal stress over the soil depth and along the length of the retaining wall (plane stress state).
- $\sigma_{h,max} \ z = \sigma_h \ 0, z \rightarrow$ horizontal stress over the soil depth at the location where the point load has the shortest distance to the retaining wall.
- $q_h = \sigma_h \ y, z_c \rightarrow$ resultant line load along the length of the quay wall at a certain soil depth.
- $q_{h,max} = \sigma_h \ 0, z_c \rightarrow$ maximum value of the resultant line load at the location where the point load has the shortest distance to the retaining wall at a certain soil depth.

In figure A-5, the described method is introduced that was based on Terzaghi's findings. At the right figure, the spreading along the quay wall is outlined.

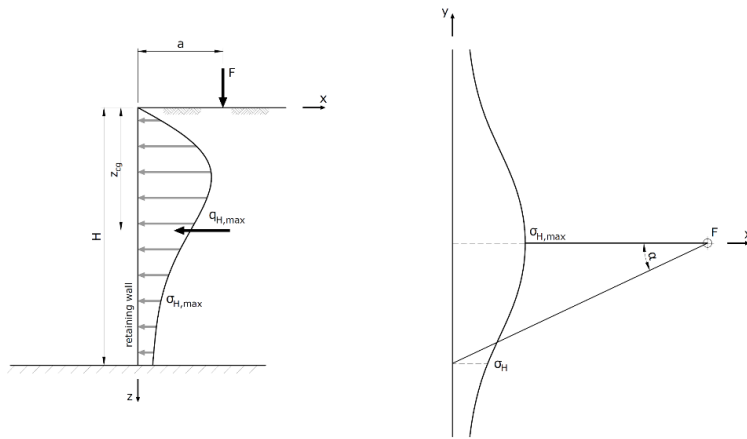


figure A-5: theoretical model based on Terzaghi's expressions for a line load; left: elevation view, right: plan view (USACE, 1994)

$$\begin{cases} \sigma_{h,max} \ z = 0.28 \frac{F}{H_{wall}^2} \times \frac{n_H^2}{0.16 + n_H^2} & \text{for } m_H \leq 0.4 \\ \sigma_{h,max} \ z = 1.77 \frac{F}{H_{wall}^2} \times \frac{m_H^2 \times n_H^2}{m_H^2 + n_H^2} & \text{for } m_H > 0.4 \end{cases} \quad \text{where } \begin{cases} m_H = \frac{a}{H_{wall}} \\ n_H = \frac{z}{H_{wall}} \end{cases} \quad \text{A.10}$$

Terzaghi derived equation (A.10) from the Boussinesq's expressions given by equation (A.6). He introduced a so-called critical distance that is located at a distance of 0.4 times the height of the structural element. The derivation of both expressions is given in 'A.14 Derivation of equation (A.10)'. A surface load in close proximity to the quay wall gives an upper bound value for the generated horizontal stress shape, so its magnitude does not depend on the actual value for the horizontal distance. The horizontal stress becomes dependent on the load location when the critical distance is exceeded. The numbers in front of the expressions in equation (A.10) were altered a few times until an agreement was reached.

In figure A-6 and figure A-7 both expressions are plotted in a 3D-graph with a distance of the load according with the criteria for the critical depth parameter.

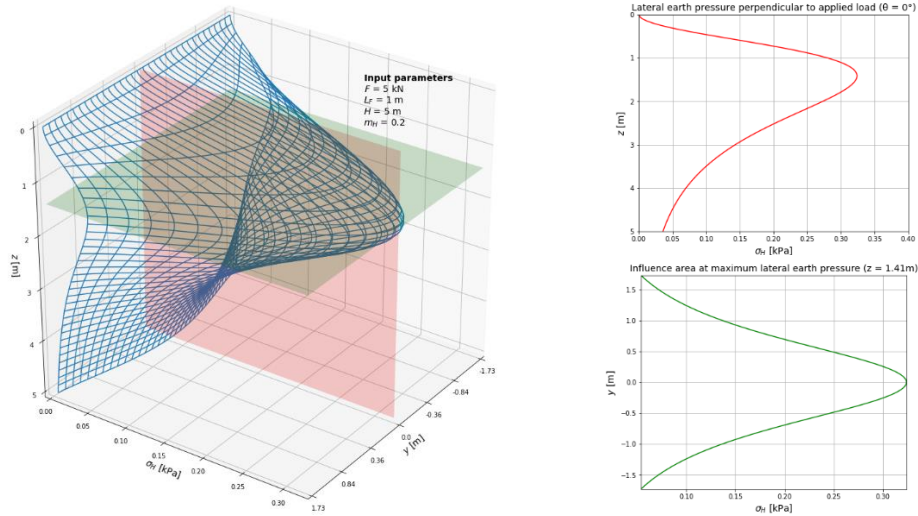


figure A-6: load spreading by a force application at a distance $a \leq 0.4H$ from the retaining wall

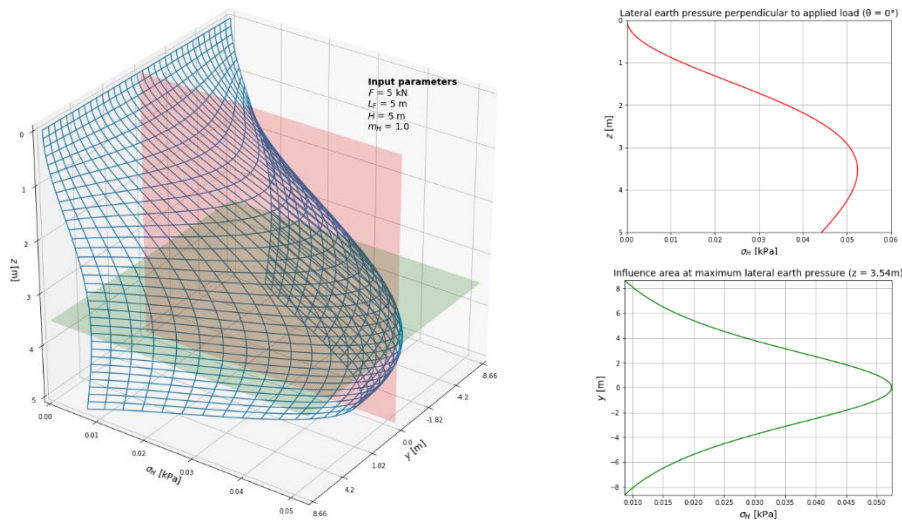


figure A-7: load spreading by a force application at a distance $a > 0.4H$ from the retaining wall

From the plots it becomes clear that the maximum occurring horizontal stress is situated deeper into the subsoil the further the point is located from the retaining wall. To determine the resultant horizontal force, the above expressions are integrated over the depth to obtain the resultant force in the form of a distributed line load and its point of application. This load description is easier to apply later on in a computer model. The resultant force gives exactly the same results as the plane stress shape because the quay wall element is assumed to be rigid and so the distribution of the force over the quay wall element is not influenced by structural deflections as mentioned in paragraph '5.2.2 Superstructure loads'.

$$\begin{cases} q_{h,max} = 0.79 \times \frac{F}{H_{wall}} \\ z_{cg} = 0.41 \times H_{wall} \end{cases} \quad \text{for } m_H \leq 0.4$$

$$\begin{cases} q_{h,max} = 0.22 \times \frac{F}{H_{wall}} \times \left(\frac{1 - m_H^2}{m_H^2 + 1} + \frac{1}{m_H} \times \tan^{-1} \left(\frac{1}{m_H} \right) \right) \\ z_{cg} = \frac{2 \times H_{wall}}{\left(1 - m_H^2 + \frac{1}{m_H} \times m_H^2 + 1 \times \tan^{-1} \left(\frac{1}{m_H} \right) \right)} \end{cases} \quad \text{for } m_H > 0.4$$
A.11

The expressions in equation (A.11) are derived in appendix 'A.15 Derivation of equation (A.11)'. To observe the influence of the distance of the point load from the retaining wall, the resultant horizontal force and its point of application are made dimensionless in the following graphs in figure A-8.

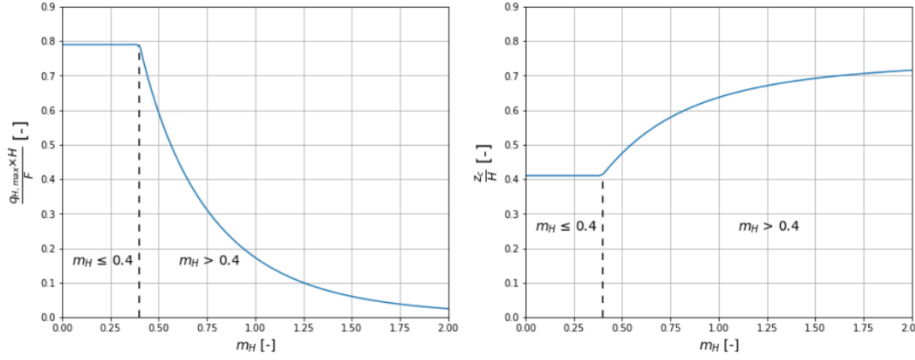


figure A-8: influence of the location of the point load on the horizontal soil response

A.2.2.2 STRIP LOADS

A similar relation is found for the horizontal stress induced by a strip load along the length of the retaining wall. Firstly, equation (A.6) is converted to a line load by the implementation of a series of concentrated loads along the y-axis (Das & Sobhan, 2014).

$$\sigma_{xx} \ x, z = \frac{2 \times Q \times x^2 \times z}{\pi \times r^4} = \frac{2 \times Q}{\pi \times r} \times \sin^2 \alpha \times \cos \alpha$$
A.12

Consequently, a strip load is created by the application of a number of line loads with an element load width. The principle of the alteration is shown in figure A-9.

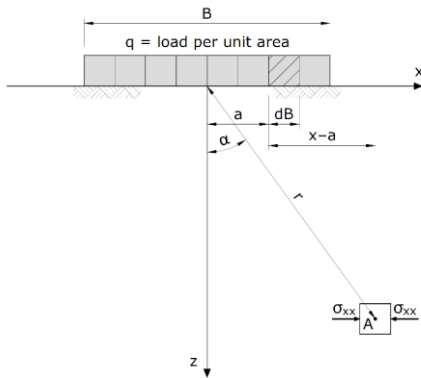


figure A-9: radial stress as a result of a vertical strip load (Das & Sobhan, 2014)

The corresponding stress value caused by a load with an elemental width is obtained by substitution.

$$d\sigma_{xx} y, z = \frac{2 \times q \, dB \times x^2 \times z}{\pi \times (x - a)^2 + z^2} \quad \text{A.13}$$

After the integration over the load width and the modification with a number of geometrical operations, the following form of the expression for the horizontal soil stress of a non-yielding retaining wall is retrieved:

$$\sigma_h z = \frac{2 \times Q}{\pi} \times (\alpha_2 - \alpha_1 - \sin \alpha_2 - \alpha_1 \times \cos \alpha_1 + \alpha_2) \quad \text{where} \quad \begin{cases} \alpha_1 = \tan^{-1} \left(\frac{a}{z} \right) \\ \alpha_2 = \tan^{-1} \left(\frac{a+b}{z} \right) \end{cases} \quad \text{A.14}$$

The used angular dimensions in above equations are depicted in *figure A-10*.

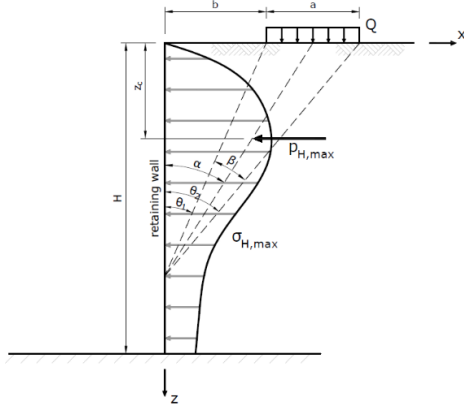


figure A-10: theoretical model based on Terzaghi's expressions for a strip load (USACE, 1994)

Jarquio (1981) found the following expression for the resultant force and the point of application on the retaining wall per running meter:

$$\begin{cases} q_{h,max} = \frac{Q \times H_{wall}}{1.57} \times C_2 - C_1 \\ z_{cg} = \frac{H_{wall}^2 \times C_2 - C_1 - C_4 - C_3 + B \times H_{wall}}{2 \times H_{wall} \times C_2 - C_1} \end{cases} \quad \text{where} \quad \begin{cases} C_1 = \tan^{-1} \left(\frac{a}{H_{wall}} \right) \\ C_2 = \tan^{-1} \left(\frac{a+B}{H_{wall}} \right) \\ C_3 = a^2 \times 1.57 - C_1 \\ C_4 = a + B^2 \times 1.57 - C_2 \end{cases} \quad \text{A.15}$$

A numerical example of the stress distribution excited by a strip load is depicted in *figure A-11*.

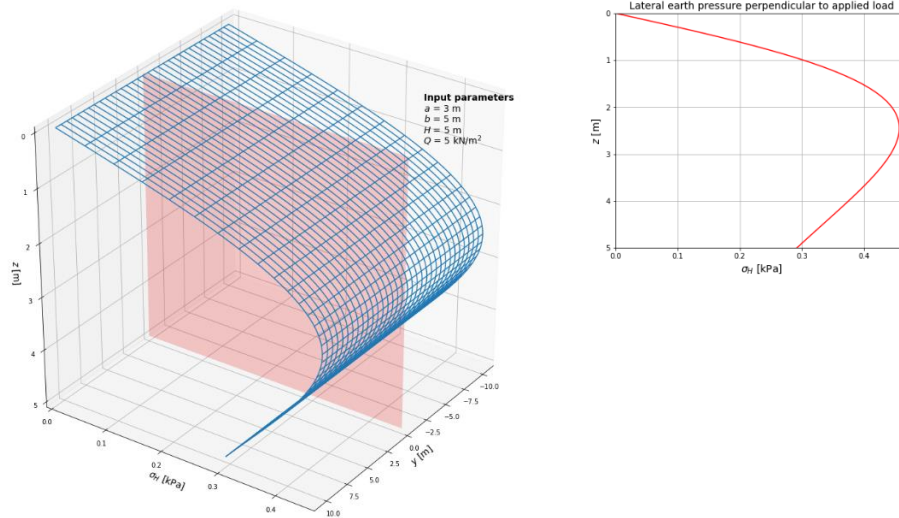


figure A-11: load spreading under the influence of a strip load

The point load and strip load models can be used as structural program with a few alterations. The exact shape of the model input is presented in paragraph 'A.2.2.3 Discretization of load spreading'.

A.2.2.3 DISCRETIZATION OF LOAD SPREADING

Loads of the traffic at ground level are transferred by the soil medium to the foundation elements and the retaining wall. The load shape defines the way of implementation into a structural calculation program. Uniformly distributed surface loads can be included immediately without any further modifications into *equation (A.1)*, *equation (A.2)*, *equation (A.3)*, or *equation (A.4)*, so no extra attention is required. Loads that are not present over the entire region behind the quay wall influences the structure in a different way that calls for a separate approach.

When a discrete load (point, line or strip load) acts at ground level, spreading occurs in two different directions which are in the horizontal plane perpendicular to the quay wall and along the vertical axis. Force spreading in horizontal direction results in stresses at the wall surface where vertical spreading results in loads on the foundation elements. A framework model is used for the structural calculations, so the continuous stress distributions are not suitable in their current form. Discretization is a good option to approximate the distributed load by discrete forces. One possibility is the application of a Riemann sum where areas of the stress distribution are divided by the midpoint rule.

$$F_i = \int_a^b f(x) dx = \lim_{n \rightarrow \infty} \sum_{i=1}^n f(x_i) \times \Delta x \quad \text{where} \quad \begin{cases} \Delta x = \frac{b-a}{n} \\ x_i = a + (i-1) \Delta x \end{cases} \quad \text{A.16}$$

This mathematical expression can be used both for the load spreading on the pile cap beams given in paragraph 'A.2.2.3.1 Vertical loads' and the spreading on the retaining wall presented in paragraph 'A.2.2.3.2 Horizontal loads'.

A.2.2.3.1 VERTICAL LOADS

A vertical point load on surface level is spread into the subsoil according to *equation (A.7)* over the loading area determined in *equation (A.8)*. When the spreading is not restricted by a vertical boundary like a quay wall, a circular stress shape appears as visualised in *figure A-4*. The pile distance along the quay wall defines the load share for each pile cap beam. The radius of the circle is derived by equating it with the standard expression for the area of a circle.

$$r = \sqrt{\frac{2}{3}} \times z \quad \text{A.17}$$

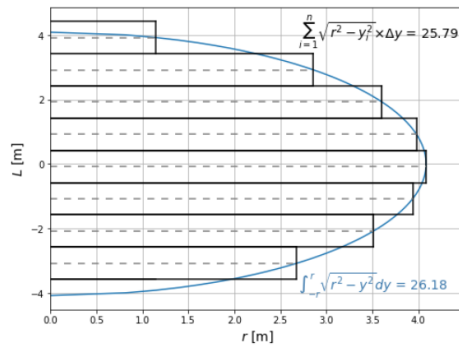
Equation (A.17) can be substituted in the expression for a circle segment.

$$x = \sqrt{r^2 - y^2} = \sqrt{\frac{2}{3} \times z^2 - y^2} \quad \text{A.18}$$

The total area from a half circle is defined by integrating *equation (A.18)* over the radius or by dividing the total area in *equation (A.8)* by two.

$$\frac{1}{2} \times A = 2 \times \int_0^r \sqrt{\frac{2}{3} \times z^2 - y^2} dy = \frac{1}{3} \times \pi \times z^2 \quad \text{A.19}$$

When a value is given for the soil depth, the load shares can be determined with a Riemann sum. In *figure A-12* and *table A-1* an example for a calculation is done for certain values of the step size and soil depth.



y_i [°]	A_i [m²]
3.92	1.15
2.92	2.86
1.92	3.60
0.92	3.98
- 0.08	4.08
- 1.08	3.94
- 2.08	3.51
- 3.08	2.68
$A = 25.79 \text{ m}^2$	

figure A-12: approximation of the distributed vertical load by a Riemann sum

table A-1: numerical values for the Riemann sum

The approximation gives almost the same values as the exact loading surfaces. To translate above calculations to a line load on a pile cap beam, above figure is mirrored around the y-axis.

$$q_{v,i} = \frac{2F \times \frac{A_i x_i}{A}}{2\Delta x_i} = \frac{F \times A_i x_i}{\Delta x_i \times A} \quad \text{A.20}$$

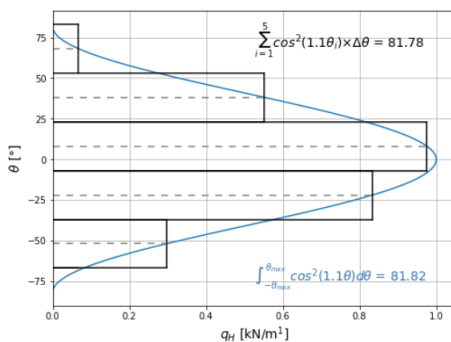
A.2.2.3.2 HORIZONTAL LOADS

The lateral stresses on the retaining wall are determined with equation (A.10) for point loads and with equation (A.12) for strip loads. The wall is not modelled as a continuous element in the framework model, so the stress has to be discretized to place the loads according to the pile grid dimensions. The stress surfaces of figure A-6, figure A-7, and figure A-11 can be simplified to a resultant line load at a certain soil depth because the retaining wall is treated as a rigid object, as mentioned in paragraph '5.2.2 Superstructure loads' and appendix 'A.2.2.1 Point loads'. Therefore, only the load spreading along the quay wall is of importance.

The resultant force is calculated with an integral over the influence range of the distributed loads given in equation (A.10). Both bounds of the integral are based on the value in the cosine function. Larger angles are physically not possible because they will result in negative force contributions.

$$F_h = \int_{-90/1.1}^{90/1.1} q_h \times \cos^2 1.1 \times \alpha \, d\theta = \frac{90}{1.1} \times q_h \quad \text{A.21}$$

Above equation can be compared to a Riemann approximation with certain values for the distributed load and the step size. This is done in figure A-13 accompanied by values in table A-2.



θ_i [°]	$F_{h,i}$ [kN]
66.82	2.01
36.82	16.57
6.82	29.27
- 23.18	25.04
- 53.18	8.90
$F_H = 81.78 \text{ kN}$	

figure A-13: approximation of the distributed horizontal load by a Riemann sum

table A-2: numerical values for the Riemann sum

Just like the approximation of the vertical load spreading, the approximation for the horizontal load spreading gives almost the same values as the exact loading surfaces. To translate above calculations to a point load on the retaining wall, the discrete values of the line load are multiplied with the load width.

$$F_{h,i} = q_{h,i} x_i \times \Delta x_i \quad \text{A.22}$$

Above approximation is quite good even for a large step size. Determination of discrete forces by a spreading angle is not very handy, so it is translated to a pile distance along the quay wall.

$$\alpha = \tan^{-1} \left(\frac{S_{pile}}{a} \right) \quad \text{A.23}$$

A.3 PILE TAPER FUNCTION

Timber foundation piles have a tapered shape which means that the pile head has a larger diameter than the pile tip. The taper rate could have a large influence on the internal force distribution depending on its magnitude. In this paragraph, three taper functions are presented to capture the taper rate of a pile element. Mathematical expressions are then fitted to empirical data. From a wide range of expressions, it was found that the taper follows from three dependencies (Duan et al., 2016):

$$d_{tree} = f(z, d_b, H_{tree}) \quad \text{A.24}$$

Those parameters are translated to the running variable along the tree axis, the diameter at breast height, and the total tree height. The breast height is a generally accepted parameter in the dendrochronological study to trees that expresses the diameter of a standing tree at a height of 1.3 m above ground level. This height is used in many calculations related to trees. One of the shorter variants of a tree taper function is given below (Sharma & Oderwald, 2001):

$$d_{tree} z = d_b \times \sqrt{\left(\frac{z}{1.3}\right)^{2-\beta_1} \times \left(\frac{H_{tree} - z}{H_{tree} - 1.3}\right)} \quad \text{for } z \geq 1.3 \quad \text{A.25}$$

The expression is quite simple because the diameter depends on only one constant. Ounekham (2009) states in her master thesis report that despite the basic arrangement of parameters, it is still an unbiased model. For several tree species located around the world, this tree shape factor was determined. In *table A-3*, an overview is given of sample sizes with their primary characteristics.

tree species	N [-]	H _{tree} [m]	d _b [m]	β ₁ [-]	reference
Loblolly pine	156	18.0	20.0	2.1852	Sharma & Oderwald, 2001
Chinese fir	183	13.49	12.52	2.0307	Duan et al., 2016
Jack pine	140	17.68	18.77	2.0399	Sharma & Zhang, 2004
Balsam fir	150	13.88	17.65	2.1152	Sharma & Zhang, 2004
Black spruce	135	15.08	16.85	2.1177	Sharma & Zhang, 2004

table A-3: properties of several tree species

From above table it follows that the constant does not differ a lot for this quite small trees. The total tree height, before it was converted to a foundation pile, is often unknown and therefore assumptions have to be made. The spruce piles found in Rotterdam originates from large and dense forests in Western Europe. At these locations, European mature spruce trees can grow up to a height of 60 m (Caudullo et al., 2016). Only the lower portion of the stem is suitable for a foundation pile because the tree has a conical shape. A simplified overview of the utilization of tree parts for structural purposes is depicted in *figure A-14*.

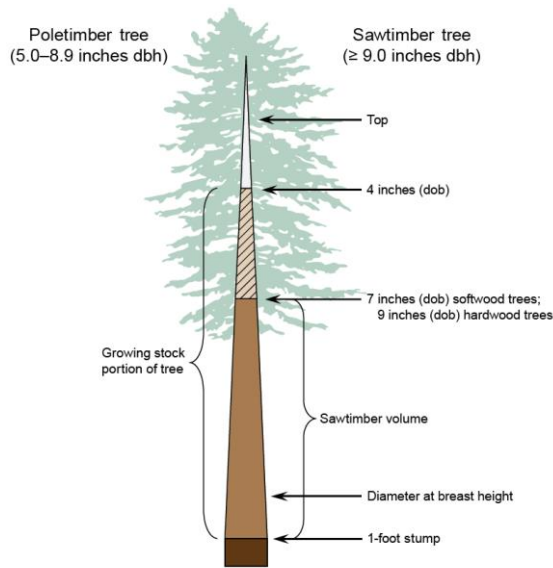


figure A-14: tree sections for processing to timber products (dbh = diameter at breast height, dob = diameter outside bark) (Simmons et al., 2016)

For a foundation pile it is required that the pile tip has a minimum diameter to prevent fracture during the pile driving process. The initial tree heights used for the long piles in Rotterdam cannot be traced, but trees with a minimum length of 40 m seems reasonable. In figure A-15, equation (A.25) is plotted for a number of possible tree heights with a tree shape factor of 2.1 and a breast diameter of 250 mm.

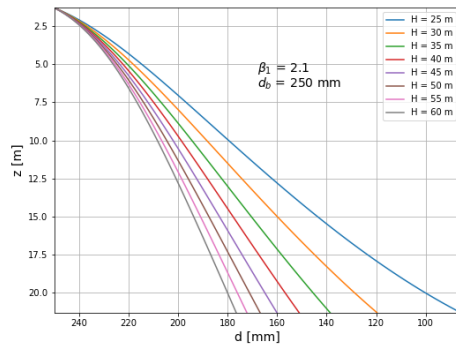


figure A-15: varying diameter along the stem axis for different tree heights

It is unknown at which height trees were sawn that were used as a foundation pile. Due to the widened base of the stem at the ground for many tree species, a breast height of 1.3 m is taken for the location of the pile head diameter.

The taper along the pile length was also estimated by numerous observations to timber foundation piles in the Netherlands. The branch organisation F3O/SBRCURnet (2016) found a relation with a linear taper rate. They took a decrease in diameter of 7.5 mm/m of the pile length.

$$d_z = d_{head} - 7.5 \times z \quad A.26$$

Another expression was composed by Sas (2007) who did an observational study to the varying cross-sectional diameter along the axis for numerous foundation piles. With a set consisting of 320 test piles with different lengths acquired from probing records and fourteen measured tree trunks, a generic expression was found unrelated to the applied wood species.

$$d_z = d_{head} \times 0.944^z \quad A.27$$

To compare this equation with the tree taper equation, the same reference system must be attained for both equations, so *equation (A.25)* is slightly adapted.

$$d_z = d_{head} \times \sqrt{\left(\frac{z+1.3}{1.3}\right)^{2-\beta_1} \times \left(\frac{H-z+1.3}{H-1.3}\right)} \quad A.28$$

The above three relations are put together in a graph to compare them with each other. A factor for β_1 in equation is not determined yet for European spruce, so its value is based on an empirical fit with the other taper equations. The above-mentioned expressions are depicted in *figure A-16* for three different pile diameters and a fixed value for the tree shape parameter.

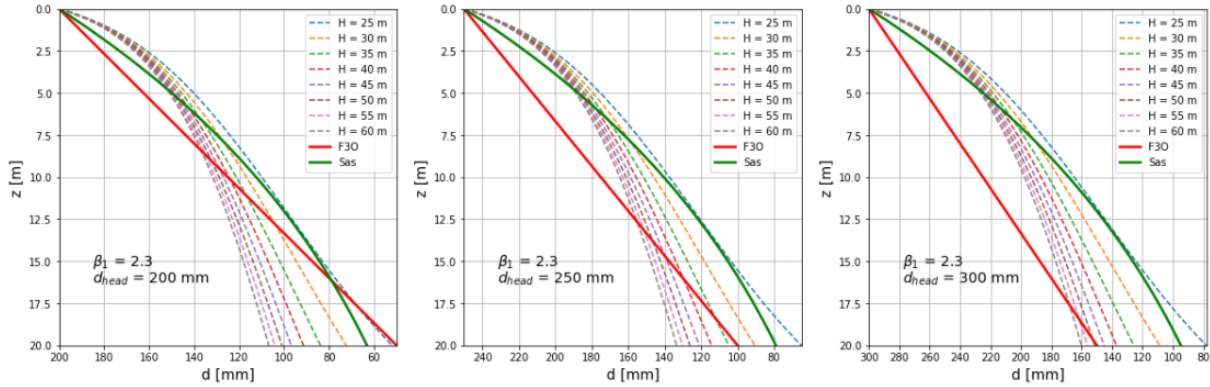


figure A-16: comparison of taper functions

The above graphs show that *equation (A.27)* is a better fit than *equation (A.26)* for this value of the tree shape parameter. The linearity of *equation (A.26)* implies that it is only applicable for shorter piles. The equation deviates too much from the actual nonlinear taper rate for longer piles. Taper expressions like *equation (A.25)* are very cumbersome to use in structural calculations, so *equation (A.27)* seems a good substitution for the estimation of the pile shape. Therefore, it will be used in further structural calculations to determine the geotechnical bearing capacity of a timber foundation pile.

A.4 BASE RESISTANCE

The determination of the pile tip capacity is possible with two different approaches. The generic method was treated already in paragraph '4.4.1.2 Shaft resistance'. Another method is based on local soil parameters that are obtained by cone penetration tests. This approach is shown below.

The resistance of the pile tip is calculated with a certain reduction factor for the compensation of the overestimated resistance value (NEN-EN 1997-1 (NB) par. 7.6.2.3 (c) and (e), 2019).

$$\begin{cases} R_{b,max,i,k} = \sigma_{b,max,i,k} \times A_b \\ \sigma_{b,max,i,k} = \frac{1}{2} \times \alpha_b \times \beta \times s \times (q_{CPT,I,avg} + q_{CPT,II,avg} + q_{CPT,III,avg}) \end{cases} \quad A.29$$

For a timber pile the values in *table A-4* are prescribed in the standards.

parameter	value	reference
α_b [-]	0.7	NEN-EN 1997-1 (NB) table 7.c, 2019
β [-]	1.0	NEN-EN 1997-1 (NB) figure 7.i, 2019
s [-]	1.0	NEN-EN 1997-1 (NB) par. 7.6.2.3 (h), 2019

table A-4: recommended values for the calculation of the pile tip bearing strength

The determination of the pile bearing resistance is based on the weighted average of three cone resistance values at regions in a CPT–diagram. The correct way of derivation of the cone resistance from a CPT–diagram is clarified with the example in *figure A-17*.

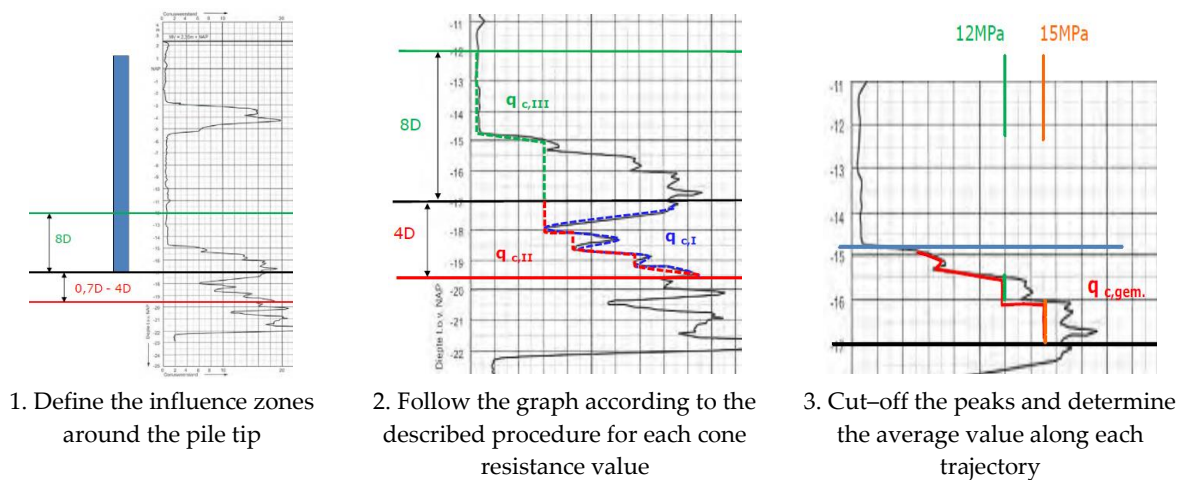


figure A-17: determination of the pile resistance with a CPT–diagram (Backhausen & Van der Stoel, 2014)

- Region I: mean value of the cone resistances that is located between the pile tip and a depth of at least 0.7 and at most 4 times the equivalent pile tip diameter below the level of the pile tip. The zone must be chosen in such a way that the parameter has a minimum value.
- Region II: mean value of the cone resistances that goes from the bottom level of region I to the pile tip where each accounted value for the cone resistance may not be higher than a cone resistance at a lower level.
- Region III: the mean value of the cone resistances over region III that can be found between the pile tip level and a level above it at a distance of 8 times the pile tip diameter from the pile tip. Each accounted value for the cone resistance may not be higher than a cone resistance at a higher level.

To prevent too optimistic outcomes for the end bearing capacity, no values higher than 15 MPa are allowed. This limit is reduced even further to a value of 12 MPa for small peaks with a width less than 1 meter.

The maximum value of the pile tip resistance is valid when the distance between the location of the driven pile and the soil probing is not too large. In this report, only publicly available soil probing diagrams are used that are retrieved from www.dinoloket.nl.

In the CPT–method given above a lot of uncertainties are involved because it is a practical approach. The pile tip resistance and pile shaft resistance are both determined with cone penetration tests, so they are combined together into a compressive resistance. The calculation for this resistance value is given in appendix ‘A.6 Total bearing capacity (compression)’.

A.5 SHAFT RESISTANCE

The shaft resistance of a pile in compression can be determined in two ways. These are the theoretical approach via the slip method and the in-situ approach with results from cone penetration tests. The description of the latter is given below in appendix ‘A.5.1 Eurocode expressions’. in appendix

‘Numerical comparison of the slip method with Eurocode 7’, the slip method and the approach according to the Eurocode are compared to each other with input for both expressions.

A.5.1 EUROCODE EXPRESSIONS

The determination of the positive shaft friction is feasible in two ways. One of them is the slip method as given in *equation (4.26)*. The second method is based on the values from cone penetration tests (CPT). Firstly, the shaft resistance was also derived from the measured cone friction, but later on it was found that the obtained results were inaccurate compared to the derivation from the cone resistance (Van Tol, 1994). The current approach for the determination of the shaft friction is based on the cone resistance values for a single soil probing over the region where an upward resisting force is expected (NEN–EN 1997–1 (NB) par. 7.6.2.3, 2019).

$$\begin{cases} R_{s,max,i,k} = \int_0^L C_{pile} z \times q_{s,i,k} dz \\ q_{s,i,k} = \alpha_s \times q_{CPT,i} \end{cases} \quad A.30$$

The integral sign includes the possibility for a change in pile circumference and shaft resistance over the soil depth. A shaft friction factor is used to apply values from the CPT–diagrams into the expression. For tapered timber piles, the following value is recommended (NEN–EN 1997–1 (NB) table 7.c, 2019):

$$\alpha_s = 0.012$$

The CPT–values are averaged over the depth of the soil layers contributing to positive shaft friction. Measured irregularities are flattened out by the removal of peak pressures. Only values with a maximum of 15 MPa may be used with a further reduction to 12 MPa when the width of the peak is less than 1 meter.

In the CPT–method given above a lot of uncertainties are involved because it is a practical approach. The pile tip and pile shaft resistance are both determined with cone penetration tests, so they are combined together into a compressive resistance. The calculation for this resistance value is given in appendix ‘A.6 Total bearing capacity (compression)’.

A.5.2 NUMERICAL COMPARISON OF THE SLIP METHOD WITH EUROCODE 7

Equation (4.26) and *equation (A.30)* are compared to each other by three numerical examples. In each case, a pile with a constant diameter of 250 mm and a length of 20 m is driven into a uniform sand, clay, or peat layer. For the required soil parameters standard values are used (NEN–EN 1997–1 (NB) table 2.b, 2019). The groundwater table is taken equal to ground level. Positive shaft friction is assumed to be present over the entire pile length. The used soil parameters are presented in *table A-5* for each case.

parameter	case 1	case 2	case 3
soil type	sand	clay	peat
consistency	dense	moderate	loose
γ_{sat} [kN/m ³]	22.0	17.0	12.0
ϕ' [°]	40.0	17.5	15.0
q_c [MPa]	15.0	2.0	0.1
K_{slip} [–]	4.0	2.5	1.5

table A-5: parameters for the comparison of the slip method and the Eurocode expression

For each case the positive shaft friction force is calculated over the soil depth according to the slip method and the Eurocode 7 expression. The obtained results are captured in *figure A-18*.

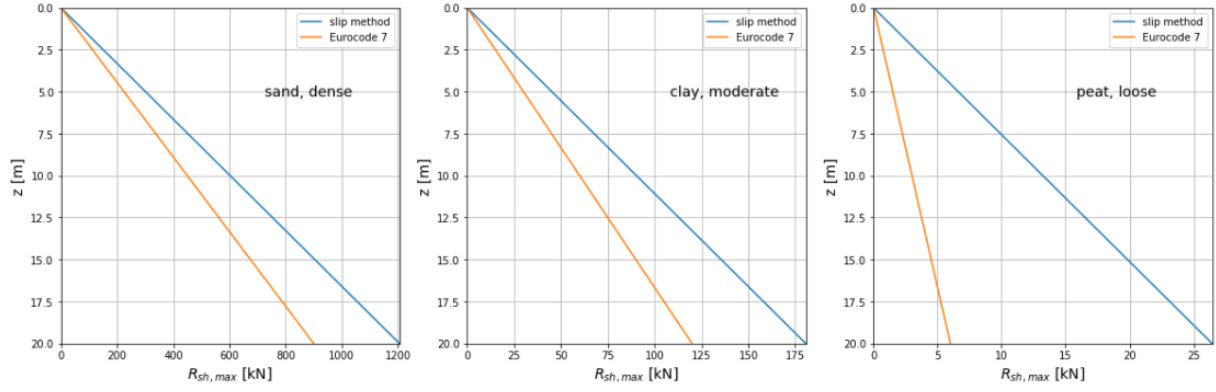


figure A-18: numerical calculations of positive shaft friction force over the soil depth

From above figure it follows that the slip method and the Eurocode 7 expression are closer to each other when the value for the alternative soil pressure coefficient in the slip method is higher. The choice for this constant is very important in acquiring the correct order of magnitude for the friction force. It seems that the slip method overestimates the total friction force and therefore this approach is very unreliable compared to the more sophisticated Eurocode 7 expression based on CPT-results.

A.6 TOTAL BEARING CAPACITY (COMPRESSION)

Both CPT-methods are robust calculation approaches for the determination of the pile tip bearing capacity and the positive shaft friction. A large part of insecurities in geotechnical parameters are diminished by these soil investigations. Uncertainties are reduced even further when more than one soil probing is performed at the project location. In this case, the total pile bearing capacity is calculated for each soil probing (NEN-EN 1997-1 (NB) par. 7.6.2.3 (c), 2019).

$$R_{c,max,i,k} = R_{b,max,i,k} + R_{s,max,i,k} \quad A.31$$

The single contributions of base resistance and pile shaft friction can be calculated with *equation (A.29)* and *equation (A.30)*, respectively. The translation to a characteristic value requires the minimum and average value of the above expression (NEN-EN 1997-1 par. 7.6.2.3 (5), 2016).

$$R_{c,avg,k} = \frac{1}{n} \times \sum_{i=1}^n R_{c,max,i,k} \quad A.32$$

$$R_{c,min,k} = \min_{i=1}^n \{R_{c,max,i,k}\} \quad A.33$$

In the computation of the characteristic value of the pile bearing capacity correlation factors are involved. This factor reduces the variability in the soil parameters and takes the ability of force redistribution in the foundation into account in case one element fails (NEN-EN 1997-1 par. 7.6.2.3 (5), 2016).

$$(R_{c,k})_{avg} = \frac{R_{c,avg,k}}{\xi_3} \quad A.34$$

$$(R_{c,k})_{min} = \frac{R_{c,min,k}}{\xi_4} \quad A.35$$

The correlation factors given above are related to driven piles and depend on the rigidity of the structure and the number of soil investigations. A structure is considered as stiff when it settles (for compression piles) or rises (for tension piles) less than 5 mm at the location of a removed pile or pile group. This check can be performed with a computational model loaded by the prescribe loading combinations in

SLS (serviceability limit state). Otherwise, the structure is regarded as non-stiff. In *table A-6*, values are given for the correlation factors.

rigidity	ξ for n =	1	2	3	4	5	7	10
stiff	ξ_3 [-]	1.26	1.20	1.18	1.17	1.17	1.15	1.14
	ξ_4 [-]	1.26	0.96	0.94	0.93	0.93	0.92	0.91
non-stiff	ξ_3 [-]	1.39	1.32	1.30	1.28	1.28	1.27	1.25
	ξ_4 [-]	1.39	1.32	1.30	1.03	1.03	1.01	1.00

table A-6: correlation factors related to the structural rigidity and the number of soil probings (NEN-EN 1997-1 (NB) table A.10a and A.10b, 2019)

The design value of the total bearing capacity follows from the average value of *equation (A.34)* and the minimum value of *equation (A.35)* divided by the safety factor for the total pile resistance given in *table 4-3* (NEN-EN 1997-1 par. 7.6.2.3 (5), 2016).

$$R_{c,d} = \frac{\min\{(R_{c,k})_{avg}; (R_{c,k})_{min}\}}{\gamma_{tot}} \quad A.36$$

Each resistance component from *equation (A.31)* can also be computed individually by the division with the resistance factor of the pile tip and the pile shaft, respectively (NEN-EN 1997-1 par. 7.6.2.3 (4), 2016).

$$R_{b,d} = \frac{R_{b,max,k}}{\max\{\xi_3; \xi_4\} \times \gamma_b} \quad A.37$$

$$R_{s,d} = \frac{R_{s,max,k}}{\max\{\xi_3; \xi_4\} \times \gamma_s} \quad A.38$$

Above calculations simplify a lot when only one soil probing is involved because the average value of *equation (A.32)* and the minimum value of *equation (A.33)* become superfluous.

A.7 NEGATIVE SKIN FRICTION

The slip method and the expression of Zeevaert-De Beer presented in paragraph '4.4.1.3 Negative skin friction' are both only applicable for homogeneous soil conditions. Where the slip method is valid only for single piles, the approach according to Zeevaert-De Beer also considers the effect of pile groups on the value for the negative skin friction force within a pile group area. To apply the correct expression for a single or group pile, *equation (4.29)* can be used.

The slip method and the Zeevaert-De Beer expression cannot be applied for stratified soil systems in their current form, so an adaptation is needed for both formulas. In the Eurocode, both expressions are extended for cases with inhomogeneous soils. Those calculation methods are given in paragraph 'A.7.1 Eurocode expressions'. To understand the influence of the group pile effect in the Zeevaert-De Beer expression, a comparison is made with the slip method in paragraph 'A.7.2 Numerical expressions of slip method with Zeevaert-De Beer' for a homogeneous soil composition.

A.7.1 EUROCODE EXPRESSIONS

For individual piles, the slip method is adjusted to an equivalent expression for a subsoil consisting of more than one layer (NEN-EN 1997-1 (NB) par. 7.3.2.2 (d), 2019).

$$\begin{cases} \sigma_{nsf,j} = K_{0,j} \times \tan(\delta_j) \times \frac{1}{2} \times (\sigma'_{v,j-1} + \sigma'_{v,j}) \\ F_{nsf,j} = \sigma_{nsf,j} \times C_{pile,avg,j} \times t_j \\ F_{nsf} = \sum_{i=1}^n F_{nsf,i} \end{cases} \quad A.39$$

Three different cases can be distinguished. Those are depicted in *figure A-19*.

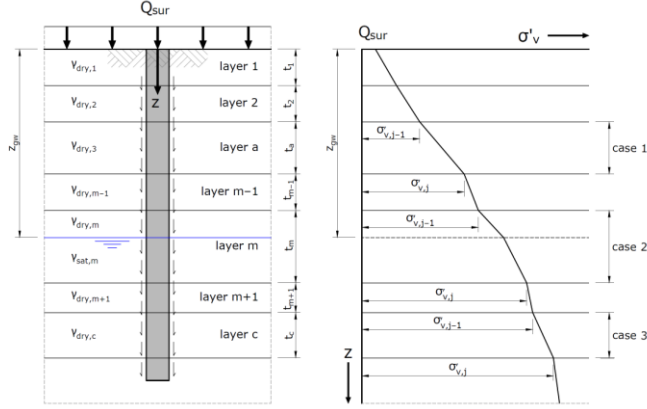


figure A-19: negative skin friction for a single pile (NEN-EN 1997-1 (NB) figure 7.a, 2019)

1. The groundwater table is situated below the soil layer of interest $j < m$:

$$\begin{cases} \sigma'_{v,j} = \sigma'_{v,j-1} + t_j \times \gamma_{dry,j} \\ \sigma'_{v,j-1} = Q_{sur} + \sum_{i=1}^{j-1} (t_i \times \gamma_{dry,i}) \end{cases} \quad A.40$$

2. The groundwater table is situated in the soil layer of interest $j = m$:

$$\begin{cases} \sigma'_{v,j} = \sigma'_{v,j-1} + \left(z_{gw} - \sum_{i=1}^{j-1} t_i \right) \times \gamma_{dry,j} + \left(\sum_{i=1}^j t_i - z_{gw} \right) \times \gamma_{sat,j} \\ \sigma'_{v,j-1} = Q_{sur} + \sum_{i=1}^{j-1} (t_i \times \gamma_{dry,i}) \end{cases} \quad A.41$$

3. The groundwater table is situated above the soil layer of interest $j > m$:

$$\begin{cases} \sigma'_{v,j} = \sigma'_{v,j-1} + t_j \times \gamma_{sat,j} \\ \sigma'_{v,j-1} = Q_{sur} + \sum_{i=1}^{j-1} (t_i \times \gamma_{dry,i}) + \left(z_{gw} - \sum_{i=1}^{j-1} t_i \right) \times \gamma_{dry,j} + \left(\sum_{i=1}^j t_i - z_{gw} \right) \times \gamma_{sat,j} + \sum_{i=m}^{j-1} (t_i \times \gamma_{sat,i}) \end{cases} \quad A.42$$

The Zeevaert-De Beer expression in *equation (A.36)* cannot be used for a layered soil system in this form, so it is extended to include a number of soil layers. A distinction is made between the upper soil layer and deeper soil layers (NEN-EN 1997-1 (NB) par. 7.3.2.2 (e), 2019). Both situations are depicted in *figure A-20*.

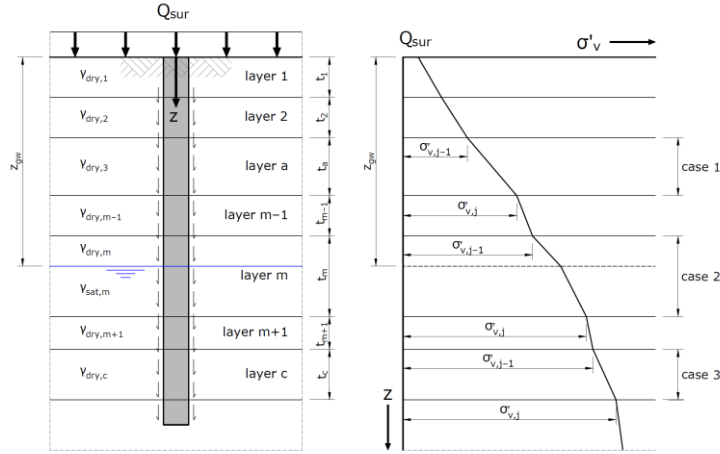


figure A-20: negative skin friction for a pile group (NEN-EN 1997-1 (NB) figure 7.b, 2019)

1. Skin friction of the upper soil layer $j = 1$:

$$\begin{cases} \sigma_{nsf,1} = \gamma'_1 \times t_1 - \left(\frac{\gamma'_1}{m_1} - Q_{sur} \right) \times 1 - e^{-m_1 \times t_1} \\ \sigma'_{m,1} = \frac{\gamma'_1}{m_1} \times 1 - e^{-m_1 \times t_1} + Q_{sur} \times e^{-m_1 \times t_1} \end{cases} \quad \text{where } m_1 = \frac{C_{pile,avg,1} \times K_{0,1} \times \tan \delta_1}{A_{gr}} \quad A.43$$

2. Skin friction for deeper soil layers $j > 1$:

$$\begin{cases} \sigma_{nsf,j} = \gamma'_j \times t_j - \left(\frac{\gamma'_j}{m_j} - \sigma'_{m,j-1} \right) \times 1 - e^{-m_j \times t_j} \\ \sigma'_{m,j-1} = \frac{\gamma'_{j-1}}{m_{j-1}} \times 1 - e^{-m_{j-1} \times t_{j-1}} + \sigma'_{m,j-2} \times e^{-m_{j-2} \times t_{j-2}} \end{cases} \quad \text{where } m_j = \frac{C_{pile,avg,j} \times K_{0,j} \times \tan(\delta_j)}{A_{gr}} \quad A.44$$

The value for the effective specific soil weight depends on the groundwater table, so if the soil is dry or saturated.

$$\begin{cases} \gamma'_j = \gamma_{dry,j} & \text{if } z_{gw} > \sum_{i=1}^j t_i \\ \gamma'_j = \frac{\gamma_{dry,j} \times (z_{gw} - \sum_{i=1}^{j-1} t_i) + (\gamma_{sat,j} - \gamma_w) \times (\sum_{i=1}^j t_i - z_{gw})}{t_h} & \text{if } \sum_{i=1}^{j-1} t_i < z_{gw} < \sum_{i=j-1}^j t_i \\ \gamma'_j = \gamma_{sat,j} - \gamma_w & \text{if } z_{gw} < \sum_{i=1}^{j-1} t_i \end{cases} \quad A.45$$

The shaft friction angle is related to the internal friction angle of the soil by a certain ratio. For timber piles, the following proportion is proposed:

$$\delta_j = 0.75 \times \varphi'_j \quad A.46$$

This ratio may be applied only when multiplication with the neutral soil pressure coefficient of equation (4.13) results in a value of at least 0.25.

$$K_{0,j} \times \tan(\delta_j) \geq 0.25 \rightarrow (1 - \sin(\varphi'_j)) \times 0.75 \times \varphi'_j \geq 0.25 \quad A.47$$

The requirement depends exclusively on the internal friction angle. The variation over this parameter in comparison with the minimum value is depicted in figure A-21.

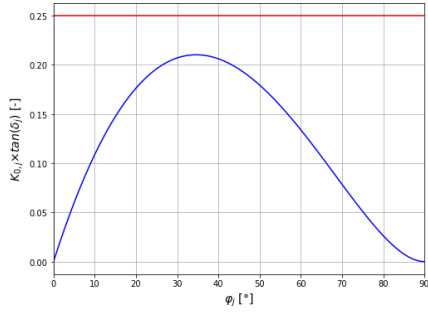


figure A-21: comparison requirement with internal friction angle values for timber piles

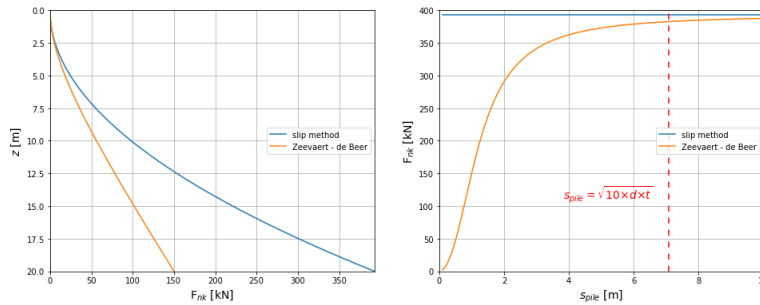
It is clear that the Eurocode requirement is governing for every value of the internal friction angle in case timber piles are applied. The simplification factor in *equation (4.28)*, *equation (A.43)*, and *equation (A.44)* becomes shorter for timber piles by uncoupling from the soil properties.

The design value of the negative skin friction is defined by the multiplication with a partial factor. The value is different for individual piles and pile groups as given in *table 4-3*.

$$F_{nsf,d} = \gamma_{nsf} \times F_{nsf,k} \quad \text{A.48}$$

A.7.2 NUMERICAL COMPARISON OF SLIP METHOD WITH ZEEVAERT-DE BEER

The differences between both approaches can be clarified with a numerical example. The used values are given in *table A-7* where the growth of the negative skin friction forces over the depth are depicted in *figure A-22* for both calculation methods.



parameter	value
soil type	sand
d [mm]	250
Q _{sur} [kPa]	0.0
t [m]	20.0
γ _{sat} [kN/m ³]	10.0
A _{gr} [m ²]	1.0

figure A-22: comparison of slip method with Zeevaert-De Beer expression table A-7: used parameters

From the left diagram it becomes clear that the calculated friction force with the slip method is a lot higher than the Zeevaert-De Beer expression because the slip method does not include a pile group effect. The influence of the pile group area is also visible in the right diagram. The slip method becomes a good approximation when the requirement according to *equation (4.29)* for individual piles is met. Both expressions give then more or less the same value for the friction force.

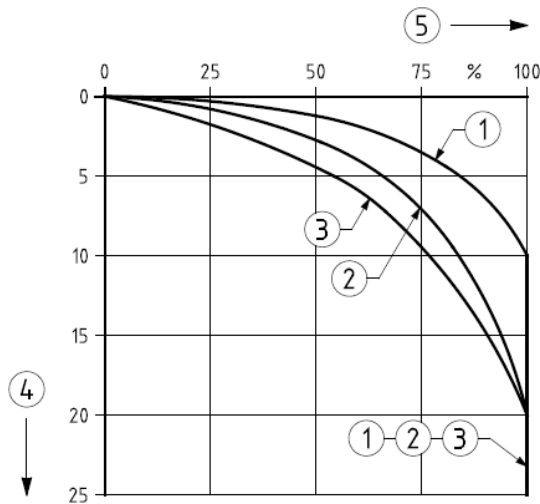
A.8 PILE SETTLEMENT

The different contributions of *equation (4.31)* and *equation (4.32)* can be determined in two ways as mentioned already in paragraph '4.4.1.4 Pile settlement'. For this thesis report, the theoretic approach follows from the building codes. The corresponding calculation rules are addressed in paragraph 'A.8.1 Eurocode expression'. In the Eurocode, an expression is used for the elastic pile elongation of an element with a constant diameter along the pile length. A timber pile has often a tapered shape, so its

deformation could deviate from the displacement according to the prescribed expression in the building codes. In paragraph 'A.8.2 Numerical comparison of prismatic with tapered pile shape', it is investigated if there are any differences between the deformations of both pile shapes.

A.8.1 EUROCODE EXPRESSION

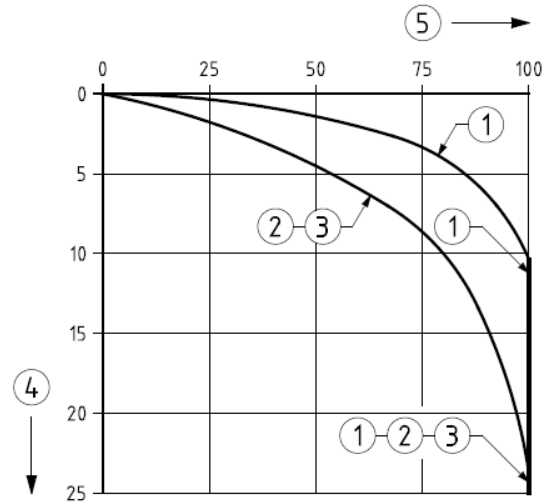
Settlements of foundation piles can be calculated by the summation of the contributions for a single pile and a pile group with *equation (4.31)* and *equation (4.32)*. This first factor in *equation (4.31)* is related to the displacement of a single pile. The pile displacement in *equation (4.32)* is split up in a settlement of the pile base and a component for the elastic pile shortening. The first factor can be derived from load–displacement diagrams in *figure A-23* and *figure A-24*.



Legend

1. load–displacement curve 1
2. load–displacement curve 2
3. load–displacement curve 3
4. $\frac{s_b}{d_{tip}}$ in %
5. $\frac{R_b}{R_{b,max}}$ in %

figure A-23: relation between the ratio of the actual and the maximum pile tip bearing force with the pile tip settlement (NEN–EN 1997–1 (NB) figure 7.n, 2019)



Legend

1. load–displacement curve 1
2. load–displacement curve 2
3. load–displacement curve 3
4. s_b in mm
5. $\frac{R_s}{R_{s,max}}$ in %

figure A-24: relation between the ratio of the actual and the maximum pile shaft friction force with the pile tip settlement (NEN–EN 1997–1 (NB) figure 7.o, 2019)

The load–displacement diagrams relate the pile tip settlement to the mobilisation ratio of both resistance parameters. In these graphs three different load–displacement curves are presented. The ultimate pile tip resistance is reached at a settlement of 10% of the equivalent pile tip diameter. The entire pile shaft resistance is mobilised at a pile tip settlement of 11 mm. When the value of the pile tip settlement lies in between those bounds, the actual force in the pile tip can be derived via vertical equilibrium.

$$R_b = F_{c,tot} - R_s \quad A.49$$

In this equation, the total compressive load consists of the pile head load and the negative skin friction component.

$$F_{c,tot} = F_{c,head} + F_{nsf} \quad A.50$$

A settlement higher than 11 mm is often not reached in practice, so in this case both shaft and tip contribute partly to the total resistance factor. The following steps are required to obtain the pile tip settlement and the corresponding resistance components from *figure A-23* and *figure A-24*:

1. Choose the correct curve based on the pile installation method. For a timber pile driven into the ground, displacement curve 1 is used.
2. Attach both graphs to each other by application of the same scaling on the y-axis.
3. Draw a horizontal line segment of the total compressive load in ULS or SLS such that both ends coincide with a curve.
4. Read the value of the pile tip displacement at the y-axis.

The second component of *equation (4.32)* follows from the elastic pile shortening at the pile head relative to the pile tip under influence of the averaged compressive load. It is found by the differential equation for axial pile deformation. The taper of a timber pile requires a slightly different expression than the one given in the standards (NEN-EN 1997-1 (NB) par. 7.6.4.2 (j), 2019).

$$u_{pile\ z} = \frac{2 \times F_{c,avg} \times 0.944^{-2 \times z} - 0.944^{-2 \times L}}{\ln 0.944 \times \pi \times E_{pile} \times d_{head}^2} \quad A.51$$

The derivation of above expressions is given in appendix 'A.16 Derivation of equation (A.50)'. By specifying the running variable at pile head level the elastic pile shortening at this level can be obtained.

$$s_{el} = u_{pile\ 0} = \frac{2 \times F_{c,avg} \times 1 - 0.944^{-2 \times L}}{\ln 0.944 \times \pi \times E_{pile} \times d_{head}^2} \quad A.52$$

Where the average pile head load in both equations is a weighted average of the axial forces and resistances with its corresponding friction zones along the pile length.

$$F_{c,avg} = \frac{F_{c,tot} \times l + 0.5 \times (F_{c,tot} + R_b) \times \Delta L}{L_{pile}} \quad A.53$$

In the deformation expressions a Young's modulus for the pile material is needed. For timber piles, the following value can be used (NEN-EN 1997-1 (NB) par. 7.6.4.2 (j), 2019).

$$E_{pile} = 3.6 \times 10^9 \text{ N/m}^2$$

The pile group settlement is caused by the compression of the soil below the pile tips as a result of pile loads. It is relevant for small pile clusters under a single footing. Poor force spreading means very high soil stresses which could induce settlements. This phenomenon may be neglected for pile groups when it fulfils a certain spacing requirement (NEN-EN 1997-1 (NB) par. 7.6.4.2 (k), 2019).

$$S_{pile} > 10 \times d_{tip} \quad A.54$$

When the pile distances do not meet this condition, the settlement follows from soil compaction at a level of four times the equivalent diameter below pile tip level.

$$s_{pile,gr} = \frac{0.9 \times m^* \times F_{gr} \times \sqrt{A_{4D}}}{E_{soil}} \quad A.55$$

The boundaries of the loaded area under the pile tip are determined by a spreading angle of 45° with respect to the pile edges as shown in *figure A-25*.

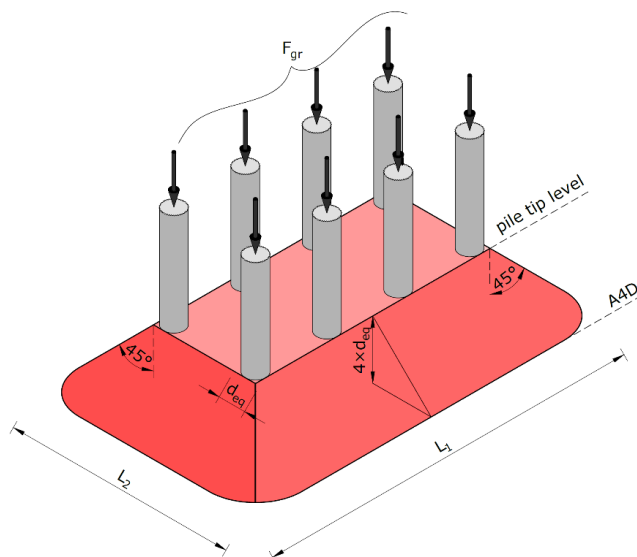


figure A-25: group pile settlement

In equation (A.55), a shape factor is included that depends on the shape of the loaded area. Values for this parameter are given in table A-8.

parameter	circle	square	rectangle L_1/L_2^a					
			1.5	2	3	5	10	100
$m^* [-]$	0.96	0.95	0.94	0.92	0.88	0.82	0.71	0.37
^a where L_1 / L_2								

table A-8: shape factor for different load areas (NEN-EN 1997-1 (NB) table 7.f, 2019)

Another term in equation is the modulus of elasticity of the soil below the pile tip. The soil under the piles is often well compacted by the exerted pile pressures. In this case, the soil stiffness follows from sand with a high consistency (NEN-EN 1997-1 (NB) table 2.b, 2019).

A quay wall structure is often widespread over many metres, so secondary settlement of the entire structure will not show up when it is subjected to a distributed load. The secondary settlement is then equal to zero. A different scenario appears when the structure has to resist a high concentrated load. For the quay wall, load model 2 described in paragraph '4.3.4 Terrain loads' falls into this category. Due to its distinct character, only a small part of the foundation becomes active when this load type appears. It is assumed that the piles under two pile cap beams forms a pile cluster by the connection of the cross-beams and the floor elements.

A.8.2 NUMERICAL COMPARISON OF PRISMATIC WITH TAPERED PILE SHAPE

The influence of the pile taper along the length can be made clear with a numerical example. The values are given in table A-9. The differences between both expressions are shown in figure A-26.

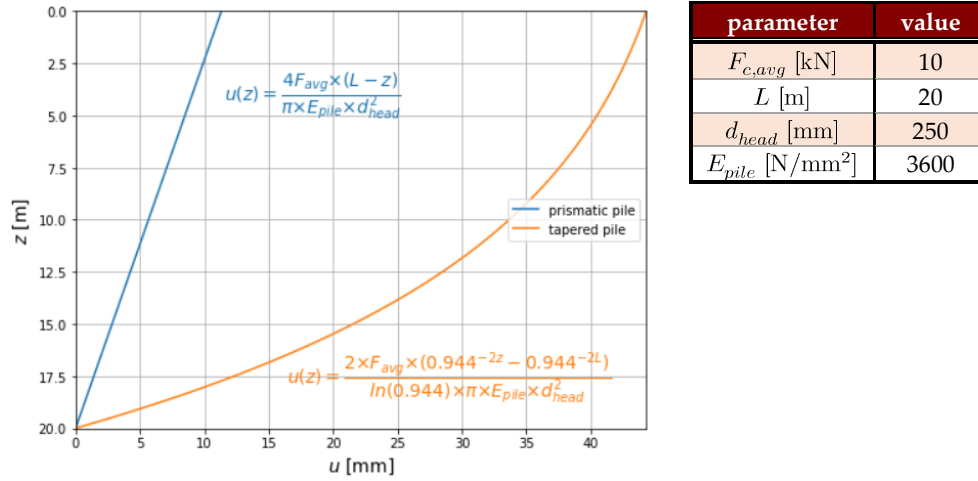


figure A-26: comparison of axial pile shortening for a pile with a prismatic shape and a tapered pile table A-9: used parameters

From above graph it follows that the tapered pile has a very different deformation behaviour than the pile with a constant cross-section. For the used parameters, the axial shortening at pile head level is four times bigger for the tapered pile than for the pile with a constant diameter over the length. From this single example it can be concluded that the taper could have a very large influence on the axial deformations and therefore it cannot be omitted in further calculations.

A.9 LOCATION OF THE NEUTRAL PLANE

As stated in paragraph '4.4.1.5 Neutral plane location', the neutral plane is located where the pile displacement is equal to the settlement of the soil given by equation (4.33). To find the neutral plane location, first the values of the friction forces have to be calculated, but those values depend on the friction zones and so the location of the neutral plane must be known beforehand. Before going into detail about this iterative process, expressions for the pile displacement and the soil settlement are required. They are given in the paragraphs 'A.9.1 Pile settlement' and 'A.9.2 Soil settlement'. The iteration process is elaborated step-by-step in paragraph 'A.9.3 Calculation approach'. It is verified in paragraph 'A.9.4 Numerical example' where three cases are shown with different parameters.

A.9.1 PILE DISPLACEMENT

Displacement of a timber foundation pile is a combination of axial pile shortening and settlement of the pile tip. It is almost similar to equation (A.51) because only the lower boundary condition of the ordinary differential equation in appendix 'A.16 Derivation of equation (A.50)' has to be changed.

$$u_{pile} z = \frac{2 \times F_{c,avg} \times (0.944^{-2 \times z} - 0.944^{-2 \times L_{pile}})}{\ln 0.944 \times \pi \times E_{pile} \times d_{head}^2} + \frac{F_{c,avg}}{k_{ax}} \quad A.56$$

The pile in above equation is modelled as an axial spring with a certain spring stiffness. Substitution of a fixed point by an axial spring has a favourable effect on the internal force transfer in a framework system because high loads can be distributed more evenly over the total number of piles (Meireman, 2016). Large differences in pile head loads are then prevented and so the probability of single pile failure decreases. The axial spring stiffness can be calculated when the pile tip displacement and the actual pile resistances are known.

$$k_{ax} = \frac{R_b + R_s}{s_b + s_2} \quad A.57$$

No contribution of the elastic pile shortening is incorporated in the axial spring stiffness because it is included already in *equation (A.56)*. The actual response of the pile tip by the application of a series of force increments is quite complicated, so for simplicity the tip is schematized as a bi-linear spring. The relation between the pile tip settlement and the pile head force is then valid until a certain settlement is reached. Increasing the force even more results in excessive displacements that could indicate geotechnical pile tip failure. According to *figure A-23*, failure occurs at a settlement higher than 10% of the pile tip diameter. The described pile tip behaviour is depicted in *figure A-27* with a force-displacement diagram.

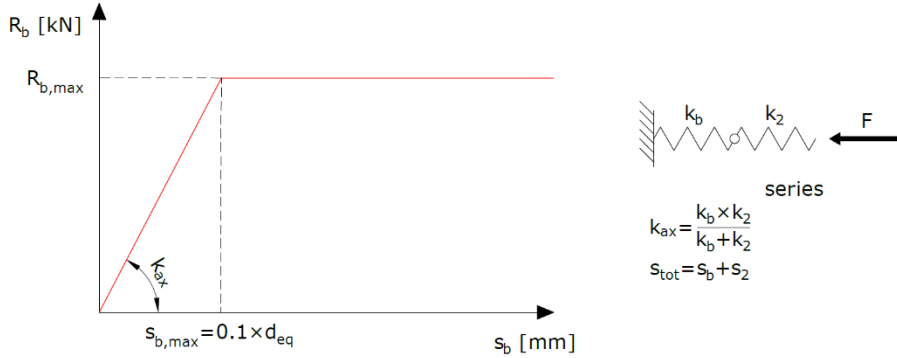


figure A-27: diagram for a support modelled as a bilinear spring

The value of the axial pile tip stiffness has a considerable impact on the load distribution over the foundation piles. In the determination of the axial pile stiffnesses many uncertainties are incorporated, so it is complicated to observe if the values are justifiable. Minimum and maximum design values can be used as variation of stiffnesses in a calculation model to investigate the response of the entire foundation structure (Backhausen & Van der Stoel, 2014).

$$\begin{cases} k_{ax,min} = \frac{k_{ax}}{\sqrt{2}} \\ k_{ax,max} = \sqrt{2} \times k_{ax} \end{cases} \quad A.58$$

A.9.2 SOIL SETTLEMENT

Soil settlements are induced by several processes during the lifetime of a structure. An enumeration of possible causes is given below (Backhausen & Van der Stoel, 2014).

- autonomous settlements
- application of a permanent surface load (elevation of the ground level)
- lowering of the groundwater table (increase of vertical effective soil stresses)
- densification of soil layers around the pile during pile driving activities that could lead to additional soil consolidation

All above described events could appear at a certain moment in the lifetime of a structure except from the first bullet point. Soil layers always consolidate for a certain amount that cannot be assigned to any external factors. The other aspects are relatable to a specific event causing a change in the soil state. The total settlement consists of two parts which are the primary and the secondary settlement.

$$s_{soil,tot} \approx s_{soil,1} + s_{soil,2} \quad A.59$$

The primary soil settlement takes a change of the initial effective stress into account by a certain stress increase (NEN-EN 1997-1 (NB) par. 6.6.2 (e), 2019).

$$s_{soil,1} z = \sum_{i=1}^{j-1} \left(\frac{C_{e,i}}{1+e_i} \times t_i \right) \times \frac{\sigma'_{v,0}(\sum_{i=1}^{j-1} t_i) + \Delta\sigma'_v(\sum_{i=1}^{j-1} t_i)}{\sigma'_{v,0}(\sum_{i=1}^{j-1} t_i)} + C_{c,i} \times \left(z - \sum_{i=1}^{j-1} t_i \right) \times \ln \left(\frac{\sigma'_{v,0} z + \Delta\sigma'_v z}{\sigma'_{v,0} z} \right) \quad A.60$$

The fraction of the primary consolidation index and the initial void ratio depends on the soil type and the value for the effective vertical soil stress (NEN-EN 1997-1 (NB) table 2.b, 2019). For the calculation of the neutral plane, only settlements below the foundation floor have to be determined. This part of the subsoil is not loaded by external forces, so no surface loads are taken into account. In this case, no stress increase appears in the soil and the primary settlement is equal to zero.

The second contribution is the secondary soil settlement and it is defined by the service life of the structure (NEN-EN 1997-1 (NB) par. 6.6.2 (g), 2019).

$$s_{soil,2} z = \left(\sum_{i=1}^{j-1} (C_{\alpha,i} \times t_i) + C_{\alpha,i} \times \left(z - \sum_{i=1}^{j-1} t_i \right) \right) \times \ln t_{\infty} \quad A.61$$

In this equation, the secondary consolidation index is related only to the soil type (NEN-EN 1997-1 (NB) table 2.b, 2019). The duration of the settlement is equal to 10.000 days. A lower value can be applied when the load duration is significantly shorter than the prescribed value. Historic quay walls are present for decades along the Dutch inland waterways, so the prescribed value is definitely valid for those kind of structures.

A.9.3 CALCULATION APPROACH

With the obtained values for the pile displacement and the soil settlement both along the soil depth, the neutral plane location can be determined according to an iterative process. The required steps are given below:

1. Calculate the maximum pile tip force with *equation (A.29)*, maximum pile shaft force with *equation (A.30)*, and the negative skin friction load with *equation (A.39)* for a chosen location of the neutral plane and correct friction zones
2. Compute the total pile head load with *equation (A.50)* for a chosen location of the neutral plane (preferred location is the depth at the transition of the weak layer to the first bearing layer).
3. Determine the pile tip settlement, actual pile tip force and actual pile shaft force from the load-settlement *figure A-23* and *figure A-24*.
4. Calculate the soil settlement with *equation (A.59)* and the pile displacement with *equation (A.56)* at the location of the neutral plane.
5. Find a new location of the neutral plane with *equation (4.33)*.
6. Repeat steps 1, 2, 3, and 4 until an agreement is reached between the force magnitudes, pile displacement, and the location of the neutral plane. It is assumed that final values are reached when the difference between the last two calculated neutral planes is smaller than 0.1 m.

The calculation steps to obtain the correct location of the neutral plane are clarified in the following paragraph 'A.9.4 Numerical example'.

A.9.4 NUMERICAL EXAMPLE

For the determination of the neutral plane location, a comparison between the pile deformation and the soil settlement has to be performed. An important part is the pile tip settlement that is derived from the load-displacement diagrams as given in *figure A-23* and *figure A-24*. When the location of the neutral

plane is determined according to an iterative process, the obtained value in every step has to be renewed. Reading values from the load–displacement diagrams is quite cumbersome and is quite complicated for the implementation into an automatic process. A small research is performed to show the influence of an alternative derivation of the adjusted pile tip settlement on the location of the neutral plane. If the influence is negligibly small, the determination with the graphs is required only at the start of the iterative cycle.

The influence of a change in the value of the pile tip settlement is investigated by three numerical cases. The generic pile set up is given in *figure A-28*.

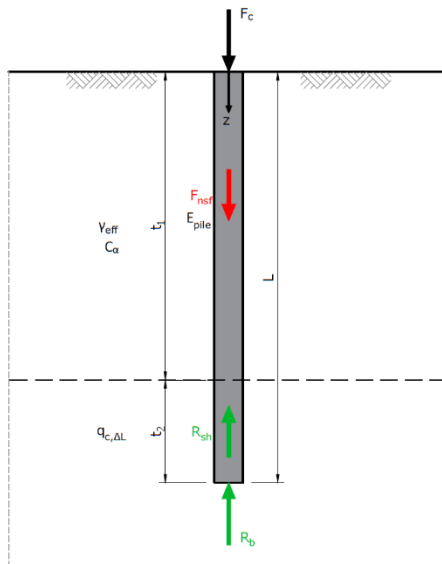


figure A-28: case for research to influence of pile settlement change

In total, three cases are considered. Case 1 has a foundation pile with a total length of 20 m that is driven 5 m into a very stable sand layer. The weak layer on top consists of clay particles without intermixing with other substances and has a thickness of 15 m. The groundwater table is equal to ground level. The pile in case 2 is 11 m long with its pile tip 2 m deep into a moderately stable sand layer. A 9 m thick peaty soil is located above this layer with a moderate degree of preloading where the groundwater level reaches ground level. In case 3 a pile with a total length of 15 m is situated for 3 m into a very stable sand layer. On top a peat layer is located with a thickness of 12 m. The groundwater table coincides with the boundary between both layers. An executive overview of required parameters is shown in *table A-10* for every numerical case.

parameter	value		
	case 1	case 2	case 3
t_1 [m]	15	9	12
t_2 [m]	5	2	3
z_{gw} [m]	0	0	12
γ_{eff} [kN/m ³]	7	3	13
C_α [–]	0.0061	0.0153	0.0153
$q_{c,1}$ [MPa]	1.0	0.2	0.2
$q_{c,\Delta L}$ [MPa]	15	12	15
F_c [kN]	150	100	200
Q_{sur} [kN/m ²]	10	0	25
d_{head} [mm]	0.25	0.20	0.30
E_{pile} [N/mm ²]	3600	3600	3600
A_{gr} [m ²]	0.50	1.50	0.75

table A-10: parameters for each case in this numerical example

The following steps are taken to investigate if a change in pile tip settlement has a considerable influence on the location of the neutral plane.

1. Determine the maximum pile tip resistance, maximum pile shaft resistance, and negative skin friction for a neutral plane at the transition between the weak and stable layer.
2. Read the actual pile tip settlement, actual pile resistance, and actual shaft resistance from *figure A-23* and *figure A-24* with the value for the total pile load.
3. Compute the elastic pile shortening along the pile axis.
4. Determine the autonomous total settlement over the soil depth.
5. Calculate the new height of the neutral plane at the depth where the pile deformation is equal to the soil settlement.
6. Read the pile tip settlement, the actual pile resistance, and actual shaft resistance from *figure A-23* and *figure A-24* for a second time with the value of the total pile load (first iteration).
7. Set up two different cases:
 - 7.1. Compute the elastic pile shortening along the pile axis with a new value for the pile tip settlement derived from the load–displacement graphs and calculate the new height for the neutral plane.
 - 7.2. Compute the elastic pile shortening along the pile axis with a new value for the pile tip settlement determined by an alternative method and calculate the new height for the neutral plane.
8. Repeat the iterative cycles until equilibrium between the pile response and the acting forces is reached.
9. Compare the final value of the neutral plane location in both methods with each other.

An overview of the performed calculations for the initial situation with a neutral plane at the transition of the weak and the stable layer is given below in *table A-11*.

parameter	value			reference
	case 1	case 2	case 3	
$R_{b,max}$ [kN]	51.41	74.27	131.73	equation (A.28)
$R_{s,max}$ [kN]	258.73	101.75	234.06	equation (A.29)
F_{nst} [kN]	44.35	11.82	94.35	equation (A.38)
$F_{c,tot}$ [kN]	194.35	111.82	294.35	equation (A.49)

table A-11: results of the initial pile forces

The actual pile forces and the resulting settlement can be determined with the load displacement diagrams from *figure A-23* and *figure A-24*. For each load case the determination of those quantities is depicted in *figure A-29*.

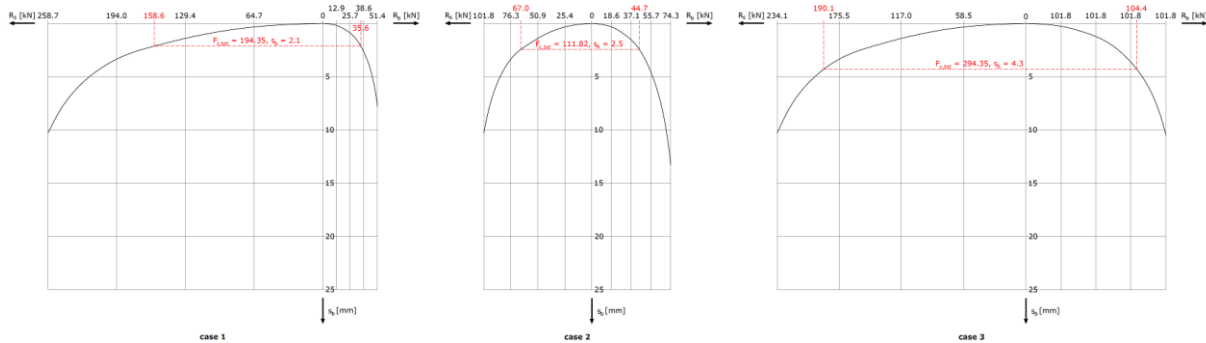


figure A-29: load–displacement diagrams of the initial situation

With above pile forces and settlements and the calculation of the averaged pile head force a new location of the neutral plane can be specified by plotting the pile deformation against the soil settlement. The visualisation of this step can be seen in *figure A-30*.

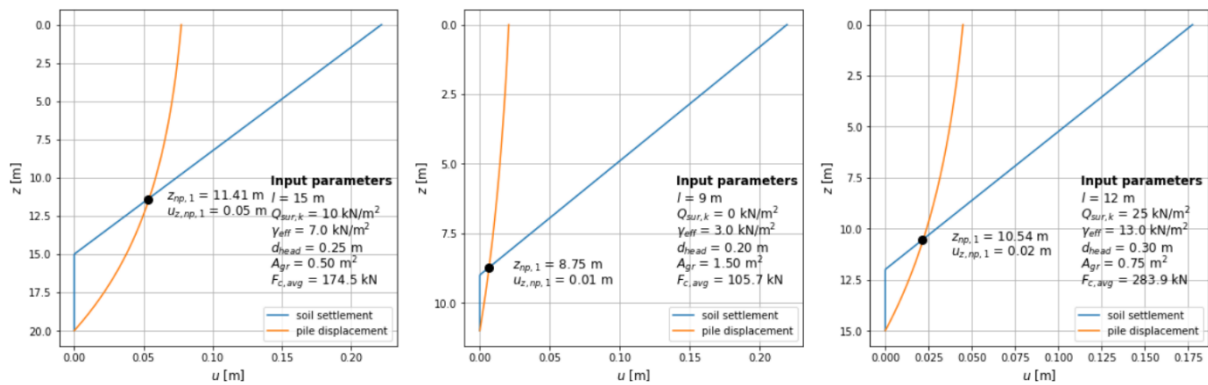


figure A-30: determination of the neutral plane in the first iteration cycle

The new location of the neutral plane leads to updated values of the pile forces in the first iteration cycle. Only the pile tip resistance remains the same. They are shown in *table A-12*.

parameter	value			reference
	case 1	case 2	case 3	
$R_{b,max,1}$ [kN]	51.41	74.27	131.73	equation (A.28)
$R_{s,max,1}$ [kN]	274.04	101.95	235.70	equation (A.29)
$F_{nsf,1}$ [kN]	33.39	11.36	82.59	equation (A.38)

table A-12: pile forces after one iteration

The shift of the neutral plane in upward direction resulted in a decrease of the skin friction and an increase of the shaft friction. This has a positive influence on the pile resistance and the pile settlement. With these forces, the next position of the neutral plane can be determined for the second iteration step where the influence of a change in pile tip settlement is investigated.

For the first method, the new pile tip settlement and the pile reaction force in each iteration step are derived from the load–displacement graphs *figure A-23* and *figure A-24*. In each iteration cycle, the total pile head force changes due to a new location of the neutral plane, so the graphs are used a lot of times.

In the second approach, the pile tip settlement is determined from the ratio with the renewed total pile head force in the current iteration step and the total pile head force and the pile tip settlement from the previous iteration step. The same approach is followed for the actual pile tip forces. In this way, the pile response is altered every iteration step without making use of the load–displacement graphs.

$$\begin{cases} s_{b,i} = \frac{F_{c,avg,i}}{F_{c,avg,i-1}} \times s_{b,i-1} \\ R_{b,i} = \frac{F_{c,avg,i}}{F_{c,avg,i-1}} \times R_{b,i-1} \end{cases} \quad A.62$$

With the different values of the pile head forces, the pile responses can be determined with the load displacement graphs of *figure A-23* and *figure A-24* or with the ratios of the pile head forces of *equation (A.62)*. In *table A-13*, the results of both approaches are shown together with the resulting averaged pile head force.

method	s _{b,1} [mm]			R _{b,1} [kN]			F _{c,avg,2} [kN]		
	case 1	case 2	case 3	case 1	case 2	case 3	case 1	case 2	case 3
graphs	1.9	2.5	3.8	34.2	44.6	100.1	151.8	104.6	255.9
pile head force	2.0	2.5	4.1	33.6	44.5	100.2	151.6	104.6	255.9

table A-13: pile reactions caused by different forces for the two calculation methods

Averaging of the pile forces over length results in the reduction of the differences between both methods to almost zero. This will also become visible in the determination of the new location of the neutral plane in the second iteration step. The graphs for the comparison of the soil settlement and the pile deformation are given below in *figure A-31* for both methods.

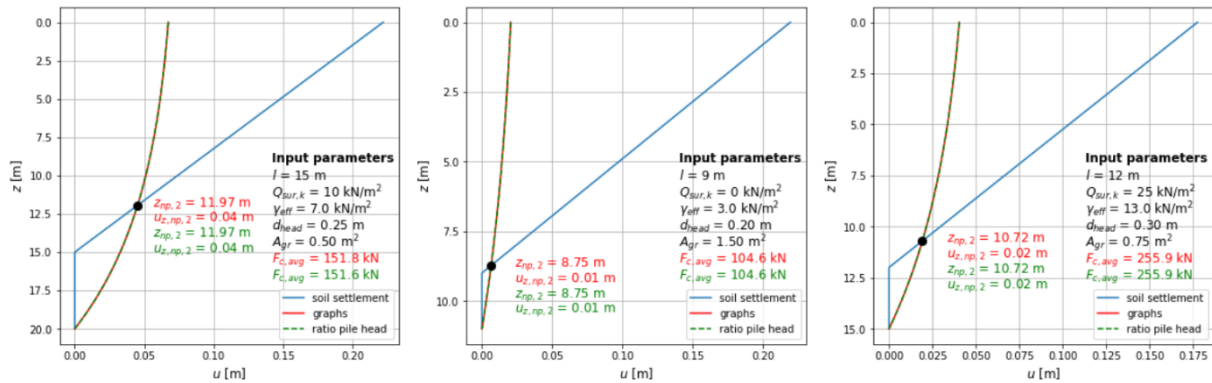


figure A-31: determination of the neutral plane in the second iteration cycle for both methods

The above process goes on further until convergence is reached between the pile forces and the neutral plane location. The remaining steps are not shown here because the final locations of the neutral planes in these examples are not of any importance.

The determination of the neutral plane via load displacement–diagrams is quite cumbersome when the pile loads changes during the iteration process. As an alternative, only the initial value of the pile tip settlement and the pile tip reaction has to be found with these diagrams and the expressions in *equation*

(A.62) It results in a reduction in the computation time because the entire iteration process can be automatised.

A.10 TENSILE RESISTANCE

The tensile resistance of a pile is similar to the CPT-method for shaft resistance of a compressive pile. In paragraph '4.4.2.1 Tensile resistance', two requirements were given related to the pile dimensions to ensure the suitability of this approach (NEN-EN 1997-1 (NB) par. 7.6.3.3 (a), 2019).

$$\begin{cases} R_{t,d} = \int_0^L C_{pile} z \times q_{t,d,i} dz \\ q_{t,d,i} = \alpha_{t,i} \times q_{CPT,d,i} \end{cases} \quad A.63$$

Unlike the derivation of the characteristic values for the bearing capacity of piles in compression, only a design value of the tensile resistance can be calculated. The tension zone is taken equal to the entire soil depth at the pile location where the pile installation factor takes the different contributions of each soil layer into account. When the largest part of the tension resistance is retrieved from a sand layer, other soil layers may be incorporated as well with a certain reduction to the installation factor. The installation factor is shown in *table A-14* for each soil type when a timber foundation pile with a tapered shape is applied.

soil type	α_t [-]
sand	0.0070
silt	0.0035
clay	0.0035
peat	0

table A-14: pile installation factor for different soil types (NEN-EN 1997-1 (NB) table 7.c and par. 7.6.3.3 (b), 2019)

In the design value of the cone resistance some partial factors are included.

$$q_{CPT,d,i} = \frac{q_{CPT,i}}{\gamma_t \times \gamma_{var} \times \xi_3} \quad A.64$$

The derivation of the cone resistance value for a soil probing diagram is determined in the same way as the shaft resistance for piles in compression. Over the considered height of the friction zone in the probing graph, only values with a maximum of 15 MPa may be used that must be reduced to 12 MPa when the width of the peak is less than 1 meter. The partial factor deals with the way how friction forces are introduced by the interface of the pile with the soil. Another constant is the load factor that incorporates the change of quasi-static loads over the lifetime of the structure (Eurocode 7 (NB) par. 7.6.3.3 (d), 2019).

$$\gamma_{var} = 1 + 0.25 \times \frac{F_{t,max} - F_{t,min}}{F_{t,max}} \quad A.65$$

Where the minimum and maximum values of the tensile force are used that can occur during the lifetime of the structure. A compressive force gets a minus sign in the given sign convention. The possible range of values is given in *figure A-32*.

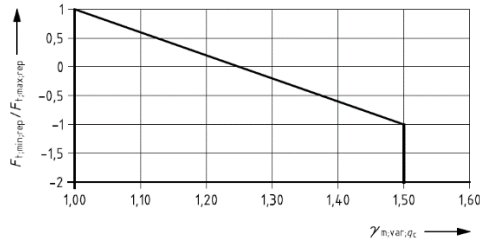


figure A-32: influence of load variability on the load combination factor (NEN-EN 1997-1 (NB) figure 7.k, 2019)

The loading history of a historic quay wall is often unknown because it is impossible to have an overview of all occurred loading situations on such structures. The maximum value in *table A-16* is applied for quay walls to cope with the uncertainties in possible loading cases. The correlation factor is the same as for compression piles, so it can be obtained from *table A-6*.

A.11 PILE RISE

When a pile is subjected to a tensile force, it moves in upward direction. This pile rise can be determined from the contributions given in *equation (4.36)* and *equation (4.37)*. Settlements of foundation piles can be calculated by the summation of the contributions for a single pile and a pile group with *equation (4.36)* and *equation (4.37)*. This first factor in *equation (4.36)* is related to the displacement of a single pile. The pile displacement in *equation (4.37)* is split up in a settlement of the pile base and a component for the elastic pile shortening. The rise of a single pile can be derived with the same load-displacement diagrams as for compressive piles. Only the diagram of the shaft resistance in *figure A-24* is needed because a pile in tension does not possess a resistance from the pile tip. A timber foundation pile under tension is also assigned to load-displacement curve 1. The pile head rise follows directly from the ratio between the actual force and the maximum tension resistance.

The second contribution is designated to the elastic pile elongation induced by an averaged tensile load. The expression for the pile displacement slightly differs from the form given in appendix 'A.14 Derivation of *equation A.10'* because the top boundary condition is changed to a tensile force.

$$u_z = \frac{2 \times F_{t,avg} \times 0.944^{-2 \times L} - 0.944^{-2 \times z}}{E_{pile} \times \pi \times d_{head}^2 \times \ln 0.944} \quad A.66$$

The elongation of the pile is obtained by specification of the running variable at pile head level.

$$r_{el} = u_0 = \frac{2 \times F_{t,avg} \times 0.944^{-2 \times L} - 1}{E_{pile} \times \pi \times d_{head}^2 \times \ln 0.944} \quad A.67$$

The average pile head force can be calculated by the weighted average of all forces along the pile length. For a pile in tension, only the axial force on the pile head is considered.

$$F_{t,avg} = \frac{1}{2} \times F_{t,head} \quad A.68$$

In the deformation expressions a Young's modulus for the pile material is needed. For timber piles, the following value can be used (NEN-EN 1997-1 (NB) par. 7.6.4.2 (j), 2019).

$$E_{pile} = 3.6 \times 10^9 \text{ N/m}^2$$

The second component of *equation (4.36)* is allocated to the soil rise caused by a group of tension piles. No pile group effects are expected at a quay wall structure, so its contribution is disregarded in this report.

A.12 STIFFNESS PROPERTIES

Besides the influence of the geotechnical resistance on the structural behaviour of a quay wall, also the properties of the individual elements play a role in the ability of the structure to transfer loads from the superstructure towards the piles. A structural system possesses two aspects that has an influence on the internal force transfer: stiffness of the structural elements and rotational stiffness of the joints in between the elements.

The distribution of loads over the structural system is partially influenced by the axial and bending stiffness of the structural components. A stiffer part of the structure attracts a large portion of the loads resulting in higher values for the internal bending moments and shear forces compared to a more flexible part. The determination of the stiffness components is described in appendix 'A.12.1 Element stiffness'. It is accompanied by a numerical example in appendix 'A.12.2 Joint stiffness' where the influence of differences in stiffness values is investigated in Scia Engineer with a framework model.

The second contribution to the stiffness of the structure is related to the joint rigidity in between the structural elements. In appendix 'A.12.3 Numerical example of joint stiffness', a calculation approach is given to estimate the rotational stiffness of the connections where calculations are performed with a structural framework program in Scia Engineer.

A.12.1 ELEMENT STIFFNESS

For the stiffnesses of the elements in a quay wall structure, a distinction is made for the foundation pile and the pile cap beam stiffness. Floor elements are not considered here because they are not used as input in a framework model as stated in paragraph '5.2.5 Axial pile head forces'. The element stiffness is comprised of a component related to axial loading and perpendicular loading which are the axial stiffness and bending stiffness, respectively. For beam elements, no axial stiffness is considered because these elements are loaded exclusively perpendicular to their element axis.

The axial and bending stiffnesses are usually written as a double letter symbol. The axial stiffness is calculated as the multiplication of the Young's modulus with the cross-sectional area where the bending stiffness consists of the Young's modulus multiplied with the second moment of area.

$$\begin{cases} EA_{pile} = E_{pile} \times A_{pile} \\ EI_{pile} = E_{pile} \times I_{pile} \end{cases} \quad A.69$$

For a pile, the value for the Young's moduli in both equations follows from appendix 'A.8 Pile settlement' where it was already used in *equation (A.51)* for the calculation of elastic pile shortening. The dimensional parameters are not constant along the pile length because of the tapered shape. When the taper expression of *equation (A.27)* is used, the following expressions are obtained:

$$\begin{cases} A_{pile} z = \frac{1}{4} \times \pi \times d_{head}^2 \times 0.944^{2 \times z} \\ I_{pile} z = \frac{1}{64} \times \pi \times d_{head}^4 \times 0.944^{4 \times z} \end{cases} \quad A.70$$

In contrast to the timber foundation piles, beam elements have a rectangular and prismatic shape along their length. The stiffness of the pile cap beam is not everywhere the same due to the presence of the retaining wall at the front end of the pile cap beam. Two different values are then needed for the correct input of the beam stiffness in a computer program. The different regions are given in *figure A-31*.

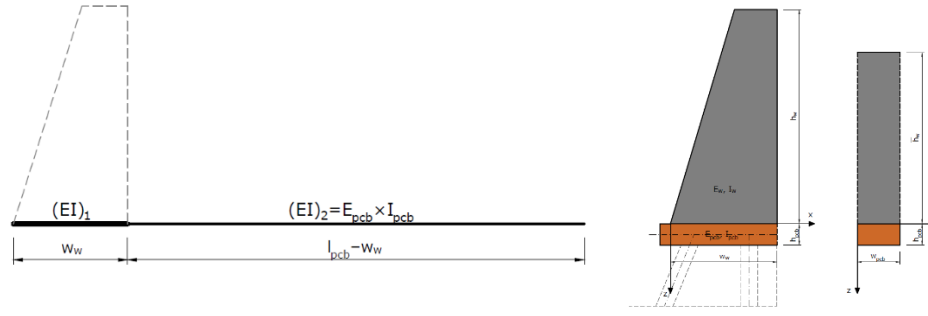


figure A-33: difference in bending stiffnesses along the pile cap beam

The beam part just below the retaining wall becomes stiffer due to the presence of the wall element. The combined stiffness of both structural elements is calculated with the Steiner rule for inhomogeneous cross-sections (Hartsuijker & Welleman, 2017). It is assumed that no slip occurs at the interface of both elements, so both contributions can be added to each other. The other part behind the retaining wall consists only of the pile cap beam, so the stiffness follows directly from its own properties.

$$\begin{cases} EI_1 = E_{wall} \times I_{wall} + E_{pcb} \times I_{pcb} \\ EI_2 = E_{pcb} \times I_{pcb} \end{cases} \quad A.71$$

For the calculation of the combined stiffness at the retaining wall, the width of the quay wall element is taken equal to the pile cap beam width. The values of the modulus of elasticity for the materials are given in table A-15. The values for the foundation piles and the pile cap beams are different because of the anisotropic behaviour of wood.

parameter	material	value	reference
E_{wall} [N/mm ²]	concrete	20×10^3	NEN-EN 1997-1 (NB)
	brick	14×10^3	par. 7.6.4.2 (j), 2019
E_{pile} [N/mm ²]	timber	3.6×10^3	NEN-EN 1997-1 (NB) par. 7.6.4.2 (j), 2019
E_{pcb} [N/mm ²]	timber	0.12×10^3	NEN-EN 384 table 2, 2018
E_{cross} [N/mm ²]	timber	0.12×10^3	NEN-EN 384 table 2, 2018

table A-15: Young's moduli for quay wall components (NEN-EN 1997-1 (NB) par. 7.6.4.2 (j), 2019)

The retaining wall is composed of various different materials, but for the simplicity of the stiffness calculations, the elastic modulus of concrete is used for the entire element.

A.12.2 JOINT STIFFNESS

Besides the stiffness of the individual elements, the internal force transfer of the foundation system is influenced by the stiffness of the joints. From paragraph '2.2 Inner-city quay wall characteristics' and the quay wall drawings in paragraph '5.1 Case study', a mortise and tenon joint is the joint type that was applied most frequent during the construction of historic quay walls. The rotational stiffness is defined by the relative rotation between the beam and the pile and the internal moment.

$$k_r = \frac{M}{\theta} \quad A.72$$

In this expression, a linear relation is assumed between the applied moment and its response. The long lifespan of the structure could have an effect on the tightness of the joint. A very loose connection

requires a certain rotation before it starts with transferring of internal forces between the connected elements. Nonlinearity of the joint response is not incorporated in the determination of the rotational stiffness as given by *equation (A.73)*.

Three different cases can be distinguished by the variation of the rotational stiffness. In *figure A-34*, three possibilities are depicted.

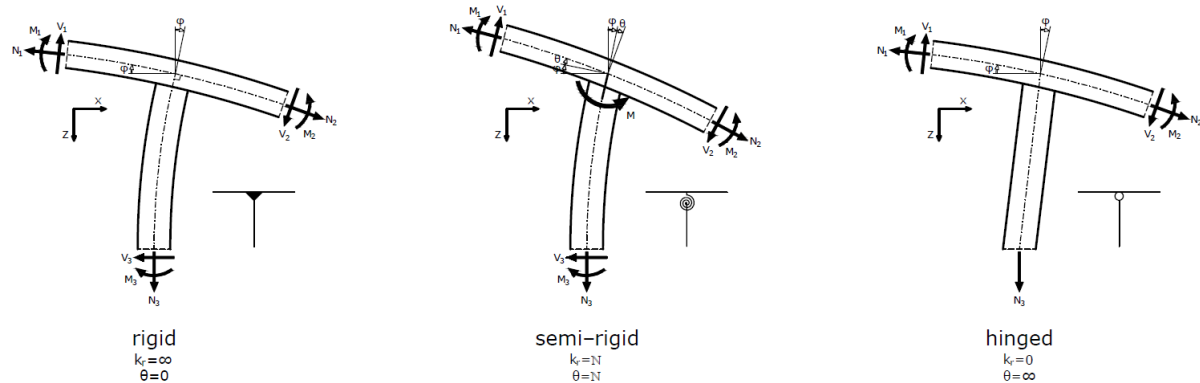


figure A-34: rotational stiffness of a beam-pile joint

Considering all three cases given above, the hinged connection is the most simple one. The pile functions here as a shuttle bar (Dutch: pendelstaaf) which means that only axial forces are transferred to the subsoil. Equilibrium is then found by a combination of batter and vertical piles with very high axial forces as the result. It is not a representative schematisation by the absence of internal shear forces and bending moments and the disability of the pile to deform in lateral direction.

The two other remaining connection types allow the occurrence of internal forces. The differences in the internal force transfer between both models depends on the rotational stiffness in the semi-rigid case. When the value is very high, the rigid case is approached and the differences in internal forces and moments diminishes. There are several ways to estimate this parameter such as measuring the joint deformation by application of force increments in a scaled set-up. Alternatively, the stiffness is estimated by a theoretical model. The obtained results are less accurate than loading tests on joints, but for this thesis report an approximation is justifiable. Moreover, the exact composition of the pile cap beam joint in historic quay wall structures includes a lot of uncertainties because documentation about the structure is often limited and data collection via inspections is complicated due to its almost unreachable location.

One of the theoretical methods is based on the component method that is widely used for steel joints. The joint is disassembled in a figurative sense by considering each joint part individually. Each part is represented by an elastic spring where the correct joint response is obtained by spring coupling. An advantage of this approach is that characterization of the joint exclusively depends on the loading direction, not on the loading type (Descamps & Guerlement, 2009). Furthermore, only geometrical and mechanical data is needed. A representation of the component method is depicted in *figure A-35*.

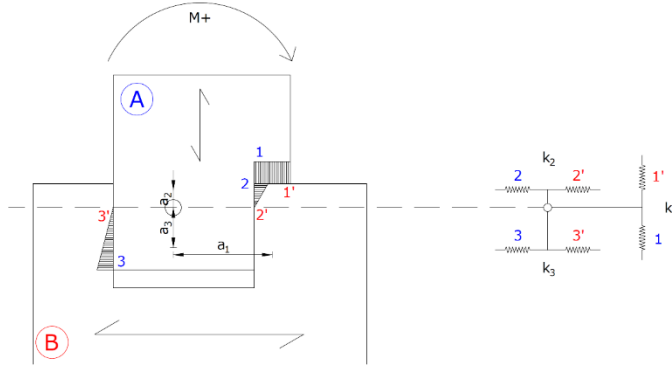


figure A-35: equivalent spring model for a mortise and tenon joint for a positive bending moment (Descamps & Guerlement, 2009)

The rotational stiffness follows from the applied bending moment and the relative rotation around the instantaneous centre of rotation (ICR).

$$k_r = \frac{M}{\theta} = \frac{\sum_{i=1}^n F_i \times a_i}{\theta} = \frac{\sum_{i=1}^n k_i \times \delta_i \times a_i}{\theta} = \frac{\sum_{i=1}^n k_i \times \theta_i \times a_i \times a_i}{\theta} = \sum_{i=1}^n k_{eq,i} \times a_i^2 \quad A.73$$

Where the distance to each stiffness component is defined by the arm between each force component to the ICR. It is difficult to find the exact location of this stationary point because the rotating mechanism must be known. Often an estimation of the location is sufficient, especially for this very basic approach. The stiffness of each component acts in a serial system with each other.

$$k_{eq} = \frac{1}{\sum_{i=1}^n \frac{1}{k_{\alpha,i}}} \quad A.74$$

The stiffness of each component depends on the stiffness of the contact area of the pile with the beam. Drdácý et al. (1999) found an expression from elastic deformation equations modified by test specimen results.

$$k_{\alpha,i} = \frac{E_{\alpha} \times \sqrt{W_i \times H_i}}{0.85} \quad A.75$$

The Young's modulus for both the pile and the beam depends on the angle relative to the fibre direction. It can be derived with Hankinson's equation for the modulus of elasticity.

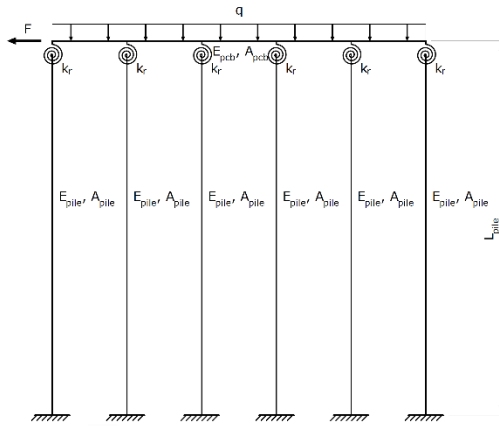
$$E_{\alpha} = \frac{E_0}{\frac{E_0}{E_{90}} \times \sin^2 \alpha + \cos^2 \alpha} \quad A.76$$

According to the researchers, equation (A.77) is a conservative and acceptable estimation for the stiffness of each component.

A.12.3 NUMERICAL EXAMPLE OF JOINT STIFFNESS

To investigate if the rotational stiffness of the connection between the pile cap beam and the piles has a considerable influence on the force transfer in a framework system, a numerical example with various stiffness values is made. Three different cases are considered as given in figure A-34. From several investigations it was examined that the pile cap beam and the pile head are often connected with each other with a mortise and tenon joint where more detailed information about the dimensions is not available. To determine a value for the rotational stiffness, no contributions of iron fasteners like barbed nails or strips are considered, so the stiffness for a certain pile diameter depends in this case entirely on

the recess depth in the pile cap beam. For the intermediate case, three different values for the recess depth are considered to analyse the influence magnitude on the internal force transfer. In total, five different calculations will be made. The used parameters for the model in *figure A-36* are given in *table A-16*.



parameter	value
F [kN]	100
q [kN/m]	50
L _{pile} [m]	5.0
S _{pile} [m]	1.0
d _{pile} [mm]	250
W _{pcb} [mm]	270
H _{pcb} [mm]	200
E _{pile} [N/mm ²]	3.6×10 ³
E _{pcb} [N/mm ²]	0.12×10 ³

figure A-36: load scheme for the determination of the rotational stiffness influence *table A-16: used parameters*

The only changing parameter is the rotational stiffness. Both hinged and rigid joints are limit cases, so the values are easy to determine. For the intermediate cases, dimensions must be chosen which are the diameter at the pile head and the depth of the recess inside the pile cap beam. As made clear in *figure 2-2* the diameter at the pile head is slightly less than the diameter of the part below. This constriction is required to provide sufficient thickness besides the gap, so shear failure of the joint is prevented. For this numerical example, a value of 40 mm is assumed for this contraction which results in the following pile head diameter:

$$d_{head} = 170 \text{ mm}$$

Different results for the rotational stiffness can be obtained by a set of values for the mortise depth in the pile cap beam. For this example, the depth is taken equal to 25%, 50%, and 75% of the pile head diameter. The shape of this joint type is depicted in *figure A-37*. In *figure A-17*, the values are given after the application of *equation (A.74)*, *equation (A.75)*, *equation (A.76)*, and *equation (A.77)*. To simplify the calculations, the height of the centre of gravity for the joint is placed at half of the joint depth.

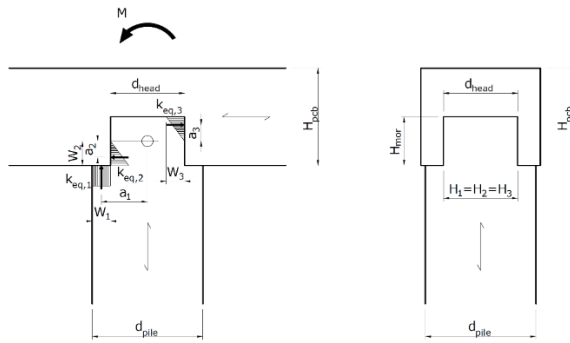


figure A-37: rotational stiffness of a mortise and tenon joint

parameter	case 2a	case 2b	case 2c
H_{mor} [mm]	50	100	150
E_0 [N/mm ²]	3.6×10^3	3.6×10^3	3.6×10^3
E_{90} [N/mm ²]	0.12×10^3	0.12×10^3	0.12×10^3
a_1 [mm]	105	105	105
a_2 [mm]	16.7	33.3	50
a_3 [mm]	16.7	33.3	50
$k_{0,1}$ [N/mm]	4.24×10^5	4.24×10^5	4.24×10^5
$k_{90,1}$ [N/mm]	1.41×10^4	1.41×10^4	1.41×10^4
$k_{0,2}$ [N/mm]	2.76×10^5	3.90×10^5	4.78×10^5
$k_{90,2}$ [N/mm]	9.20×10^3	1.30×10^4	1.59×10^4
$k_{0,3}$ [N/mm]	2.76×10^5	3.90×10^5	4.78×10^5
$k_{90,3}$ [N/mm]	9.20×10^3	1.30×10^4	1.59×10^4
$k_{eq,1}$ [N/mm]	1.37×10^4	1.37×10^4	1.37×10^4
$k_{eq,2}$ [N/mm]	8.91×10^3	1.26×10^4	1.54×10^4
$k_{eq,3}$ [N/mm]	8.91×10^3	1.26×10^4	1.54×10^4
k_r [Nmm/rad]	1.56×10^8	1.79×10^8	2.28×10^8

table A-17: used parameters

These rotational stiffnesses are used together with the structural dimensions and loads as input in Scia Engineer to find the influence of the rotational stiffness on the internal forces and bending moments. The results of the calculations are found below in table A-18.

parameter	case 1 ($k_r = 0$ kNm/rad)	case 2a ($k_r = 156$ kNm/rad)	case 2b ($k_r = 179$ kNm/rad)	case 2c ($k_r = 228$ kNm/rad)	case 3 ($k_r = \infty$ kNm/rad)
pile cap beam					
N_{min} [kN]	16.66	16.37	16.33	16.25	15.06
N_{max} [kN]	83.32	83.37	83.39	83.43	84.07
V_{min} [kN]	-29.05	-3.66	-2.26	0.14	16.36
V_{max} [kN]	29.05	61.36	63.32	66.64	85.73
M_{min} [kNm]	-4.26	-21.51	-22.83	-25.04	-37.79
M_{max} [kNm]	4.22	21.52	21.97	24.03	34.95
foundation piles					
N_{min} [kN]	-53.84	-64.53	-65.09	-65.99	-80.87
N_{max} [kN]	-20.95	11.36	13.32	16.64	35.73
V_{min} [kN]	-16.68	-16.77	-16.79	-16.82	-17.34
V_{max} [kN]	-16.66	-16.37	-16.33	-16.25	-15.06
M_{min} [kNm]	-83.40	-61.83	-60.49	-58.22	-44.18
M_{max} [kNm]	0	20.74	23.45	25.90	42.53
global					
$u_{x,max}$ [mm]	-1009.7	-616.8	-592.0	-549.8	-280.1
$u_{z,max}$ [mm]	-1.5	-1.8	-1.8	-1.9	-2.3

table A-18: calculation results from Scia Engineer

From above calculation results it follows that there are no large differences by a variation of the recess depth in the pile cap beam. For this thesis report, a depth of 50% of the pile cap beam thickness is a reasonable estimation.

A.13 DERIVATION OF EQUATION 4.28

The method Zeevaert–De Beer follows from the vertical equilibrium of a very small amount of soil around a pile. In this method the vertical effective stress is reduced with the stress caused by skin friction. The reduction is realized by the application of the mean vertical stress at the top and bottom side of a very thin slice of soil. The maximum shear resistance of the pile is assumed over the total height of the soil around the pile which results in:

$$\tau_z = \sigma'_{z,pile} \times K_0 \times \tan \varphi'$$

$$\sigma'_{z,pile} z = \sigma'_{0,z} z - \sigma'_z z$$

$$\sigma'_{0,z} z = Q_{sur} + \gamma' \times z$$

The increase of a vertical soil stress over a slice with an infinitesimal thickness is given by:

$$\frac{d\sigma'_{0,z}}{dz} = \gamma'$$

To determine the vertical stress at a depth below the ground level, the equation for vertical equilibrium of forces is used derived from *figure 4-10*. In this case, stresses must be translated first to internal forces.

$$F_z - F_z + \frac{dF_z}{dz} - V = 0$$

$$\frac{dF_z}{dz} - V = 0$$

The force contributions in this ordinary differential equation are:

$$F_z = A_{gr} \times \sigma'_z = A_{gr} \times (Q_{sur} + \gamma' \times z - \sigma'_{z,pile})$$

$$\frac{dF_z}{dz} = A_{gr} \times \left(\gamma' - \frac{d\sigma'_{z,pile}}{dz} \right)$$

$$V = \sigma'_{z,pile} \times K_0 \times \tan \varphi' \times C_{pile}$$

Substitution of the forces into the equilibrium equation gives:

$$A_{gr} \times \left(\gamma' - \frac{d\sigma'_{z,pile}}{dz} \right) - \sigma'_{z,pile} \times K_0 \times \tan \varphi' \times C_{pile} = 0$$

$$\gamma' - \frac{d\sigma'_{z,pile}}{dz} - \frac{K_0 \times \tan \varphi' \times C}{A_{gr}} \times \sigma'_{z,pile} = 0$$

$$\gamma' - \frac{d\sigma'_{z,pile}}{dz} - m \times \sigma'_{z,pile} = 0 \quad \text{where } m = \frac{K_0 \times \tan \varphi' \times C_{pile}}{A_{gr}}$$

$$\frac{d\sigma'_{z,pile}}{dz} + m \times \sigma'_{z,pile} = \gamma'$$

The total solution to this ordinary differential equation consists of a homogenous solution and a particular solution.

$$\sigma'_{z,pile} z = \sigma'_{z,pile,hom} z + \sigma'_{z,pile,part} z$$

The characteristic equation of the homogenous differential equation can be found by substitution of the following exponential function:

$$\sigma'_{z,pile} z = e^{r \times z}$$

$$\frac{d\sigma'_{z,pile}}{dz} = r \times e^{r \times z}$$

Substitution of the function in the homogeneous form of differential equation results in:

$$r \times e^{r \times z} + m \times e^{r \times z} = 0$$

$$e^{r \times z} \times r + m = 0$$

$$r + m = 0$$

$$r = -m$$

The homogeneous solution is then:

$$\sigma'_{z,pile,hom} z = C_1 \times e^{-m \times z}$$

A particular solution can be sought in the form:

$$\sigma'_{z,pile,part} z = C_2$$

$$\frac{d\sigma'_{z,pile,part} z}{dz} = 0$$

Substitution of this particular solution in the particular form of the differential equation results in:

$$0 + m \times C_2 = \gamma'$$

$$C_2 = \frac{\gamma'}{m}$$

A particular solution of the ordinary differential equation is then:

$$\sigma'_{z,pile,part} z = \frac{\gamma'}{m}$$

The total solution is the summation of the homogeneous and particular solution.

$$\sigma'_{z,pile} z = C_1 \times e^{-m \times z} + \frac{\gamma'}{m}$$

The above equation contains one unknown, so only one boundary condition is required to obtain a solution for the ordinary differential equation.

$$\sigma'_{z,pile} 0 = Q_{sur}$$

Substitution of this boundary condition in the ordinary differential equation gives:

$$C_1 \times e^{-m \times 0} + \frac{\gamma'}{m} = Q_{sur}$$

$$C_1 = Q_{sur} - \frac{\gamma'}{m}$$

The total solution is equal to:

$$\sigma'_{z,pile} z = \left(Q_{sur} - \frac{\gamma'}{m} \right) \times e^{-m \times z} + \frac{\gamma'}{m}$$

$$\sigma'_{z,pile} z = \frac{\gamma'}{m} \times 1 - e^{-m \times z} + Q_{sur} \times e^{-m \times z}$$

The negative skin friction can be determined by the difference between the stress state of the situation including the pile and without the pile.

$$\sigma_{nsf} z = \sigma'_{0,z} z - \sigma'_{z,pile} z$$

$$\sigma_{nsf} z = Q_{sur} + \gamma' \times z - \frac{\gamma'}{m} \times 1 - e^{-m \times z} + Q_{sur} \times e^{-m \times z}$$

$$\sigma_{nsf} z = \gamma' \times z \times \left(\frac{Q_{sur}}{\gamma' \times z} + 1 - \frac{1}{m \times z} \times 1 - e^{-m \times z} + \frac{Q_{sur}}{\gamma' \times z} \times e^{-m \times z} \right)$$

$$\sigma_{nsf} z = \gamma' \times z \times \left(1 - \frac{1}{m \times z} \times 1 - e^{-m \times z} + \frac{Q_{sur}}{\gamma' \times z} \times 1 - e^{-m \times z} \right)$$

$$\sigma_{nsf} z = \gamma' \times z \times \left(1 - \left(\frac{1}{m \times z} - \frac{Q_{sur}}{\gamma' \times z} \right) \times 1 - e^{-m \times z} \right)$$

A.14 DERIVATION OF EQUATION A.10

$$\sigma_h z = \frac{3 \times F \times z^3}{2\pi \times R^5}$$

$$y = 0 \rightarrow R = \sqrt{x^2 + z^2} \rightarrow \sigma_{h,max} z = \frac{3 \times F}{2\pi} \times \frac{z^3}{(\sqrt{x^2 + z^2})^5}$$

$$x = m_H \times H_{wall}, z = n_H \times H_{wall} \rightarrow \sigma_{h,max} z = \frac{3 \times F}{2\pi} \times \frac{n_H \times H_{wall}^3}{(\sqrt{m_H \times H_{wall}^2 + n_H \times H_{wall}^2})^5}$$

$$\sigma_{h,max} z = \frac{3 \times F}{2\pi} \times \frac{n_H^3 \times H_{wall}^3}{(m_H^2 \times H_{wall}^2 + n_H^2 \times H_{wall}^2)^{5/2}}$$

$$\sigma_{h,max} z = \frac{3 \times F}{2\pi} \times \frac{n_H^3 \times H_{wall}^3}{(H_{wall}^2 \times m_H^2 + n_H^2)^{5/2}}$$

$$\sigma_{h,max} z = \frac{3 \times F}{2\pi} \times \frac{n_H^3 \times H_{wall}^3}{H_{wall}^5 \times m_H^2 + n_H^2^{5/2}}$$

$$\sigma_{h,max} z = \frac{3 \times F}{2\pi \times H_{wall}^2} \times \frac{n_H^3 \times \sqrt{m_H^2 + n_H^2}}{m_H^2 + n_H^2^3}$$

$$\text{Taylor at } m_H \neq 0 \rightarrow n_H^3 \times \sqrt{m_H^2 + n_H^2} \approx \frac{1}{2} \times m_H^2 \times n_H^2 - \frac{1}{8} \times m_H^4 + \dots$$

$$\sigma_{h,max} z = \frac{3 \times F}{2\pi \times H_{wall}^2} \times \frac{\frac{1}{2} \times m_H^2 \times n_H^2}{m_H^2 + n_H^2^3}$$

$$\sigma_{h,max} z = \frac{3 \times F}{4\pi \times H_{wall}^2} \times \frac{m_H^2 \times n_H^2}{m_H^2 + n_H^2^3}$$

$$\sigma_{h,max} z = C \times \frac{F}{H_{wall}^2} \times \frac{m_H^2 \times n_H^2}{m_H^2 + n_H^2^3}$$

For $m_H \leq 0.4$ $C = 1.77$, $m_H = 0.4$:

$$\sigma_{h,max} z = 1.77 \times \frac{F}{H_{wall}^2} \times \frac{0.4^2 \times n_H^2}{0.4^2 + n_H^2^3}$$

$$\sigma_{h,max} z = 0.28 \times \frac{F}{H_{wall}^2} \times \frac{n_H^2}{0.16 + n_H^2^3}$$

For $m_H > 0.4$ $C = 1.77$:

$$\sigma_{h,max} z = 1.77 \times \frac{F}{H_{wall}^2} \times \frac{m_H^2 \times n_H^2}{m_H^2 + n_H^2^3}$$

A.15 DERIVATION OF EQUATION A.11

Derivation of the force resultant (C1 and C2 are factors for the interchangeability of both stress equations)

$$q_{h,max} = \int_0^{H_{wall}} \sigma_{H,max} z \, dz$$

$$q_{h,max} = \int_0^{H_{wall}} C \times \frac{F}{H_{wall}^2} \times \frac{C_1 \times n_H^2}{C_2 + n_H^2} dz$$

$$m_H = \frac{x}{H_{wall}}, n_H = \frac{z}{H_{wall}} \rightarrow q_{h,max} = \int_0^{H_{wall}} C \times \frac{F}{H_{wall}^2} \times \frac{C_1 \times \left(\frac{z}{H_{wall}}\right)^2}{\left(C_2 + \left(\frac{z}{H_{wall}}\right)^2\right)} dz$$

$$q_{h,max} = C \times \frac{F}{H_{wall}^4} \times \int_0^{H_{wall}} \frac{C_1 \times z^2}{\left(C_2 + \left(\frac{z}{H_{wall}}\right)^2\right)} dz$$

$$\boxed{\int \frac{u^2}{\left(a^2 + \left(\frac{1}{b}\right)^2\right)} du = b^3 \times \left(\frac{\sqrt{a} \times b \times u \times u^2 - a \times b^2}{a^2 \times b^2 + u^2} + \tan^{-1} \left(\frac{u}{\sqrt{a} \times b} \right) \right) + c}$$

For $m \leq 0.4$ $C = 0.28$, $C_1 = 1$, $C_2 = 0.16$:

$$q_{h,max} = 0.28 \times \frac{F}{H_{wall}^4} \times \left[\frac{1}{8} \times 0.16^{-3/2} \times H_{wall}^3 \times \left(\frac{\sqrt{0.16} \times H_{wall} \times z \times z^2 - 0.16 \times H^2}{(0.16 \times H_{wall}^2 + z^2)^2} + \tan^{-1} \left(\frac{z}{\sqrt{0.16} \times H_{wall}} \right) \right) \right]_0^{H_{wall}}$$

$$q_{h,max} = 0.28 \times \frac{F}{H_{wall}^4} \times \frac{1}{8} \times 0.16^{-3/2} \times H_{wall}^3 \times \left(\frac{\sqrt{0.16} \times H_{wall} \times H_{wall} \times (H_{wall}^2 - 0.16 \times H_{wall}^2)}{(0.16 \times H_{wall}^2 + H_{wall}^2)^2} + \tan^{-1} \left(\frac{H_{wall}}{\sqrt{0.16} \times H_{wall}} \right) \right)$$

$$q_{h,max} = 0.55 \times \frac{F}{H_{wall}} \times \left(\frac{0.34 \times H_{wall}^4}{1.35 \times H_{wall}^4} + \tan^{-1} 2.5 \right)$$

$$q_{h,max} = 0.79 \times \frac{F}{H_{wall}}$$

For $m > 0.4$ $C = 1.77$, $C_1 = C_2 = m_H^2$:

$$q_{h,max} = 1.77 \times \frac{F \times m_H^2}{H_{wall}^4} \times \left[\frac{1}{8} \times m_H^{-3} \times H_{wall}^3 \times \frac{m_H \times H_{wall} \times z \times z^2 - m_H^2 \times H_{wall}^2}{m_H^2 \times H_{wall}^2 + z^2} + \tan^{-1} \left(\frac{z}{m_H \times H_{wall}} \right) \right]_0^{H_{wall}}$$

$$q_{h,max} = 1.77 \times \frac{F \times m_H^2}{H_{wall}^4} \times \frac{1}{8} \times m_H^{-3} \times H_{wall}^3 \times \left(\frac{m_H \times H_{wall} \times H_{wall} \times (H_{wall}^2 - m_H^2 \times H_{wall}^2)}{(m_H^2 \times H_{wall}^2 + H_{wall}^2)^2} + \tan^{-1} \left(\frac{H_{wall}}{m_H \times H_{wall}} \right) \right)$$

$$q_{h,max} = 0.22 \times \frac{F}{m_H \times H_{wall}} \times \left(\frac{m_H \times H_{wall}^2 \times H_{wall}^2 \times 1 - m_H^2}{(H_{wall}^2 \times m_H^2 + 1)^2} + \tan^{-1} \left(\frac{H_{wall}}{m_H \times H_{wall}} \right) \right)$$

$$q_{h,max} = 0.22 \times \frac{F}{m_H \times H_{wall}} \times \left(\frac{m_H \times H_{wall}^2 \times H_{wall}^2 \times 1 - m_H^2}{H_{wall}^4 \times m_H^2 + 1^2} + \tan^{-1} \left(\frac{1}{m_H} \right) \right)$$

$$q_{h,max} = 0.22 \times \frac{F}{H_{wall}} \times \left(\frac{1 - m_H^2}{m_H^2 + 1^2} + \frac{1}{m_H} \times \tan^{-1} \left(\frac{1}{m_H} \right) \right)$$

Derivation of the point of application (c_1 and c_2 are factors for the interchangeability of both stress equations)

$$z_{cg} = \frac{S_z}{q_{h,max}}$$

$$S_z = \int_0^{H_{wall}} z \times \sigma_{h,max} dz$$

$$S_z = \int_0^{H_{wall}} z \times C \times \frac{F}{H_{wall}^2} \times \frac{C_1 \times n_H^2}{C_2 + n_H^2} dz$$

$$m_H = \frac{x}{H_{wall}}, n_H = \frac{z}{H_{wall}} \rightarrow q_{h,max} = \int_0^{H_{wall}} z \times C \times \frac{F}{H_{wall}^2} \times \frac{C_1 \times \left(\frac{z}{H_{wall}}\right)^2}{\left(C_2 + \left(\frac{z}{H_{wall}}\right)^2\right)^3} dz$$

$$q_{h,max} = C \times \frac{F}{H_{wall}^4} \times \int_0^{H_{wall}} \frac{C_1 \times z^3}{\left(C_2 + \left(\frac{z}{H_{wall}}\right)^2\right)^3} dz$$

$$\boxed{\int \frac{u^3}{\left(a^2 + \left(\frac{1}{b}\right)^2\right)^3} du = -\frac{b^6 \times a \times b^2 + 2 \times u^2}{4 \times a \times b^2 + u^2} + c}$$

For $m \leq 0.4$ $C = 0.28$, $C_1 = 1$, $C_2 = 0.16$:

$$S_z = 0.28 \times \frac{F}{H_{wall}^4} \times \left[-\frac{H_{wall}^6 \times (0.16 \times H_{wall}^2 + 2 \times z^2)}{4 \times (0.16 \times H_{wall}^2 + z^2)^2} \right]_0^{H_{wall}}$$

$$S_z = 0.28 \times \frac{F}{H_{wall}^4} \times \left(-\frac{H_{wall}^6 \times (0.16 \times H_{wall}^2 + 2 \times H_{wall}^2)}{4 \times (0.16 \times H_{wall}^2 + H_{wall}^2)^2} + \frac{H_{wall}^6 \times (0.16 \times H_{wall}^2 + 2 \times 0^2)}{4 \times (0.16 \times H_{wall}^2 + 0^2)^2} \right)$$

$$S_z = 0.28 \times \frac{F}{H_{wall}^4} \times \left(-\frac{H_{wall}^6 \times 2.16 \times H_{wall}^2}{4 \times (1.16 \times H_{wall}^2)^2} + \frac{H_{wall}^6 \times 0.16 \times H_{wall}^2}{4 \times (0.16 \times H_{wall}^2)^2} \right)$$

$$S_z = 0.28 \times \frac{F}{H_{wall}^4} \times \left(-\frac{2.16 \times H_{wall}^8}{5.38 \times H_{wall}^4} + \frac{0.16 \times H_{wall}^8}{0.10 \times H_{wall}^4} \right)$$

$$S_z = 0.28 \times \frac{F}{H_{wall}^4} \times (-0.20 \times H_{wall}^4 + 1.60 \times H_{wall}^4)$$

$$S_z = 0.33 \times F$$

$$z_{cg} = \frac{0.33 \times F}{0.79 \times \frac{F}{H_{wall}}}$$

$$z_{cg} = 0.41 \times H_{wall}$$

For $m > 0.4$ $C = 1.77$, $C_1 = C_2 = m_H^2$:

$$S_z = 1.77 \times \frac{F \times m_H^2}{H_{wall}^4} \times \left[-\frac{H_{wall}^6 \times (m_H^2 \times H_{wall}^2 + 2 \times z^2)}{4 \times (m_H^2 \times H_{wall}^2 + z^2)^2} \right]_0^{H_{wall}}$$

$$S_z = 1.77 \times \frac{F \times m_H^2}{H_{wall}^4} \times \left(-\frac{H_{wall}^6 \times (m_H^2 \times H_{wall}^2 + 2 \times H_{wall}^2)}{4 \times (m_H^2 \times H_{wall}^2 + H_{wall}^2)^2} + \frac{H_{wall}^6 \times (m_H^2 \times H_{wall}^2 + 2 \times 0^2)}{4 \times (m_H^2 \times H_{wall}^2 + 0^2)^2} \right)$$

$$S_z = 1.77 \times \frac{F \times m_H^2}{H_{wall}^4} \times \left(-\frac{H_{wall}^6 \times H_{wall}^2 \times m_H^2 + 2}{4 \times (H_{wall}^2 \times m_H^2 + 1)^2} + \frac{H_{wall}^6 \times m_H^2 \times H_{wall}^2}{4 \times (m_H^2 \times H_{wall}^2)^2} \right)$$

$$S_z = 1.77 \times \frac{F \times m_H^2}{H_{wall}^4} \times \left(-\frac{H_{wall}^8 \times m_H^2 + 2}{4 \times H_{wall}^4 \times m_H^2 + 1^2} + \frac{m_H^2 \times H_{wall}^8}{4 \times m_H^4 \times H_{wall}^4} \right)$$

$$S_z = 1.77 \times \frac{F \times m_H^2}{H_{wall}^4} \times \left(-\frac{H_{wall}^4 \times m_H^2 + 2}{4 \times m_H^2 + 1^2} + \frac{H_{wall}^4}{4 \times m_H^2} \right)$$

$$S_z = 1.77 \times \frac{F \times m_H^2}{H_{wall}^4} \times \left(\frac{1}{4} \times H_{wall}^4 \times \left(\frac{1}{m_H^2} - \frac{m_H^2 + 2}{m_H^2 + 1^2} \right) \right)$$

$$S_z = 0.44 \times F \times m_H^2 \times \left(\frac{m_H^2 + 1^2}{m_H^2 \times m_H^2 + 1^2} - \frac{m_H^2 \times m_H^2 + 2}{m_H^2 \times m_H^2 + 1^2} \right)$$

$$S_z = 0.44 \times F \times m_H^2 \times \frac{m_H^4 + 2 \times m_H^2 + 1 - m_H^4 - 2 \times m_H^2}{m_H^2 \times m_H^2 + 1^2}$$

$$S_z = 0.44 \times F \times m_H^2 \times \frac{1}{m_H^2 \times m_H^2 + 1^2}$$

$$S_z = \frac{0.44 \times F}{m_H^2 + 1^2}$$

$$z_{cg} = \frac{\frac{0.44 \times F}{m_H^2 + 1^2}}{0.22 \times \frac{F}{H_{wall}} \times \left(\frac{1 - m_H^2}{m_H^2 + 1^2} + \frac{1}{m_H} \times \tan^{-1} \left(\frac{1}{m_H} \right) \right)}$$

$$z_{cg} = \frac{0.44 \times F \times H_{wall}}{0.22 \times F \times m_H^2 + 1^2 \times \left(\frac{1 - m_H^2}{m_H^2 + 1^2} + \frac{1}{m_H} \times \tan^{-1} \left(\frac{1}{m_H} \right) \right)}$$

$$z_{cg} = \frac{2 \times H_{wall}}{m_H^2 + 1^2 \times \left(1 - m_H^2 + \frac{1}{m_H} \times m_H^2 + 1^2 \times \tan^{-1} \left(\frac{1}{m_H} \right) \right)}$$

A.16 DERIVATION OF EQUATION A.51

The deformation of a pile under an axial load can be calculated with the differential equation for axial shortening. The relations which are required for the formulation of the differential equation can be found in figure A-38.

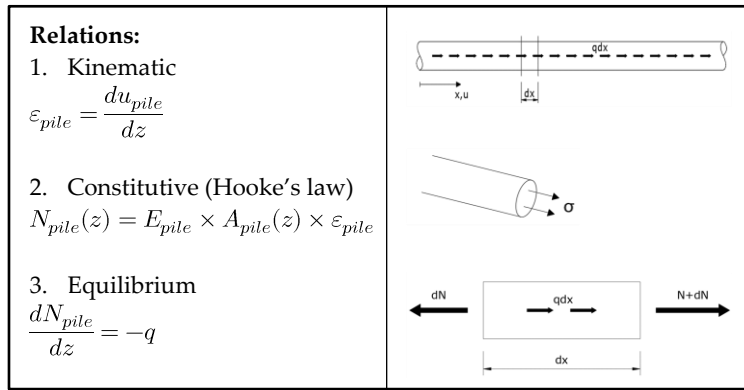


figure A-38: relations for the axial deformation of an element with an infinitesimal length

The differential equation for a non-prismatic homogeneous cross-section is given as:

$$-\frac{d}{dz} \left(E_{pile} \times A_{pile}(z) \times \frac{du_{pile}}{dz} \right) = q$$

For the determination of equation (A.51), no axial distributed load is present. The constitutive relation and integration of the ordinary equation over the depth results in the following general solution for the normal force distribution and the displacement field:

$$\frac{du_{pile}}{dz} = \frac{C_1}{E_{pile} \times A_{pile}(z)}$$

$$N_{pile}(z) = C_1$$

$$u_{pile}(z) = \int \frac{C_1}{E_{pile} \times A_{pile}(z)} dz + C_2$$

The varying cross-sectional area over the pile depth is calculated with the taper expression of equation (A.27).

$$A_{pile\ z} = \frac{1}{4} \times \pi \times d_{head}^2 \times 0.944^{2 \times z}$$

Substitution of the cross-sectional area in the expression for the displacement field leads to:

$$u_{pile\ z} = \int \frac{C_1}{E_{pile} \times \frac{1}{4} \times \pi \times d_{head}^2 \times 0.944^{2 \times z}} dz + C_2$$

$$u_{pile\ z} = \frac{4 \times C_1}{E_{pile} \times \pi \times d_{head}^2} \times \int \frac{1}{0.944^{2 \times z}} dz + C_2$$

$$\boxed{\int \frac{1}{a^{b \times u}} du = -\frac{a^{-b \times x}}{b \times \ln a} + C}$$

$$u_{pile\ z} = \frac{4 \times C_1}{E_{pile} \times \pi \times d_{head}^2} \times -\frac{0.944^{-2 \times z}}{2 \times \ln 0.944} + C_2$$

$$u_{pile\ z} = -\frac{2 \times C_1 \times 0.944^{-2 \times z}}{E_{pile} \times \pi \times d_{head}^2 \times \ln 0.944} + C_2$$

$$u'_{pile\ z} = \frac{4 \times \ln 0.944 \times C_1 \times 0.944^{-2 \times z}}{E_{pile} \times \pi \times d_{head}^2 \times \ln 0.944}$$

$$u'_{pile\ z} = \frac{4 \times C_1 \times 0.944^{-2 \times z}}{E_{pile} \times \pi \times d_{head}^2}$$

Two boundary conditions are required to obtain a displacement field for a pile with the inclusion of only elastic shortening.

$$N_{pile\ 0} = -F_{c,avg}$$

$$u_{pile\ L} = 0$$

Substitution of the boundary conditions in the total solution results in:

$$N\ 0 = -F_{c,avg} \rightarrow E_{pile} \times \frac{1}{4} \times \pi \times d_{head}^2 \times 0.944^{2 \times z} \times \frac{4 \times C_1 \times 0.944^{-2 \times z}}{E_{pile} \times \pi \times d_{head}^2} = -F_{c,avg}$$

$$C_1 = -F_{c,avg}$$

$$u_{pile\ L} = 0 \rightarrow -\frac{2 \times C_1 \times 0.944^{-2 \times L}}{E_{pile} \times \pi \times d_{head}^2 \times \ln 0.944} + C_2 = 0$$

$$C_2 = \frac{2 \times C_1 \times 0.944^{-2 \times L}}{E_{pile} \times \pi \times d_{head}^2 \times \ln 0.944}$$

Substitution of the constants into the general solution gives the expressions for the normal force distribution and the displacement field.

$$N\ z = -F_{c,avg}$$

$$u_{pile\ z} = \frac{2 \times F_{c,avg} \times 0.944^{-2 \times z}}{E_{pile} \times \pi \times d_{head}^2 \times \ln 0.944} - \frac{2 \times F_{c,avg} \times 0.944^{-2 \times L}}{E_{pile} \times \pi \times d_{head}^2 \times \ln 0.944}$$

$$u_{pile\ z} = \frac{2 \times F_{c,avg} \times (0.944^{-2 \times z} - 0.944^{-2 \times L})}{E_{pile} \times \pi \times d_{head}^2 \times \ln 0.944}$$

Appendix B: Assessment results of quay walls

B.1 BOOMPJESKADE, ROTTERDAM

Deformation measurements of the Boompjeskade started in 1998 (Gemeente Rotterdam, personal communications, 2013). When the last assessment report was finished in 2013, a vertical displacement of 30 mm downwards and a horizontal displacement of 90 mm towards the waterside were measured. Along the considered section, a kink is observed in the direction of the Nieuwe Maas. This deviation is present for a quite long time already because the placement of the current pavement along the quay wall was adapted to the deformed shape. The development of the bend is in the same direction as the deformation of the straight sections. The movement of the measuring points shows a consistent pattern during the assessment period, so there is no reason for immediate actions.

The current condition of the structure is assessed with visual inspections to detect possible deficiencies. The assessment comprises a survey from the waterside with a diving team and observations from the landside. The following perceptions were captured from both approaches:

- Minor local settlements were observed at ground level. No anomalies were found in the substructure to clarify those deformations in the subsoil. The settlements were probably caused by the application of a concrete floor and a geotextile in 2012.
- No damages were observed at the timber foundation.

At 28 locations along the quay wall with a timber foundation, penetrometer measurements were performed. The exact locations of the impact hammer tests are not given in the report. The impact hammer was applied to foundation piles, pile cap beams, and floor elements with a total of six measurement per location. A brief summary of the obtained results can be seen in *table B-1*.

element	t [mm]	p _m [mm]
foundation piles	276	4
pile cap beams	241	4
floor elements	60	2

table B-1: penetration values of the Boompjeskade (Gemeente Rotterdam, personal communications, 2013)

A total of fourteen samples were retrieved from the foundation piles along the Boompjeskade and investigated in the laboratory on the degree of degradation by bacteria and fungi. From this obtained data, an estimation of the residual compression strength was made based on *equation (3.2)*. The sampling sites are given below in *figure B-1*.

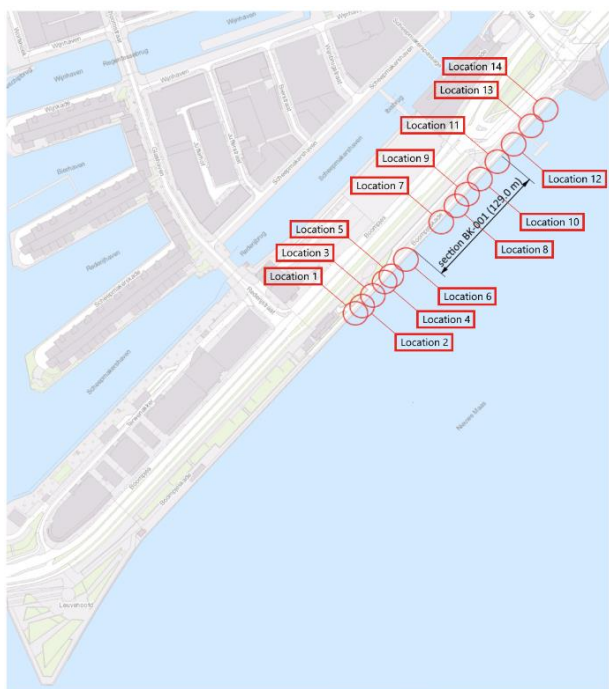


figure B-1: sample locations of the Boompjeskade (GeoStart, n.d.)

A wood increment borer with an internal diameter of 10 mm was used to retrieve wood core samples with a length of at least half of the pile diameter. The specimens are investigated at a laboratory for the determination of the wood species, the degree of degradation, and the degrading species based on the observed decay patterns. The obtained results of the microscopic research are shown in *table B-2* and the estimation of the residual compressive strength is given in *table B-3*.

no. (location)	element	wood species	L _{spec} [mm]	mean depth of decay [mm]					main degraders
				I	II	III	IV	V	
1 (1)	pile Ø280	spruce	143	6	4	3	19	111	EB
2 (2)	pile Ø270	spruce	135	0	0	14	0	121	EB
3 (3)	pile Ø260	spruce	135	0	0	6	0	129	EB, SR
4 (4)	pile Ø300	spruce	177	0	0	10	5	162	EB, SR
5 (5)	pile Ø300	fir	165	0	0	3	0	162	EB, SR
6 (6)	pile Ø270	spruce	113	0	0	8	9	96	EB
7 (7)	pile Ø280	spruce	140	0	5	4	13	118	EB
8 (8)	pile Ø290	spruce	145	7	0	8	0	130	EB
9 (9)	pile Ø290	spruce	126	5	1	0	0	120	EB, SR
10 (10)	pile Ø260	spruce	135	0	4	0	4	127	EB, SR
11 (11)	pile Ø250	spruce	147	0	6	0	7	134	EB, SR
12 (12)	pile Ø300	spruce	143	0	0	0	17	126	EB
13 (13)	pile Ø300	spruce	143	0	5	9	4	125	EB, SR
14 (14)	pile Ø260	spruce	153	0	3	7	0	143	EB, SR
degradation classes: I – total disruption of the wood structure II – severe decay III – moderate decay IV – weak decay V – none decay				degrader types: EB – erosion bacteria TB – tunnelling bacteria SR – soft rot fungi WR – white rot fungi BR – brown rot fungi					

table B-2: microscopic results of the Boompjeskade (Gemeente Rotterdam, personal communications, 2013)

no. (location)	L _{spec} [mm]	f _c (left) [N/mm ²] and L _{spec} (right) [mm] per segment																	
		1		2		3		4		5		6		7		8		9	
1 (1)	143	1.0	6	8.5	8	14.4	18	15.6	19	15.8	19	14.3	19	15.0	24	14.6	13	10.0	18
2 (2)	135	–	14	21.3	21	20.6	19	17.6	22	15.2	21	16.8	19	9.2	17	N/A		N/A	
3 (3)	135	9.3	20	15.9	20	15.4	19	14.2	21	14.0	18	14.3	22	13.4	15	N/A		N/A	
4 (4)	177	4.4	15	15.4	17	18.2	20	19.2	16	17.9	20	12.4	21	11.0	26	12.1	24	10.3	18
5 (5)	165	5.0	19	8.3	18	15.2	18	10.9	21	8.2	19	12.1	24	13.0	22	12.2	24	N/A	
6 (6)	113	7.6	8	12.0	18	18.7	18	18.5	20	15.2	24	8.5	23	N/A		N/A		N/A	
7 (7)	140	6.6	13	14.1	18	12.6	19	13.1	20	15.5	19	15.0	16	14.1	17	10.5	17	N/A	
8 (8)	145	5.2	15	13.4	18	14.9	18	15.3	16	12.7	18	13.6	18	12.3	21	12.6	20	N/A	
9 (9)	126	–	6	7.5	16	14.6	18	14.7	14	13.1	18	13.5	18	13.5	19	11.4	16	N/A	
10 (10)	135	6.3	8	10.6	21	15.3	18	14.7	17	13.7	17	12.7	20	13.8	22	18.4	11	N/A	
11 (11)	147	9.2	8	13.6	19	13.3	17	13.9	18	14.2	21	13.0	20	11.5	21	12.7	22	N/A	
12 (12)	143	10.3	17	14.8	18	16.5	17	15.6	19	11.7	22	13.4	19	14.3	18	13.5	18	N/A	
13 (13)	143	4.4	14	9.2	16	12.7	17	12.8	17	8.9	17	9.7	19	12.0	23	12.5	20	N/A	
14 (14)	153	8.4	10	12.9	18	16.3	20	16.8	19	15.8	20	11.8	20	10.9	23	7.9	23	N/A	

table B-3: estimation residual strength of the foundation elements at the Boompjeskade (Gemeente Rotterdam, personal communications, 2013)

B.2 HARINGVLIET, ROTTERDAM

To estimate the actual condition of the quay wall structures in the Haringvliet harbour, the monitoring of structural translations is performed from 2001 onwards (Gemeente Rotterdam, personal communications, 2012). The last assessment report was written in 2013, so records over a period of 12 years are documented. From the measurement data it follows that the sections have moved 1 cm in downward direction and 12 cm towards the waterside. The large differences in both values probably comes from the horizontal impact forces of cars bumping into parking curbs for parking lots situated perpendicular to the quay wall. The deformations have grown gradually over the years, which are indications for the presence of structural deficiencies.

The following action in the analysis of the structural condition is the visual inspection. The sections with a timber foundation are observed both from the landside and the waterfront where for the later a diving team was used for the underwater inspection. The following observations were reported:

- No settlements are found at ground level.
- The timber foundation is in a good condition; no defects were observed at the timber floor.
- No height differences by uneven settlements were observed between the sections.

The condition of the timber foundation elements is determined at three locations around the Haringvliet area with penetrometer measurements and microscopic analysis. The three locations are given below in *figure B-2*.

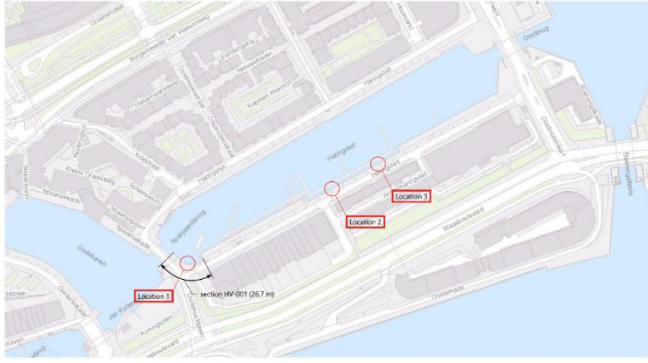


figure B-2: sample locations of the Haringvliet (GeoStart, n.d.)

The hardness of each foundation element was measured two times per location with a penetrometer device with exclusion of the foundation floor at location 2. In *table B-4*, the obtained results are shown.

element	location	t [mm]	p _m [mm]
foundation piles	1	250	4
	1	250	4
	2	270	2
	2	260	2
	2	270	4
	3	260	0
pile cap beams	1	180	0
	1	180	5
	2	200	0
	2	200	0
	3	200	0.8
	3	200	0
floor elements	1	60	5
	2	60	0
	2	60	0
	3	60	0
	3	60	1.6

table B-4: penetration values of the Haringvliet (Gemeente Rotterdam, personal communications, 2012)

At the same locations as the penetrometer measurements, one sample was retrieved per location from the foundation piles. An increment borer with a diameter of 10 mm was used to extract the wood cores from the piles and they were sent in sealed packages to the laboratory. Each sample was investigated on the timber species, degree of degradation and the type of organisms responsible for the degradation patterns. The results of the microscopic research are stated in *table B-5* and in *table B-6* the results of the estimations for the residual compressive strengths are listed based on *equation (3.2)*.

no. (location)	element	wood species	L _{spec} [mm]	mean depth of decay [mm]					main degraders
				I	II	III	IV	V	
1 (1)	pile Ø250	spruce	117	0	2	13	1	101	EB
2 (2)	pile Ø270	spruce	124	0	2	0	18	104	EB, SR, BR
3 (3)	pile Ø270	spruce	114	0	0	2	26	86	EB, SR
degradation classes: I – total disruption of the wood structure II – severe decay III – moderate decay IV – weak decay V – none decay				degrader types: EB – erosion bacteria TB – tunnelling bacteria SR – soft rot fungi WR – white rot fungi BR – brown rot fungi					

table B-5: microscopic results of the Haringvliet (Gemeente Rotterdam, personal communications, 2012)

no. (location)	L _{spec} [mm]	f _c [N/mm ²] per segment						
		1	2	3	4	5	6	7
1 (1)	117	5.8	13.9	20.1	18.1	17.5	18.9	N/A
2 (2)	124	0.6	8.8	14.6	14.3	16.5	16.9	12.5
3 (3)	114	12.8	13.1	12.4	13.8	12.6	N/A	N/A

table B-6: estimation residual strength of the foundation elements at the Haringvliet (Gemeente Rotterdam, personal communications, 2012)

B.3 NOORDWAL, THE HAGUE

The deformation of the Noordwal is monitored from 2009 onwards (Ingenieursbureau Den Haag, 2020). In 2017, around 50% of the measurement points on the quay wall reached a certain intervention value that implies the need for a more intensive inspection regime. The frequency of inspections increased further over the years until a weekly recurrence in 2019. The records from this year indicate a sharp increase of the mean displacement rate along the length from 3 mm/year to 7 mm/year in a period of one year with an outlier of 16 mm/year at the Kalkoenstraat. No requirements are given in the building codes for maximum displacement rates of quay walls, but for buildings a value of 5 mm/year is prescribed. Above measurements are higher than this restriction, however, a quay wall is much stiffer than a masonry wall in a building. The prescribed values are probably too restrictive for quay walls, but the measurements still indicate a very poor condition of the quay wall structure.

The structure was visually assessed in 2016 and 2018 both from land- and waterside. The following observations were done with respect to the timber foundation:

- The connection of the pile cap beam with the piles is almost not present anymore so the current force transfer between both elements is very ineffective.
- Around 70% of the pile cap beams and the piles is heavily degraded in the forms of cleaves and cracks and most of the piles has lost their bearing function.
- The seepage screen contains gaps at the connection with the brick wall.

At the same moments as the visual inspections, the residual strength of the foundation elements was determined with penetrometer measurements and microscopic investigations of retrieved samples. The obtained information was not made publicly, so a detailed summary of the findings is not possible. To get an indication of the degree of degradation of the Noordwal, timber quality results of the former structure at the Toussaintkade in appendix 'B.5 Toussaintkade, The Hague' can be used as a reference.

B.4 STIELTJESKADE, ROTTERDAM

Measurements to deformations of the structure already started in 1993 (Gemeente Rotterdam, personal communications, 2013). At the moment the report was published, the structure has displaced 7 mm in downward direction and 30 mm in the direction of the waterside. The development of the movement was consistent during the measurement period, so the structural integrity seems to be quite good.

The second step shows the structural condition by photos made from both the quay side and the water side. Not the entire part of the structure was accessible because of the dense pile grid. The following anomalies were observed:

- Around 50% of the pile connections with the beams contains a gap of 20 mm. As a result, only 50% of the pile area is accounted for load bearing.
- The connection of the piles with the beams is a combination of a bolted steel strip and a mortise and tenon joint. The strip is partly corroded but still functions quite well.
- At the middle part of the section a large crack is found which stretches over the full height of the wall. The maximum crack width is 10 mm and has a maximum depth of 250 mm. No evidence is found at the foundation elements that could clarify the cause of the crack.

Estimation of the residual strength of the timber foundation elements was examined at two locations. They are shown below in *figure B-3*.

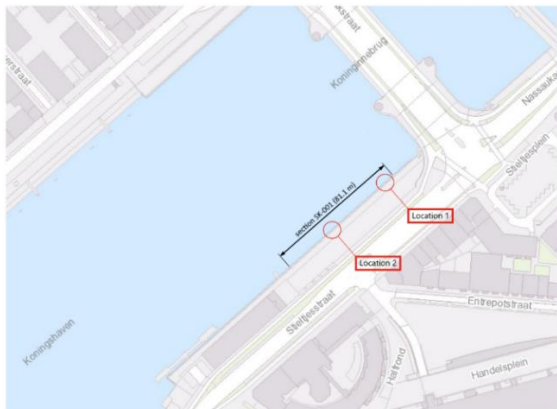


figure B-3: sample locations of the Stieltjeskade (Geostart, n.d.)

Penetrometer measurements were performed on piles, floor elements, and pile cap beams. Only the front row region was accessible, so the number of measurements is limited. Results are given in *table B-7*.

element	location	t [mm]	p _m [mm]
foundation piles	1	250	8
	1	250	4
	2	250	4
	2	250	4
	2	250	5
pile cap beams	1	200	5
	2	200	6
	2	200	5
floor elements	1	50	7
	2	50	6

table B-7: penetration values of the Stieltjeskade (Gemeente Rotterdam, personal communications, 2013)

Three samples were retrieved from the same two locations as the penetrometer tests. A wood core was drilled with a diameter of 10 mm and a length equal to at least half of the pile diameter. The specimens are investigated at a laboratory for the determination of wood species, the degree of degradation, and the degrading species based on the observed decay patterns. In *table B-8*, an overview is given of the obtained results. An overview of the estimated residual compressive strength of the foundation elements with *equation (3.2)* is provided in *table B-9*.

no. (location)	element	wood species	L _{spec} [mm]	mean depth of decay [mm]					main degraders
				I	II	III	IV	V	
1 (1)	pile Ø250	spruce	153	0	4	4	25	120	EB
2 (1)	pile Ø250	spruce	118	0	2	8	8	100	EB, SR
3 (2)	pile Ø250	spruce	112	0	1	1	1	109	EB
degradation classes: I – total disruption of the wood structure II – severe decay III – moderate decay IV – weak decay V – none decay				degrader types: EB – erosion bacteria TB – tunnelling bacteria SR – soft rot fungi WR – white rot fungi BR – brown rot fungi					

table B-8: microscopic results of the Stieltjeskade (Gemeente Rotterdam, personal communications, 2013)

no. (location)	L _{spec} [mm]	f _c [N/mm ²] per segment							
		1	2	3	4	5	6	7	8
1 (1)	153	8.0	14.6	17.3	17.6	19.7	11.4	N/A	N/A
2 (1)	118	12.5	15.2	14.9	16.4	18.0	17.1	17.9	23.2
3 (2)	112	7.7	13.6	16.0	13.6	14.5	13.8	N/A	N/A

table B-9: estimation residual strength of the foundation elements at the Stieltjeskade (Gemeente Rotterdam, personal communications, 2013)

B.5 TOUSSAINTKADE, THE HAGUE

There is not a lot known about the deformations of the Toussaintkade because the collection of measurement data started just after the renovations in 2012 (Ingenieursbureau Amsterdam, 2016). It means that no information is known about the structural responses before the application of the purlins and the grout anchor. These structural elements have a significant influence on the internal force transfers, so the deformation measurements after the changes do not contribute a lot to the understanding of the behaviour of the analysed composition. Therefore, the deformation records are not considered in this report.

Besides the deformation measurements, the structure was inspected visually in 2009, 2011, and 2015 from both land and water side. A collection of the observed features is given below:

The front part of one of the pile cap beams is broken/cracked, so no transfer of the wall deadweight via the beam to the front pile is possible. Around 50% of the pile connections is deteriorated by wood decay in such a way that the cross-sectional area of the bearing part is significantly decreased.

- The seepage screen contains large gaps of 10 mm near the connection with the other elements. Behind the screen, erosion holes of 20 cm deep are found in the compacted clay layer.

- A few trees are inclined in the direction of the canal, probably due to deformations of the older part of the wall towards the water.
- The pavement behind the quay wall shows settlements in the form of rutting along the entire length. The exact same cause as the tree movements seems plausible.

To obtain a judgment about the residual strength of the timber foundation, five locations along the Toussaintkade were examined. The locations are given in *figure B-4*.

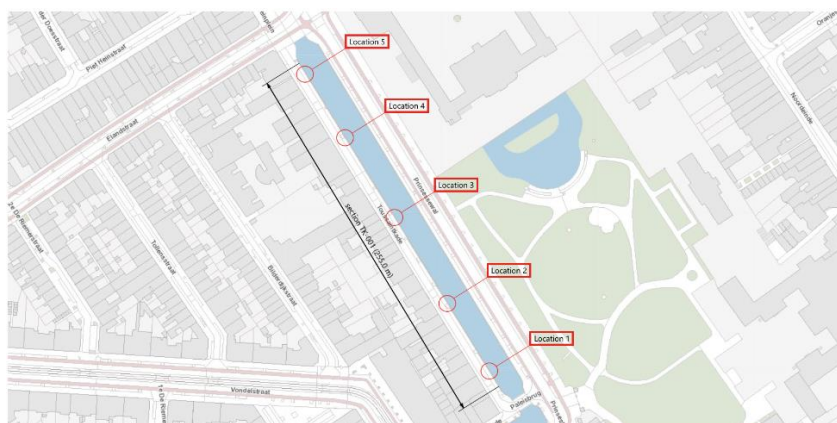


figure B-4: sample locations of the Toussaintkade (ArcGIS, n.d.)

At all five sites, penetrometer measurements were performed and samples were retrieved for further microscopic investigation in the laboratory. In *table B-10*, the results of the impact hammer assessment are presented. The mean value of the penetration depth was determined by doing six trials for each pile.

location	t [mm]	p _m [mm]
1	180	25
2	180	30
3	180	32
4	170	31
5	170	26

table B-10: penetration values for the piles at the Toussaintkade (Gemeente Rotterdam, internal documents, 2009)

The wood specimen for microscopic research were removed from the piles with an increment borer that has a diameter of 10 mm. A brief overview of the outcomes is shown in *table B-11*. It is accompanied by estimated calculations of the residual compressive strength in *table B-12* based on *equation (3.2)*.

no. (location)	element	wood species	L _{spec} [mm]	mean depth of decay [mm]					main degraders
				I	II	III	IV	V	
1 (1)	pile Ø180	pine	95	0	27	18	22	28	EB
2 (2)	pile Ø180	pine	73	6	17	7	8	35	EB
3 (3)	pile Ø180	pine	80	8	36	0	0	0	EB
4 (4)	pile Ø170	pine	103	10	52	3	0	38	EB
5 (5)	pile Ø170	pine	80	0	43	2	0	35	EB
degradation classes: I – total disruption of the wood structure II – severe decay III – moderate decay IV – weak decay V – none decay				degrader types: EB – erosion bacteria TB – tunnelling bacteria SR – soft rot fungi WR – white rot fungi BR – brown rot fungi					

table B-11: microscopic results of the Toussaintkade (Gemeente Rotterdam, internal documents, 2009)

no. (location)	L _{spec} [mm]	f _c [N/mm ²] per segment							
		1	2	3	4	5	6	7	8
1 (1)	153	8.0	14.6	17.3	17.6	19.7	11.4	N/A	N/A
2 (1)	118	12.5	15.2	14.9	16.4	18.0	17.1	17.9	23.2
3 (2)	112	7.7	13.6	16.0	13.6	14.5	13.8	N/A	N/A

table B-12: estimation residual strength of the foundation elements at the Toussaintkade (Gemeente Rotterdam, internal documents, 2009)

Right after the demolition and renovation of the Toussaintkade, thirteen timber piles and an unknown number of sole beam lengths were reclaimed from the soil and brought to a laboratory for several tests. The extracting locations are shown in *figure B-5*.

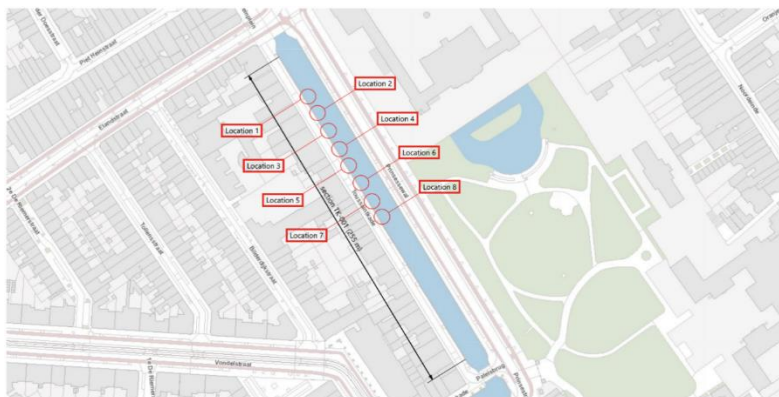


figure B-5: retrieved pile locations of the Toussaintkade (ArcGIS, n.d.)

Samples were taken from ten piles and five sole beams for further microscopic investigations. For the determination of the ultimate compression resistance, sections were sawn into sections with a length-to-diameter ratio of 1:1. Sections with a length-to-diameter ratio of 2:1 were used for the determination of the Young's modulus. The results in *table B-13* are complete for eight piles, so those are presented here. In this table, also a comparison is made with the values of the compression strength according to *equation (3.2)*.

no.	L _{pile} [mm]	d [mm]		F _c [kN]			E _{pile} [N/mm ²]
		head	tip	destructive testing	equation 3.2		
					head	tip	
1	3.10	190	160	169	196	169	817
2	3.80	210	180	233	294	216	1018
3	3.10	170	140	146	270	122	645
4	3.80	160	130	176	143	84	574
5	3.95	190	150	238	250	126	1346
6	4.00	230	150	328	274	83	416
7	3.60	200	180	213	138	189	954
8	3.20	180	140	200	290	137	958

table B-13: mechanical testing results from the timber foundation piles at the Toussaintkade (Gemeente Rotterdam, internal documents, 2009)

Appendix C: Calculation results

C.1 BOOMPJESKADE, ROTTERDAM

C.1.1 COLLECTION OF DATA

terrain loads	
parameter	value
$F_{LM1,rep,i}$ [kN]	150
$Q_{LM1,rep,i}$ [kN/m ²]	9.0
$Q_{LM1,rep}$ [kN/m ²]	2.5
α_Q [-]	0.6
W_{LM1} [m]	3.0
$a_{LM1,x}$ [m]	3.0
$S_{LM1,x}$ [m]	2.0
$S_{LM1,y}$ [m]	1.2

mooring forces			
no.	$y_{mr,i}$ [m]	$F_{mr,i}$ [kN]	$\alpha_{mr,i}$ [°]
1	5.00	50	30
2	10.00	50	45
3	15.00	50	90

surface water	
parameter	value
z_{MHW} [m NAP]	+1.30
γ_w [kN/m ³]	10.0

retaining wall	
parameter	value
γ_{wall} [kN/m ³]	16.0
$z_{wall,top}$ [m NAP]	+2.85
$z_{wall,btm}$ [m NAP]	-0.75
$x_{wall,top}$ [m]	0.160
E_{wall} [N/mm ²]	2.00×10^4

retaining wall coordinates		
no.	$x_{wall,i}$ [m]	$z_{wall,i}$ [m NAP]
1	0	-0.75
2	2.00	-0.75
3	2.00	0.65
4	1.65	0.65
5	1.11	2.55
6	0.66	2.60
7	0.66	2.85
8	0.16	2.85
9	0.16	2.60

pile row									
no.	$x_{pile,i}$ [m]	$z_{head,i}$ [m NAP]	$z_{tip,i}$ [m NAP]	$d_{head,i}$ [mm]	$d_{tip,i}$ [mm]	$\alpha_{pile,i}$ [°]	$A_{gr,i}$ [m ²]	E_{pile} [N/mm ²]	$z_{soil,top,i}$ [m NAP]
1	0.40	-1.04	-18.50	280	102.4	0	0.39	3.6×10^3	-2.65
2	1.20	-1.04	-18.50	280	102.4	0	0.44	3.6×10^3	-2.55
3	2.20	-1.04	-18.50	280	102.4	0	0.49	3.6×10^3	-1.74
4	3.20	-1.04	-18.50	280	102.4	0	0.49	3.6×10^3	-1.06
5	4.20	-1.04	-18.50	280	102.4	0	0.49	3.6×10^3	-1.20
6	5.20	-1.04	-18.50	280	102.4	0	0.49	3.6×10^3	-1.34
7	6.20	-1.04	-18.50	280	102.4	0	0.49	3.6×10^3	-1.48
1sub	1.70	-1.04	-18.50	280	102.4	-18.4	0.49	3.6×10^3	-2.63
2sub	3.70	-1.04	-18.50	280	102.4	-18.4	0.49	3.6×10^3	-1.12

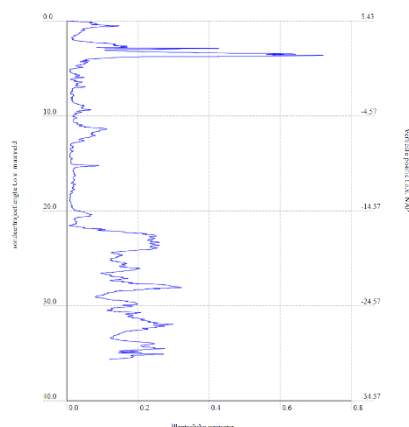
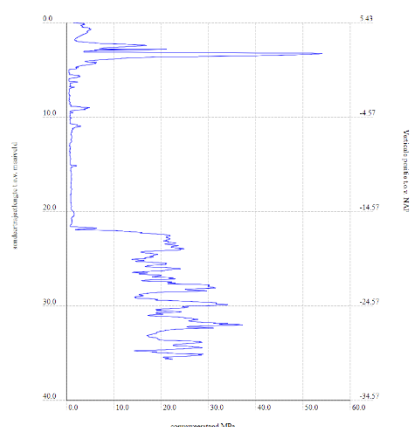
pile cap beam	
parameter	value
γ_{pcb} [kN/m ³]	4.20
W_{pcb} [mm]	300
H_{pcb} [mm]	200
L_{pcb} [mm]	6970
S_{pcb} [m]	0.975
E_{pcb} [N/mm ²]	0.12×10^3

floor element	
parameter	value
γ_{floor} [kN/m ³]	4.20
W_{floor} [mm]	230
H_{floor} [mm]	60
L_{floor} [mm]	975

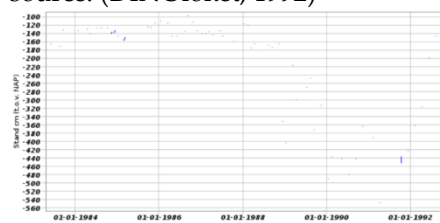
cross-beam	
parameter	value
γ_{cross} [kN/m ³]	4.20
$x_{cross,1}$ [m]	1.70
$x_{cross,2}$ [m]	3.70
W_{cross} [mm]	320
H_{cross} [mm]	220
L_{cross} [mm]	975
E_{cross} [N/mm ²]	0.12×10^3



id: CPT000000079657
 date: 14-01-2017
 coord: 93327.690, 436850.760 (RD)
 ground level: +5.43 m NAP
 total depth: 35.66 m
 source: (DINOloket, 2017)



id: B37H0520
date: 18-04-1983 / 14-12-1992
coord: 93380, 437090 (RD)
ground level: +2.48 m NAP
source: (DINOloket, 1992)

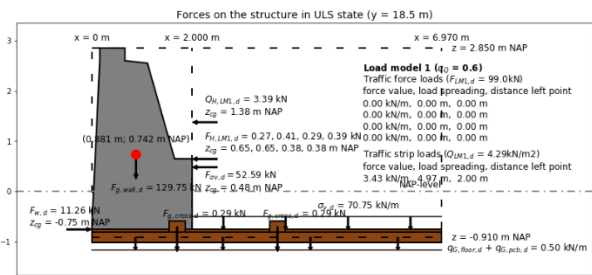
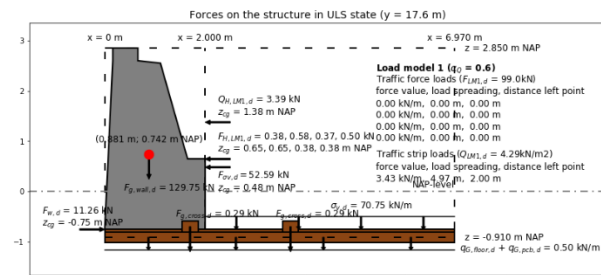
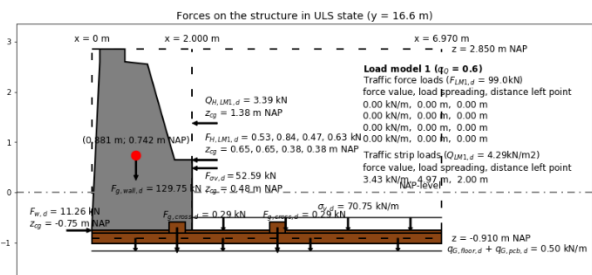
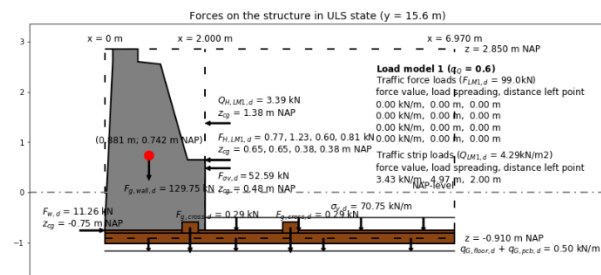
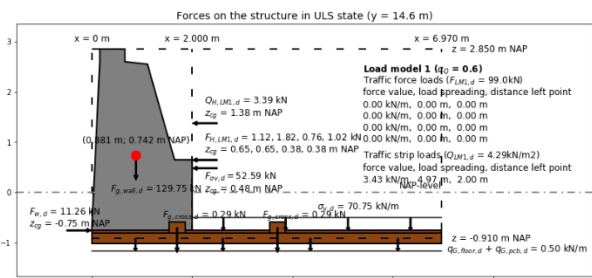
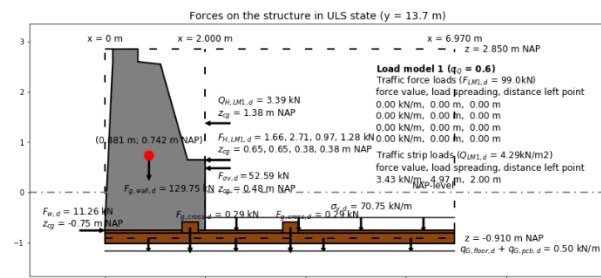
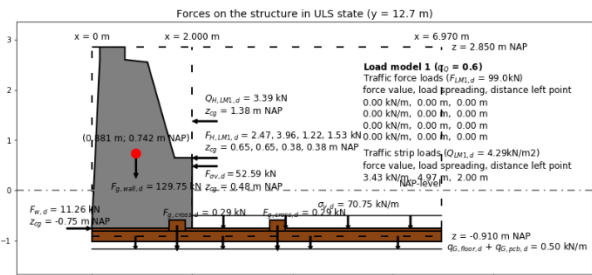
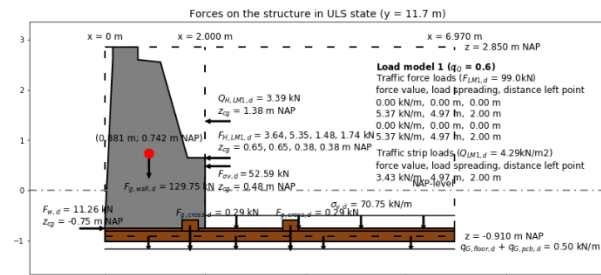
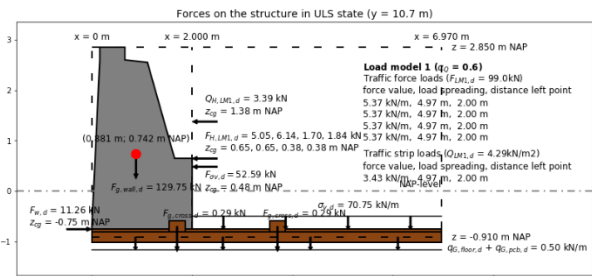
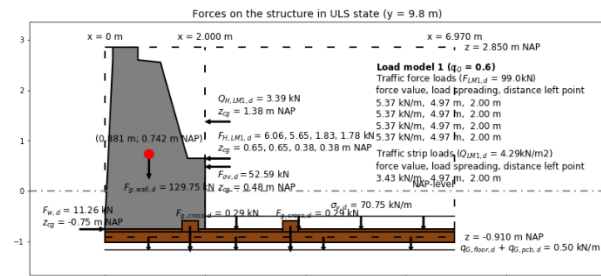
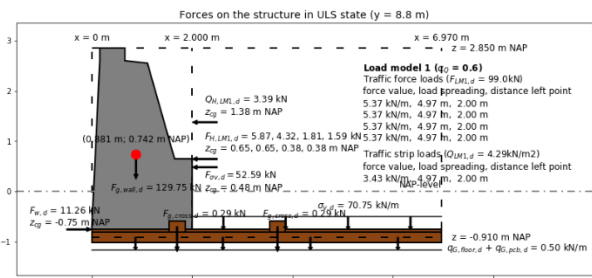
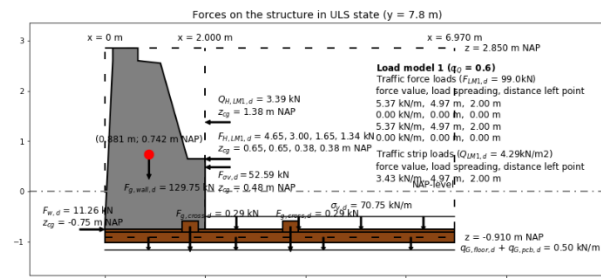


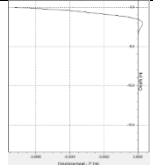
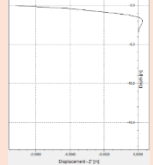
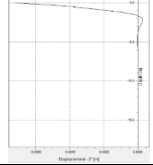
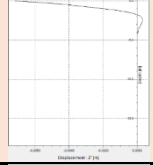
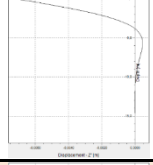
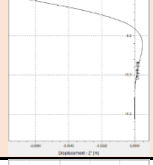
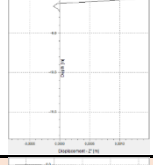
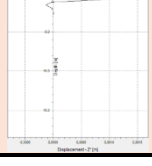
general soil information	
parameter	value
n_{probe} [-]	1
ξ_3 [-]	1.26
ξ_4 [-]	1.26
z_{gw} [m NAP]	-1.40
γ_{gw} [kN/m ³]	10.0

soil type classification					
z_{soil} [m NAP]		$q_{CPT,avg}$ [MPa]	$f_{CPT,avg}$ [MPa]	$R_{CPT,avg}$ [%]	soil type
from	to				
+2.85	+1.30	21.3	0.375	1.77	sand, weak silty/ clayey
+1.30	-5.20	1.5	0.026	1.97	clay, slight sandy, moderate
-5.20	-8.70	1.0	0.041	4.30	peat, moderate
-8.70	-14.20	1.0	0.019	1.89	clay, slight sandy, moderate
-14.20	-16.70	1.1	0.034	3.28	clay, clean, moderate
-16.70	-30.20	21.6	0.180	0.84	sand, clean, dense

C.1.2 SUPERSTRUCTURE LOADS





	-16.70	-18.50	-17.60	-16.69	0	
104	-1.74	-5.20	-3.47	-2.56	1.29×10^{-4}	
	-5.20	-8.70	-6.95	-6.04	0	
	-8.70	-14.20	-11.45	-10.54	0	
	-14.20	-16.70	-15.45	-14.54	0	
	-16.70	-18.50	-17.60	-16.69	0	
105	-1.06	-5.20	-3.13	-2.22	2.99×10^{-4}	
	-5.20	-8.70	-6.95	-6.04	1.00×10^{-6}	
	-8.70	-14.20	-11.45	-10.54	0	
	-14.20	-16.70	-15.45	-14.54	0	
	-16.70	-18.50	-17.60	-16.69	0	
106	-1.20	-5.20	-3.20	-2.29	3.05×10^{-4}	
	-5.20	-8.70	-6.95	-6.04	-4.00×10^{-6}	
	-8.70	-14.20	-11.45	-10.54	0	
	-14.20	-16.70	-15.45	-14.54	0	
	-16.70	-18.50	-17.60	-16.69	0	
107	-1.34	-5.20	-3.27	-2.36	-1.79×10^{-3}	
	-5.20	-8.70	-6.95	-6.04	4.29×10^{-4}	
	-8.70	-14.20	-11.45	-10.54	1.40×10^{-5}	
	-14.20	-16.70	-15.45	-14.54	-1.40×10^{-5}	
	-16.70	-18.50	-17.60	-16.69	-2.00×10^{-6}	
108	-1.48	-5.20	-3.34	-2.43	-1.55×10^{-3}	
	-5.20	-8.70	-6.95	-6.04	4.61×10^{-4}	
	-8.70	-14.20	-11.45	-10.54	5.30×10^{-5}	
	-14.20	-16.70	-15.45	-14.54	-2.00×10^{-5}	
	-16.70	-18.50	-17.60	-16.69	-8.00×10^{-6}	
187	-2.63	-5.20	-3.92	-3.01	1.00×10^{-6}	
	-5.20	-8.70	-6.95	-6.04	0	
	-8.70	-14.20	-11.45	-10.54	0	
	-14.20	-16.70	-15.45	-14.54	0	
	-16.70	-18.50	-17.60	-16.69	0	
188	-1.12	-5.20	-3.16	-2.25	2.00×10^{-6}	
	-5.20	-8.70	-6.95	-6.04	0	
	-8.70	-14.20	-11.45	-10.54	0	
	-14.20	-16.70	-15.45	-14.54	0	
	-16.70	-18.50	-17.60	-16.69	0	

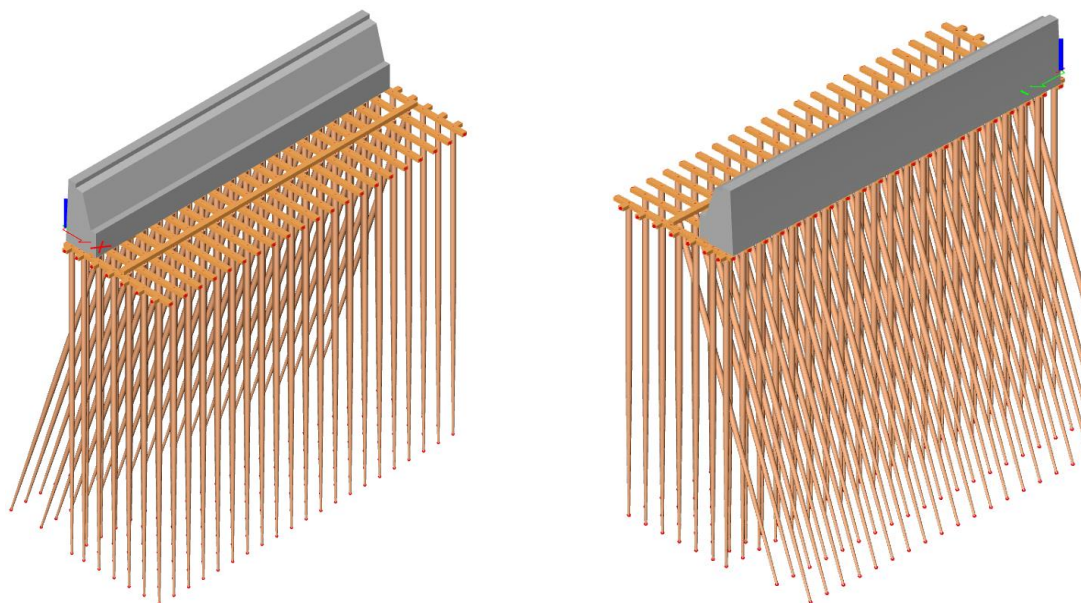
horizontal soil response							
pile no.	Z _{soil} [m NAP]		soil type	α [-]	β [-]	k _s [MN/m ³]	p _{soil} [MN/m ²]
	from	to					
1	-2.65	-5.20	clay	2/3	2.0	1.66×10^{-4}	5.22
	-5.20	-8.70	peat	1	3.0	1.45×10^{-4}	0.32
	-8.70	-14.20	clay	2/3	2.0	1.11×10^{-4}	0
	-14.20	-16.70	clay	2/3	2.0	1.22×10^{-4}	0
	-16.70	-18.50	sand	1/3	0.7	9.75×10^{-4}	0
2	-2.55	-5.20	clay	2/3	2.0	1.66×10^{-4}	1.24
	-5.20	-8.70	peat	1	3.0	1.45×10^{-4}	0.01
	-8.70	-14.20	clay	2/3	2.0	1.11×10^{-4}	0

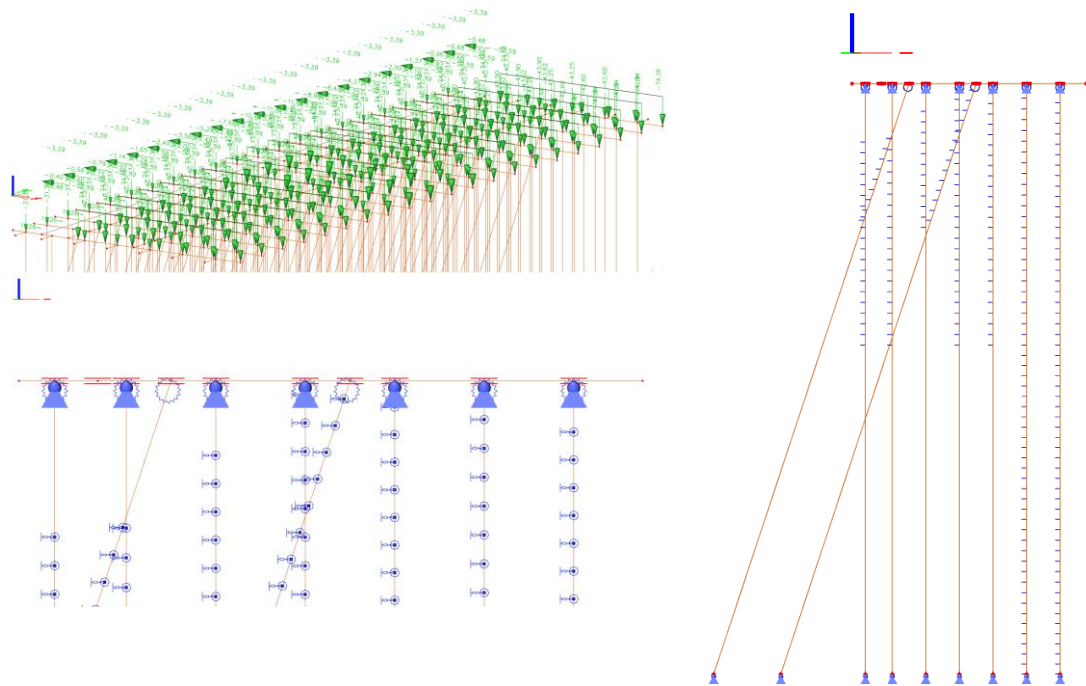
	-14.20	-16.70	clay	2/3	2.0	1.22×10^{-4}	0
	-16.70	-18.50	sand	1/3	0.7	9.75×10^{-4}	0
3	-1.74	-5.20	clay	2/3	2.0	1.66×10^{-4}	2.14
	-5.20	-8.70	peat	1	3.0	1.45×10^{-4}	0
	-8.70	-14.20	clay	2/3	2.0	1.11×10^{-4}	0
	-14.20	-16.70	clay	2/3	2.0	1.22×10^{-4}	0
	-16.70	-18.50	sand	1/3	0.7	9.75×10^{-4}	0
4	-1.06	-5.20	clay	2/3	2.0	1.66×10^{-4}	4.96
	-5.20	-8.70	peat	1	3.0	1.45×10^{-4}	0.01
	-8.70	-14.20	clay	2/3	2.0	1.11×10^{-4}	0
	-14.20	-16.70	clay	2/3	2.0	1.22×10^{-4}	0
	-16.70	-18.50	sand	1/3	0.7	9.75×10^{-4}	0
5	-1.20	-5.20	clay	2/3	2.0	1.66×10^{-4}	5.06
	-5.20	-8.70	peat	1	3.0	1.45×10^{-4}	0.06
	-8.70	-14.20	clay	2/3	2.0	1.11×10^{-4}	0
	-14.20	-16.70	clay	2/3	2.0	1.22×10^{-4}	0
	-16.70	-18.50	sand	1/3	0.7	9.75×10^{-4}	0
6	-1.34	-5.20	clay	2/3	2.0	1.66×10^{-4}	29.67
	-5.20	-8.70	peat	1	3.0	1.45×10^{-4}	6.20
	-8.70	-14.20	clay	2/3	2.0	1.11×10^{-4}	0.15
	-14.20	-16.70	clay	2/3	2.0	1.22×10^{-4}	0.17
	-16.70	-18.50	sand	1/3	0.7	9.75×10^{-4}	0.19
7	-1.48	-5.20	clay	2/3	2.0	1.66×10^{-4}	25.70
	-5.20	-8.70	peat	1	3.0	1.45×10^{-4}	6.66
	-8.70	-14.20	clay	2/3	2.0	1.11×10^{-4}	0.59
	-14.20	-16.70	clay	2/3	2.0	1.22×10^{-4}	0.24
	-16.70	-18.50	sand	1/3	0.7	9.75×10^{-4}	0.78
1sub	-2.63	-5.20	clay	2/3	2.0	1.66×10^{-4}	0.02
	-5.20	-8.70	peat	1	3.0	1.45×10^{-4}	0
	-8.70	-14.20	clay	2/3	2.0	1.11×10^{-4}	0
	-14.20	-16.70	clay	2/3	2.0	1.22×10^{-4}	0
	-16.70	-18.50	sand	1/3	0.7	9.75×10^{-4}	0
2sub	-1.12	-5.20	clay	2/3	2.0	1.66×10^{-4}	0.03
	-5.20	-8.70	peat	1	3.0	1.45×10^{-4}	0
	-8.70	-14.20	clay	2/3	2.0	1.11×10^{-4}	0
	-14.20	-16.70	clay	2/3	2.0	1.22×10^{-4}	0
	-16.70	-18.50	sand	1/3	0.7	9.75×10^{-4}	0

C.1.4 JOINT STIFFNESS

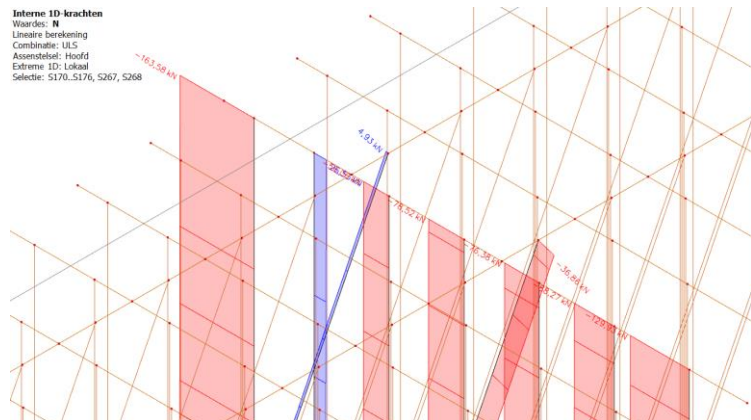
calculation joint stiffness	
parameter	value
H_{mor} [mm]	90
W_{notch} [mm]	28
a_1 [mm]	126
a_2 [mm]	30
a_3 [mm]	30
$k_{0,1}$ [N/mm]	3.01×10^5
$k_{90,1}$ [N/mm]	1.00×10^4
$k_{0,2}$ [N/mm]	6.72×10^5
$k_{90,2}$ [N/mm]	2.24×10^4
$k_{0,3}$ [N/mm]	6.72×10^5
$k_{90,3}$ [N/mm]	2.24×10^4
$k_{\text{eq},1}$ [N/mm]	9.73×10^3
$k_{\text{eq},2}$ [N/mm]	2.17×10^4
$k_{\text{eq},3}$ [N/mm]	2.17×10^4
k_r [MNm/rad]	0.19

C.1.5 AXIAL PILE HEAD FORCES

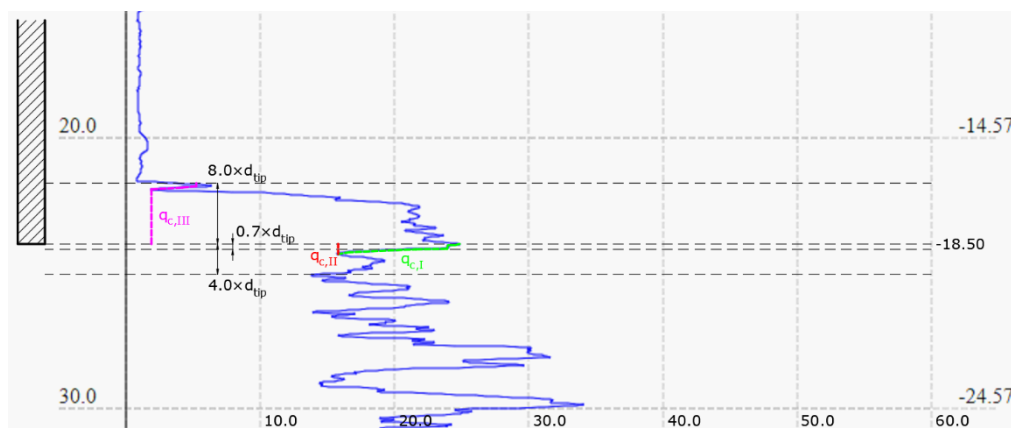




axial pile head forces (y = 9.75 m)	
pile row	F _{head,d} [kN]
1	-163.58
2	+26.53
3	-56.06
4	-78.52
5	-76.38
6	-88.27
7	-129.93
1sub	+4.93
2sub	-36.86



C.1.6 AXIAL PILE FORCES AND RESISTANCES



cone resistances	
parameter	value
$q_{CPT,I}$ [MPa]	15.0
$q_{CPT,II}$ [MPa]	15.0
$q_{CPT,III}$ [MPa]	2.5

maximum pile tip resistance				
pile row	A_{tip} [mm ²]	$q_{b,max}$ [MPa]	$R_{b,max,k}$ [kN]	$R_{b,max,d}$ [kN]
1	8.23×10^3	6.13	50.41	30.22
3	8.23×10^3	6.13	50.41	30.22
4	8.23×10^3	6.13	50.41	30.22
5	8.23×10^3	6.13	50.41	30.22
6	8.23×10^3	6.13	50.41	30.22
7	8.23×10^3	6.13	50.41	30.22
2sub	8.23×10^3	6.13	50.41	30.22

maximum pile shaft resistance ($z_{ip} = -16.7$ m NAP)							
pile row	ΔL [m]	$Z_{\Delta L,avg}$ [m]	$d_{\Delta L,avg}$ [mm]	$C_{\Delta L,avg}$ [mm]	$q_{s,max}$ [MPa]	$R_{s,max,k}$ [kN]	$R_{s,max,d}$ [kN]
1	1.80	16.56	107.8	338.7	0.18	109.75	65.80
3	1.80	16.56	107.8	338.7	0.18	109.75	65.80
4	1.80	16.56	107.8	338.7	0.18	109.75	65.80
5	1.80	16.56	107.8	338.7	0.18	109.75	65.80
6	1.80	16.56	107.8	338.7	0.18	109.75	65.80
7	1.80	16.56	107.8	338.7	0.18	109.75	65.80
2sub	1.80	16.56	107.8	338.7	0.18	109.75	65.80

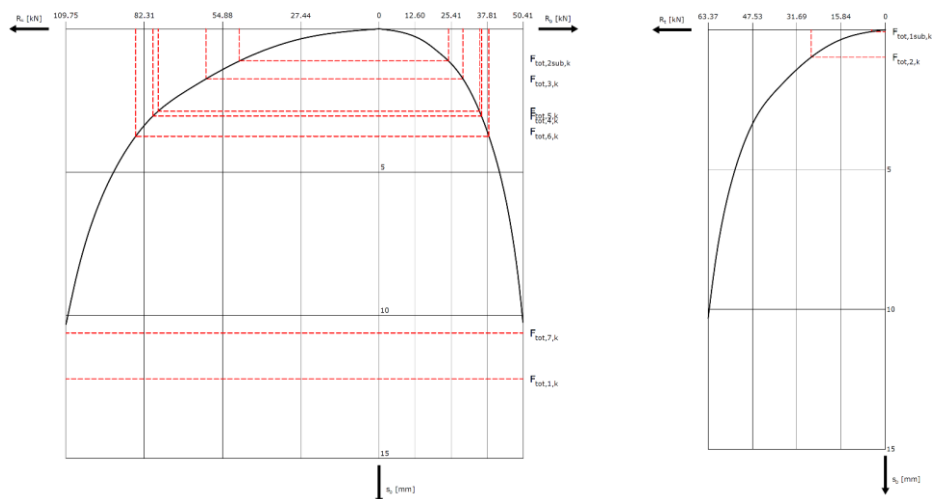
negative skin friction ($z_{ip} = -16.7$ m NAP)											
pile row	Z_{mid} [m NAP]	t_i [m]	γ'_i [kN/m ³]	$Z_{pile,mid}$ [m]	$C_{pile,mid}$ [m]	m_i [-]	$\sigma'_{m,i}$ [kN/m ²]	$\sigma_{nsf,i}$ [kN/m ²]	$F_{nsf,i}$ [kN]	$F_{nsf,k}$ [kN]	$F_{nsf,d}$ [kN]
1	-3.93	2.55	8.0	2.89	0.74	0.48	11.80	8.60	3.36	26.15	31.38
	-6.95	3.50	3.0	5.91	0.63	0.40	8.54	13.76	5.36		
	-11.45	5.50	8.0	10.41	0.48	0.31	22.69	29.85	11.64		
	-15.45	2.50	7.0	14.41	0.38	0.25	25.35	14.84	5.79		
3	-3.47	3.46	8.0	2.43	0.76	0.39	15.19	12.49	6.12	33.94	40.73
	-6.95	3.50	3.0	5.91	0.63	0.32	11.29	14.40	7.05		
	-11.45	5.50	8.0	10.41	0.48	0.25	27.01	28.28	13.86		
	-15.45	2.50	7.0	14.41	0.38	0.20	30.40	14.11	6.91		
4	-3.13	4.14	8.0	2.09	0.78	0.40	16.23	16.89	8.27	36.58	43.90
	-6.95	3.50	3.0	5.91	0.63	0.32	11.63	15.10	7.40		
	-11.45	5.50	8.0	10.41	0.48	0.25	27.10	28.53	13.98		
	-15.45	2.50	7.0	14.41	0.38	0.20	30.46	14.14	6.93		
5	-3.20	4.00	8.0	2.16	0.78	0.40	16.05	15.95	7.81	36.04	43.25
	-6.95	3.50	3.0	5.91	0.63	0.32	11.57	14.98	7.34		
	-11.45	5.50	8.0	10.41	0.48	0.25	27.08	28.49	13.96		
	-15.45	2.50	7.0	14.41	0.38	0.20	30.45	14.13	6.93		
6	-3.27	3.86	8.0	2.23	0.77	0.39	15.85	15.03	7.36	35.50	42.60
	-6.95	3.50	3.0	5.91	0.63	0.32	11.51	14.84	7.27		
	-11.45	5.50	8.0	10.41	0.48	0.25	27.07	28.44	13.94		
	-15.45	2.50	7.0	14.41	0.38	0.20	30.44	14.13	6.92		
7	-3.34	3.72	8.0	2.30	0.77	0.39	15.64	14.12	6.92	34.95	41.94
	-6.95	3.50	3.0	5.91	0.63	0.32	11.44	14.70	7.20		
	-11.45	5.50	8.0	10.41	0.48	0.25	27.05	28.39	13.91		

	-15.45	2.50	7.0	14.41	0.38	0.20	30.43	14.12	6.92		
2sub	-3.16	4.08	8.0	2.12	0.78	0.40	16.16	16.48	8.08	36.35	43.62
	-6.95	3.50	3.0	5.91	0.63	0.32	11.61	15.05	7.37		
	-11.45	5.50	8.0	10.41	0.48	0.25	27.09	28.52	13.97		
	-15.45	2.50	7.0	14.41	0.38	0.20	30.45	14.14	6.93		

tensile resistance										
pile row	Zmid [m NAP]	t _i [m]	Z _{pile,mid} [m]	C _{pile,mid} [m]	α _{t,i} [-]	q _{CPT,d,i} [MPa]	q _{t,d,i} [MPa]	R _{t,d,i} [kN]	R _{t,d} [kN]	R _{t,k} [kN]
2	-3.88	2.65	2.84	0.747	0.0035	0.533	0.002	3.69	33.77	63.37
	-6.95	3.50	5.91	0.626	0.0035	0.355	0.001	2.72		
	-11.45	5.50	10.41	0.483	0.0035	0.355	0.001	3.30		
	-15.45	2.50	14.41	0.383	0.0035	0.391	0.001	1.31		
	-17.60	1.80	16.56	0.339	0.0070	5.329	0.037	22.74		
1sub	-3.92	2.57	2.88	0.745	0.0035	0.533	0.002	3.57	33.65	63.14
	-6.95	3.50	5.91	0.626	0.0035	0.355	0.001	2.72		
	-11.45	5.50	10.41	0.483	0.0035	0.355	0.001	3.30		
	-15.45	2.50	14.41	0.383	0.0035	0.391	0.001	1.31		
	-17.60	1.80	16.56	0.339	0.0070	5.329	0.037	22.74		

C.1.7 PILE TIP SETTLEMENT AND FORCE

total pile head force	
pile row	F _{tot} [kN]
1	-193.57
2	+31.70
3	-92.42
4	-117.06
5	-113.79
6	-123.35
7	-165.25
1sub	+5.90
2sub	-70.22



pile settlement and rise					
pile row	R _b [kN]	R _s [kN]	s _b [mm]	R _t [kN]	s _{head} [mm]
1	59.7	130.0	12.2	–	–
2	–	–	–	26.5	1.0
3	29.3	60.7	1.7	–	–
4	35.8	79.3	3.0	–	–
5	35.7	77.3	2.8	–	–
6	38.5	85.3	3.7	–	–
7	51.9	113.0	10.6	–	–
1sub	–	–	–	4.9	0.1
2sub	48.9	24.3	1.1	–	–

axial pile tip stiffness	
pile row	k _{ax} [MN/m]
1	15.5
2	26.5
3	52.9
4	38.4
5	40.4
6	33.5
7	15.6
1sub	49.0
2sub	66.5

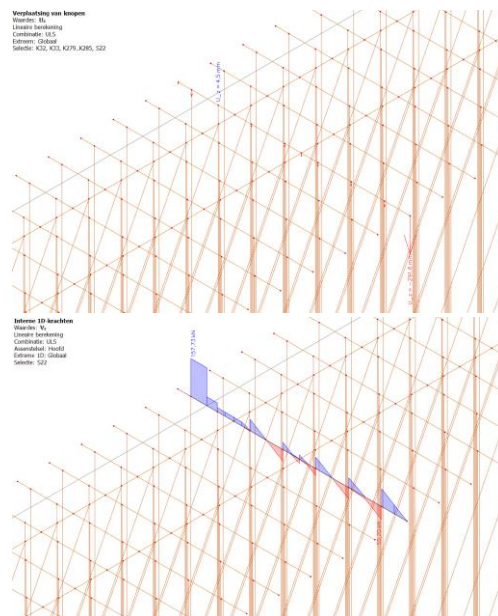
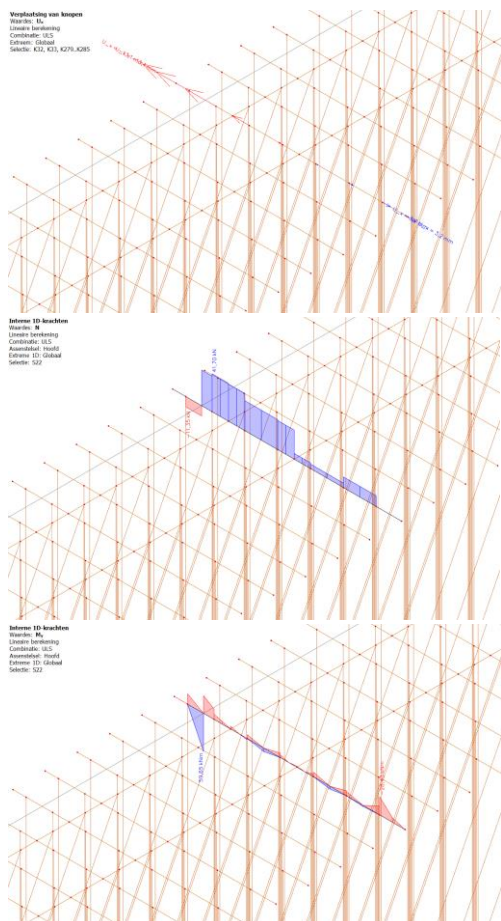
C.1.8 NEUTRAL PLANE

total soil settlement				
pile row	Z _{top} [m NAP]	t _i [m]	S _{soil,tot,i} [m]	S _{soil,tot} [m]
1	–2.65	2.55	0.047	0.531
	–5.20	3.50	0.322	
	–8.70	5.50	0.101	
	–14.20	2.50	0.061	
3	–1.74	3.46	0.064	0.548
	–5.20	3.50	0.322	
	–8.70	5.50	0.101	
	–14.20	2.50	0.061	
4	–1.06	4.14	0.076	0.560
	–5.20	3.50	0.322	
	–8.70	5.50	0.101	
	–14.20	2.50	0.061	
5	–1.20	4.00	0.074	0.558
	–5.20	3.50	0.322	
	–8.70	5.50	0.101	
	–14.20	2.50	0.061	
6	–1.34	3.86	0.071	0.555
	–5.20	3.50	0.322	
	–8.70	5.50	0.101	
	–14.20	2.50	0.061	
7	–1.48	3.72	0.068	0.553
	–5.20	3.50	0.322	

	-8.70	5.50	0.101	
	-14.20	2.50	0.061	
2sub	-1.12	4.08	0.075	0.559
	-5.20	3.50	0.322	
	-8.70	5.50	0.101	
	-14.20	2.50	0.061	

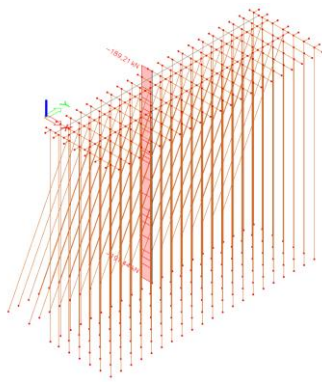
influence neutral plane					
pile row	value	R _{s,max,k} [kN]	R _{s,max,d} [kN]	F _{nsf,k} [kN]	F _{nsf,d} [kN]
1	maximum	109.75	65.80	26.15	31.38
3	maximum	109.75	65.80	33.94	40.73
4	maximum	109.75	65.80	36.58	43.90
5	maximum	109.75	65.80	36.04	43.25
6	maximum	109.75	65.80	35.50	42.60
7	maximum	109.75	65.80	34.95	41.94
2sub	maximum	109.75	65.80	36.35	43.62

C.1.9 CALCULATION MODEL

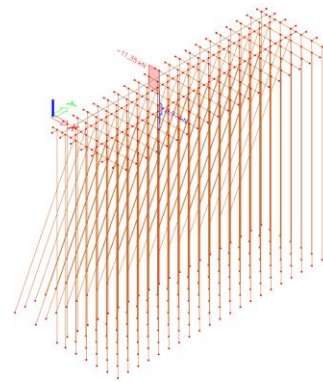


extreme values in pile cap beam (y = 9.75 m)				
parameter	minimum		maximum	
	value	pile row	value	pile row
u _{x,int} [mm]	-13.1	1	3.2	7
u _{z,int} [mm]	-291.6	7	4.5	2
N _{int} [kN]	-11.4	1-2	41.7	2-3
V _{z,int} [kN]	-55.2	7	157.7	1-2
M _{y,int} [kNm]	-28.4	7	59.7	1-2

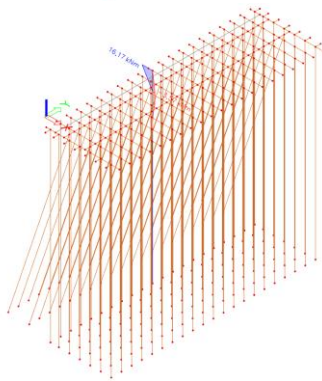
Inferno 1D-brachten
 Waarden: M_x
 Lineaire berekening
 Combinator: ULS
 Assumefact: Hoofd
 Extreme 1D: Global
 Selectie: 5170



Inferno 1D-brachten
 Waarden: V_z
 Lineaire berekening
 Combinator: ULS
 Assumefact: Hoofd
 Extreme 1D: Global
 Selectie: 5170



Inferno 1D-brachten
 Waarden: M_y
 Lineaire berekening
 Combinator: ULS
 Assumefact: Hoofd
 Extreme 1D: Global
 Selectie: 5170



extreme values in pile at first row (x = 0.40 m, y = 9.75 m)

parameter	minimum value	maximum value
N _{int} [kN]	-191.4	-189.2
V _{z,int} [kN]	-11.4	3.0
M _{y,int} [kNm]	-3.6	16.2

C.1.10 STRUCTURAL DEFICIENCIES

changes in structural model		
modification	changing variable	adaptations
1	$p_m = 5 \text{ mm}$	d _{head,1...7} (y = 0.00 m), ..., d _{head,1...7} (y = 19.50 m): 280 mm → 260 mm
		d _{tip,1...7} (y = 0.00 m), ..., d _{tip,1...7} (y = 19.50 m): 102.4 mm → 87.4 mm
		d _{head,sub,1,2} (y = 0.49 m), ..., d _{head,sub,1,2} (y = 19.01 m): 280 mm → 260 mm
		d _{tip,sub,1,2} (y = 0.49 m), ..., d _{tip,sub,1,2} (y = 19.01 m): 102.4 mm → 87.4 mm
2	$p_m = 5 \text{ mm}$	d _{head,1...7} (y = 9.75 m): 280 mm → 260 mm
		d _{tip,1...7} (y = 9.75 m): 102.4 mm → 87.4 mm
		d _{head,sub,1,2} (y = 10.24 m): 280 mm → 260 mm
		d _{tip,sub,1,2} (y = 10.24 m): 102.4 mm → 87.4 mm
3	$p_m = 5 \text{ mm}$	d _{head,1,2} (y = 0.00 m), ..., d _{head,1,2} (y = 19.50 m): 280 mm → 260 mm
		d _{tip,1,2} (y = 0.00 m), ..., d _{tip,1,2} (y = 19.50 m): 102.4 mm → 87.4 mm
4	$p_m = 15 \text{ mm}$	d _{head,1...7} (y = 0.00 m), ..., d _{head,1...7} (y = 19.50 m): 280 mm → 240 mm
		d _{tip,1...7} (y = 0.00 m), ..., d _{tip,1...7} (y = 19.50 m): 102.4 mm → 77.4 mm
		d _{head,sub,1,2} (y = 0.49 m), ..., d _{head,sub,1,2} (y = 19.01 m): 280 mm → 240 mm
		d _{tip,sub,1,2} (y = 0.49 m), ..., d _{tip,sub,1,2} (y = 19.01 m): 102.4 mm → 77.4 mm
		W _{pcb} (y = 0.00 m), ..., W _{pcb} (y = 19.50 m): 300 mm → 290 mm
		W _{cross,1} (x = 1.70 m): 320 mm → 310 mm
		W _{cross,2} (x = 3.70 m): 320 mm → 310 mm
5	$p_m = 15 \text{ mm}$	d _{head,1...7} (y = 9.75 m): 280 mm → 240 mm
		d _{tip,1...7} (y = 9.75 m): 102.4 mm → 77.4 mm
		d _{head,sub,1,2} (y = 10.24 m): 280 mm → 240 mm
		d _{tip,sub,1,2} (y = 10.24 m): 102.4 mm → 77.4 mm
		W _{pcb} (y = 9.75 m): 300 mm → 290 mm
		W _{cross,1} (x = 1.70 m): 320 mm → 310 mm
		W _{cross,2} (x = 3.70 m): 320 mm → 310 mm

6	$p_m = 15 \text{ mm}$	$d_{\text{head},1,2} (y = 0.00 \text{ m}), \dots, d_{\text{head},1,2} (y = 19.50 \text{ m}): 280 \text{ mm} \rightarrow 240 \text{ mm}$ $d_{\text{tip},1,2} (y = 0.00 \text{ m}), \dots, d_{\text{tip},1,2} (y = 19.50 \text{ m}): 102.4 \text{ mm} \rightarrow 77.4 \text{ mm}$ $W_{\text{pcb}} (y = 0.00 \text{ m}), \dots, W_{\text{pcb}} (y = 19.50 \text{ m}): 300 \text{ mm} \rightarrow 290 \text{ mm}$
7	$p_m = 30 \text{ mm}$	$d_{\text{head},1,\dots,7} (y = 0.00 \text{ m}), \dots, d_{\text{head},1,\dots,7} (y = 19.50 \text{ m}): 280 \text{ mm} \rightarrow 210 \text{ mm}$ $d_{\text{tip},1,\dots,7} (y = 0.00 \text{ m}), \dots, d_{\text{tip},1,\dots,7} (y = 19.50 \text{ m}): 102.4 \text{ mm} \rightarrow 62.4 \text{ mm}$ $d_{\text{head},\text{sub},1,2} (y = 0.49 \text{ m}), \dots, d_{\text{head},\text{sub},1,2} (y = 19.01 \text{ m}): 280 \text{ mm} \rightarrow 210 \text{ mm}$ $d_{\text{tip},\text{sub},1,2} (y = 0.49 \text{ m}), \dots, d_{\text{tip},\text{sub},1,2} (y = 19.01 \text{ m}): 102.4 \text{ mm} \rightarrow 62.4 \text{ mm}$ $W_{\text{pcb}} (y = 0.00 \text{ m}), \dots, W_{\text{pcb}} (y = 19.50 \text{ m}): 300 \rightarrow 260 \text{ mm}$ $W_{\text{cross},1} (x = 1.70 \text{ m}): 320 \text{ mm} \rightarrow 280 \text{ mm}$ $W_{\text{cross},2} (x = 3.70 \text{ m}): 320 \text{ mm} \rightarrow 280 \text{ mm}$
8	$p_m = 30 \text{ mm}$	$d_{\text{head},1,\dots,7} (y = 9.75 \text{ m}): 280 \text{ mm} \rightarrow 210 \text{ mm}$ $d_{\text{tip},1,\dots,7} (y = 9.75 \text{ m}): 102.4 \text{ mm} \rightarrow 62.4 \text{ mm}$ $d_{\text{head},\text{sub},1,2} (y = 10.24 \text{ m}): 280 \text{ mm} \rightarrow 210 \text{ mm}$ $d_{\text{tip},\text{sub},1,2} (y = 10.24 \text{ m}): 102.4 \text{ mm} \rightarrow 62.4 \text{ mm}$ $W_{\text{pcb}} (y = 9.75 \text{ m}): 300 \text{ mm} \rightarrow 260 \text{ mm}$ $W_{\text{cross},1} (x = 1.70 \text{ m}): 320 \text{ mm} \rightarrow 280 \text{ mm}$ $W_{\text{cross},2} (x = 3.70 \text{ m}): 320 \text{ mm} \rightarrow 280 \text{ mm}$
9	$p_m = 30 \text{ mm}$	$d_{\text{head},1,2} (y = 0.00 \text{ m}), \dots, d_{\text{head},1,2} (y = 19.50 \text{ m}): 280 \text{ mm} \rightarrow 210 \text{ mm}$ $d_{\text{tip},1,2} (y = 0.00 \text{ m}), \dots, d_{\text{tip},1,2} (y = 19.50 \text{ m}): 102.4 \text{ mm} \rightarrow 62.4 \text{ mm}$ $W_{\text{pcb}} (y = 0.00 \text{ m}), \dots, W_{\text{pcb}} (y = 19.50 \text{ m}): 300 \text{ mm} \rightarrow 260 \text{ mm}$
10	$e_y = 25 \text{ mm}$	$e_{y,\text{pcb}} (y = 9.75 \text{ m}): 0 \rightarrow 25 \text{ mm}$
11	$e_y = 50 \text{ mm}$	$e_{y,\text{pcb}} (y = 9.75 \text{ m}): 0 \rightarrow 50 \text{ mm}$
12	$e_y = 100 \text{ mm}$	$e_{y,\text{pcb}} (y = 9.75 \text{ m}): 0 \rightarrow 100 \text{ mm}$
13	$R_{c,\text{max}} = 0 \text{ kN}$, $R_{t,\text{max}} = 0 \text{ kN}$	$R_{c,\text{pile},1,d} (x = 0.40 \text{ m}, y = 9.75 \text{ m}): 96.02 \text{ kN} \rightarrow 0 \text{ kN}$ $R_{t,\text{pile},2,d} (x = 1.20 \text{ m}, y = 9.75 \text{ m}): 33.77 \text{ kN} \rightarrow 0 \text{ kN}$
14	$R_{c,\text{max}} = 0 \text{ kN}$, $R_{t,\text{max}} = 0 \text{ kN}$	$R_{c,\text{pile},6} (x = 5.20 \text{ m}, y = 9.75 \text{ m}): 96.02 \text{ kN} \rightarrow 0 \text{ kN}$ $R_{c,\text{pile},7} (x = 6.20 \text{ m}, y = 9.75 \text{ m}): 96.02 \text{ kN} \rightarrow 0 \text{ kN}$
15	$S_b = 5 \text{ mm}$, $S_{\text{head}} = 5 \text{ mm}$	$k_{ax,1} (x = 0.40 \text{ m}, y = 9.75 \text{ m}): 15.5 \text{ MN/m} \rightarrow 37.9 \text{ MN/m}$ $k_{ax,2} (x = 1.20 \text{ m}, y = 9.75 \text{ m}): 26.5 \text{ MN/m} \rightarrow 5.3 \text{ MN/m}$ $k_{ax,3} (x = 2.20 \text{ m}, y = 9.75 \text{ m}): 52.9 \text{ MN/m} \rightarrow 18.0 \text{ MN/m}$ $k_{ax,4} (x = 3.20 \text{ m}, y = 9.75 \text{ m}): 38.4 \text{ MN/m} \rightarrow 23.0 \text{ MN/m}$ $k_{ax,5} (x = 4.20 \text{ m}, y = 9.75 \text{ m}): 40.4 \text{ MN/m} \rightarrow 22.6 \text{ MN/m}$ $k_{ax,6} (x = 5.20 \text{ m}, y = 9.75 \text{ m}): 33.5 \text{ MN/m} \rightarrow 24.8 \text{ MN/m}$ $k_{ax,7} (x = 6.20 \text{ m}, y = 9.75 \text{ m}): 15.6 \text{ MN/m} \rightarrow 33.0 \text{ MN/m}$ $k_{ax,1\text{sub}} (x = 1.70 \text{ m}, y = 10.24 \text{ m}): 49.0 \text{ MN/m} \rightarrow 1.0 \text{ MN/m}$ $k_{ax,2\text{sub}} (x = 3.70 \text{ m}, y = 10.24 \text{ m}): 66.5 \text{ MN/m} \rightarrow 14.6 \text{ MN/m}$
16	$S_b = 5 \text{ mm}$, $S_{\text{head}} = 5 \text{ mm}$	$k_{ax,1} (x = 0.40 \text{ m}, y = 0.00 \text{ m}), \dots, k_{ax,1} (x = 0.40 \text{ m}, y = 19.50 \text{ m}): 15.5 \text{ MN/m} \rightarrow 37.9 \text{ MN/m}$ $k_{ax,2} (x = 1.20 \text{ m}, y = 0.00 \text{ m}), \dots, k_{ax,2} (x = 1.20 \text{ m}, y = 19.50 \text{ m}): 26.5 \text{ MN/m} \rightarrow 5.3 \text{ MN/m}$
17	$S_b = 10 \text{ mm}$, $S_{\text{head}} = 10 \text{ mm}$	$k_{ax,1} (x = 0.40 \text{ m}, y = 9.75 \text{ m}): 15.5 \text{ MN/m} \rightarrow 19.0 \text{ MN/m}$ $k_{ax,2} (x = 1.20 \text{ m}, y = 9.75 \text{ m}): 26.5 \text{ MN/m} \rightarrow 2.7 \text{ MN/m}$ $k_{ax,3} (x = 2.20 \text{ m}, y = 9.75 \text{ m}): 52.9 \text{ MN/m} \rightarrow 9.0 \text{ MN/m}$ $k_{ax,4} (x = 3.20 \text{ m}, y = 9.75 \text{ m}): 38.4 \text{ MN/m} \rightarrow 11.5 \text{ MN/m}$ $k_{ax,5} (x = 4.20 \text{ m}, y = 9.75 \text{ m}): 40.4 \text{ MN/m} \rightarrow 11.3 \text{ MN/m}$ $k_{ax,6} (x = 5.20 \text{ m}, y = 9.75 \text{ m}): 33.5 \text{ MN/m} \rightarrow 12.4 \text{ MN/m}$ $k_{ax,7} (x = 6.20 \text{ m}, y = 9.75 \text{ m}): 15.6 \text{ MN/m} \rightarrow 16.5 \text{ MN/m}$ $k_{ax,1\text{sub}} (x = 1.70 \text{ m}, y = 10.24 \text{ m}): 49.0 \text{ MN/m} \rightarrow 0.5 \text{ MN/m}$ $k_{ax,2\text{sub}} (x = 3.70 \text{ m}, y = 10.24 \text{ m}): 66.5 \text{ MN/m} \rightarrow 7.3 \text{ MN/m}$
18	$S_b = 10 \text{ mm}$, $S_{\text{head}} = 10 \text{ mm}$	$k_{ax,1} (x = 0.40 \text{ m}, y = 0.00 \text{ m}), \dots, k_{ax,1} (x = 0.40 \text{ m}, y = 19.50 \text{ m}): 15.5 \text{ MN/m} \rightarrow 19.0 \text{ MN/m}$ $k_{ax,2} (x = 1.20 \text{ m}, y = 0.00 \text{ m}), \dots, k_{ax,2} (x = 1.20 \text{ m}, y = 19.50 \text{ m}): 26.5 \text{ MN/m} \rightarrow 2.7 \text{ MN/m}$
19	$S_b = 20 \text{ mm}$, $S_{\text{head}} = 20 \text{ mm}$	$k_{ax,1} (x = 0.40 \text{ m}, y = 9.75 \text{ m}): 15.5 \text{ MN/m} \rightarrow 9.5 \text{ MN/m}$ $k_{ax,2} (x = 1.20 \text{ m}, y = 9.75 \text{ m}): 26.5 \text{ MN/m} \rightarrow 1.3 \text{ MN/m}$ $k_{ax,3} (x = 2.20 \text{ m}, y = 9.75 \text{ m}): 52.9 \text{ MN/m} \rightarrow 4.5 \text{ MN/m}$ $k_{ax,4} (x = 3.20 \text{ m}, y = 9.75 \text{ m}): 38.4 \text{ MN/m} \rightarrow 5.8 \text{ MN/m}$

		$k_{ax,5}$ (x = 4.20 m, y = 9.75 m): 40.4 MN/m --> 5.7 MN/m
		$k_{ax,6}$ (x = 5.20 m, y = 9.75 m): 33.5 MN/m --> 6.2 MN/m
		$k_{ax,7}$ (x = 6.20 m, y = 9.75 m): 15.6 MN/m --> 8.2 MN/m
		$k_{ax,1sub}$ (x = 1.70 m, y = 9.75 m): 49.0 MN/m --> 0.2 MN/m
		$k_{ax,2sub}$ (x = 3.70 m, y = 9.75 m): 66.5 MN/m --> 3.7 MN/m
20	S _b = 20 mm, S _{head} = 20 mm	$k_{ax,1}$ (x = 0.40 m, y = 0.00 m),..., $k_{ax,1}$ (x = 0.40 m, y = 19.50 m): 15.5 MN/m --> 9.5 MN/m
		$k_{ax,2}$ (x = 1.20 m, y = 0.00 m),..., $k_{ax,2}$ (x = 1.20 m, y = 19.50 m): 26.5 MN/m --> 1.3 MN/m

calculation results for pile cap beam (y = 9.75 m)										
mod.	u _{x,mod} [mm]		u _{z,mod} [mm]		N _{mod} [kN]		V _{z,mod} [kN]		M _{y,mod} [kNm]	
	min.	max.	min.	max.	min.	max.	min.	max.	min.	max.
1	-13.3	3.7	-303.1	4.3	-10.6	43.3	-55.1	154.6	-28.4	59.4
2	-13.2	3.8	-303.1	4.7	-10.0	42.5	-55.1	147.2	-28.4	56.7
3	-13.7	3.1	-291.5	4.3	-10.6	42.9	-55.2	154.7	-28.4	59.4
4	-13.8	4.5	-322.4	4.2	-10.0	44.6	-54.9	152.1	-28.4	59.1
5	-13.3	4.6	-322.5	4.8	-8.8	42.5	-55.0	134.6	-28.4	52.6
6	-14.7	3.1	-298.1	4.1	-10.1	43.8	-55.1	152.4	-28.4	59.2
7	-15.2	6.5	-374.3	3.8	-9.2	46.7	-54.5	148.2	-28.7	58.6
8	-13.4	6.8	-374.6	4.7	-6.6	41.5	-54.7	110.0	-28.4	44.0
9	-17.1	3.4	-320.8	4.9	-9.4	45.2	-54.6	148.7	-28.5	58.7
10	-13.1	3.2	-291.6	4.5	-11.3	41.7	-55.2	157.7	-28.4	59.6
11	-13.1	3.3	-291.7	4.5	-11.3	41.6	-55.2	157.5	-28.4	59.6
12	-13.3	3.8	-292.2	4.4	-11.3	41.5	-55.2	156.9	-28.4	59.4
13	-14.0	3.1	-487.0	9.4	0.0	42.3	-55.2	73.9	-28.4	5.5
14	-11.9	45.4	-4.4×10 ⁴	4.2	-11.1	234.2	-418.3	350.2	-494.4	59.6
15	-13.0	3.0	-283.5	5.0	-12.2	41.5	-56.3	165.4	-28.4	61.9
16	-13.0	3.2	-291.6	7.0	-11.6	41.2	-55.2	158.9	-28.4	59.8
17	-13.1	3.0	-288.8	5.2	-11.6	41.9	-56.3	160.0	-28.4	60.3
18	-13.2	3.2	-291.6	6.5	-11.4	41.6	-55.2	157.6	-28.4	59.6
19	-13.1	3.1	-299.5	5.2	-10.5	42.7	-56.5	150.0	-28.4	57.4
20	-13.8	3.1	-291.5	9.2	-10.7	42.6	-55.2	153.7	-28.4	59.1

calculation results for pile in first pile row (x = 0.40 m, y = 9.75 m)						
mod.	N _{mod} [kN]		V _{z,mod} [kN]		M _{y,mod} [kNm]	
	min.	max.	min.	max.	min.	max.
1	-187,9	-186,0	-10,6	2,6	-3,4	14,9
2	-180,5	-178,7	-10,0	2,5	-3,4	14,1
3	-188,0	-186,2	-10,6	2,6	-3,5	15,0
4	-185,1	-183,6	-10,0	2,2	-3,4	14,0
5	-167,7	-166,1	-8,8	2,0	-3,2	12,2
6	-185,4	-183,8	-10,1	2,2	-3,5	14,1
7	-180,9	-179,7	-9,2	2,3	-3,3	12,7
8	-142,7	-141,5	-6,6	1,9	-2,7	8,9
9	-181,4	-180,2	-9,4	2,5	-3,6	12,8
10	-191,4	-189,2	-11,3	3,0	-3,6	16,2
11	-191,2	-189,0	-11,3	3,0	-3,6	16,1
12	-190,6	-188,4	-11,3	3,0	-3,6	16,0
13	-	-	-	-	-	-
14	-191,3	-189,1	-11,1	2,8	-3,2	16,1
15	-199,1	-196,9	-12,2	3,1	-3,5	17,6
16	-192,6	-190,4	-11,6	3,0	-3,5	16,6
17	-193,7	-191,5	-11,6	3,0	-3,6	16,6

18	-191,3	-189,1	-11,4	3,0	-3,6	16,2
19	-183,8	-181,5	-10,5	2,9	-3,6	14,7
20	-187,4	-185,2	-10,7	2,9	-3,8	14,8

C.2 HARINGVLIET, ROTTERDAM

C.2.1 COLLECTION OF DATA

terrain loads	
parameter	value
$F_{LM1,rep,i}$ [kN]	150
$Q_{LM1,rep,i}$ [kN/m ²]	9.0
$Q_{LM1,rep}$ [kN/m ²]	2.5
α_Q [-]	0.7
W_{LM1} [m]	3.5
$a_{LM1,x}$ [m]	5.0
$S_{LM1,x}$ [m]	2.0
$S_{LM1,y}$ [m]	1.2

trees			
no.	$x_{tree,i}$ [m]	$y_{tree,i}$ [m]	$F_{tree,i}$ [kN]
1	0.50	17.72	25.0

surface water	
parameter	value
z_{MHW} [m NAP]	+1.30
γ_w [kN/m ³]	10.0

retaining wall	
parameter	value
γ_{wall} [kN/m ³]	16.0
$z_{wall,top}$ [m NAP]	+2.90
$z_{wall,btm}$ [m NAP]	-1.03
$x_{wall,top}$ [m]	0.44
E_{wall} [N/mm ²]	1.40×10^4

retaining wall coordinates		
no.	X _{wall,i} [m]	Z _{wall,i} [m NAP]
1	0.16	-1.03
2	1.63	-1.03
3	1.71	0.00
4	1.61	0.00
5	1.64	+0.50
6	1.54	+0.50
7	1.57	+1.00
8	1.47	+1.00
9	1.50	+1.50
10	1.40	+1.50
11	1.47	+2.40
12	1.16	+2.70
13	0.99	+2.70
14	0.99	+2.90
15	0.44	+2.90
16	0.44	+2.70

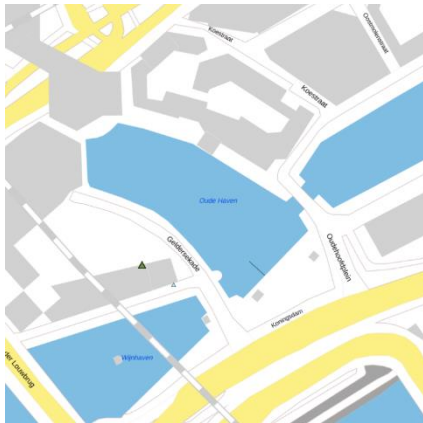
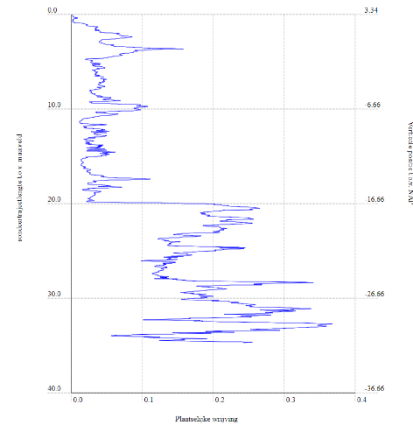
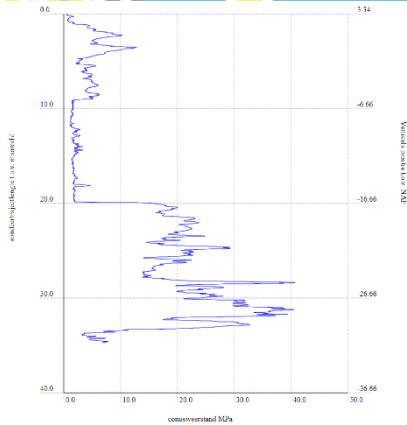
pile row									
no.	X _{pile,i} [m]	Z _{head,i} [m NAP]	Z _{tip,i} [m NAP]	d _{head,i} [mm]	d _{tip,i} [mm]	α _{pile,i} [°]	A _{gr,i} [m ²]	E _{pile} [N/mm ²]	Z _{low,i} [m NAP]
1	0.18	-1.27	-18.00	250	95.3	0	0.28	3.6×10 ³	-3.00
2	0.82	-1.27	-18.00	250	95.3	0	0.28	3.6×10 ³	-3.00
3	1.48	-1.27	-18.00	250	95.3	0	0.28	3.6×10 ³	-1.27

pile cap beam	
parameter	value
γ _{pcb} [kN/m ³]	4.20
W _{pcb} [mm]	270
H _{pcb} [mm]	180
L _{pcb} [mm]	1780
S _{pcb} [m]	0.85
E _{pcb} [N/mm ²]	0.12×10 ³

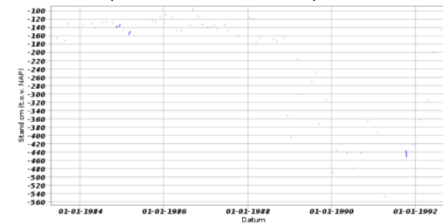
floor element	
parameter	value
γ _{floor} [kN/m ³]	4.20
W _{floor} [mm]	250
H _{floor} [mm]	60
L _{floor} [mm]	850
E _{floor} [N/mm ²]	0.12×10 ³



id: CPT000000149445
 date: 14-01-2017
 coord: 93502.270, 437098.230 (RD)
 ground level: +3.34 m NAP
 total depth: 34.68 m
 source: (DINOloket, 2017)



id: B37H0520
 date: 18-04-1983 / 14-12-1992
 coord: 93380, 437090 (RD)
 ground level: +2.48 m NAP
 source: (DINOloket, 1992)

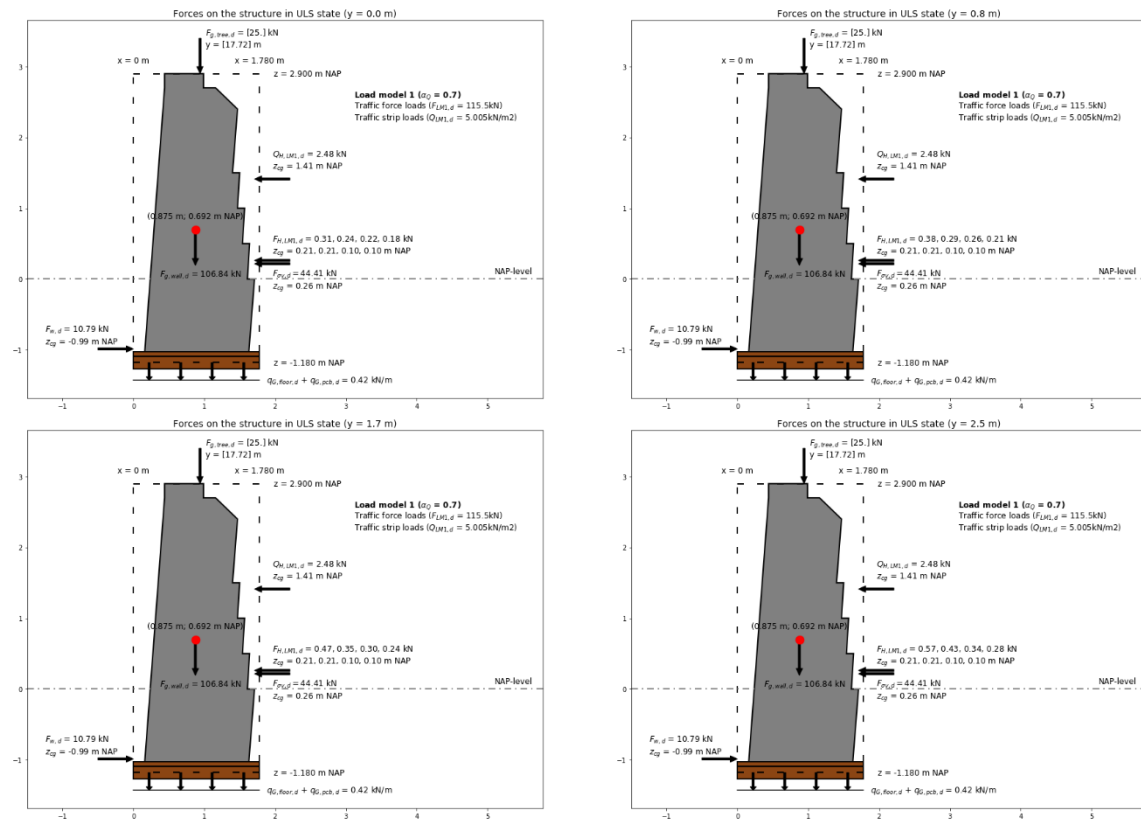


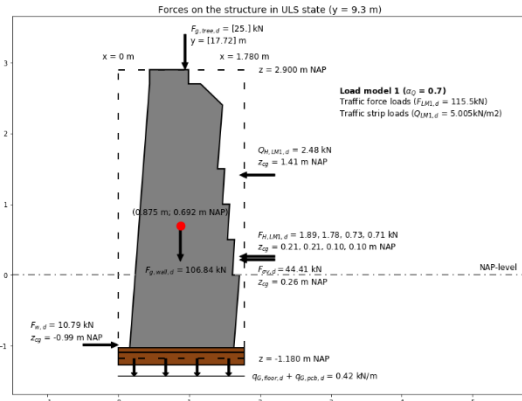
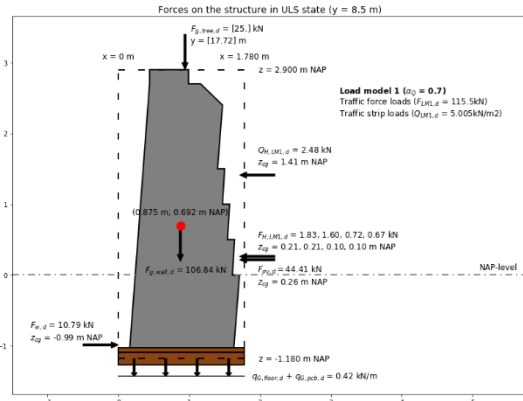
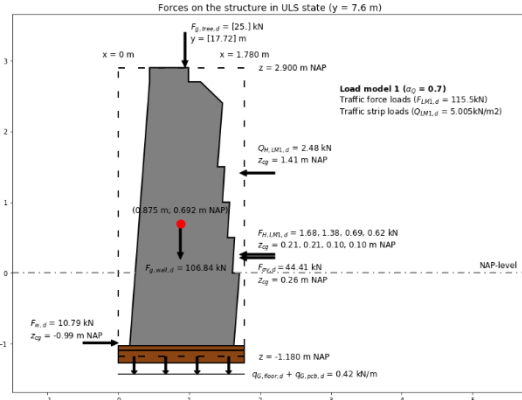
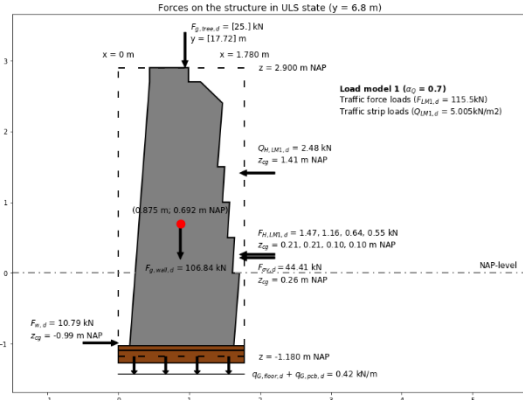
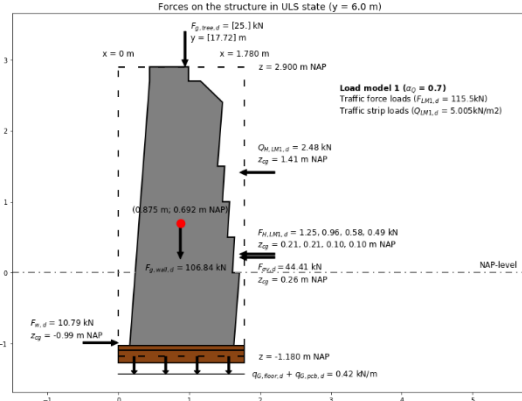
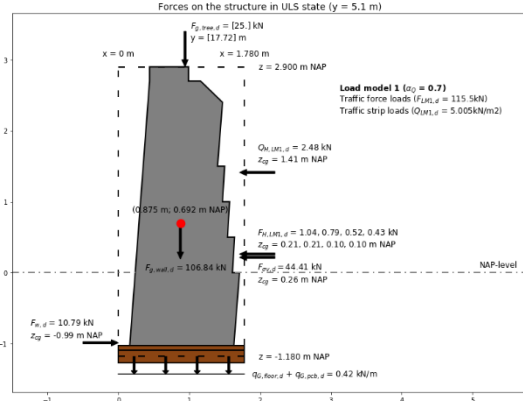
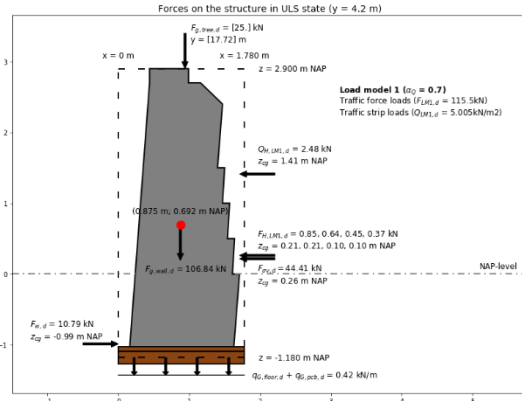
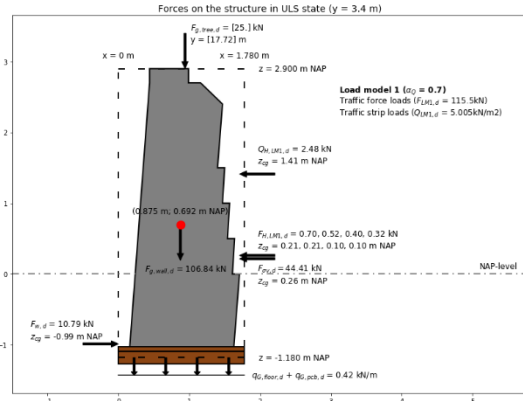
general soil information	
parameter	value
$n_{\text{probe}} [-]$	1
$\xi_3 [-]$	1.26
$\xi_4 [-]$	1.26
$z_{\text{gw}} [\text{m NAP}]$	-1.40
$\gamma_{\text{gw}} [\text{kN/m}^3]$	10.0

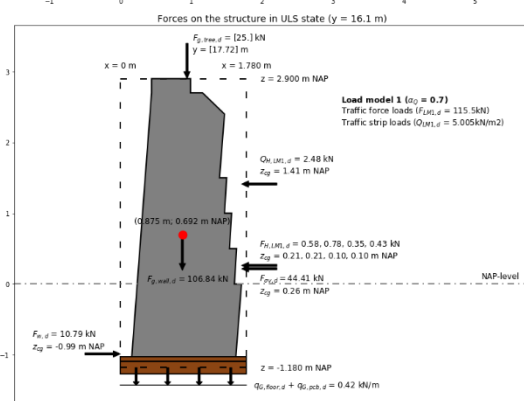
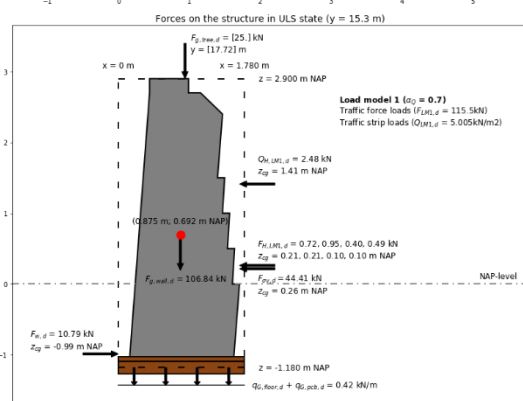
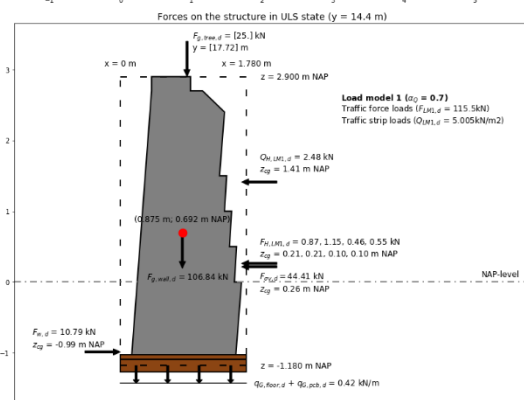
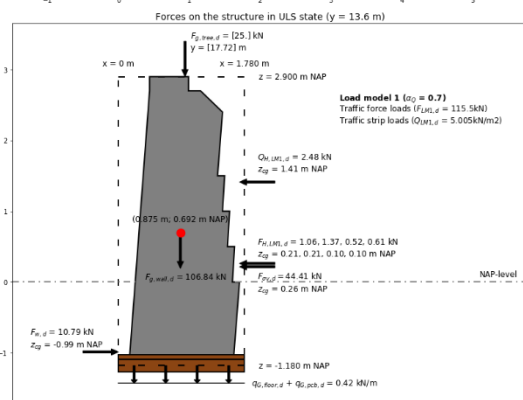
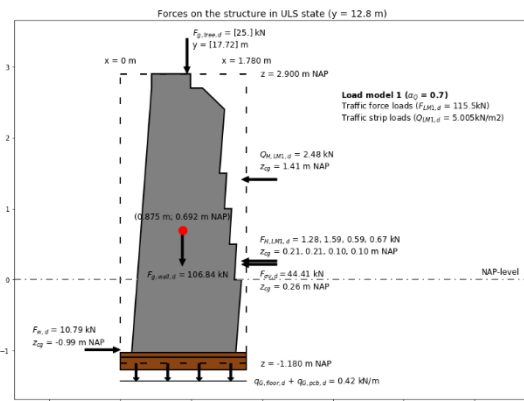
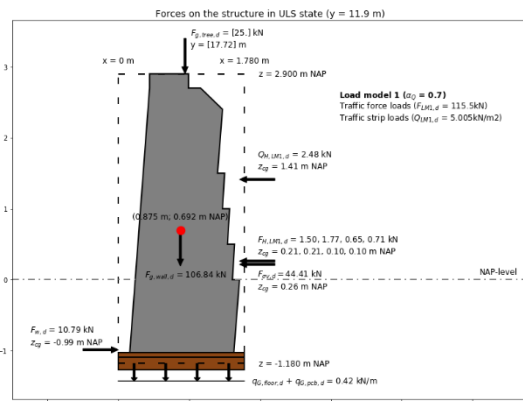
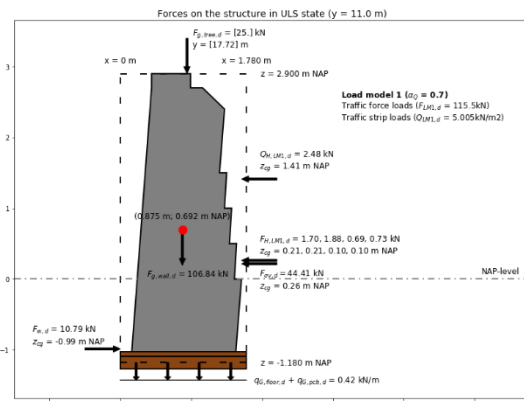
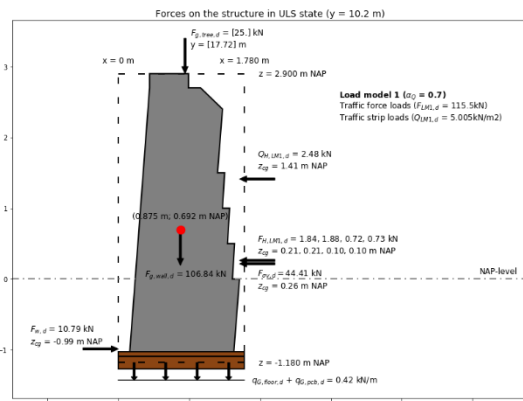
soil type classification					
NAP-level		qcPT,avg [MPa]	fcPT,avg [MPa]	RCPT,avg [%]	soil type
from	to				
+2.90	-6.10	5.3	0.048	0.91	loam, strong sandy
-6.10	-8.60	1.4	0.040	2.88	peat, loose
-8.60	-16.60	1.8	0.041	2.24	clay, clean, dense
-16.60	-18.10	17.1	0.227	1.32	sand, slight silty/ clayey
-18.10	-30.10	23.7	0.200	0.84	sand, clean, dense
-30.10	-31.10	6.0	0.116	1.93	clay, slight sandy, dense

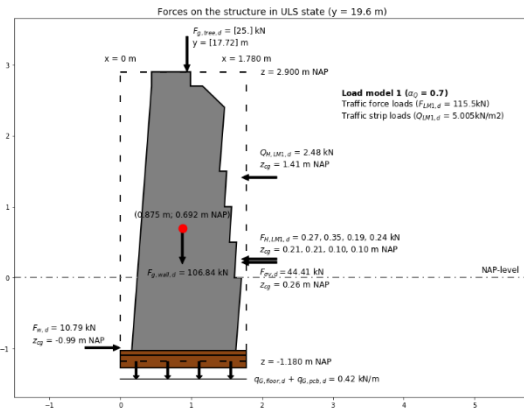
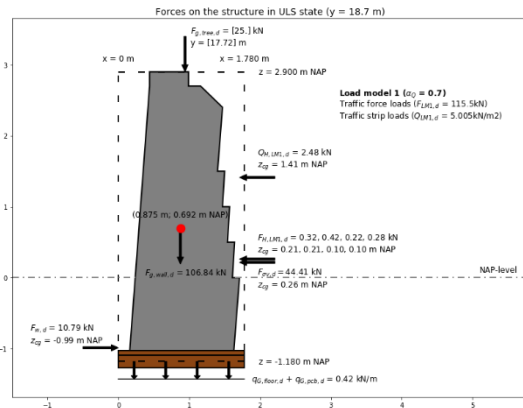
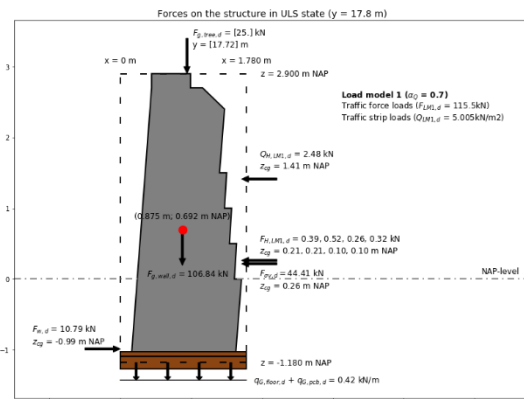
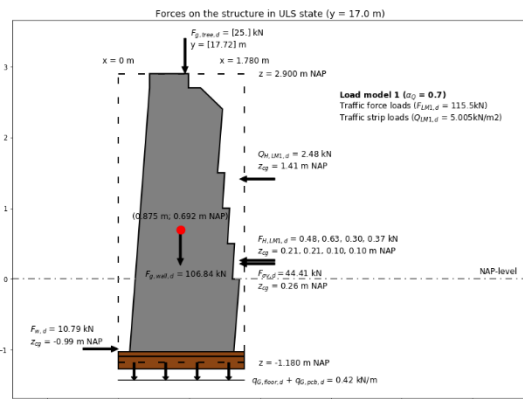
soil parameters							
NAP-level		γ_{dry} [kN/m ³]	γ_{sat} [kN/m ³]	φ' [°]	c' [kPa]	C_α [-]	E_{soil} [-]
from	to						
+2.90	-6.10	20.0	20.0	35.0	1.0	0.0020	4.0
-6.10	-8.60	12.0	12.0	15.0	1.0	0.0230	0.5
-8.60	-16.60	20.0	20.0	25.0	13.0	0.0037	7.0
-16.60	-18.10	19.0	21.0	32.5	0	0	40.0
-18.10	-30.10	20.0	22.0	40.0	0	0	95.0
-30.10	-31.10	21.0	21.0	27.5	13.0	0.0031	7.0

C.2.2 SUPERSTRUCTURE LOADS



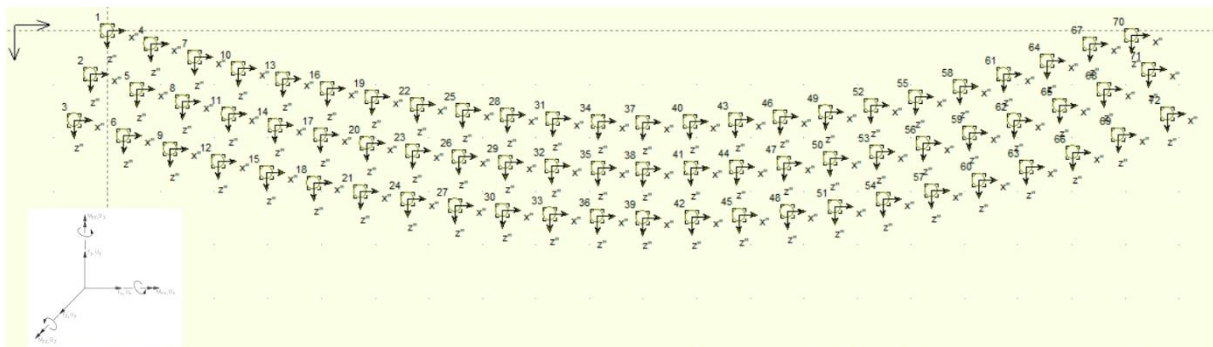


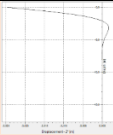
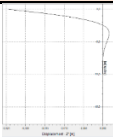





C.2.3 LATERAL SOIL RESISTANCE

input D-pile group	
parameter	value
v [-]	0.499
$z_{soil,top,avg}$ [m]	1.15
$E_{soil,top}$ [kN/m ²]	4.0×10^3
$E_{soil,btm}$ [kN/m ²]	70.0×10^3
x_{cap} [m]	10.00
y_{cap} [m]	0
z_{cap} [m]	2.58
fixity	free
F_y [kN]	-2.56×10^3
F_z [kN]	-1.07×10^3
M_x [kNm]	-1.57×10^3



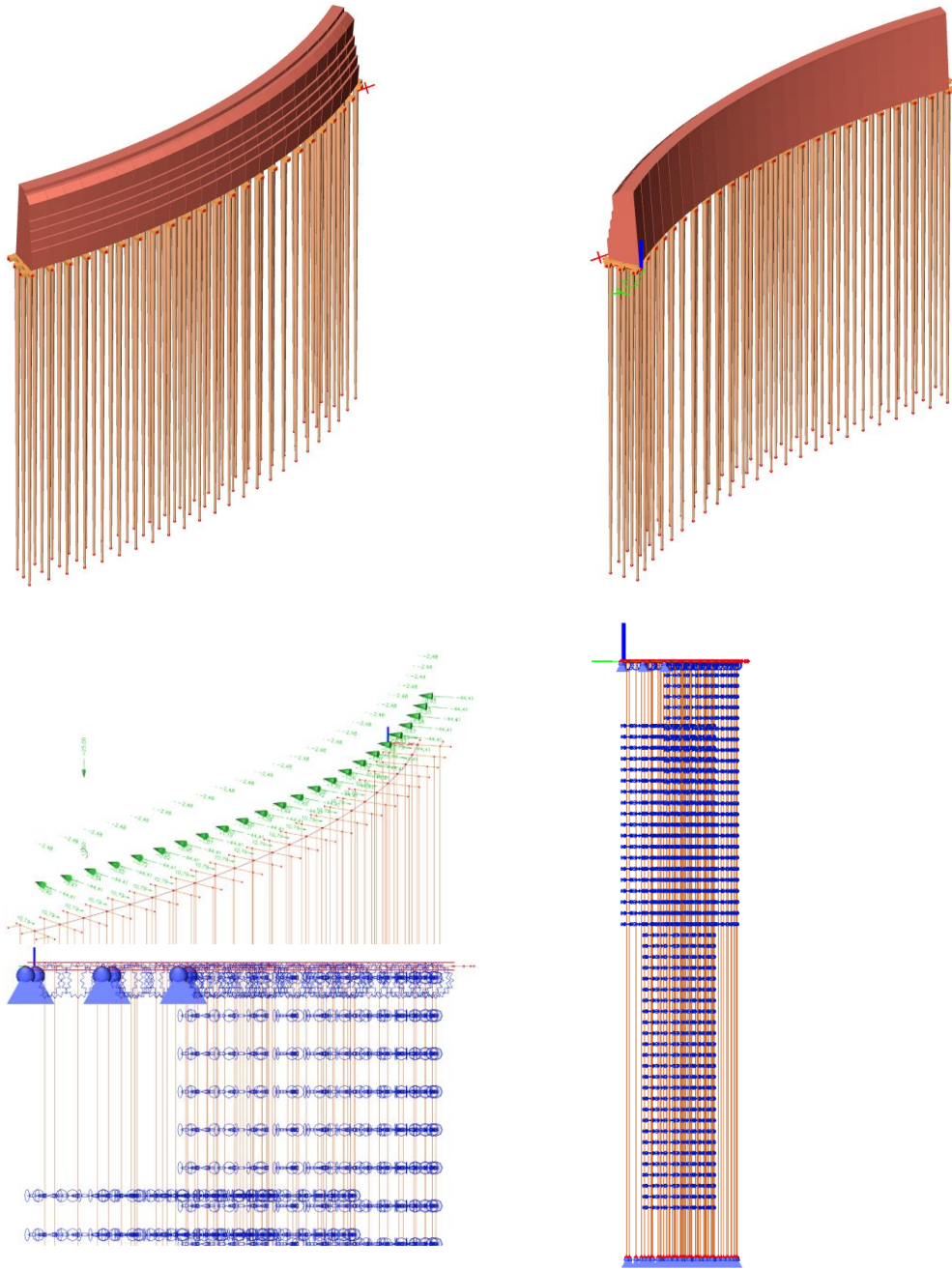
horizontal pile displacement						
pile no.	Z _{soil} [m NAP]		Z _{mid} [m NAP]	Z _{mid} [m]	V _{pile} [m]	figures
	from	to				
37	-3.00	-6.10	-4.65	-3.47	1.60×10^{-3}	
	-6.10	-8.60	-7.35	-6.17	4.00×10^{-5}	
	-8.60	-16.60	-12.60	-11.42	0	
	-16.60	-18.00	-17.30	-16.12	0	
38	-3.00	-6.10	-4.65	-3.47	1.57×10^{-3}	
	-6.10	-8.60	-7.35	-6.17	3.80×10^{-4}	
	-8.60	-16.60	-12.60	-11.42	-1.00×10^{-5}	
	-16.60	-18.00	-17.30	-16.12	0	
39	-1.27	-6.10	-3.69	-2.51	8.50×10^{-4}	
	-6.10	-8.60	-7.35	-6.17	4.00×10^{-5}	
	-8.60	-16.60	-12.60	-11.42	0	
	-16.60	-18.00	-17.30	-16.12	0	

horizontal soil response							
pile no.	Z _{soil} [m NAP]		soil type	α [-]	β [-]	k _s [MN/m ³]	p _{soil} [MN/m ²]
	from	to					
1	-3.00	-6.10	loam	1/2	1.0	3.16×10^4	50.49
	-6.10	-8.60	peat	1	3.0	2.02×10^4	0.81
	-8.60	-16.60	clay	2/3	2.0	1.99×10^4	0
	-16.60	-18.00	sand	1/3	0.7	7.72×10^4	0
2	-3.00	-6.10	loam	1/2	1.0	3.16×10^4	49.54
	-6.10	-8.60	peat	1	3.0	2.02×10^4	7.69
	-8.60	-16.60	clay	2/3	2.0	1.99×10^4	0.20
	-16.60	-18.00	sand	1/3	0.7	7.72×10^4	0
3	-1.27	-6.10	loam	1/2	1.0	3.16×10^4	26.82
	-6.10	-8.60	peat	1	3.0	2.02×10^4	0.81
	-8.60	-16.60	clay	2/3	2.0	1.99×10^4	0
	-16.60	-18.00	sand	1/3	0.7	7.72×10^4	0

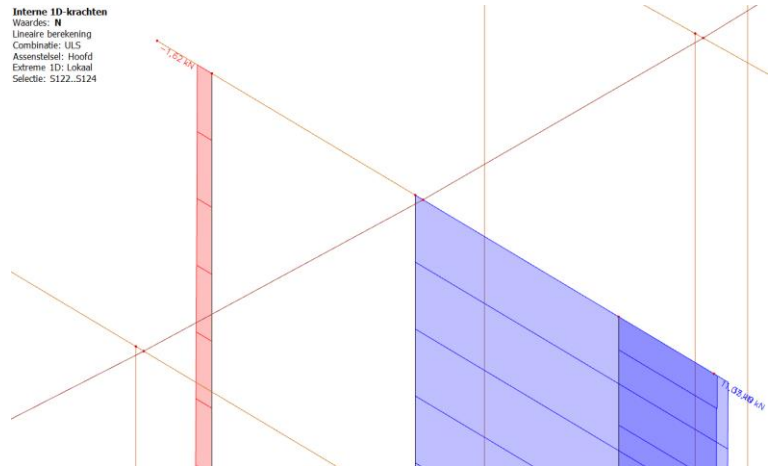
C.2.4 JOINT STIFFNESS

calculation joint stiffness	
parameter	value
H _{mor} [mm]	90
W _{notch} [mm]	25
a ₁ [mm]	113
a ₂ [mm]	30
a ₃ [mm]	30
k _{0,1} [N/mm]	2.84×10^5
k _{90,1} [N/mm]	9.47×10^3
k _{0,2} [N/mm]	6.35×10^5
k _{90,2} [N/mm]	2.12×10^4
k _{0,3} [N/mm]	6.35×10^5
k _{90,3} [N/mm]	2.12×10^4
k _{eq,1} [N/mm]	9.16×10^3
k _{eq,2} [N/mm]	2.05×10^4
k _{eq,3} [N/mm]	2.05×10^4
k _r [MNm/rad]	0.15

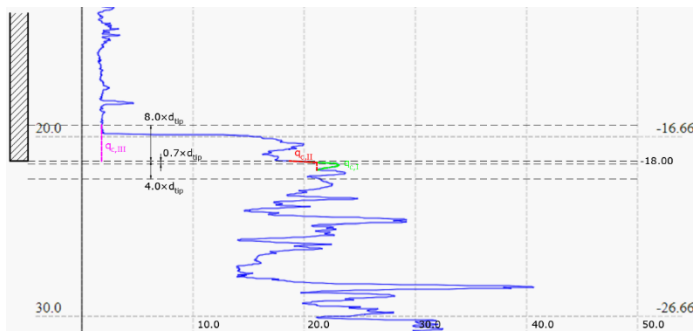
C.2.5 AXIAL PILE HEAD FORCES



axial pile head forces (y = 10.20 m)	
pile row	F _{head,d} [kN]
1	-1.62
2	11.07
3	35.10



C.2.6 AXIAL PILE FORCES AND RESISTANCES



cone resistances	
parameter	value
q _{CPT,I} [MPa]	15.0
q _{CPT,II} [MPa]	15.0
q _{CPT,III} [MPa]	2.0

maximum pile tip resistance				
pile row	A _{tip} [mm ²]	q _{b,max} [MPa]	R _{b,max,k} [kN]	R _{b,max,d} [kN]
1	7.14×10 ³	5.95	42.47	25.46

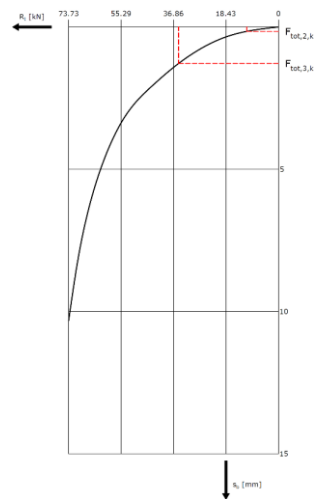
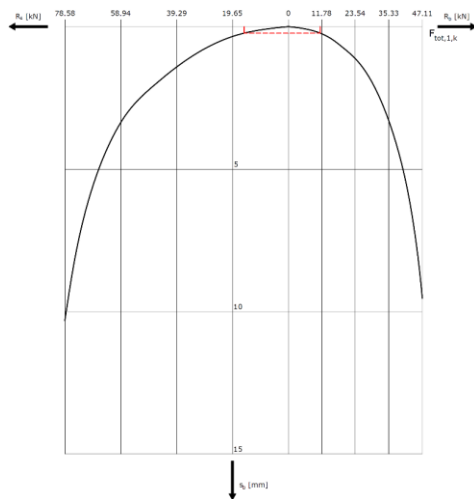
maximum pile shaft resistance (z _{tp} = -18.10 m NAP)							
pile row	ΔL [m]	Z _{ΔL,avg} [m]	d _{ΔL,avg} [m]	C _{ΔL,avg} [m]	q _{s,max} [MPa]	R _{s,max,k} [kN]	R _{s,max,d} [kN]
1	1.40	16.03	99.3	311.8	0.18	78.58	47.11

negative skin friction (z _{tp} = −18.10 m NAP)											
pile row	Z _{mid} [m NAP]	t _i [m]	γ' _i [kN/m³]	Z _{pile,mid} [m]	C _{pile,mid} [m]	m _i [−]	σ' _{m,i} [kN/m²]	σ _{nsf,i} [kN/m²]	F _{nsf,i} [kN]	F _{nsf,k} [kN]	F _{nsf,d} [kN]
1	−4.55	3.1	10.0	3.28	0.650	0.58	14.38	16.62	4.65	25.12	30.14
	−7.35	2.5	2.0	6.08	0.553	0.49	7.05	12.33	3.45		
	−12.60	8.0	10.0	11.33	0.409	0.37	26.30	60.75	17.01		

tensile resistance										
pile row	z_{mid} [m NAP]	t_i [m]	$z_{pile,mid}$ [m]	$C_{pile,mid}$ [m]	$\alpha_{t,i}$ [-]	$q_{CPT,d,i}$ [MPa]	$q_{t,d,i}$ [MPa]	$R_{t,d,i}$ [kN]	$R_{t,d}$ [kN]	$R_{t,k}$ [kN]
2	-4.55	3.10	3.28	0.650	0.0035	1.88	0.007	13.28	39.29	73.73
	-7.35	2.50	6.08	0.553	0.0035	0.50	0.002	2.41		
	-12.60	8.00	11.33	0.409	0.0035	0.64	0.002	7.32		
	-17.30	1.40	16.03	0.312	0.0070	5.33	0.037	16.28		
3	-3.69	4.83	2.42	0.683	0.0035	1.88	0.007	21.75	47.76	89.62
	-7.35	2.50	6.08	0.553	0.0035	0.50	0.002	2.41		
	-12.60	8.00	11.33	0.409	0.0035	0.64	0.002	7.32		
	-17.30	1.40	16.03	0.312	0.0070	5.33	0.037	16.28		

C.2.7 PILE TIP SETTLEMENT AND FORCE

total pile head force	
pile row	F_{head} [kN]
1	-26.74
2	11.07
3	35.10



pile settlement and rise					
pile row	$R_{b,k}$ [kN]	$R_{s,k}$ [kN]	s_b [mm]	$R_{t,k}$ [kN]	s_{head} [mm]
1	11.2	15.5	0.2	—	—
2	—	—	—	11.1	0.2
3	—	—	—	35.1	1.3

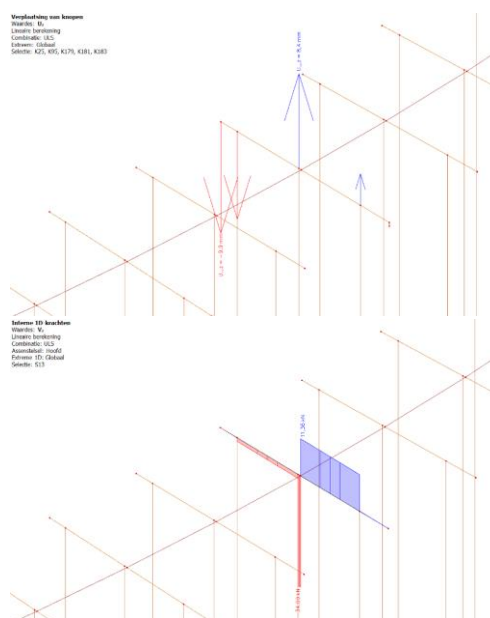
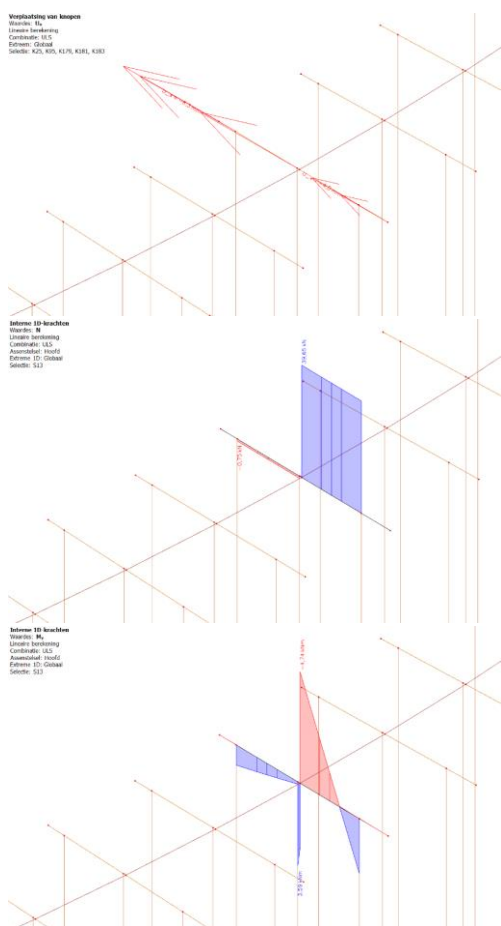
axial pile tip stiffness	
pile row	k_{ax} [MN/m]
1	133.5
2	55.5
3	27.0

C.2.8 NEUTRAL PLANE

total soil settlement				
pile row	Z _{top} [m NAP]	t _i [m]	S _{soil,tot,i} [m]	S _{soil,tot} [m]
1	-3.00	3.1	0.118	0.373
	-6.10	2.5	0.229	
	-8.60	8.0	0.119	

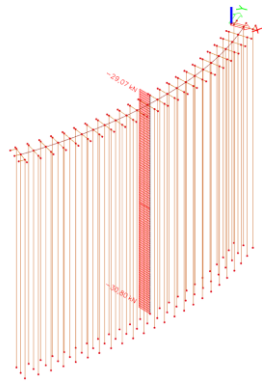
influence neutral plane					
pile row	value	R _{s,max,k} [kN]	R _{s,max,d} [kN]	F _{nsf,k} [kN]	F _{nsf,d} [kN]
1	maximum	78.58	47.11	25.12	30.14

C.2.9 CALCULATION MODEL

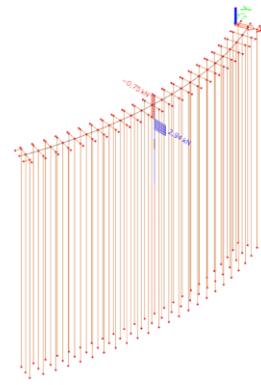


extreme values in pile cap beam (y = 10.20 m)				
parameter	minimum		maximum	
	value	pile row	value	pile row
u _{x,int} [mm]	-8.3	2	-4.0	3
u _{z,int} [mm]	-9.9	1	8.4	2
N _{int} [kN]	-0.8	1-2	39.7	2-3
V _{z,int} [kN]	-34.1	2	11.4	2-3
M _{y,int} [kNm]	-4.7	2	3.6	2

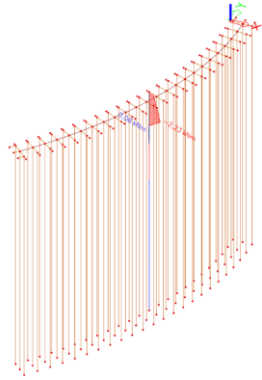
Interne 1D-brachten
 Waarden: M_x
 Lineaire berekening
 Combinatie: ULS
 Assumtel: Hoofd
 Extreme 1D: Global
 Selectie: S122



Interne 1D-brachten
 Waarden: V_z
 Lineaire berekening
 Combinatie: ULS
 Assumtel: Hoofd
 Extreme 1D: Global
 Selectie: S122



Interne 1D-brachten
 Waarden: M_y
 Lineaire berekening
 Combinatie: ULS
 Assumtel: Hoofd
 Extreme 1D: Global
 Selectie: S122



extreme values in pile at first row ($x = 0.18$ m, $y = 10.20$ m)

parameter	minimum value	maximum value
N_{int} [kN]	-30.8	-29.1
$V_{z,int}$ [kN]	-0.8	2.9
$M_{y,int}$ [kNm]	-2.2	0.1

C.2.10 STRUCTURAL DEFICIENCIES

changes in structural model		
modification	changing variable	adaptations
1	$p_m = 5$ mm	$d_{head,1...3}$ ($y = 0.00$ m), ..., $d_{head,1...3}$ ($y = 19.55$ m): 250 mm \rightarrow 230 mm
		$d_{tip,1...3}$ ($y = 0.00$ m), ..., $d_{tip,1...3}$ ($y = 19.55$ m): 95.3 mm \rightarrow 80.3 mm
2	$p_m = 5$ mm	$d_{head,1...3}$ ($y = 10.20$ m): 250 mm \rightarrow 230 mm
		$d_{tip,1...3}$ ($y = 10.20$ m): 95.3 mm \rightarrow 80.3 mm
3	$p_m = 5$ mm	$d_{head,1,2}$ ($y = 0.00$ m), ..., $d_{head,1,2}$ ($y = 19.55$ m): 250 mm \rightarrow 230 mm
		$d_{tip,1,2}$ ($y = 0.00$ m), ..., $d_{tip,1,2}$ ($y = 19.55$ m): 95.3 mm \rightarrow 80.3 mm
4	$p_m = 15$ mm	$d_{head,1...3}$ ($y = 0.00$ m), ..., $d_{head,1...3}$ ($y = 19.55$ m): 250 mm \rightarrow 210 mm
		$d_{tip,1...3}$ ($y = 0.00$ m), ..., $d_{tip,1...3}$ ($y = 19.55$ m): 95.3 mm \rightarrow 70.3 mm
		W_{pcb} ($y = 0.00$ m), ..., W_{pcb} ($y = 19.55$ m): 270 mm \rightarrow 260 mm
5	$p_m = 15$ mm	$d_{head,1...3}$ ($y = 10.20$ m): 250 mm \rightarrow 210 mm
		$d_{tip,1...3}$ ($y = 10.20$ m): 95.3 mm \rightarrow 70.3 mm
		W_{pcb} ($y = 10.20$ m): 270 mm \rightarrow 260 mm
6	$p_m = 15$ mm	$d_{head,1,2}$ ($y = 0.00$ m), ..., $d_{head,1,2}$ ($y = 19.55$ m): 250 mm \rightarrow 210 mm
		$d_{tip,1,2}$ ($y = 0.00$ m), ..., $d_{tip,1,2}$ ($y = 19.55$ m): 95.3 mm \rightarrow 70.3 mm
		W_{pcb} ($y = 0.00$ m), ..., W_{pcb} ($y = 19.55$ m): 270 mm \rightarrow 260 mm
7	$p_m = 30$ mm	$d_{head,1...3}$ ($y = 0.00$ m), ..., $d_{head,1...3}$ ($y = 19.55$ m): 250 mm \rightarrow 180 mm
		$d_{tip,1...3}$ ($y = 0.00$ m), ..., $d_{tip,1...3}$ ($y = 19.55$ m): 95.3 mm \rightarrow 55.3 mm
		W_{pcb} ($y = 0.00$ m), ..., W_{pcb} ($y = 19.55$ m): 270 mm \rightarrow 230 mm
8	$p_m = 30$ mm	$d_{head,1...3}$ ($y = 10.20$ m): 250 mm \rightarrow 180 mm
		$d_{tip,1...3}$ ($y = 10.20$ m): 95.3 mm \rightarrow 55.3 mm
		W_{pcb} ($y = 10.20$ m): 270 mm \rightarrow 230 mm
9	$p_m = 30$ mm	$d_{head,1,2}$ ($y = 0.00$ m), ..., $d_{head,1,2}$ ($y = 19.55$ m): 250 mm \rightarrow 180 mm
		$d_{tip,1,2}$ ($y = 0.00$ m), ..., $d_{tip,1,2}$ ($y = 19.55$ m): 95.3 mm \rightarrow 55.3 mm

		$W_{pcb} (y = 0.00 \text{ m}), \dots, W_{pcb} (y = 19.55 \text{ m}): 270 \text{ mm} \rightarrow 230 \text{ mm}$
10	$e_y = 25 \text{ mm}$	$e_{y,pcb} (y = 10.20 \text{ m}): 0 \rightarrow 25 \text{ mm}$
11	$e_y = 50 \text{ mm}$	$e_{y,pcb} (y = 10.20 \text{ m}): 0 \rightarrow 50 \text{ mm}$
12	$e_y = 100 \text{ mm}$	$e_{y,pcb} (y = 10.20 \text{ m}): 0 \rightarrow 100 \text{ mm}$
13	$R_{c,max} = 0 \text{ kN},$ $R_{t,max} = 0 \text{ kN}$	$R_{c,pile,1,d} (x = 0.18 \text{ m}, y = 10.20 \text{ m}): 104.04 \text{ kN} \rightarrow 0 \text{ kN}$ $R_{t,pile,2,d} (x = 0.83 \text{ m}, y = 10.20 \text{ m}): 39.29 \text{ kN} \rightarrow 0 \text{ kN}$
14	$R_{c,max} = 0 \text{ kN},$ $R_{t,max} = 0 \text{ kN}$	$R_{c,pile,2,d} (x = 0.83 \text{ m}, y = 10.20 \text{ m}): 39.29 \text{ kN} \rightarrow 0 \text{ kN}$ $R_{c,pile,3,d} (x = 1.48 \text{ m}, y = 10.20 \text{ m}): 47.76 \text{ kN} \rightarrow 0 \text{ kN}$
15	$S_b = 5 \text{ mm},$ $S_{head} = 5 \text{ mm}$	$k_{ax,1} (x = 0.18 \text{ m}, y = 10.20 \text{ m}): 133.5 \text{ MN/m} \rightarrow 5.3 \text{ MN/m}$ $k_{ax,2} (x = 0.83 \text{ m}, y = 10.20 \text{ m}): 55.5 \text{ MN/m} \rightarrow 2.2 \text{ MN/m}$ $k_{ax,3} (x = 1.48 \text{ m}, y = 10.20 \text{ m}): 27.0 \text{ MN/m} \rightarrow 7.0 \text{ MN/m}$
16	$S_b = 5 \text{ mm},$ $S_{head} = 5 \text{ mm}$	$k_{ax,1} (x = 0.18 \text{ m}, y = 0.00 \text{ m}), \dots, k_{ax,1} (x = 0.18 \text{ m}, y = 19.55 \text{ m}): 133.5 \text{ MN/m} \rightarrow 5.3 \text{ MN/m}$ $k_{ax,2} (x = 0.83 \text{ m}, y = 0.00 \text{ m}), \dots, k_{ax,2} (x = 0.83 \text{ m}, y = 19.55 \text{ m}): 55.5 \text{ MN/m} \rightarrow 2.2 \text{ MN/m}$
17	$S_b = 10 \text{ mm},$ $S_{head} = 10 \text{ mm}$	$k_{ax,1} (x = 0.18 \text{ m}, y = 10.20 \text{ m}): 133.5 \text{ MN/m} \rightarrow 2.7 \text{ MN/m}$ $k_{ax,2} (x = 0.83 \text{ m}, y = 10.20 \text{ m}): 55.5 \text{ MN/m} \rightarrow 1.1 \text{ MN/m}$ $k_{ax,3} (x = 1.48 \text{ m}, y = 10.20 \text{ m}): 27.0 \text{ MN/m} \rightarrow 3.5 \text{ MN/m}$
18	$S_b = 10 \text{ mm},$ $S_{head} = 10 \text{ mm}$	$k_{ax,1} (x = 0.18 \text{ m}, y = 0.00 \text{ m}), \dots, k_{ax,1} (x = 0.18 \text{ m}, y = 19.55 \text{ m}): 133.5 \text{ MN/m} \rightarrow 2.7 \text{ MN/m}$ $k_{ax,2} (x = 0.83 \text{ m}, y = 0.00 \text{ m}), \dots, k_{ax,2} (x = 0.83 \text{ m}, y = 19.55 \text{ m}): 55.5 \text{ MN/m} \rightarrow 1.1 \text{ MN/m}$
19	$S_b = 20 \text{ mm},$ $S_{head} = 20 \text{ mm}$	$k_{ax,1} (x = 0.18 \text{ m}, y = 10.20 \text{ m}): 133.5 \text{ MN/m} \rightarrow 1.3 \text{ MN/m}$ $k_{ax,2} (x = 0.83 \text{ m}, y = 10.20 \text{ m}): 55.5 \text{ MN/m} \rightarrow 0.6 \text{ MN/m}$ $k_{ax,3} (x = 1.48 \text{ m}, y = 10.20 \text{ m}): 27.0 \text{ MN/m} \rightarrow 1.8 \text{ MN/m}$
20	$S_b = 20 \text{ mm},$ $S_{head} = 20 \text{ mm}$	$k_{ax,1} (x = 0.18 \text{ m}, y = 0.00 \text{ m}), \dots, k_{ax,1} (x = 0.18 \text{ m}, y = 19.55 \text{ m}): 133.5 \text{ MN/m} \rightarrow 1.3 \text{ MN/m}$ $k_{ax,2} (x = 0.83 \text{ m}, y = 0.00 \text{ m}), \dots, k_{ax,2} (x = 0.83 \text{ m}, y = 19.55 \text{ m}): 55.5 \text{ MN/m} \rightarrow 0.6 \text{ MN/m}$

calculation results for pile cap beam (y = 10.20 m)										
mod.	$u_{x,mod} [\text{mm}]$		$u_{z,mod} [\text{mm}]$		$N_{mod} [\text{kN}]$		$V_{z,mod} [\text{kN}]$		$M_{y,mod} [\text{kNm}]$	
	min.	max.	min.	max.	min.	max.	min.	max.	min.	max.
1	-8,7	-4,3	-12,2	9,3	-0,3	40,9	-30,2	12,6	-5,3	4,1
2	-8,3	-4,1	-12,0	8,5	-0,3	39,0	-28,3	11,1	-4,7	3,2
3	-8,5	-4,1	-12,2	9,2	-0,3	40,8	-30,0	12,9	-5,4	4,1
4	-9,2	-4,5	-14,8	10,3	0,0	41,9	-27,3	13,5	-5,7	4,5
5	-8,3	-4,1	-14,4	8,6	0,0	37,7	-24,2	10,6	-4,4	2,8
6	-8,8	-4,2	-14,7	10,1	0,0	41,6	-26,9	14,1	-5,9	4,5
7	-10,5	-4,9	-20,8	12,2	0,0	43,5	-22,8	14,5	-6,2	5,0
8	-8,5	-4,0	-19,7	8,8	0,0	34,5	-18,9	9,3	-3,8	1,9
9	-9,7	-4,2	-20,7	11,7	0,0	42,7	-22,1	15,8	-6,7	5,0
10	-8,3	-3,9	-9,9	8,4	-0,8	39,1	-34,1	11,4	-4,7	3,6
11	-8,3	-3,7	-9,9	8,4	-0,8	37,5	-34,1	11,3	-4,7	3,6
12	-8,4	-3,1	-9,9	8,4	-0,7	32,4	-34,0	11,2	-4,7	3,6
13	-8,3	-4,0	-296,5	8,4	0,0	39,7	-30,3	11,7	-20,4	2,4
14	-8,7	-8,6	-10,0	44,5	-0,8	0,0	-0,8	0,2	-0,1	0,8
15	-8,3	-4,0	-15,3	8,7	-0,4	39,6	-17,4	11,1	-4,7	2,9
16	-8,7	-4,2	-16,1	9,0	-0,7	42,3	-15,1	16,2	-7,0	6,8
17	-8,3	-4,1	-20,1	8,8	0,0	39,6	-14,4	10,6	-4,5	2,4
18	-9,1	-4,4	-22,2	6,2	-0,6	43,8	-7,2	17,3	-7,7	8,6
19	-8,4	-4,1	-28,8	8,8	0,0	34,9	-14,6	9,8	-4,2	2,9
20	-4,6	-9,5	-34,8	4,4	-0,5	45,6	-2,6	17,0	-7,9	10,0

calculation results for pile in first pile row ($x = 0.18$ m, $y = 10.20$ m)						
mod.	N_{mod} [kN]		$V_{z,mod}$ [kN]		$M_{y,mod}$ [kNm]	
	min.	max.	min.	max.	min.	max.
1	-30,2	-28,8	-0,3	2,3	-1,6	0,1
2	-29,7	-28,3	-0,3	2,1	-1,5	0,1
3	-30,2	-28,8	-0,3	2,2	-1,6	0,1
4	-29,7	-28,5	-0,2	1,6	-1,2	0,1
5	-28,8	-27,6	-0,2	1,4	-1,2	0,1
6	-29,7	-28,5	-0,2	1,6	-1,2	0,1
7	-29,0	-28,1	-0,1	0,8	-1,4	0,1
8	-27,2	-26,4	-0,1	0,7	-1,5	0,1
9	-28,9	-28,1	-0,1	0,7	-1,4	0,1
10	-30,8	-29,1	-0,8	2,9	-2,2	0,1
11	-30,8	-29,1	-0,8	2,9	-2,2	0,1
12	-30,8	-29,1	-0,7	2,9	-2,2	0,1
13	-	-	-	-	-	-
14	-31,3	-29,5	-0,8	3,1	-2,4	0,1
15	-28,7	-26,9	-0,4	2,8	-2,1	0,1
16	-31,4	-29,7	-0,7	3,1	-2,3	0,1
17	-26,9	-25,1	-0,1	2,7	-2,0	0,1
18	-31,8	-30,1	-0,6	3,2	-2,4	0,1
19	-23,7	-22,0	-0,1	2,5	-2,9	0,1
20	-31,1	-29,4	-0,5	3,2	-2,4	0,1

C.3 NOORDWAL, THE HAGUE

C.3.1 COLLECTION OF DATA

terrain loads	
parameter	value
$F_{LM1,rep,i}$ [kN]	150
$Q_{LM1,rep,i}$ [kN/m ²]	9.0
$Q_{LM1,rep}$ [kN/m ²]	2.5
α_Q [-]	0.7
W_{LM1} [m]	5.5
$a_{LM1,x}$ [m]	3.44
$S_{LM1,x}$ [m]	2.0
$S_{LM1,y}$ [m]	1.2

trees			
no.	$x_{tree,i}$ [m]	$y_{tree,i}$ [m]	$F_{tree,i}$ [kN]
1	1.60	3.00	25
2	1.60	17.00	25

surface water	
parameter	value
z_{MHW} [m NAP]	-0.43
γ_w [kN/m ³]	10.0

retaining wall	
parameter	value
γ_{wall} [kN/m ³]	16.0
$z_{\text{wall,top}}$ [m NAP]	+0.59
$z_{\text{wall,btm}}$ [m NAP]	-1.16
$x_{\text{wall,top}}$ [m NAP]	0.15
E_{wall} [N/mm ²]	1.40×10^4

fortification		
no. [-]	$y_{\text{wall,fort}}$ [m]	$W_{\text{wall,fort}}$ [m]
1	10.00	1.00

retaining wall coordinates				
no.	$x_{\text{wall},i}$ [m]	$z_{\text{wall},i}$ [m NAP]	$x_{\text{wall,fort},i}$ [m]	$z_{\text{wall,fort},i}$ [m]
1	0.15	-1.03	0.15	-1.03
2	0.33	-1.03	0.33	-1.03
3	0.33	-1.10	0.33	-1.10
4	0.81	-1.10	1.21	-1.10
5	0.81	-0.41	1.21	-0.60
6	0.86	-0.41	1.10	-0.60
7	0.86	+0.09	1.10	-0.20
8	0.59	+0.34	0.86	-0.20
9	0.59	+0.59	0.86	+0.09
10	0.15	+0.59	0.59	+0.34
11	–	–	0.59	+0.59
12	–	–	0.15	+0.59

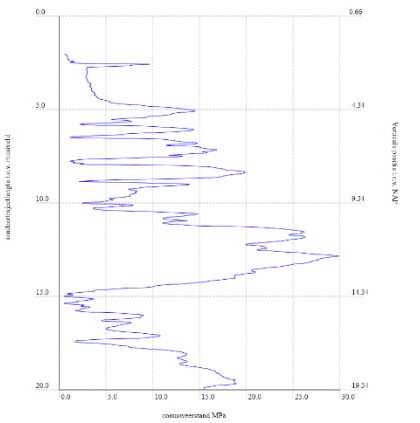
pile row									
no.	$x_{\text{pile},i}$ [m]	$z_{\text{head},i}$ [m NAP]	$z_{\text{tip},i}$ [m NAP]	$d_{\text{head},i}$ [mm]	$d_{\text{tip},i}$ [mm]	$\alpha_{\text{pile},i}$ [°]	$A_{\text{gr},i}$ [m ²]	E_{pile} [N/mm ²]	$z_{\text{low},i}$ [m NAP]
1	0.12	-1.30	-5.30	180	142.9	0	0.30	3.6×10^3	-1.30
2	0.64	-1.30	-5.30	180	142.9	0	0.49	3.6×10^3	-1.30
fort	2.81	-1.30	-5.30	180	142.9	-14.0	0.67	3.6×10^3	-1.30

pile cap beam	
parameter	value
γ_{pcb} [kN/m ³]	4.20
W_{pcb} [mm]	160
H_{pcb} [mm]	140
L_{pcb} [mm]	900
S_{pcb} [m]	1.16
E_{pcb} [N/mm ²]	0.12×10^3

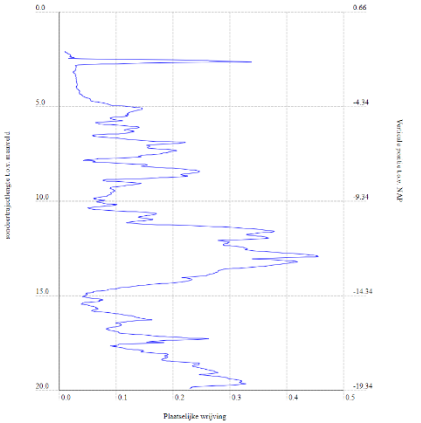
floor element	
parameter	value
γ_{floor} [kN/m ³]	4.20
W_{floor} [mm]	200
H_{floor} [mm]	60
L_{floor} [mm]	1160

E_{floor} [N/mm ²]	0.12×10^3
---	--------------------

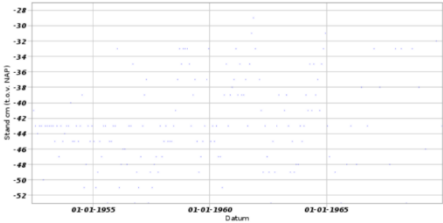
cross-beam	
parameter	value
γ_{cross} [kN/m ³]	4.20
x_{cross} [m]	0.25
W_{cross} [mm]	160
H_{cross} [mm]	130
L_{cross} [mm]	1160
E_{cross} [N/mm ²]	0.12×10^3

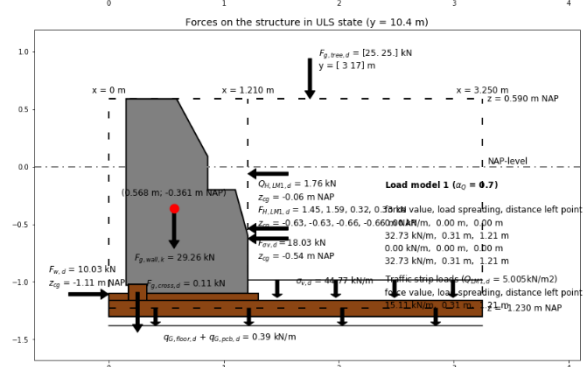
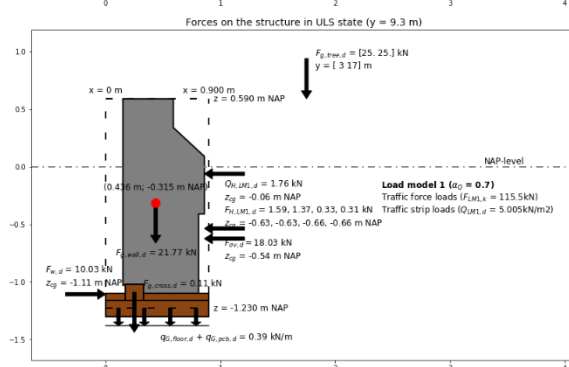
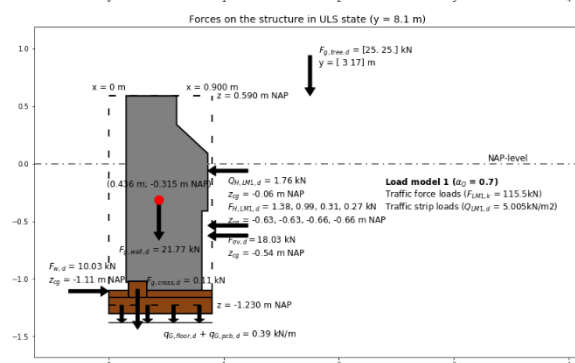
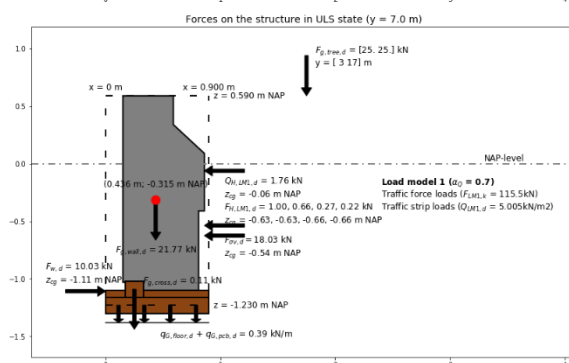
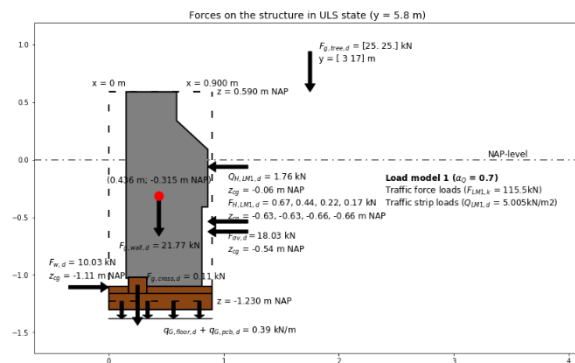
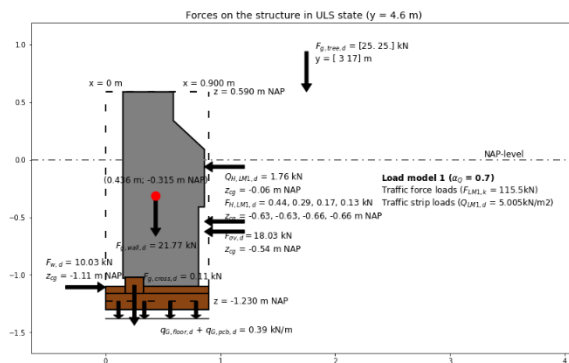
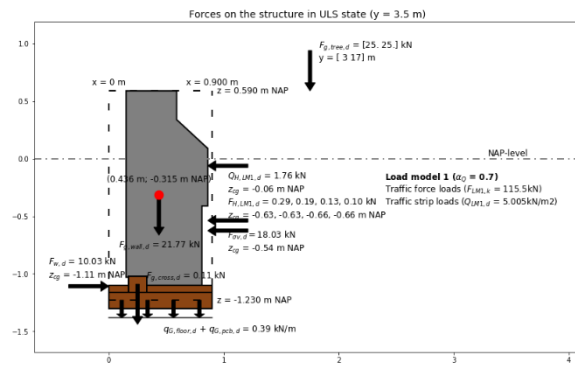
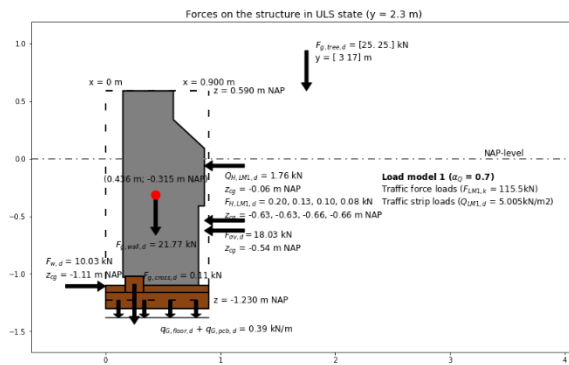


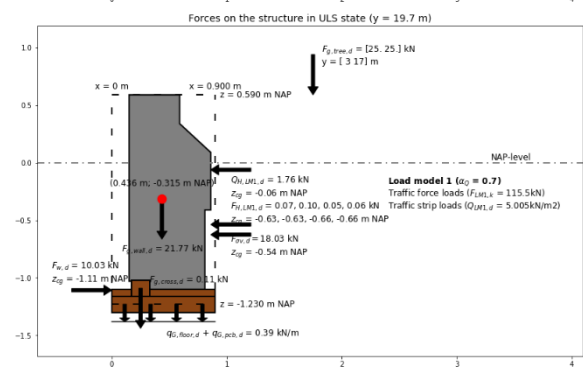
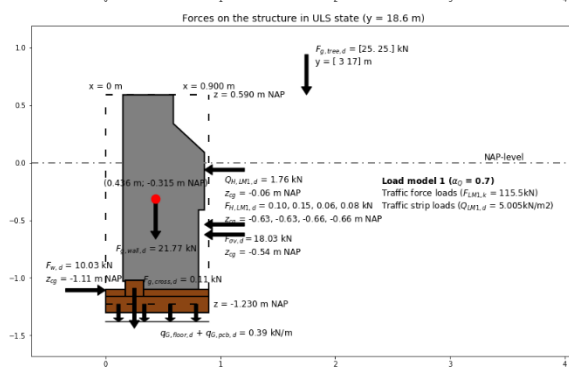
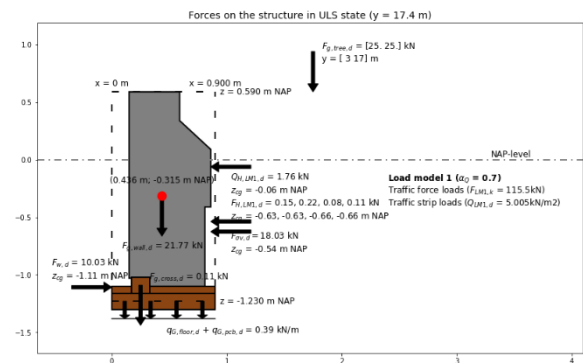
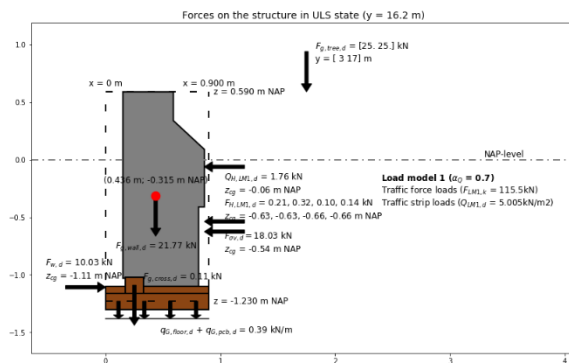
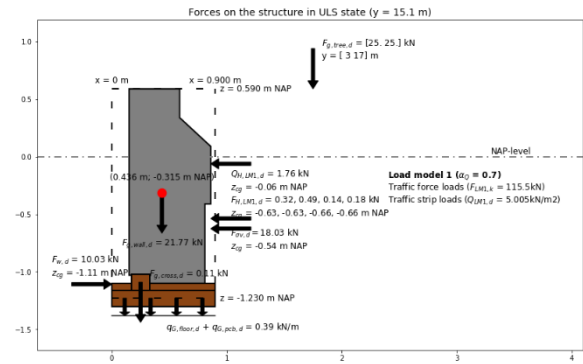
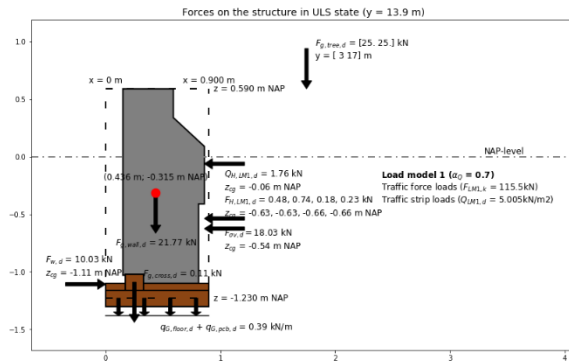
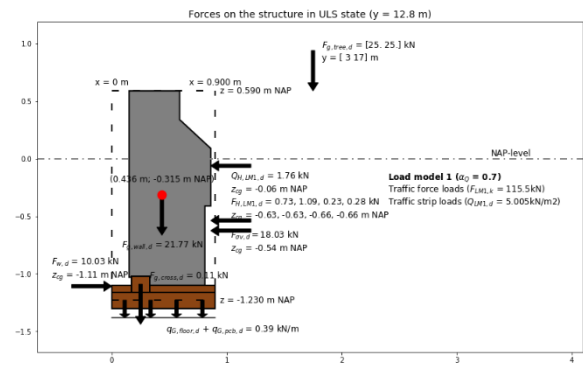
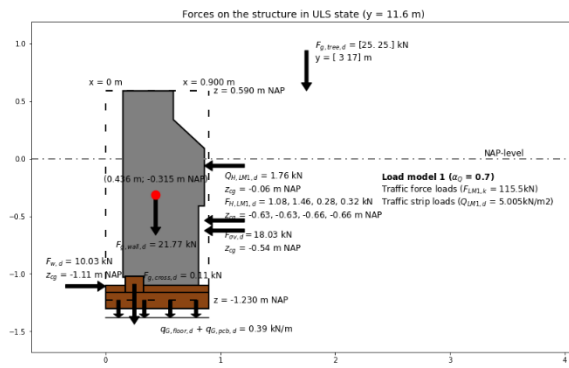
id: CPT000000097103
date: 10-06-2010
coord: 80594.840, 455139.130 (RD)
ground level: +0.66 m NAP
total depth: 19.94 m
source: (DINOloket, 2010)



id: B30G1071
date: 14-05-1952 / 14-12-1969
coord: 80520, 454860 (RD)
ground level: +1.67 m NAP
source: (DINOloket, 1969)

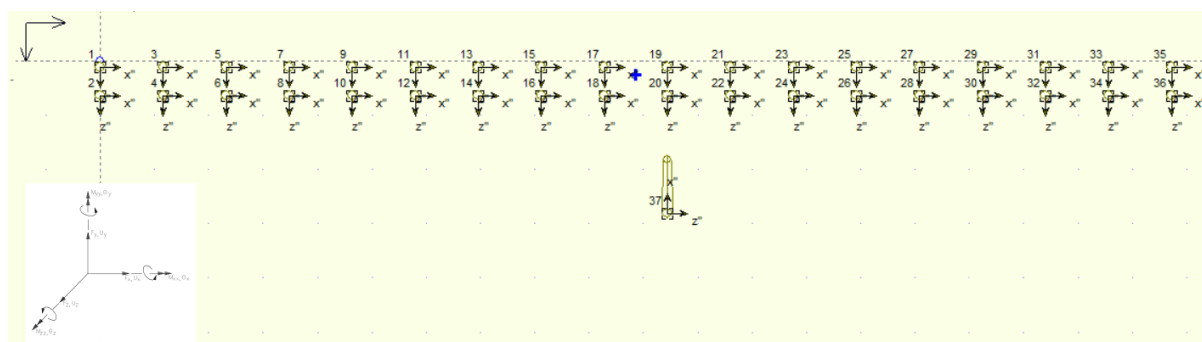






C.3.3 LATERAL SOIL RESISTANCE

input D-pile group	
parameter	value
ν [-]	0.499
$z_{\text{soil,top,avg}}$ [m]	0
$E_{\text{soil,top}}$ [kN/m ²]	3.0×10^3
$E_{\text{soil,btm}}$ [kN/m ²]	45.0×10^3
x_{cap} [m]	9.86
y_{cap} [m]	0
z_{cap} [m]	0.26
fixity	free
F_y [kN]	-4.84×10^2
F_z [kN]	-2.97×10^2
M_x [kNm]	-1.88×10^2



horizontal pile displacement (main cross-section)						
pile no.	z_{soil} [m NAP]		z_{mid} [m NAP]	z_{mid} [m]	v_{pile} [m]	figures
	from	to				
11	-1.30	-1.90	-1.60	-0.37	-8.45×10^{-3}	
	-1.90	-4.40	-3.15	-1.92	1.03×10^{-3}	
	-4.40	-5.40	-4.90	-3.67	-5.00×10^{-6}	
12	-1.30	-1.90	-1.60	-0.37	-8.46×10^{-3}	
	-1.90	-4.40	-3.15	-1.92	1.03×10^{-3}	
	-4.40	-5.40	-4.90	-3.67	-4.00×10^{-6}	

horizontal pile displacement (fortified cross-section)						
pile no.	z_{soil} [m NAP]		z_{mid} [m NAP]	z_{mid} [m]	v_{pile} [m]	figures
	from	to				
19	-1.30	-1.90	-1.60	-0.37	-8.49×10^{-3}	
	-1.90	-4.40	-3.15	-1.92	1.02×10^{-3}	
	-4.40	-5.40	-4.90	-3.67	2.00×10^{-6}	
20	-1.30	-1.90	-1.60	-0.37	-8.54×10^{-3}	
	-1.90	-4.40	-3.15	-1.92	1.02×10^{-3}	
	-4.40	-5.40	-4.90	-3.67	1.00×10^{-5}	
37	-1.30	-1.90	-1.60	-0.37	7.81×10^{-3}	
	-1.90	-4.40	-3.15	-1.92	-1.00×10^{-3}	
	-4.40	-5.40	-4.90	-3.67	8.00×10^{-5}	

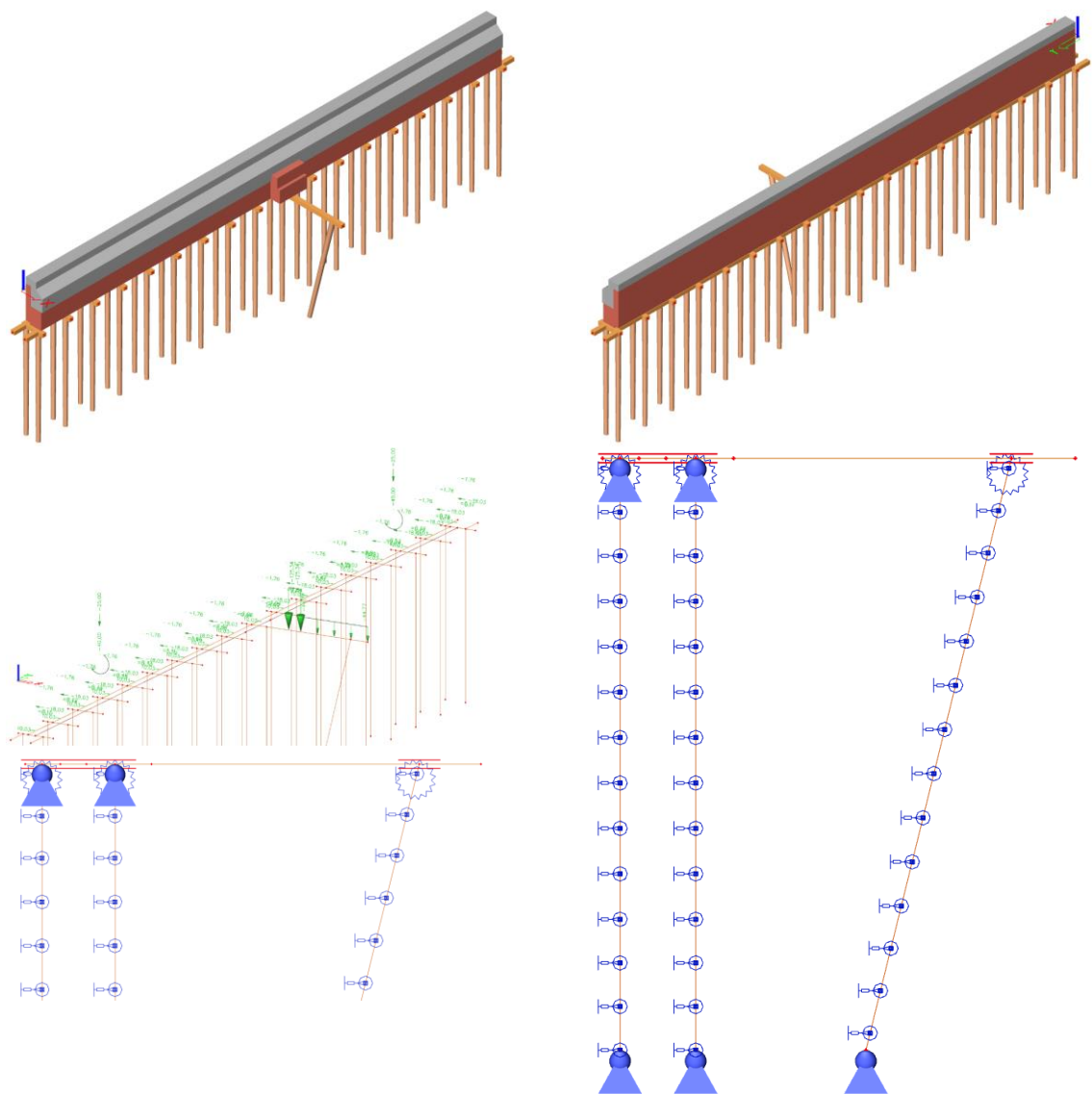
horizontal soil response (main cross-section)							
pile no.	z _{soil} [m NAP]		soil type	α [-]	β [-]	k _s [MN/m ³]	p _{soil} [MN/m ²]
	from	to					
1	-1.30	-1.90	loam	1/2	1.0	4.17×10 ³	35.22
	-1.90	-4.40	clay	2/3	2.0	5.08×10 ⁴	52.36
	-4.40	-5.40	sand	1/3	0.7	5.23×10 ⁴	0.26
2	-1.30	-1.90	loam	1/2	1.0	4.17×10 ³	35.22
	-1.90	-4.40	clay	2/3	2.0	5.08×10 ⁴	52.36
	-4.40	-5.40	sand	1/3	0.7	5.23×10 ⁴	0.26

horizontal soil response (fortified cross-section)							
pile no.	z _{soil} [m NAP]		soil type	α [-]	β [-]	k _s [kN/m ³]	p _{soil} [kN/m ²]
	from	to					
1	-1.30	-1.90	loam	1/2	1.0	4.17×10 ³	35.38
	-1.90	-4.40	clay	2/3	2.0	5.08×10 ⁴	51.86
	-4.40	-5.30	sand	1/3	0.7	5.23×10 ⁴	0.10
2	-1.30	-1.90	loam	1/3	1.0	4.17×10 ³	35.59
	-1.90	-4.40	clay	2/3	2.0	5.08×10 ⁴	51.86
	-4.40	-5.30	sand	1/3	0.7	5.23×10 ⁴	0.52
fort	-1.30	-1.90	loam	1/2	1.0	4.17×10 ³	32.55
	-1.90	-4.40	clay	2/3	2.0	5.08×10 ⁴	50.84
	-4.40	-5.30	sand	1/3	0.7	5.23×10 ⁴	4.19

C.3.4 JOINT STIFFNESS

calculation joint stiffness	
parameter	value
H _{mor} [mm]	70.0
W _{notch} [mm]	18.0
a ₁ [mm]	81.0
a ₂ [mm]	23.3
a ₃ [mm]	23.3
k _{0,1} [N/mm]	2.13×10 ⁵
k _{90,1} [N/mm]	7,09×10 ³
k _{0,2} [N/mm]	4.75×10 ⁵
k _{90,2} [N/mm]	1.58×10 ⁴
k _{0,3} [N/mm]	4.75×10 ⁵
k _{90,3} [N/mm]	1.58×10 ⁴
k _{eq,1} [N/mm]	6.86×10 ³
k _{eq,2} [N/mm]	1.53×10 ⁴
k _{eq,3} [N/mm]	1.53×10 ⁴
k _r [MNm/rad]	0.06

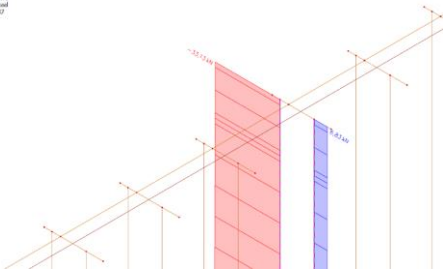
C.3.5 AXIAL PILE HEAD FORCES

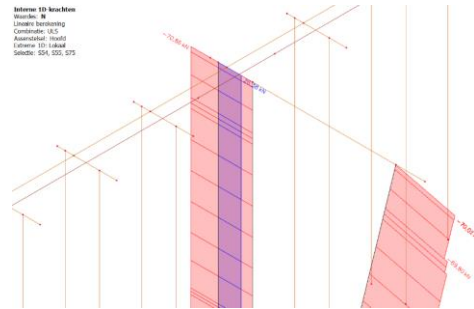


axial pile head forces (y = 5.8 m)	
pile row	F _{head,d} [kN]
1	-33.13
2	+6.83

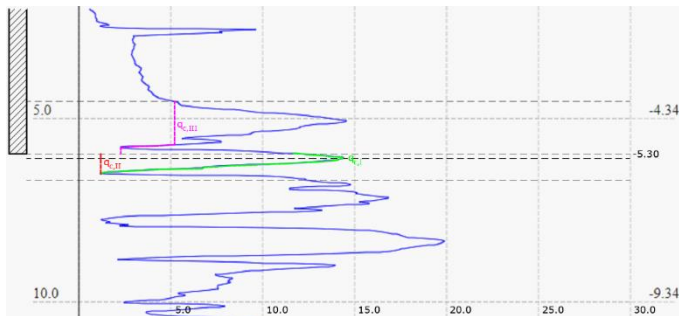
axial pile head forces (y = 10.2 m)	
pile row	F _{head,d} [kN]
1	-70.86
2	+26.38
fort	-70.02

Software: 10-Frame
Version: 8
Created: 10/10/2010
Coordinates: 10.2
Dimensions: 10.2
Pile: 10.2
Collection: 10.2





C.3.6 AXIAL PILE FORCES AND RESISTANCES



cone resistances	
parameter	value
$q_{CPT,I}$ [MPa]	9.0
$q_{CPT,II}$ [MPa]	1.0
$q_{CPT,III}$ [MPa]	4.5

maximum pile tip resistance (main cross-section)				
pile row	A_{tip} [mm ²]	$q_{b,max}$ [MPa]	$R_{b,max,k}$ [kN]	$R_{b,max,d}$ [kN]
1	1.60×10^4	3.32	53.36	31.99

maximum pile tip resistance (fortified cross-section)				
pile row	A_{tip} [mm ²]	$q_{b,max}$ [MPa]	$R_{b,max,k}$ [kN]	$R_{b,max,d}$ [kN]
1	1.60×10^4	3.32	53.36	31.99
fort	1.60×10^4	3.32	53.36	31.99

maximum pile shaft resistance (main cross-section) ($z_{tp} = -4.40$ m NAP)							
pile row	ΔL [m]	$z_{\Delta L,avg}$ [m]	$d_{\Delta L,avg}$ [mm]	$C_{\Delta L,avg}$ [mm]	$q_{s,max}$ [MPa]	$R_{s,max,k}$ [kN]	$R_{s,max,d}$ [kN]
1	0.90	3.55	146.7	460.9	0.14	57.74	34.62

maximum pile shaft resistance (fortified cross-section) ($z_{tp} = -4.40$ m NAP)							
pile row	ΔL [m]	$z_{\Delta L,avg}$ [m]	$d_{\Delta L,avg}$ [mm]	$C_{\Delta L,avg}$ [mm]	$q_{s,max}$ [MPa]	$R_{s,max,k}$ [kN]	$R_{s,max,d}$ [kN]
1	0.90	3.55	146.7	460.9	0.14	57.74	34.62
fort	0.90	3.55	146.7	460.9	0.14	57.74	34.62

negative skin friction (main cross-section) ($z_{tp} = -4.40$ m NAP)											
pile row	z_{mid} [m NAP]	t_i [m]	γ'_i [kN/m ³]	$z_{pile,mid}$ [m]	$C_{pile,mid}$ [m]	m_i [–]	$\sigma'_{m,i}$ [kN/m ²]	$\sigma_{nsf,i}$ [kN/m ²]	$F_{nsf,i}$ [kN]	$F_{nsf,k}$ [kN]	$F_{nsf,d}$ [kN]
1	–1.60	0.60	9.0	0.30	0.556	0.46	4.71	0.69	0.21	3.43	4.11
	–3.15	2.50	8.0	1.85	0.508	0.42	13.97	10.74	3.22		

negative skin friction (fortified cross-section) ($z_{tp} = -4.40$ m NAP)											
pile row	z_{mid} [m NAP]	t_i [m]	γ'_i [kN/m ³]	$z_{pile,mid}$ [m]	$C_{pile,mid}$ [m]	m_i [–]	$\sigma'_{m,i}$ [kN/m ²]	$\sigma_{nsf,i}$ [kN/m ²]	$F_{nsf,i}$ [kN]	$F_{nsf,k}$ [kN]	$F_{nsf,d}$ [kN]
1	–1.60	0.60	9.0	0.30	0.556	0.46	4.71	0.69	0.21	3.43	4.11
	–3.15	2.50	8.0	1.85	0.508	0.42	13.97	10.74	3.22		
fort	–1.60	0.60	9.0	0.30	0.556	0.20	5.08	0.32	0.22	4.23	5.08
	–3.15	2.50	8.0	1.85	0.508	0.19	19.09	5.99	4.01		

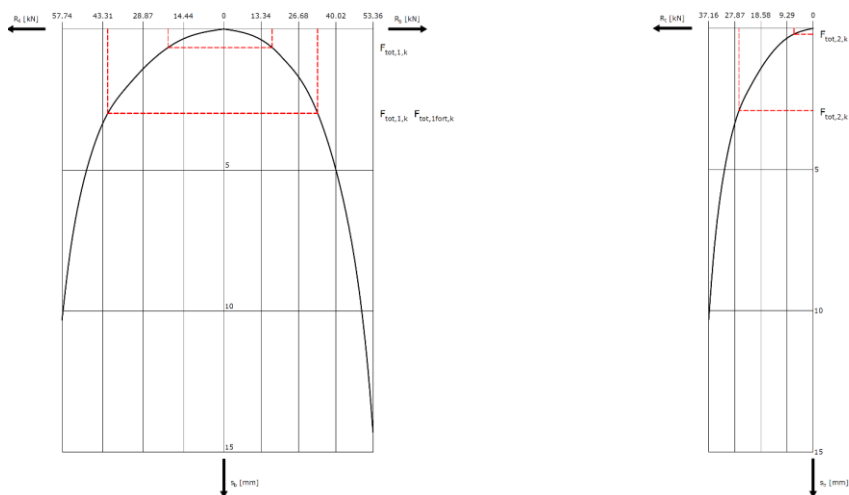
tensile resistance (main cross-section)										
pile row	z_{mid} [m NAP]	t_i [m]	$z_{pile,mid}$ [m]	$C_{pile,mid}$ [m]	$\alpha_{t,i}$ [–]	$q_{CPT,d,i}$ [MPa]	$q_{t,d,i}$ [MPa]	$R_{t,d,i}$ [kN]	$R_{t,d}$ [kN]	$R_{t,k}$ [kN]
2	–1.60	0.60	0.30	0.556	0.0070	0.249	0.002	0.58	19.81	37.16
	–3.15	2.50	1.85	0.508	0.0035	1.634	0.006	7.27		
	–4.85	0.90	3.50	0.461	0.0070	4.121	0.029	11.97		

tensile resistance (fortified cross-section)										
pile row	z_{mid} [m NAP]	t_i [m]	$z_{pile,mid}$ [m]	$C_{pile,mid}$ [m]	$\alpha_{t,i}$ [–]	$q_{CPT,d,i}$ [MPa]	$q_{t,d,i}$ [MPa]	$R_{t,d,i}$ [kN]	$R_{t,d}$ [kN]	$R_{t,k}$ [kN]
2	–1.60	0.60	0.30	0.556	0.0070	0.249	0.002	0.58	19.81	37.16
	–3.15	2.50	1.85	0.508	0.0035	1.634	0.006	7.27		
	–4.85	0.90	3.50	0.461	0.0070	4.121	0.029	11.97		

C.3.7 PILE TIP SETTLEMENT AND FORCE

total pile head force (main cross-section)	
pile row	F_{tot} [kN]
1	–37.24
2	6.83

total pile head force (fortified cross-section)	
pile row	F_{tot} [kN]
1	–74.97
2	26.38
fort	–75.10



pile settlement and rise (main cross-section)					
pile row	$R_{b,k}$ [kN]	$R_{s,k}$ [kN]	s_b [mm]	$R_{t,k}$ [kN]	s_{head} [mm]
1	17.3	19.9	0.7	–	–
2	–	–	–	6.8	0.2

pile settlement and rise (fortified cross-section)					
pile row	$R_{b,k}$ [kN]	$R_{s,k}$ [kN]	s_b [mm]	$R_{t,k}$ [kN]	s_{head} [mm]
1	33.5	41.5	3.0	–	–
2	–	–	–	26.4	2.9
fort	33.6	41.5	3.0	–	–

axial pile tip stiffness (main cross-section)	
pile row	k_{ax} [MN/m]
1	53.1
2	34.0

pile tip stiffness (fortified cross-section)	
pile row	k_{ax} [MN/m]
1	25.0
2	9.1
fort	25.0

C.3.8 NEUTRAL PLANE

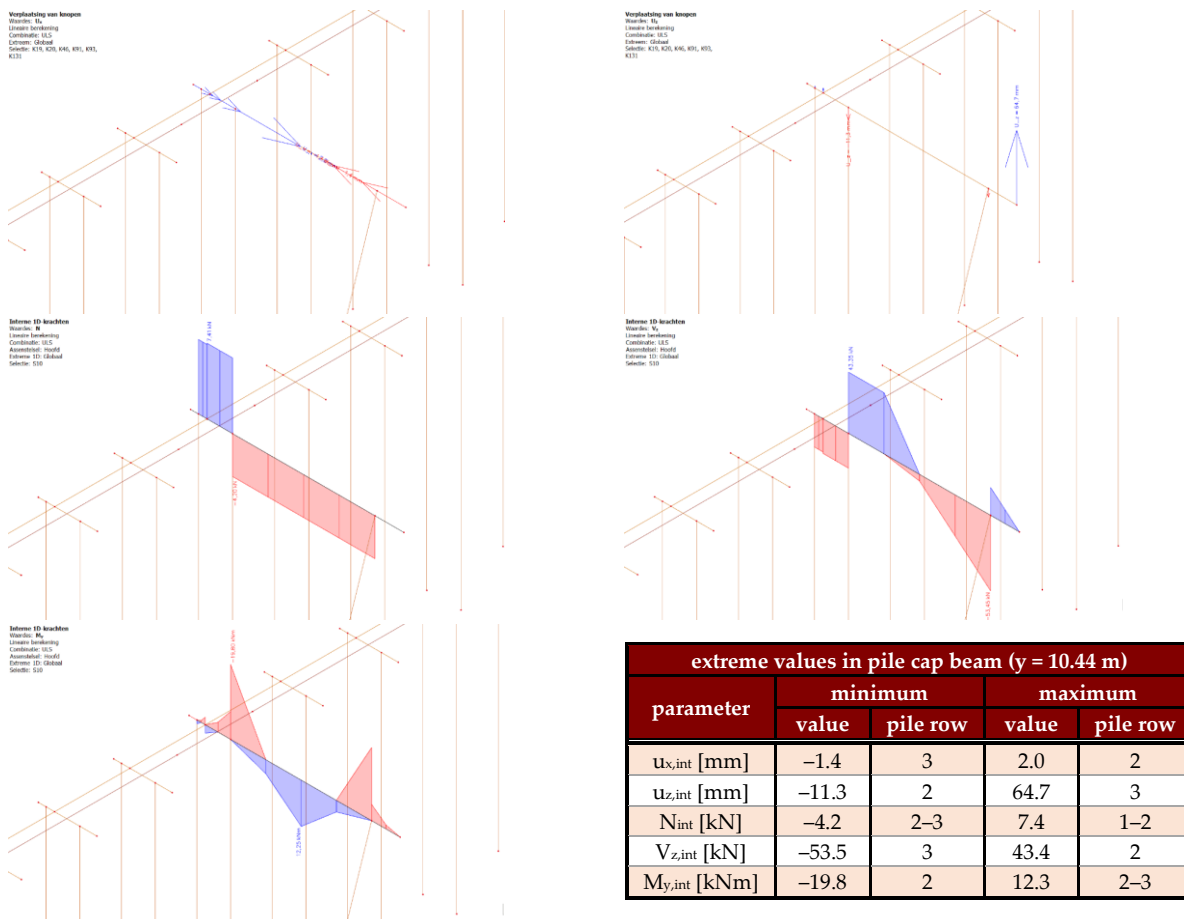
total soil settlement (main cross-section)				
pile row	Z_{top} [m NAP]	t_i [m]	$s_{soil,tot,i}$ [m]	$s_{soil,tot}$ [m]
1	–1.30	0.60	0.009	0.055
	–1.90	2.50	0.046	

total soil settlement (fortified cross-section)				
pile row	Z _{top} [m NAP]	t _i [m]	S _{soil,tot,i} [m]	S _{soil,tot} [m]
1	-1.30	0.60	0.009	0.055
	-1.90	2.50	0.046	
fort	-1.30	0.60	0.009	0.055
	-1.90	2.50	0.046	

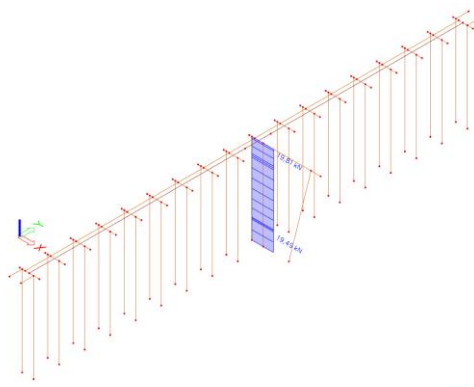
influence neutral plane (main cross-section)						
pile row	value	Z _{tp} [kN]	R _{s,max,k} [kN]	R _{s,max,d} [kN]	F _{nsf,k} [kN]	F _{nsf,d} [kN]
1	interaction	-4.34	59.31	35.56	3.33	3.99

influence neutral plane (fortified cross-section)						
pile row	value	Z _{tp} [kN]	R _{s,max,k} [kN]	R _{s,max,d} [kN]	F _{nsf,k} [kN]	F _{nsf,d} [kN]
1	interaction	-4.21	62.72	37.60	3.11	3.73
fort	interaction	-4.21	62.72	37.60	3.80	4.55

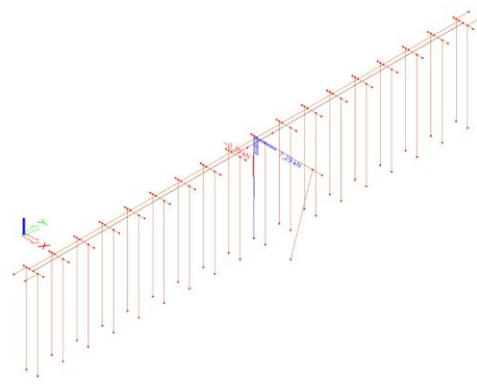
C.3.9 CALCULATION MODEL



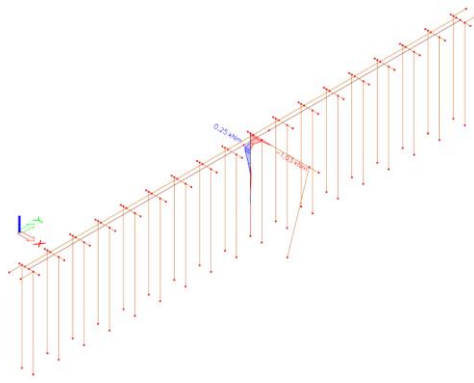
Interne 1D-brachten
Waarde: M_x
Lineaire berekening
Combinatie: ULS
Assumestel: Hoofd
Extremie 1D: Globaal
Selectie: 554



Interne 1D-brachten
Waarde: V_z
Lineaire berekening
Combinatie: ULS
Assumestel: Hoofd
Extremie 1D: Globaal
Selectie: 554



Interne 1D-brachten
Waarde: M_y
Lineaire berekening
Combinatie: ULS
Assumestel: Hoofd
Extremie 1D: Globaal
Selectie: 554



extreme values in pile at first row ($x = 0.12$ m, $y = 10.44$ m)		
parameter	minimum value	maximum value
N [kN]	19.5	19.8
V_z [kN]	-0.4	7.3
M_y [kNm]	-1.0	0.3

C.3.10 STRUCTURAL DEFICIENCIES

changes in structural model		
modification	changing variable	adaptations
1	$p_m = 5$ mm	$d_{head,1,2}$ ($y = 0.00$ m), ..., $d_{head,1,2}$ ($y = 19.72$ m): 180 mm \rightarrow 160 mm
		$d_{tip,1,2}$ ($y = 0.00$ m), ..., $d_{tip,1,2}$ ($y = 19.72$ m): 142.9 mm \rightarrow 127.9 mm
		$d_{head,fort}$ ($y = 10.44$ m): 180 mm \rightarrow 160 mm
		$d_{tip,fort}$ ($y = 10.44$ m): 142.9 mm \rightarrow 127.9 mm
2	$p_m = 5$ mm	$d_{head,1,2}$ ($y = 10.44$ m): 180 mm \rightarrow 160 mm
		$d_{tip,1,2}$ ($y = 10.44$ m): 142.9 mm \rightarrow 127.9 mm
		$d_{head,fort}$ ($y = 10.44$ m): 180 mm \rightarrow 160 mm
		$d_{tip,fort}$ ($y = 10.44$ m): 142.9 mm \rightarrow 127.9 mm
3	$p_m = 5$ mm	$d_{head,1,2}$ ($y = 0.00$ m), ..., $d_{head,1,2}$ ($y = 19.72$ m): 180 mm \rightarrow 160 mm
		$d_{tip,1,2}$ ($y = 0.00$ m), ..., $d_{tip,1,2}$ ($y = 19.72$ m): 142.9 mm \rightarrow 127.9 mm
4	$p_m = 15$ mm	$d_{head,1,2}$ ($y = 0.00$ m), ..., $d_{head,1,2}$ ($y = 19.72$ m): 180 mm \rightarrow 140 mm
		$d_{tip,1,2}$ ($y = 0.00$ m), ..., $d_{tip,1,2}$ ($y = 19.72$ m): 142.9 mm \rightarrow 117.9 mm
		$d_{head,fort}$ ($y = 10.44$ m): 180 mm \rightarrow 140 mm
		$d_{tip,fort}$ ($y = 10.44$ m): 142.9 mm \rightarrow 117.9 mm
		W_{pcb} ($y = 0.00$ m), ..., W_{pcb} ($y = 19.72$ m): 160 mm \rightarrow 150 mm
		W_{cross} ($x = 0.25$ m): 160 mm \rightarrow 150 mm
5	$p_m = 15$ mm	$d_{head,1,2}$ ($y = 10.44$ m): 180 mm \rightarrow 140 mm
		$d_{tip,1,2}$ ($y = 10.44$ m): 142.9 mm \rightarrow 117.9 mm
		$d_{head,fort}$ ($y = 10.44$ m): 180 mm \rightarrow 140 mm
		$d_{tip,fort}$ ($y = 10.44$ m): 142.9 mm \rightarrow 117.9 mm
		W_{pcb} ($y = 10.44$ m): 160 mm \rightarrow 150 mm
		W_{cross} ($x = 0.25$ m): 160 mm \rightarrow 150 mm
6	$p_m = 15$ mm	$d_{head,1,2}$ ($y = 0.00$ m), ..., $d_{head,1,2}$ ($y = 19.72$ m): 180 mm \rightarrow 140 mm
		$d_{tip,1,2}$ ($y = 0.00$ m), ..., $d_{tip,1,2}$ ($y = 19.72$ m): 142.9 mm \rightarrow 117.9 mm

		$W_{pcb} (y = 0.00 \text{ m}), \dots, W_{pcb} (y = 19.72 \text{ m}): 160 \text{ mm} \rightarrow 150 \text{ mm}$
7	$p_m = 30 \text{ mm}$	$d_{head,1,2} (y = 0.00 \text{ m}), \dots, d_{head,1,2} (y = 19.72 \text{ m}): 180 \text{ mm} \rightarrow 110 \text{ mm}$
		$d_{tip,1,2} (y = 0.00 \text{ m}), \dots, d_{tip,1,2} (y = 19.72 \text{ m}): 142.9 \text{ mm} \rightarrow 102.9 \text{ mm}$
		$d_{head,fort} (y = 9.86 \text{ m}): 180 \text{ mm} \rightarrow 110 \text{ mm}$
		$d_{tip,fort} (y = 9.86 \text{ m}): 142.9 \text{ mm} \rightarrow 102.9 \text{ mm}$
		$W_{pcb} (y = 0.00 \text{ m}), \dots, W_{pcb} (y = 19.72 \text{ m}): 160 \text{ mm} \rightarrow 120 \text{ mm}$
		$W_{cross} (x = 0.25 \text{ m}): 160 \text{ mm} \rightarrow 120 \text{ mm}$
8	$p_m = 30 \text{ mm}$	$d_{head,1,2} (y = 10.44 \text{ m}): 180 \text{ mm} \rightarrow 110 \text{ mm}$
		$d_{tip,1,2} (y = 10.44 \text{ m}): 142.9 \text{ mm} \rightarrow 102.9 \text{ mm}$
		$d_{head,fort} (y = 10.44 \text{ m}): 180 \text{ mm} \rightarrow 110 \text{ mm}$
		$d_{tip,fort} (y = 10.44 \text{ m}): 142.9 \text{ mm} \rightarrow 102.9 \text{ mm}$
		$W_{pcb} (y = 10.44 \text{ m}): 160 \text{ mm} \rightarrow 120 \text{ mm}$
		$W_{cross} (x = 0.25 \text{ m}): 160 \text{ mm} \rightarrow 120 \text{ mm}$
9	$p_m = 30 \text{ mm}$	$d_{head,1,2} (y = 0.00 \text{ m}), \dots, d_{head,1,2} (y = 19.72 \text{ m}): 180 \text{ mm} \rightarrow 110 \text{ mm}$
		$d_{tip,1,2} (y = 0.00 \text{ m}), \dots, d_{tip,1,2} (y = 19.72 \text{ m}): 142.9 \text{ mm} \rightarrow 102.9 \text{ mm}$
		$W_{pcb} (y = 0.00 \text{ m}), \dots, W_{pcb} (y = 19.72 \text{ m}): 160 \text{ mm} \rightarrow 120 \text{ mm}$
10	$e_y = 25 \text{ mm}$	$e_{y,pcb} (y = 10.44 \text{ m}): 0 \rightarrow 25 \text{ mm}$
11	$e_y = 50 \text{ mm}$	$e_{y,pcb} (y = 10.44 \text{ m}): 0 \rightarrow 50 \text{ mm}$
12	$e_y = 100 \text{ mm}$	$e_{y,pcb} (y = 10.44 \text{ m}): 0 \rightarrow 100 \text{ mm}$
13	$R_{c,max} = 0 \text{ kN},$ $R_{t,max} = 0 \text{ kN}$	$R_{c,pile,1,d} (x = 0.12 \text{ m}, y = 10.44 \text{ m}): 66.61 \text{ kN} \rightarrow 0 \text{ kN}$
		$R_{t,pile,2,d} (x = 0.64 \text{ m}, y = 10.44 \text{ m}): 37.16 \text{ kN} \rightarrow 0 \text{ kN}$
14	$R_{c,max} = 0 \text{ kN},$ $R_{t,max} = 0 \text{ kN}$	$R_{t,pile,2,d} (x = 0.64 \text{ m}, y = 10.44 \text{ m}): 37.16 \text{ kN} \rightarrow 0 \text{ kN}$
		$R_{c,pile,fort} (x = 2.81 \text{ m}, y = 10.44 \text{ m}): 66.61 \text{ kN} \rightarrow 0 \text{ kN}$
15	$S_b = 5 \text{ mm},$ $S_{head} = 5 \text{ mm}$	$k_{ax,1} (x = 0.12 \text{ m}, y = 10.44 \text{ m}): 25.0 \text{ MN/m} \rightarrow 15.0 \text{ MN/m}$
		$k_{ax,2} (x = 0.64 \text{ m}, y = 10.44 \text{ m}): 9.1 \text{ MN/m} \rightarrow 5.3 \text{ MN/m}$
		$k_{ax,fort} (x = 2.81 \text{ m}, y = 10.44 \text{ m}): 25.0 \text{ MN/m} \rightarrow 15.0 \text{ MN/m}$
16	$S_b = 5 \text{ mm},$ $S_{head} = 5 \text{ mm}$	$k_{ax,1} (x = 0.12 \text{ m}, y = 0.00 \text{ m}), \dots, k_{ax,1} (x = 0.12 \text{ m}, y = 9.28 \text{ m}): 53.1 \text{ MN/m} \rightarrow 7.4 \text{ MN/m}$
		$k_{ax,1} (x = 0.12 \text{ m}, y = 10.44 \text{ m}): 25.0 \text{ MN/m} \rightarrow 15.0 \text{ MN/m}$
		$k_{ax,1} (x = 0.12 \text{ m}, y = 11.60 \text{ m}), \dots, k_{ax,1} (x = 0.12 \text{ m}, y = 19.72 \text{ m}): 53.1 \text{ MN/m} \rightarrow 7.4 \text{ MN/m}$
		$k_{ax,2} (x = 0.64 \text{ m}, y = 0.00 \text{ m}), \dots, k_{ax,2} (x = 0.64 \text{ m}, y = 9.28 \text{ m}): 34.0 \text{ MN/m} \rightarrow 1.4 \text{ MN/m}$
		$k_{ax,2} (x = 0.64 \text{ m}, y = 10.44 \text{ m}): 9.1 \text{ MN/m} \rightarrow 5.3 \text{ MN/m}$
		$k_{ax,2} (x = 0.64 \text{ m}, y = 11.60 \text{ m}), \dots, k_{ax,2} (x = 0.64 \text{ m}, y = 19.72 \text{ m}): 34.0 \text{ MN/m} \rightarrow 1.4 \text{ MN/m}$
17	$S_b = 10 \text{ mm},$ $S_{head} = 10 \text{ mm}$	$k_{ax,1} (x = 0.12 \text{ m}, y = 10.44 \text{ m}): 25.0 \text{ MN/m} \rightarrow 7.5 \text{ MN/m}$
		$k_{ax,2} (x = 0.64 \text{ m}, y = 10.44 \text{ m}): 9.1 \text{ MN/m} \rightarrow 2.6 \text{ MN/m}$
		$k_{ax,fort} (x = 2.81 \text{ m}, y = 10.44 \text{ m}): 25.0 \text{ MN/m} \rightarrow 7.5 \text{ MN/m}$
18	$S_b = 10 \text{ mm},$ $S_{head} = 10 \text{ mm}$	$k_{ax,1} (x = 0.12 \text{ m}, y = 0.00 \text{ m}), \dots, k_{ax,1} (x = 0.12 \text{ m}, y = 9.28 \text{ m}): 53.1 \text{ MN/m} \rightarrow 3.7 \text{ MN/m}$
		$k_{ax,1} (x = 0.12 \text{ m}, y = 10.44 \text{ m}): 25.0 \text{ MN/m} \rightarrow 7.5 \text{ MN/m}$
		$k_{ax,1} (x = 0.12 \text{ m}, y = 11.60 \text{ m}), \dots, k_{ax,1} (x = 0.12 \text{ m}, y = 19.72 \text{ m}): 53.1 \text{ MN/m} \rightarrow 3.7 \text{ MN/m}$
		$k_{ax,2} (x = 0.64 \text{ m}, y = 0.00 \text{ m}), \dots, k_{ax,2} (x = 0.64 \text{ m}, y = 9.28 \text{ m}): 34.0 \text{ MN/m} \rightarrow 0.7 \text{ MN/m}$
		$k_{ax,2} (x = 0.64 \text{ m}, y = 10.44 \text{ m}): 9.1 \text{ MN/m} \rightarrow 2.6 \text{ MN/m}$
		$k_{ax,2} (x = 0.64 \text{ m}, y = 11.60 \text{ m}), \dots, k_{ax,2} (x = 0.64 \text{ m}, y = 19.72 \text{ m}): 34.0 \text{ MN/m} \rightarrow 0.7 \text{ MN/m}$
19	$S_b = 20 \text{ mm},$ $S_{head} = 20 \text{ mm}$	$k_{ax,1} (x = 0.12 \text{ m}, y = 10.44 \text{ m}): 25.0 \text{ MN/m} \rightarrow 3.8 \text{ MN/m}$
		$k_{ax,2} (x = 0.64 \text{ m}, y = 10.44 \text{ m}): 9.1 \text{ MN/m} \rightarrow 1.3 \text{ MN/m}$
		$k_{ax,fort} (x = 2.81 \text{ m}, y = 10.44 \text{ m}): 25.0 \text{ MN/m} \rightarrow 3.8 \text{ MN/m}$
20	$S_b = 20 \text{ mm},$ $S_{head} = 20 \text{ mm}$	$k_{ax,1} (x = 0.12 \text{ m}, y = 0.00 \text{ m}), \dots, k_{ax,1} (x = 0.12 \text{ m}, y = 9.28 \text{ m}): 53.1 \text{ MN/m} \rightarrow 1.9 \text{ MN/m}$
		$k_{ax,1} (x = 0.12 \text{ m}, y = 10.44 \text{ m}): 25.0 \text{ MN/m} \rightarrow 3.8 \text{ MN/m}$
		$k_{ax,1} (x = 0.12 \text{ m}, y = 11.60 \text{ m}), \dots, k_{ax,1} (x = 0.12 \text{ m}, y = 19.72 \text{ m}): 53.1 \text{ MN/m} \rightarrow 1.9 \text{ MN/m}$
		$k_{ax,2} (x = 0.64 \text{ m}, y = 0.00 \text{ m}), \dots, k_{ax,2} (x = 0.64 \text{ m}, y = 9.28 \text{ m}): 34.0 \text{ MN/m} \rightarrow 0.3 \text{ MN/m}$
		$k_{ax,2} (x = 0.64 \text{ m}, y = 10.44 \text{ m}): 9.1 \text{ MN/m} \rightarrow 1.3 \text{ MN/m}$
		$k_{ax,2} (x = 0.64 \text{ m}, y = 11.60 \text{ m}), \dots, k_{ax,2} (x = 0.64 \text{ m}, y = 19.72 \text{ m}): 34.0 \text{ MN/m} \rightarrow 0.3 \text{ MN/m}$

calculation results for pile cap beam (y = 10.44 m)										
mod.	u _{x,mod} [mm]		u _{z,mod} [mm]		N _{mod} [kN]		V _{z,mod} [kN]		M _{y,mod} [kNm]	
	min.	max.	min.	max.	min.	max.	min.	max.	min.	max.
1	-2,4	2,0	-12,3	68,6	-5,5	8,6	-53,4	43,4	-19,8	12,3
2	-2,0	2,4	-12,3	68,6	-5,5	8,6	-53,4	43,4	-19,8	12,3
3	-1,3	2,5	-12,3	64,8	-4,7	8,8	-53,5	43,3	-19,7	12,3
4	-3,1	3,1	-13,4	73,8	-7,3	10,5	-53,4	43,4	-19,8	12,3
5	-3,1	3,1	-13,4	73,8	-7,3	10,5	-53,4	43,4	-19,8	12,3
6	-1,3	3,3	-13,4	62,6	-5,3	10,9	-53,6	43,2	-19,7	12,2
7	-7,1	5,6	-16,5	92,8	-11,9	15,1	-53,4	43,4	-19,8	12,3
8	-7,1	5,7	-15,8	92,9	-11,9	15,9	-53,4	43,4	-19,8	12,3
9	-1,2	6,1	-16,1	52,5	-6,8	16,6	-53,8	42,9	-19,9	12,1
10	-1,5	2,3	-11,3	64,9	-2,8	6,9	-53,5	43,4	-19,8	12,3
11	-1,9	2,8	-11,3	65,3	0,0	5,8	-53,5	43,4	-19,8	12,3
12	-2,8	3,6	-11,3	66,2	0,0	6,5	-53,5	43,4	-19,8	12,3
13	-4,2	-3,8	-1084,6	141,1	-0,4	0,0	-64,5	32,3	-28,6	15,0
14	18,9	18,9	-1,3×10 ⁴	142,8	-1,4	0,0	0,0	121,1	-220,8	0,0
15	-1,4	2,1	-16,3	62,7	-4,3	7,5	-53,5	43,3	-19,7	12,3
16	-1,4	2,1	-16,0	65,0	-4,3	7,6	-53,5	43,3	-19,7	12,3
17	-1,3	2,3	-27,5	57,8	-4,5	7,5	-53,6	43,2	-19,6	12,3
18	-1,4	2,3	-26,7	65,8	-4,5	7,7	-53,6	43,2	-19,6	12,3
19	-1,3	2,5	-46,1	48,2	-4,8	7,7	-53,7	43,1	-19,6	12,3
20	-1,4	2,5	-44,3	67,0	-4,8	7,9	-53,8	43,0	-19,6	12,3

calculation results for pile in first pile row (x = 0.12 m, y = 10.44 m)						
mod.	N _{mod} [kN]		V _{z,mod} [kN]		M _{y,mod} [kNm]	
	min.	max.	min.	max.	min.	max.
1	19,7	19,9	-0,3	8,5	-1,0	0,2
2	19,8	20,0	-0,3	8,5	-1,0	0,2
3	19,6	19,9	-0,3	8,7	-1,0	0,2
4	19,2	19,4	-0,5	10,4	-1,1	0,2
5	19,4	19,6	-0,5	10,4	-1,1	0,2
6	19,6	19,8	-0,5	10,8	-1,0	0,2
7	20,7	20,8	-0,6	14,9	-1,0	0,1
8	18,2	18,4	-0,8	15,7	-1,3	0,2
9	19,6	19,7	-0,7	16,3	-1,1	0,2
10	19,5	19,8	-0,3	6,7	-1,0	0,2
11	19,5	19,8	-0,3	5,7	-1,0	0,2
12	19,2	19,6	-0,3	5,0	-1,0	0,2
13	-	-	-	-	-	-
14	-110,4	-110,1	-109,2	5,2	-4,1	68,4
15	17,7	18,0	-0,3	7,3	-0,8	0,3
16	16,6	16,9	-0,4	7,4	-0,9	0,3
17	13,8	14,1	-0,6	7,4	-0,4	0,3
18	11,8	12,1	-0,4	7,6	-0,5	0,3
19	7,6	7,9	-1,1	7,5	0,0	0,9
20	4,7	5,1	-0,9	7,8	0,0	0,6

C.4 STIELTJESKADE, ROTTERDAM

C.4.1 COLLECTION OF DATA

terrain loads	
parameter	value
$F_{LM1,rep,i}$ [kN]	150
$Q_{LM1,rep,i}$ [kN/m ²]	9.0
$Q_{LM1,rep}$ [kN/m ²]	2.5
α_Q [-]	0.6
W_{LM1} [m]	12.0
$a_{LM1,x}$ [m]	4.0
$S_{LM1,x}$ [m]	2.0
$S_{LM1,y}$ [m]	1.2

mooring forces			
no. [-]	$y_{mr,i}$ [m]	$F_{mr,i}$ [kN]	$\alpha_{mr,i}$ [°]
1	5.00	50	30
2	15.00	50	60

surface water	
parameter	value
Z_{MHW} [m NAP]	+1.27
γ_w [kN/m ³]	10.0

retaining wall	
parameter	value
γ_{wall} [kN/m ³]	16.0
$Z_{wall,top}$ [m NAP]	+3.60
$Z_{wall,btm}$ [m NAP]	-0.35
$X_{wall,top}$ [m NAP]	0.510
E_{wall} [N/mm ²]	2.00×10^4

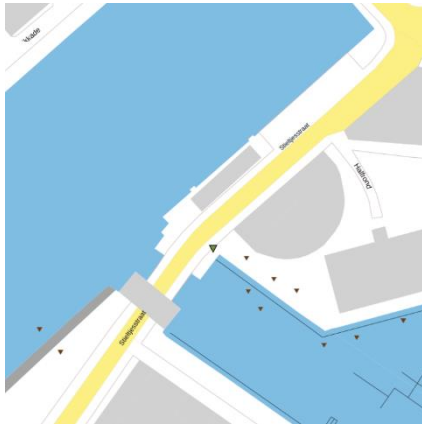
retaining wall coordinates		
no.	$X_{wall,i}$ [m]	$Z_{wall,i}$ [m NAP]
1	0.13	-0.35
2	2.12	-0.35
3	2.12	+1.05
4	1.52	+1.05
5	1.52	+3.20
6	1.12	+3.30
7	1.12	+3.60
8	0.51	+3.60

pile row									
no.	$x_{pile,i}$ [m]	$z_{head,i}$ [m NAP]	$z_{tip,i}$ [m NAP]	$d_{head,i}$ [mm]	$d_{tip,i}$ [mm]	$\alpha_{pile,i}$ [°]	$A_{gr,i}$ [m ²]	E_{pile} [N/mm ²]	$z_{low,i}$ [m NAP]
1	0.33	-0.60	-20.00	250	81.7	-5.7	0.45	3.6×10^3	-4.65
2	1.33	-0.60	-20.00	250	81.7	-3.8	0.45	3.6×10^3	-4.21
3	2.33	-0.60	-20.00	250	81.7	-2.9	0.45	3.6×10^3	-3.35
4	3.33	-0.60	-20.00	250	81.7	0	0.45	3.6×10^3	-2.46
5	4.33	-0.60	-20.00	250	81.7	0	0.45	3.6×10^3	-1.68
6	5.33	-0.60	-20.00	250	81.7	0	0.45	3.6×10^3	-0.91
7	6.33	-0.60	-20.00	250	81.7	0	0.45	3.6×10^3	-0.60
1sub	0.85	-0.60	-20.00	250	81.7	-18.4	0.45	3.6×10^3	-4.65
2sub	2.85	-0.60	-20.00	250	81.7	-18.4	0.45	3.6×10^3	-3.65

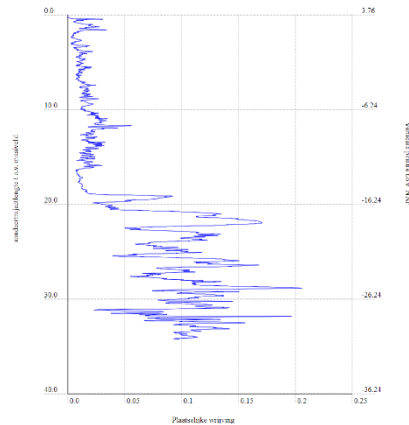
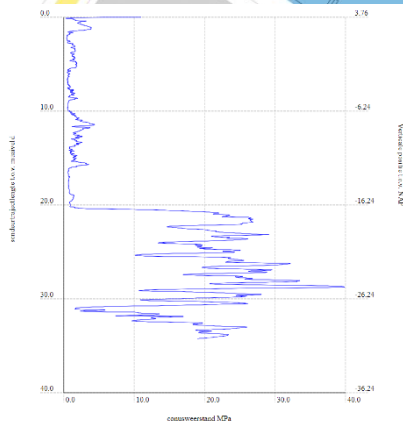
pile cap beam	
parameter	value
γ_{pcb} [kN/m ³]	4.20
W_{pcb} [mm]	310
H_{pcb} [mm]	180
L_{pcb} [mm]	6805
S_{pcb} [m]	0.90
E_{pcb} [N/mm ²]	0.12×10^3

floor element	
parameter	value
γ_{floor} [kN/m ³]	4.20
W_{floor} [mm]	250
H_{floor} [mm]	70
L_{floor} [mm]	900
E_{floor} [N/mm ²]	0.12×10^3

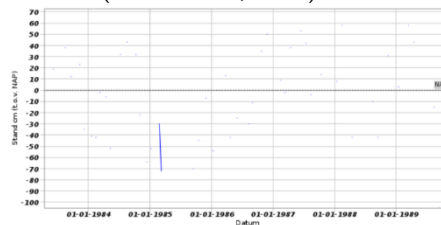
cross-beam	
parameter	value
γ_{cross} [kN/m ³]	4.20
$x_{cross,1}$ [m]	0.88
$x_{cross,2}$ [m]	2.88
W_{cross} [mm]	280
H_{cross} [mm]	250
L_{cross} [mm]	900
E_{cross} [N/mm ²]	0.12×10^3



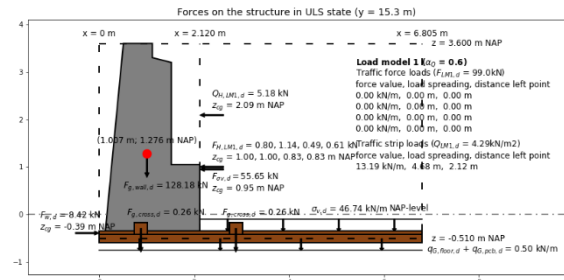
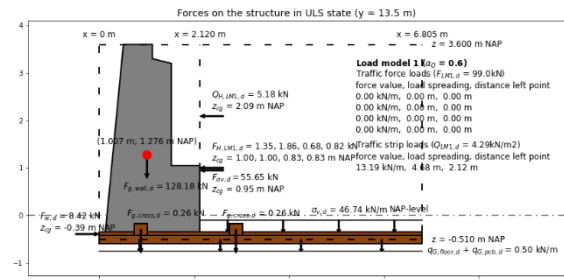
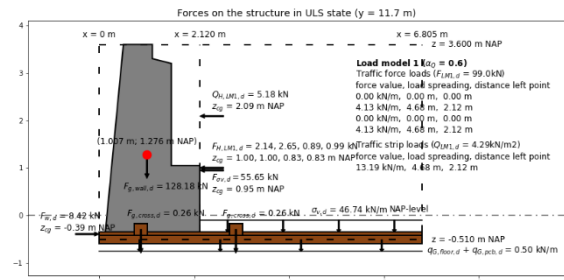
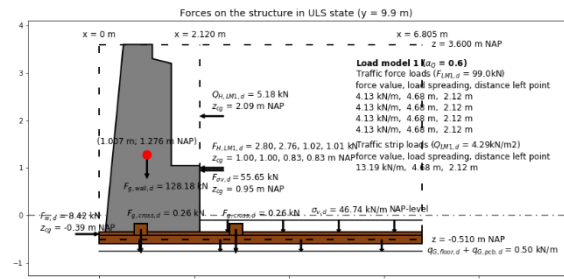
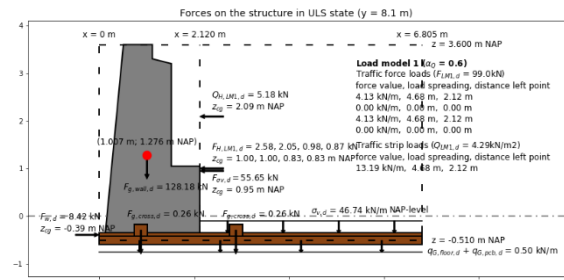
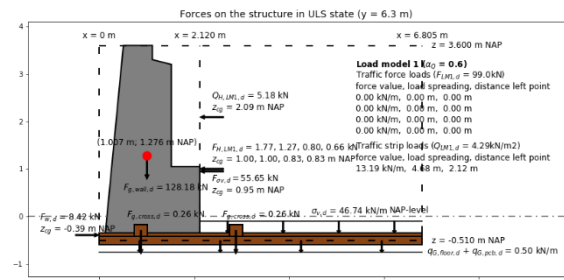
id: CPT000000056860
 date: 13-01-2017
 coord: 93723.680, 436182.710 (RD)
 ground level: +3.76 m NAP
 total depth: 34.26 m
 source: (DINOloket, 2017)

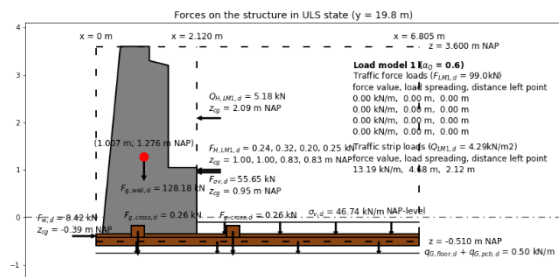
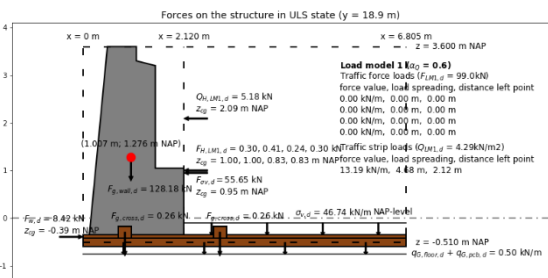
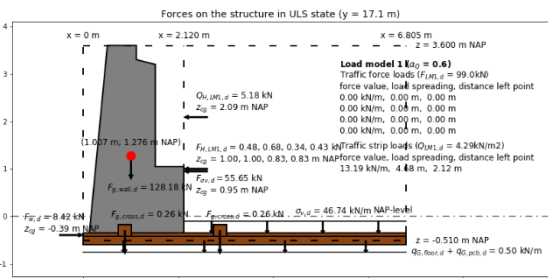


id: B37H0522-001
 date: 13-04-1983 / 14-11-1989
 coord: 93962, 436401 (RD)
 ground level: 3.62 m NAP
 source: (DINOloket, 1989)

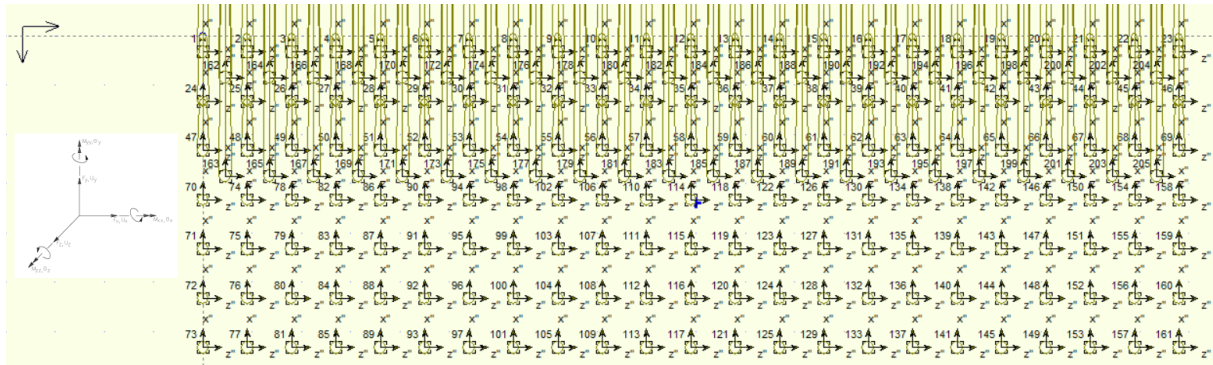


general soil information	
parameter	value
$n_{\text{probe}} [-]$	1
$\xi_3 [-]$	1.26
$\xi_4 [-]$	1.26
$z_{\text{gw}} [\text{m NAP}]$	-0.10
$\gamma_{\text{gw}} [\text{kN/m}^3]$	10.0





input D-pile group	
parameter	value
v [–]	0.499
$z_{\text{soil,top,avg}}$ [m]	–2.40
$E_{\text{soil,top}}$ [kN/m ²]	4.0×10^3
$E_{\text{soil,btm}}$ [kN/m ²]	85.0×10^3
x_{cap} [m]	10.0
y_{cap} [m]	0
z_{cap} [m]	3.40
fixity	free
F_y [kN]	-7.98×10^3
F_z [kN]	-1.28×10^3
M_x [kNm]	-4.01×10^3



horizontal pile displacement						
pile no.	Zsoil [m NAP]		Zmid [m NAP]	Zmid [m]	v _{pile} [m]	figures
	from	to				
12	-4.65	-6.90	-5.78	-5.27	-9.00×10 ⁻⁵	
	-6.90	-12.40	-9.65	-9.14	0	
	-12.40	-16.90	-14.65	-14.14	0	
	-16.90	-20.00	-18.45	-17.94	0	
35	-4.21	-6.90	-5.56	-5.05	6.40×10 ⁻⁵	
	-6.90	-12.40	-9.65	-9.14	0	
	-12.40	-16.90	-14.65	-14.14	0	
	-16.90	-20.00	-18.45	-17.94	0	
58	-3.35	-6.90	-5.13	-4.62	3.68×10 ⁻⁴	
	-6.90	-12.40	-9.65	-9.14	1.60×10 ⁻⁵	
	-12.40	-16.90	-14.65	-14.14	-1.00×10 ⁻⁶	
	-16.90	-20.00	-18.45	-17.94	0	
114	-2.46	-6.90	-4.68	-4.17	-2.91×10 ⁻⁴	
	-6.90	-12.40	-9.65	-9.14	4.00×10 ⁻⁶	
	-12.40	-16.90	-14.65	-14.14	0	
	-16.90	-20.00	-18.45	-17.94	0	
115	-1.68	-6.90	-4.29	-3.78	6.27×10 ⁻³	
	-6.90	-12.40	-9.65	-9.14	-8.66×10 ⁻⁴	
	-12.40	-16.90	-14.65	-14.14	-7.90×10 ⁻⁴	
	-16.90	-20.00	-18.45	-17.94	-1.78×10 ⁻⁴	
116	-0.91	-6.90	-3.91	-3.40	6.57×10 ⁻³	
	-6.90	-12.40	-9.65	-9.14	-1.02×10 ⁻³	
	-12.40	-16.90	-14.65	-14.14	-2.70×10 ⁻⁵	
	-16.90	-20.00	-18.45	-17.94	5.20×10 ⁻⁵	
117	-0.60	-6.90	-3.75	-3.24	6.02×10 ⁻³	
	-6.90	-12.40	-9.65	-9.14	-7.85×10 ⁻⁴	
	-12.40	-16.90	-14.65	-14.14	5.00×10 ⁻⁵	
	-16.90	-20.00	-18.45	-17.94	1.40×10 ⁻⁵	
184	-4.65	-6.90	-5.78	-5.27	-1.46×10 ⁻³	
	-6.90	-12.40	-9.65	-9.14	5.00×10 ⁻⁵	
	-12.40	-16.90	-14.65	-14.14	0	
	-16.90	-20.00	-18.45	-17.94	0	
185	-3.65	-6.90	-5.28	-4.77	-1.22×10 ⁻³	
	-6.90	-12.40	-9.65	-9.14	6.00×10 ⁻⁵	
	-12.40	-16.90	-14.65	-14.14	0	
	-16.90	-20.00	-18.45	-17.94	0	

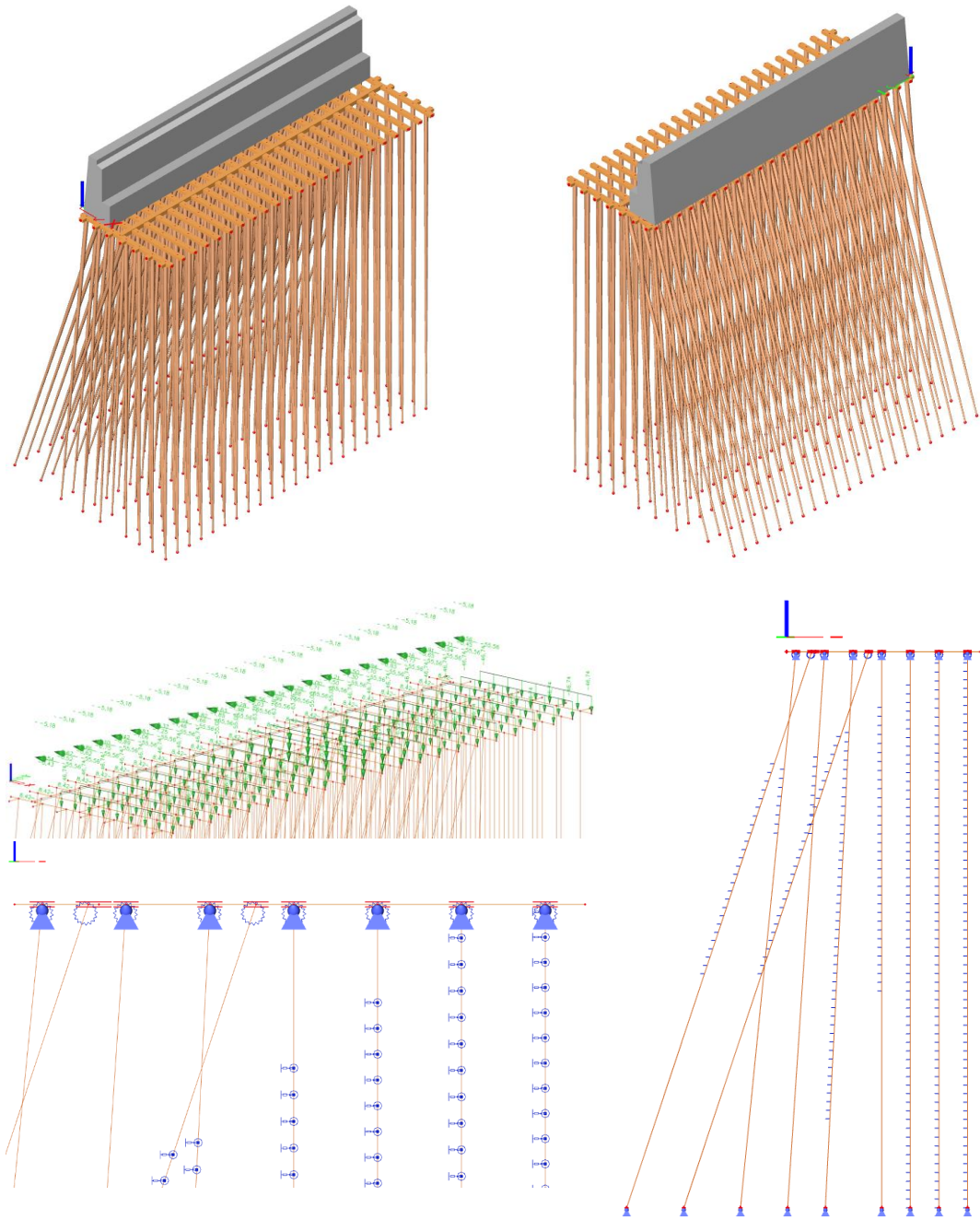
horizontal soil response							
pile no.	z _{soil} [m NAP]		soil type	α [-]	β [-]	k _s [MN/m ³]	p _{soil} [MN/m ²]
	from	to					
1	-4.65	-6.90	peat	1	3.0	1.73×10 ⁻⁴	1.56
	-6.90	-12.40	clay	2/3	2.0	1.99×10 ⁻⁴	0
	-12.40	-16.90	peat	1	3.0	1.30×10 ⁻⁴	0
	-16.90	-20.00	sand	1/3	0.7	9.48×10 ⁻⁴	0
2	-4.21	-6.90	peat	1	3.0	1.73×10 ⁻⁴	1.11
	-6.90	-12.40	clay	2/3	2.0	1.99×10 ⁻⁴	0
	-12.40	-16.90	peat	1	3.0	1.30×10 ⁻⁴	0
	-16.90	-20.00	sand	1/3	0.7	9.48×10 ⁻⁴	0
3	-3.35	-6.90	peat	1	3.0	1.73×10 ⁻⁴	6.38
	-6.90	-12.40	clay	2/3	2.0	1.99×10 ⁻⁴	0.32
	-12.40	-16.90	peat	1	3.0	1.30×10 ⁻⁴	0.01
	-16.90	-20.00	sand	1/3	0.7	9.48×10 ⁻⁴	0
4	-2.46	-6.90	peat	1	3.0	1.73×10 ⁻⁴	5.05
	-6.90	-12.40	clay	2/3	2.0	1.99×10 ⁻⁴	0.08
	-12.40	-16.90	peat	1	3.0	1.30×10 ⁻⁴	0
	-16.90	-20.00	sand	1/3	0.7	9.48×10 ⁻⁴	0
5	-1.68	-6.90	peat	1	3.0	1.73×10 ⁻⁴	108.75
	-6.90	-12.40	clay	2/3	2.0	1.99×10 ⁻⁴	17.23
	-12.40	-16.90	peat	1	3.0	1.30×10 ⁻⁴	10.28
	-16.90	-20.00	sand	1/3	0.7	9.48×10 ⁻⁴	16.87
6	-0.91	-6.90	peat	1	3.0	1.73×10 ⁻⁴	113.96
	-6.90	-12.40	clay	2/3	2.0	1.99×10 ⁻⁴	20.29
	-12.40	-16.90	peat	1	3.0	1.30×10 ⁻⁴	0.35
	-16.90	-20.00	sand	1/3	0.7	9.48×10 ⁻⁴	4.93
7	-0.60	-6.90	peat	1	3.0	1.73×10 ⁻⁴	104.42
	-6.90	-12.40	clay	2/3	2.0	1.99×10 ⁻⁴	15.62
	-12.40	-16.90	peat	1	3.0	1.30×10 ⁻⁴	0.65
	-16.90	-20.00	sand	1/3	0.7	9.48×10 ⁻⁴	1.33
1sub	-4.65	-6.90	peat	1	3.0	1.73×10 ⁻⁴	25.32
	-6.90	-12.40	clay	2/3	2.0	1.99×10 ⁻⁴	0.99
	-12.40	-16.90	peat	1	3.0	1.30×10 ⁻⁴	0
	-16.90	-20.00	sand	1/3	0.7	9.48×10 ⁻⁴	0
2sub	-3.65	-6.90	peat	1	3.0	1.73×10 ⁻⁴	21.16
	-6.90	-12.40	clay	2/3	2.0	1.99×10 ⁻⁴	1.19
	-12.40	-16.90	peat	1	3.0	1.30×10 ⁻⁴	0
	-16.90	-20.00	sand	1/3	0.7	9.48×10 ⁻⁴	0

C.4.4 JOINT STIFFNESS

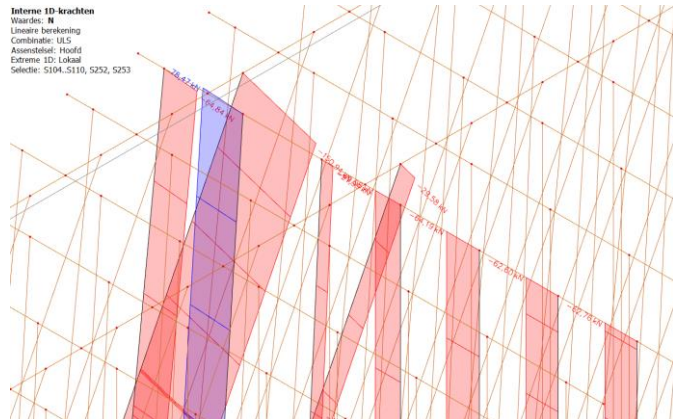
calculation joint stiffness	
parameter	value
H _{mor} [mm]	90.0
W _{notch} [mm]	25.0
a ₁ [mm]	113.0
a ₂ [mm]	30.0
a ₃ [mm]	30.0
k _{0,1} [N/mm]	2.84×10 ⁵
k _{90,1} [N/mm]	9.47×10 ³

$k_{0,2}$ [N/mm]	6.35×10^5
$k_{90,2}$ [N/mm]	2.12×10^4
$k_{0,3}$ [N/mm]	6.35×10^5
$k_{90,3}$ [N/mm]	2.12×10^4
$k_{eq,1}$ [N/mm]	9.16×10^3
$k_{eq,2}$ [N/mm]	2.05×10^4
$k_{eq,3}$ [N/mm]	2.05×10^4
k_r [MNm/rad]	0.15

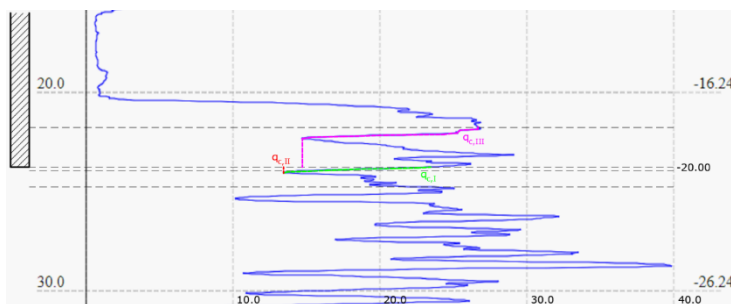
C.4.5 AXIAL PILE HEAD FORCES



axial pile head forces (y = 9.90 m)	
pile row	F _{head,d} [kN]
1	-64.84
2	+78.47
3	-21.99
4	-49.08
5	-64.19
6	-62.60
7	-62.76
1sub	-150.94
2sub	-29.58



C.4.6 AXIAL PILE FORCES AND RESISTANCES



cone resistances	
parameter	value
q _{CPT,I} [MPa]	15.0
q _{CPT,II} [MPa]	13.5
q _{CPT,III} [MPa]	15.0

maximum pile tip resistance				
pile row	A _{tip} [mm ²]	q _{b,max} [MPa]	R _{b,max,k} [kN]	R _{b,max,d} [kN]
1	5.25×10 ³	10.24	53.71	32.20
3	5.25×10 ³	10.24	53.71	32.20
4	5.25×10 ³	10.24	53.71	32.20
5	5.25×10 ³	10.24	53.71	32.20
6	5.25×10 ³	10.24	53.71	32.20
7	5.25×10 ³	10.24	53.71	32.20
1sub	5.25×10 ³	10.24	53.71	32.20
2sub	5.25×10 ³	10.24	53.71	32.20

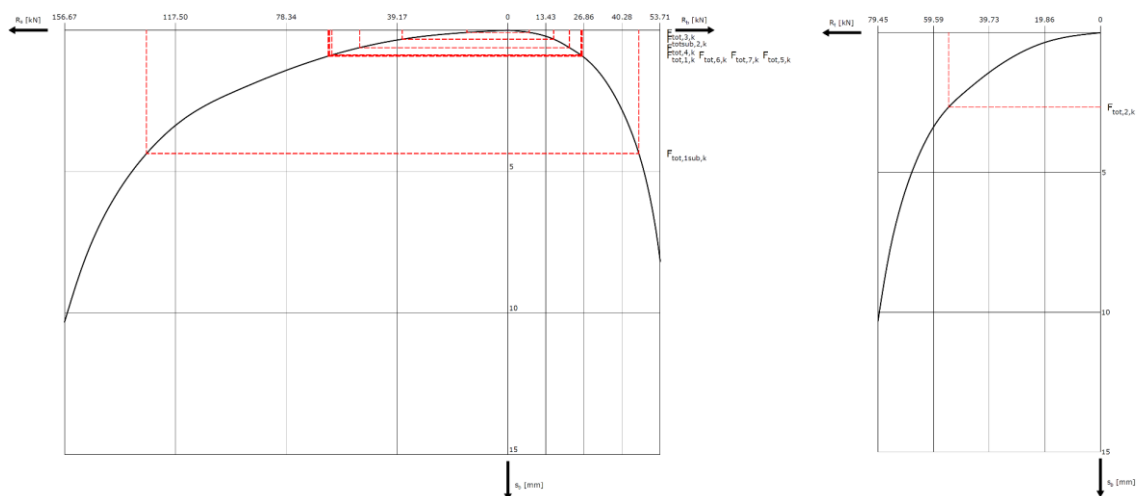
maximum pile shaft resistance ($z_{tp} = -16.90$ m NAP)							
pile row	ΔL [m]	$z_{\Delta L,avg}$ [m]	$d_{\Delta L,avg}$ [mm]	$C_{\Delta L,avg}$ [mm]	$q_{s,max}$ [MPa]	$R_{s,max,k}$ [kN]	$R_{s,max,d}$ [kN]
1	3.10	17.85	89.4	280.8	0.18	156.67	93.92
3	3.10	17.85	89.4	280.8	0.18	156.67	93.92
4	3.10	17.85	89.4	280.8	0.18	156.67	93.92
5	3.10	17.85	89.4	280.8	0.18	156.67	93.92
6	3.10	17.85	89.4	280.8	0.18	156.67	93.92
7	3.10	17.85	89.4	280.8	0.18	156.67	93.92
1sub	3.10	17.85	89.4	280.8	0.18	156.67	93.92
2sub	3.10	17.85	89.4	280.8	0.18	156.67	93.92

negative skin friction ($z_{tp} = -16.90$ m NAP)											
pile row	z_{mid} [m NAP]	t_i [m]	γ'_i [kN/m ³]	$z_{pile,mid}$ [m]	$C_{pile,mid}$ [m]	m_i [–]	$\sigma'_{m,i}$ [kN/m ²]	$\sigma_{nsf,i}$ [kN/m ²]	$F_{nsf,i}$ [kN]	$F_{nsf,k}$ [kN]	$F_{nsf,d}$ [kN]
1	–5.78	2.25	2.0	5.18	0.583	0.32	3.20	1.30	0.59	23.15	27.78
	–9.65	5.50	10.0	9.05	0.466	0.26	30.19	28.11	12.65		
	–14.65	4.50	3.0	14.05	0.349	0.19	21.56	22.03	9.91		
3	–5.13	3.55	2.0	4.53	0.605	0.34	4.15	2.95	1.33	24.28	29.13
	–9.65	5.50	10.0	9.05	0.466	0.26	30.32	28.83	12.97		
	–14.65	4.50	3.0	14.05	0.349	0.19	21.66	22.16	9.97		
4	–4.68	4.44	2.0	4.08	0.621	0.34	4.54	4.34	1.95	25.06	30.07
	–9.65	5.50	10.0	9.05	0.466	0.26	30.41	29.13	13.11		
	–14.65	4.50	3.0	14.05	0.349	0.19	21.70	22.22	10.00		
5	–4.29	5.22	2.0	3.69	0.635	0.35	4.77	5.67	2.55	25.75	30.90
	–9.65	5.50	10.0	9.05	0.466	0.26	30.47	29.30	13.19		
	–14.65	4.50	3.0	14.05	0.349	0.19	21.72	22.25	10.01		
6	–3.91	5.99	2.0	3.31	0.649	0.36	4.91	7.07	3.18	26.44	31.72
	–9.65	5.50	10.0	9.05	0.466	0.26	30.50	29.41	13.23		
	–14.65	4.50	3.0	14.05	0.349	0.19	21.73	22.27	10.02		
7	–3.75	6.30	2.0	3.15	0.655	0.36	4.94	7.66	3.45	26.71	32.06
	–9.65	5.50	10.0	9.05	0.466	0.26	30.51	29.43	13.24		
	–14.65	4.50	3.0	14.05	0.349	0.19	21.74	22.27	10.02		
1sub	–5.78	2.25	2.0	5.18	0.583	0.32	3.20	1.30	0.59	23.15	27.78
	–9.65	5.50	10.0	9.05	0.467	0.26	30.09	28.11	12.65		
	–14.65	4.50	3.0	14.05	0.349	0.19	21.56	22.03	9.91		
2sub	–5.28	3.25	2.0	4.68	0.600	0.33	3.97	2.53	1.14	24.01	28.82
	–9.65	5.50	10.0	9.05	0.466	0.26	30.27	28.70	12.91		
	–14.65	4.50	3.0	14.05	0.349	0.19	21.64	22.14	9.96		

tensile resistance										
pile row	z_{mid} [m NAP]	t_i [m]	$z_{pile,mid}$ [m]	$C_{pile,mid}$ [m]	$\alpha_{t,i}$ [–]	$q_{CPT,d,i}$ [MPa]	$q'_{t,d,i}$ [MPa]	$R_{t,d,i}$ [kN]	$R_{t,d}$ [kN]	$R_{t,k}$ [kN]
2	–5.56	2.69	4.96	0.590	0.0035	0.426	0.001	2.37	42.34	79.45
	–9.65	5.50	9.05	0.466	0.0035	0.639	0.002	5.74		
	–14.65	4.50	14.05	0.349	0.0035	0.320	0.001	1.76		
	–18.45	3.10	17.85	0.281	0.0070	5.33	0.037	32.47		

C.4.7 PILE TIP SETTLEMENT AND FORCE

total pile head force	
pile row	F_{tot} [kN]
1	-82.77
2	72.44
3	-24.94
4	-75.27
5	-90.13
6	-89.02
7	-89.50
1sub	-196.72
2sub	-51.94



pile settlement and rise					
pile row	$R_{b,k}$ [kN]	$R_{s,k}$ [kN]	s_b [mm]	$R_{t,k}$ [kN]	s_{head} [mm]
1	25.8	62.2	0.9	—	—
2	—	—	—	54.2	2.7
3	7.5	14.5	0.1	—	—
4	21.7	52.4	0.6	—	—
5	26.3	63.6	0.9	—	—
6	26.0	63.0	0.9	—	—
7	26.2	63.3	0.9	—	—
1sub	46.3	127.8	4.4	—	—
2sub	16.2	37.4	0.3	—	—

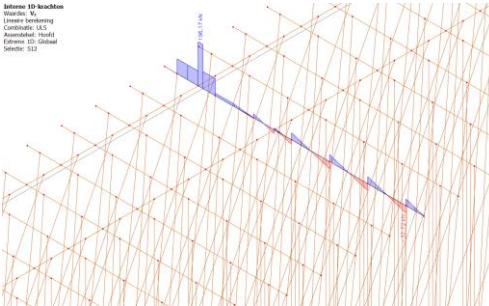
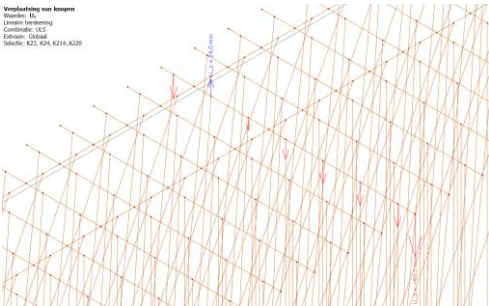
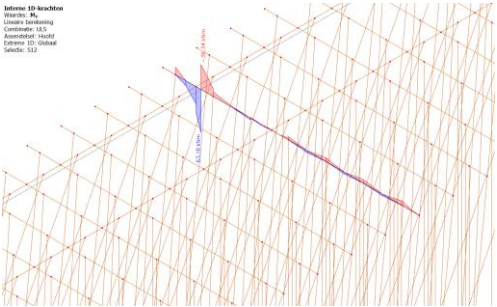
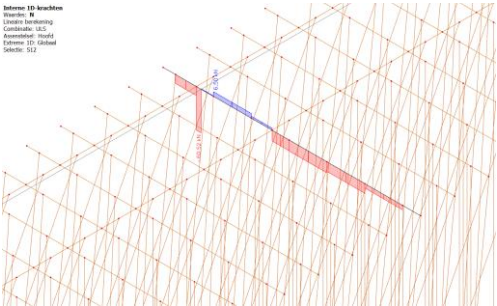
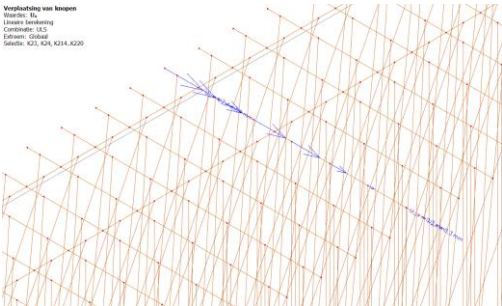
axial pile tip stiffness	
pile row	k_{ax} [MN/m]
1	97.8
2	20.1
3	220.0
4	123.5
5	99.9
6	98.9
7	99.4
1sub	39.6
2sub	178.7

C.4.8 NEUTRAL PLANE

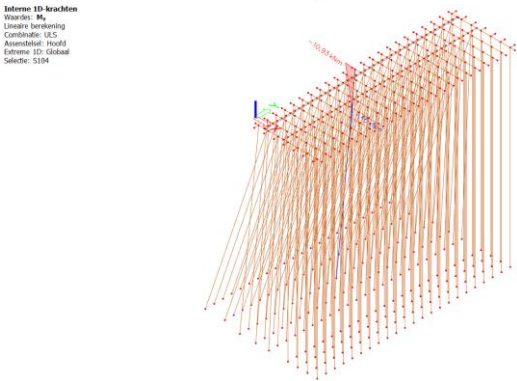
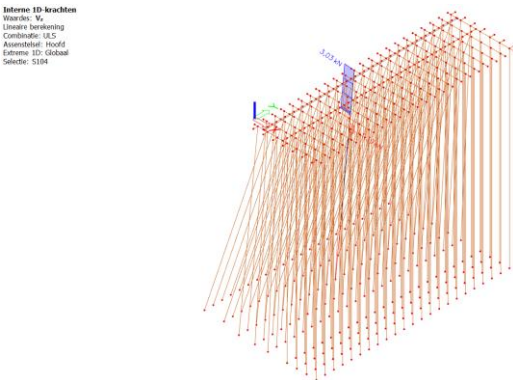
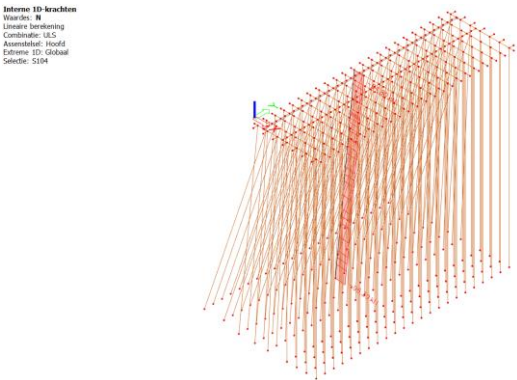
total soil settlement				
pile row	Z _{top} [m NAP]	t _i [m]	S _{soil,tot,i} [m]	S _{soil,tot} [m]
1	-4.65	2.25	0.207	0.563
	-6.90	5.50	0.081	
	-12.40	4.50	0.275	
3	-3.35	3.55	0.327	0.683
	-6.90	5.50	0.081	
	-12.40	4.50	0.275	
4	-2.46	4.44	0.408	0.764
	-6.90	5.50	0.081	
	-12.40	4.50	0.275	
5	-1.68	5.22	0.480	0.836
	-6.90	5.50	0.081	
	-12.40	4.50	0.275	
6	-0.91	5.99	0.551	0.907
	-6.90	5.50	0.081	
	-12.40	4.50	0.275	
7	-0.60	6.30	0.580	0.936
	-6.90	5.50	0.081	
	-12.40	4.50	0.275	
1sub	-4.65	2.25	0.207	0.563
	-6.90	5.50	0.081	
	-12.40	4.50	0.275	
2sub	-3.65	3.25	0.299	0.655
	-6.90	5.50	0.081	
	-12.40	4.50	0.275	

influence neutral plane					
pile row	value	R _{s,max,k} [kN]	R _{s,max,d} [kN]	F _{nsf,k} [kN]	F _{nsf,d} [kN]
1	maximum	156.67	93.92	23.15	27.78
3	maximum	156.67	93.92	24.28	29.13
4	maximum	156.67	93.92	25.06	30.07
5	maximum	156.67	93.92	25.75	30.90
6	maximum	156.67	93.92	26.44	31.72
7	maximum	156.67	93.92	26.71	32.06
1sub	maximum	156.67	93.92	23.15	27.78
2sub	maximum	156.67	93.92	24.01	28.82

C.4.9 CALCULATION MODEL



extreme values (y = 9.90 m)				
parameter	minimum		maximum	
	value	pile row	value	pile row
$u_{x,int}$ [mm]	0.3	7	7.4	1
$u_{z,int}$ [mm]	-60.2	7	24.0	2
N_{int} [kN]	-60.5	1-2	6.5	2-3
$V_{z,int}$ [kN]	-32.7	7	196.2	1-2
$M_{y,int}$ [kNm]	-36.3	1-2	63.2	1-2



extreme values in pile at first row (x = 0.33 m, y = 9.90 m)		
parameter	minimum value	maximum value
N_{int} [kN]	-96.4	-94.8
$V_{z,int}$ [kN]	-1.4	3.0
$M_{y,int}$ [kNm]	-10.9	1.5

C.4.10 STRUCTURAL DEFICIENCIES

changes in structural model		
modification	changing variable	adaptations
1	$p_m = 5 \text{ mm}$	$d_{head,1...7} (y = 0.00 \text{ m}), \dots, d_{head,1...7} (y = 19.80 \text{ m}): 250 \text{ mm} \rightarrow 230 \text{ mm}$
		$d_{tip,1...7} (y = 0.00 \text{ m}), \dots, d_{tip,1...7} (y = 19.80 \text{ m}): 81.7 \text{ mm} \rightarrow 66.7 \text{ mm}$
		$d_{head,sub,1,2} (y = 0.45 \text{ m}), \dots, d_{head,sub,1,2} (y = 19.35 \text{ m}): 250 \text{ mm} \rightarrow 230 \text{ mm}$
		$d_{tip,sub,1,2} (y = 0.45 \text{ m}), \dots, d_{tip,sub,1,2} (y = 19.35 \text{ m}): 81.7 \text{ mm} \rightarrow 66.7 \text{ mm}$
2	$p_m = 5 \text{ mm}$	$d_{head,1...7} (y = 9.90 \text{ m}): 250 \text{ mm} \rightarrow 230 \text{ mm}$
		$d_{tip,1...7} (y = 9.90 \text{ m}): 81.7 \text{ mm} \rightarrow 66.7 \text{ mm}$
		$d_{head,sub,1,2} (y = 10.35 \text{ m}): 250 \text{ mm} \rightarrow 230 \text{ mm}$
		$d_{tip,sub,1,2} (y = 10.35 \text{ m}): 81.7 \text{ mm} \rightarrow 66.7 \text{ mm}$
3	$p_m = 5 \text{ mm}$	$d_{head,1,2} (y = 0.00 \text{ m}), \dots, d_{head,1,2} (y = 19.80 \text{ m}): 250 \text{ mm} \rightarrow 230 \text{ mm}$
		$d_{tip,1,2} (y = 0.00 \text{ m}), \dots, d_{tip,1,2} (y = 19.80 \text{ m}): 81.7 \text{ mm} \rightarrow 66.7 \text{ mm}$
4	$p_m = 15 \text{ mm}$	$d_{head,1...7} (y = 0.00 \text{ m}), \dots, d_{head,1...7} (y = 19.80 \text{ m}): 250 \text{ mm} \rightarrow 210 \text{ mm}$
		$d_{tip,1...7} (y = 0.00 \text{ m}), \dots, d_{tip,1...7} (y = 19.80 \text{ m}): 81.7 \text{ mm} \rightarrow 56.7 \text{ mm}$
		$d_{head,sub,1,2} (y = 0.45 \text{ m}), \dots, d_{head,sub,1,2} (y = 19.35 \text{ m}): 250 \text{ mm} \rightarrow 210 \text{ mm}$
		$d_{tip,sub,1,2} (y = 0.45 \text{ m}), \dots, d_{tip,sub,1,2} (y = 19.35 \text{ m}): 81.7 \text{ mm} \rightarrow 56.7 \text{ mm}$
		$W_{pcb} (y = 0.00 \text{ m}), \dots, W_{pcb} (y = 19.80 \text{ m}): 310 \text{ mm} \rightarrow 300 \text{ mm}$
		$W_{cross,1} (x = 0.88 \text{ m}): 280 \text{ mm} \rightarrow 270 \text{ mm}$
5	$p_m = 15 \text{ mm}$	$W_{cross,2} (x = 2.88 \text{ m}): 280 \text{ mm} \rightarrow 270 \text{ mm}$
		$d_{head,1...7} (y = 9.90 \text{ m}): 250 \text{ mm} \rightarrow 210 \text{ mm}$
		$d_{tip,1...7} (y = 9.90 \text{ m}): 81.7 \text{ mm} \rightarrow 56.7 \text{ mm}$
		$d_{head,sub,1,2} (y = 10.35 \text{ m}): 250 \text{ mm} \rightarrow 210 \text{ mm}$
		$d_{tip,sub,1,2} (y = 10.35 \text{ m}): 81.7 \text{ mm} \rightarrow 56.7 \text{ mm}$
		$W_{pcb} (y = 9.90 \text{ m}): 310 \text{ mm} \rightarrow 300 \text{ mm}$
6	$p_m = 15 \text{ mm}$	$W_{cross,1} (x = 0.88 \text{ m}): 280 \text{ mm} \rightarrow 270 \text{ mm}$
		$W_{cross,2} (x = 2.88 \text{ m}): 280 \text{ mm} \rightarrow 270 \text{ mm}$
		$d_{head,1,2} (y = 0.00 \text{ m}), \dots, d_{head,1,2} (y = 19.80 \text{ m}): 250 \text{ mm} \rightarrow 210 \text{ mm}$
7	$p_m = 15 \text{ mm}$	$d_{tip,1,2} (y = 0.00 \text{ m}), \dots, d_{tip,1,2} (y = 19.80 \text{ m}): 81.7 \text{ mm} \rightarrow 56.7 \text{ mm}$
		$W_{pcb} (y = 0.00 \text{ m}), \dots, W_{pcb} (y = 19.80 \text{ m}): 310 \text{ mm} \rightarrow 300 \text{ mm}$
		$d_{head,1...7} (y = 0.00 \text{ m}), \dots, d_{head,1...7} (y = 19.80 \text{ m}): 250 \text{ mm} \rightarrow 180 \text{ mm}$
8	$p_m = 30 \text{ mm}$	$d_{tip,1...7} (y = 0.00 \text{ m}), \dots, d_{tip,1...7} (y = 19.80 \text{ m}): 81.7 \text{ mm} \rightarrow 41.7 \text{ mm}$
		$d_{head,sub,1,2} (y = 0.45 \text{ m}), \dots, d_{head,sub,1,2} (y = 19.35 \text{ m}): 250 \text{ mm} \rightarrow 180 \text{ mm}$
		$d_{tip,sub,1,2} (y = 0.45 \text{ m}), \dots, d_{tip,sub,1,2} (y = 19.35 \text{ m}): 81.7 \text{ mm} \rightarrow 41.7 \text{ mm}$
		$W_{pcb} (y = 0.00 \text{ m}), \dots, W_{pcb} (y = 19.80 \text{ m}): 310 \text{ mm} \rightarrow 270 \text{ mm}$
		$W_{cross,1} (x = 0.88 \text{ m}): 280 \text{ mm} \rightarrow 240 \text{ mm}$
		$W_{cross,2} (x = 2.88 \text{ m}): 280 \text{ mm} \rightarrow 240 \text{ mm}$
9	$p_m = 30 \text{ mm}$	$d_{head,1...7} (y = 9.90 \text{ m}): 250 \text{ mm} \rightarrow 180 \text{ mm}$
		$d_{tip,1...7} (y = 9.90 \text{ m}): 81.7 \text{ mm} \rightarrow 41.7 \text{ mm}$
		$d_{head,sub,1,2} (y = 10.35 \text{ m}): 250 \text{ mm} \rightarrow 180 \text{ mm}$
		$d_{tip,sub,1,2} (y = 10.35 \text{ m}): 81.7 \text{ mm} \rightarrow 41.7 \text{ mm}$
		$W_{pcb} (y = 9.90 \text{ m}): 310 \text{ mm} \rightarrow 270 \text{ mm}$
		$W_{cross,1} (x = 0.88 \text{ m}): 280 \text{ mm} \rightarrow 240 \text{ mm}$
10	$p_m = 30 \text{ mm}$	$W_{cross,1,2} (x = 2.88 \text{ m}): 280 \text{ mm} \rightarrow 240 \text{ mm}$
		$d_{head,1,2} (y = 0.00 \text{ m}), \dots, d_{head,1,2} (y = 19.80 \text{ m}): 250 \text{ mm} \rightarrow 180 \text{ mm}$
		$d_{tip,1,2} (y = 0.00 \text{ m}), \dots, d_{tip,1,2} (y = 19.80 \text{ m}): 81.7 \text{ mm} \rightarrow 41.7 \text{ mm}$
11	$e_y = 25 \text{ mm}$	$W_{pcb} (y = 0.00 \text{ m}), \dots, W_{pcb} (y = 19.80 \text{ m}): 310 \text{ mm} \rightarrow 270 \text{ mm}$
		$e_{y,pcb} (y = 9.90 \text{ m}): 0 \rightarrow 25 \text{ mm}$
	$e_y = 50 \text{ mm}$	$e_{y,pcb} (y = 9.90 \text{ m}): 0 \rightarrow 50 \text{ mm}$

12	$e_y = 100 \text{ mm}$	$e_{y,pcb} (y = 9.90 \text{ m}): 0 \rightarrow 100 \text{ mm}$
13	$R_{c,max} = 0 \text{ kN}$, $R_{t,max} = 0 \text{ kN}$	$R_{c,pile,1,d} (x = 0.33 \text{ m}, y = 9.90 \text{ m}): 126.12 \text{ kN} \rightarrow 0 \text{ kN}$ $R_{t,pile,2,d} (x = 1.33 \text{ m}, y = 9.90 \text{ m}): 42.34 \text{ kN} \rightarrow 0 \text{ kN}$
14	$R_{c,max} = 0 \text{ kN}$, $R_{t,max} = 0 \text{ kN}$	$R_{c,pile,6} (x = 5.33 \text{ m}, y = 9.90 \text{ m}): 126.12 \text{ kN} \rightarrow 0 \text{ kN}$ $R_{c,pile,7} (x = 6.33 \text{ m}, y = 9.90 \text{ m}): 126.12 \text{ kN} \rightarrow 0 \text{ kN}$
15	$S_b = 5 \text{ mm}$, $S_{head} = 5 \text{ mm}$	$k_{ax,1} (x = 0.33 \text{ m}, y = 9.90 \text{ m}): 97.8 \text{ MN/m} \rightarrow 17.6 \text{ MN/m}$ $k_{ax,2} (x = 1.33 \text{ m}, y = 9.90 \text{ m}): 20.1 \text{ MN/m} \rightarrow 10.8 \text{ MN/m}$ $k_{ax,3} (x = 2.33 \text{ m}, y = 9.90 \text{ m}): 220.0 \text{ MN/m} \rightarrow 4.4 \text{ MN/m}$ $k_{ax,4} (x = 3.33 \text{ m}, y = 9.90 \text{ m}): 123.5 \text{ MN/m} \rightarrow 14.8 \text{ MN/m}$ $k_{ax,5} (x = 4.33 \text{ m}, y = 9.90 \text{ m}): 99.9 \text{ MN/m} \rightarrow 18.0 \text{ MN/m}$ $k_{ax,6} (x = 5.33 \text{ m}, y = 9.90 \text{ m}): 98.9 \text{ MN/m} \rightarrow 17.8 \text{ MN/m}$ $k_{ax,7} (x = 6.33 \text{ m}, y = 9.90 \text{ m}): 99.4 \text{ MN/m} \rightarrow 17.9 \text{ MN/m}$ $k_{ax,1sub} (x = 0.88 \text{ m}, y = 10.35 \text{ m}): 39.6 \text{ MN/m} \rightarrow 34.8 \text{ MN/m}$ $k_{ax,2sub} (x = 2.88 \text{ m}, y = 10.35 \text{ m}): 178.7 \text{ MN/m} \rightarrow 10.7 \text{ MN/m}$
16	$S_b = 5 \text{ mm}$, $S_{head} = 5 \text{ mm}$	$k_{ax,1} (x = 0.33 \text{ m}, y = 0.00 \text{ m}), \dots, k_{ax,1} (x = 0.33 \text{ m}, y = 19.80 \text{ m}): 97.8 \text{ MN/m} \rightarrow 17.6 \text{ MN/m}$ $k_{ax,2} (x = 1.33 \text{ m}, y = 0.00 \text{ m}), \dots, k_{ax,2} (x = 1.33 \text{ m}, y = 19.80 \text{ m}): 20.1 \text{ MN/m} \rightarrow 10.8 \text{ MN/m}$
17	$S_b = 10 \text{ mm}$, $S_{head} = 10 \text{ mm}$	$k_{ax,1} (x = 0.33 \text{ m}, y = 9.90 \text{ m}): 97.8 \text{ MN/m} \rightarrow 8.8 \text{ MN/m}$ $k_{ax,2} (x = 1.33 \text{ m}, y = 9.90 \text{ m}): 20.1 \text{ MN/m} \rightarrow 5.4 \text{ MN/m}$ $k_{ax,3} (x = 2.33 \text{ m}, y = 9.90 \text{ m}): 220.0 \text{ MN/m} \rightarrow 2.2 \text{ MN/m}$ $k_{ax,4} (x = 3.33 \text{ m}, y = 9.90 \text{ m}): 123.5 \text{ MN/m} \rightarrow 7.4 \text{ MN/m}$ $k_{ax,5} (x = 5.33 \text{ m}, y = 9.90 \text{ m}): 99.9 \text{ MN/m} \rightarrow 9.0 \text{ MN/m}$ $k_{ax,6} (x = 6.33 \text{ m}, y = 9.90 \text{ m}): 98.9 \text{ MN/m} \rightarrow 8.9 \text{ MN/m}$ $k_{ax,7} (x = 7.33 \text{ m}, y = 9.90 \text{ m}): 99.4 \text{ MN/m} \rightarrow 9.0 \text{ MN/m}$ $k_{ax,1sub} (x = 0.88 \text{ m}, y = 10.35 \text{ m}): 39.6 \text{ MN/m} \rightarrow 17.4 \text{ MN/m}$ $k_{ax,2sub} (x = 2.88 \text{ m}, y = 10.35 \text{ m}): 178.7 \text{ MN/m} \rightarrow 5.4 \text{ MN/m}$
18	$S_b = 10 \text{ mm}$, $S_{head} = 10 \text{ mm}$	$k_{ax,1} (x = 0.33 \text{ m}, y = 0.00 \text{ m}), \dots, k_{ax,1} (x = 0.33 \text{ m}, y = 19.80 \text{ m}): 97.8 \text{ MN/m} \rightarrow 8.8 \text{ MN/m}$ $k_{ax,2} (x = 1.33 \text{ m}, y = 0.00 \text{ m}), \dots, k_{ax,2} (x = 1.33 \text{ m}, y = 19.80 \text{ m}): 20.1 \text{ MN/m} \rightarrow 5.4 \text{ MN/m}$
19	$S_b = 20 \text{ mm}$, $S_{head} = 20 \text{ mm}$	$k_{ax,1} (x = 0.33 \text{ m}, y = 9.90 \text{ m}): 97.8 \text{ MN/m} \rightarrow 4.4 \text{ MN/m}$ $k_{ax,2} (x = 1.33 \text{ m}, y = 9.90 \text{ m}): 20.1 \text{ MN/m} \rightarrow 2.7 \text{ MN/m}$ $k_{ax,3} (x = 2.33 \text{ m}, y = 9.90 \text{ m}): 220.0 \text{ MN/m} \rightarrow 1.1 \text{ MN/m}$ $k_{ax,4} (x = 3.33 \text{ m}, y = 9.90 \text{ m}): 123.5 \text{ MN/m} \rightarrow 1.8 \text{ MN/m}$ $k_{ax,5} (x = 4.33 \text{ m}, y = 9.90 \text{ m}): 99.9 \text{ MN/m} \rightarrow 4.5 \text{ MN/m}$ $k_{ax,6} (x = 5.33 \text{ m}, y = 9.90 \text{ m}): 98.9 \text{ MN/m} \rightarrow 4.5 \text{ MN/m}$ $k_{ax,7} (x = 6.33 \text{ m}, y = 9.90 \text{ m}): 99.4 \text{ MN/m} \rightarrow 4.5 \text{ MN/m}$ $k_{ax,1sub} (x = 0.88 \text{ m}, y = 10.35 \text{ m}): 39.6 \text{ MN/m} \rightarrow 8.7 \text{ MN/m}$ $k_{ax,2sub} (x = 2.88 \text{ m}, y = 10.35 \text{ m}): 178.7 \text{ MN/m} \rightarrow 2.7 \text{ MN/m}$
20	$S_b = 20 \text{ mm}$, $S_{head} = 20 \text{ mm}$	$k_{ax,1} (x = 0.33 \text{ m}, y = 0.00 \text{ m}), \dots, k_{ax,1} (x = 0.33 \text{ m}, y = 19.80 \text{ m}): 97.8 \text{ MN/m} \rightarrow 4.4 \text{ MN/m}$ $k_{ax,2} (x = 1.33 \text{ m}, y = 0.00 \text{ m}), \dots, k_{ax,2} (x = 1.33 \text{ m}, y = 19.80 \text{ m}): 20.1 \text{ MN/m} \rightarrow 2.7 \text{ MN/m}$

calculation results for pile cap beam ($y = 9.90 \text{ m}$)										
mod.	$u_{x,mod} [\text{mm}]$		$u_{z,mod} [\text{mm}]$		$N_{mod} [\text{kN}]$		$V_{z,mod} [\text{kN}]$		$M_{y,mod} [\text{kNm}]$	
	min.	max.	min.	max.	min.	max.	min.	max.	min.	max.
1	0,3	5,6	-70,7	25,1	-56,3	9,9	-32,7	185,5	-35,5	64,0
2	0,4	7,2	-70,8	26,2	-54,9	7,4	-32,8	177,2	-34,8	61,4
3	0,3	7,1	-60,2	28,9	-59,8	7,0	-32,7	193,2	-36,3	63,2
4	0,4	4,5	-83,7	26,1	-53,1	12,5	-32,8	177,6	-34,9	64,5
5	0,5	7,0	-83,8	27,8	-50,0	8,4	-32,8	159,6	-32,6	58,3
6	0,3	7,2	-61,0	34,7	-59,5	7,1	-32,7	191,6	-36,3	63,2
7	0,5	4,1	-118,1	27,0	-48,3	16,3	-32,8	165,5	-34,1	65,2
8	0,7	7,3	-118,4	29,9	-42,3	10,2	-32,9	129,8	-28,2	51,1
9	0,3	9,8	-68,1	53,6	-61,0	5,6	-32,6	193,8	-36,4	63,0

10	0,3	7,5	-60,2	24,0	-60,4	6,5	-32,7	196,0	-36,3	63,2
11	0,3	7,7	-60,2	23,9	-60,2	6,5	-32,7	195,5	-36,3	63,1
12	0,3	8,3	-60,2	23,8	-59,2	6,6	-32,7	193,3	-36,2	62,9
13	0,3	6,6	-407,5	49,7	-50,8	6,2	-32,7	118,7	-22,8	50,7
14	10,9	74,4	-2.9×10 ⁴	23,5	-60,1	158,3	-147,7	220,9	-290,3	63,2
15	0,3	7,4	-64,7	24,4	-60,0	6,7	-32,7	193,6	-35,9	62,9
16	0,3	7,3	-60,2	26,0	-60,2	6,8	-32,7	194,9	-36,4	63,1
17	0,3	7,3	-70,0	25,6	-58,1	7,0	-32,7	187,2	-34,8	62,3
18	0,3	6,8	-60,2	29,9	-59,3	7,4	-32,7	192,3	-36,3	63,2
19	0,3	7,2	-80,8	27,2	-54,9	8,8	-34,9	175,9	-33,5	61,2
20	0,3	6,1	-60,2	36,6	-57,9	8,4	-32,7	187,9	-36,2	63,2

calculation results for pile in first pile row (x = 0.33 m, y = 9.90 m)						
mod.	N _{mod} [kN]		V _{z,mod} [kN]		M _{y,mod} [kNm]	
	min.	max.	min.	max.	min.	max.
1	-98,7	-97,4	-1,5	3,1	-10,8	1,8
2	-90,7	-89,4	-1,3	2,7	-9,4	1,5
3	-91,8	-90,5	-1,3	2,7	-9,5	1,5
4	-100,1	-99,2	-1,5	3,1	-10,4	2,1
5	-83,6	-82,6	-1,1	2,3	-7,8	1,5
6	-86,6	-85,6	-1,1	2,3	-8,1	1,5
7	-102,1	-101,4	-1,8	2,9	-9,5	2,3
8	-69,5	-68,7	-0,9	1,5	-5,0	1,1
9	-74,7	-74,0	-1,0	1,7	-5,7	1,3
10	-96,4	-94,8	-1,4	3,0	-10,9	1,5
11	-96,3	-94,7	-1,4	3,0	-10,9	1,5
12	-95,8	-94,2	-1,4	3,0	-10,8	1,4
13	-	-	-	-	-	-
14	-96,5	-94,9	-1,3	3,0	-10,9	1,4
15	-94,1	-92,5	-1,3	2,9	-10,4	1,4
16	-94,8	-93,2	-1,3	2,9	-10,5	1,4
17	-91,6	-89,9	-1,2	2,7	-9,8	1,3
18	-93,0	-91,4	-1,3	2,8	-9,9	1,3
19	-86,9	-85,2	-1,1	2,4	-8,8	1,1
20	-89,5	-87,8	-1,1	2,5	-8,8	1,2

C.5 TOUSSAINTKADE, THE HAGUE

C.5.1 COLLECTION OF DATA

terrain loads	
parameter	value
F _{LM1,rep,i} [kN]	150
Q _{LM1,rep,i} [kN/m ²]	9.0
Q _{LM1,rep} [kN/m ²]	2.5
α _Q [-]	0.7
W _{LM1} [m]	2.46
a _{LM1,x} [m]	0.44
S _{LM1,x} [m]	2.0
S _{LM1,y} [m]	1.2

trees			
no. [-]	$x_{tree,i}$ [m]	$y_{tree,i}$ [m]	$F_{tree,i}$ [kN]
1	1.50	5.00	25
2	1.50	15.00	25

surface water	
parameter	value
z_{MHW} [m NAP]	-0.43
γ_w [kN/m ³]	10.0

retaining wall	
parameter	value
γ_{wall} [kN/m ³]	16.0
$z_{wall,top}$ [m NAP]	+0.55
$z_{wall,btm}$ [m NAP]	-1.30
$x_{wall,top}$ [m NAP]	0.28
E_{wall} [N/mm ²]	10.0
γ_{wall} [kN/m ³]	1.0
$z_{wall,top}$ [m NAP]	1.40×10^4

fortification		
no. [-]	$y_{wall,fort}$ [m]	$W_{wall,fort}$ [m]
1	10.00	1.00

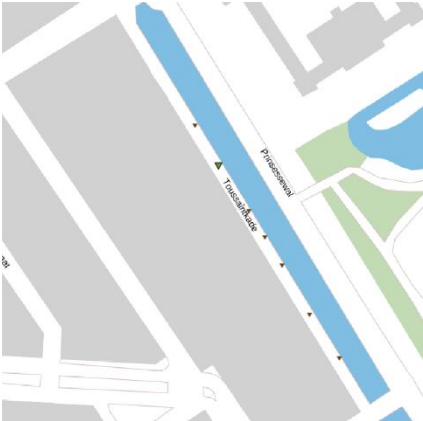
retaining wall coordinates				
no. [-]	$x_{wall,i}$ [m]	$z_{wall,i}$ [m NAP]	$x_{wall,fort,i}$ [m]	$z_{wall,fort,i}$ [m]
1	0.20	-1.24	0.20	-1.24
2	1.00	-1.24	1.50	-1.24
3	1.00	-0.95	1.50	-0.95
4	0.90	-0.95	1.40	-0.95
5	0.90	-0.65	1.40	-0.65
6	0.80	-0.65	1.29	-0.65
7	0.80	-0.43	1.29	-0.25
8	0.95	-0.43	1.22	+0.35
9	0.95	-0.13	0.72	+0.35
10	0.72	+0.35	0.72	+0.55
11	0.72	+0.55	0.28	+0.55
12	0.28	+0.55	0.28	+0.35
13	0.28	+0.35	–	–

pile row									
no.	$x_{pile,i}$ [m]	$z_{head,i}$ [m NAP]	$z_{tip,i}$ [m NAP]	$d_{head,i}$ [mm]	$d_{tip,i}$ [mm]	$\alpha_{pile,i}$ [°]	$A_{gr,i}$ [m ²]	E_{pile} [N/mm ²]	$z_{low,i}$ [m NAP]
1	0.29	-1.42	-5.50	180	142.3	0	0.38	3.6×10^3	-1.83
2	0.78	-1.42	-5.50	180	142.3	0	0.38	3.6×10^3	-1.42
fort	2.80	-1.42	-5.50	180	142.3	-14.0	0.50	3.6×10^3	-1.42

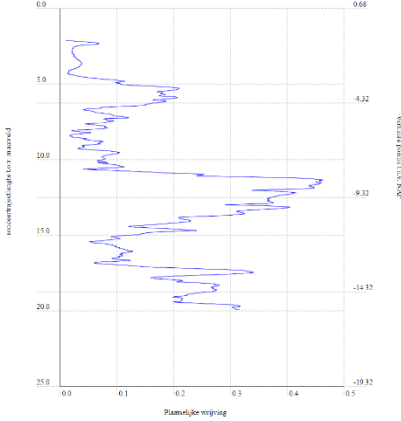
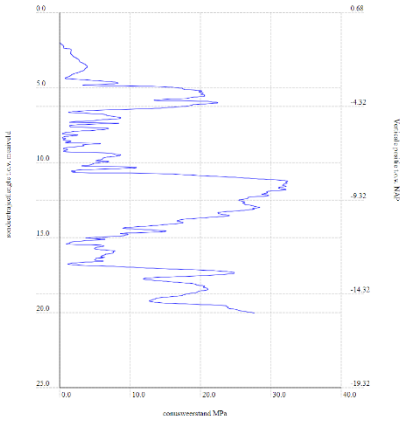
pile cap beam	
parameter	value
γ_{pcb} [kN/m ³]	4.20
W_{pcb} [mm]	160
H_{pcb} [mm]	120
L_{pcb} [mm]	1100
S_{pcb} [m]	3200
E_{pcb} [N/mm ²]	1.00
γ_{pcb} [kN/m ³]	0.12×10^3

floor element	
parameter	value
γ_{floor} [kN/m ³]	4.20
W_{floor} [mm]	200
H_{floor} [mm]	60
L_{floor} [mm]	1000
E_{floor} [N/mm ²]	0.12×10^3

cross-beam	
parameter	value
γ_{cross} [kN/m ³]	4.20
x_{cross} [m]	0.30
W_{cross} [mm]	180
H_{cross} [mm]	180
L_{cross} [mm]	1160
E_{cross} [N/mm ²]	0.12×10^3

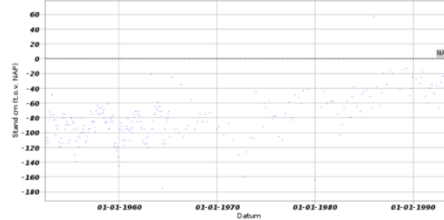


id: CPT000000097117
date: 11-06-2010
coord: 80616.370, 455361.600 (RD)
ground level: +0.68 m NAP
total depth: 19.98 m
source: (DINOloket, 2010)





id: B30G0946
date: 28-05-1952 / 16-12-1993
coord: 80950, 455340 (RD)
ground level: +2.25 m NAP
source: (DINOloket, 1993)



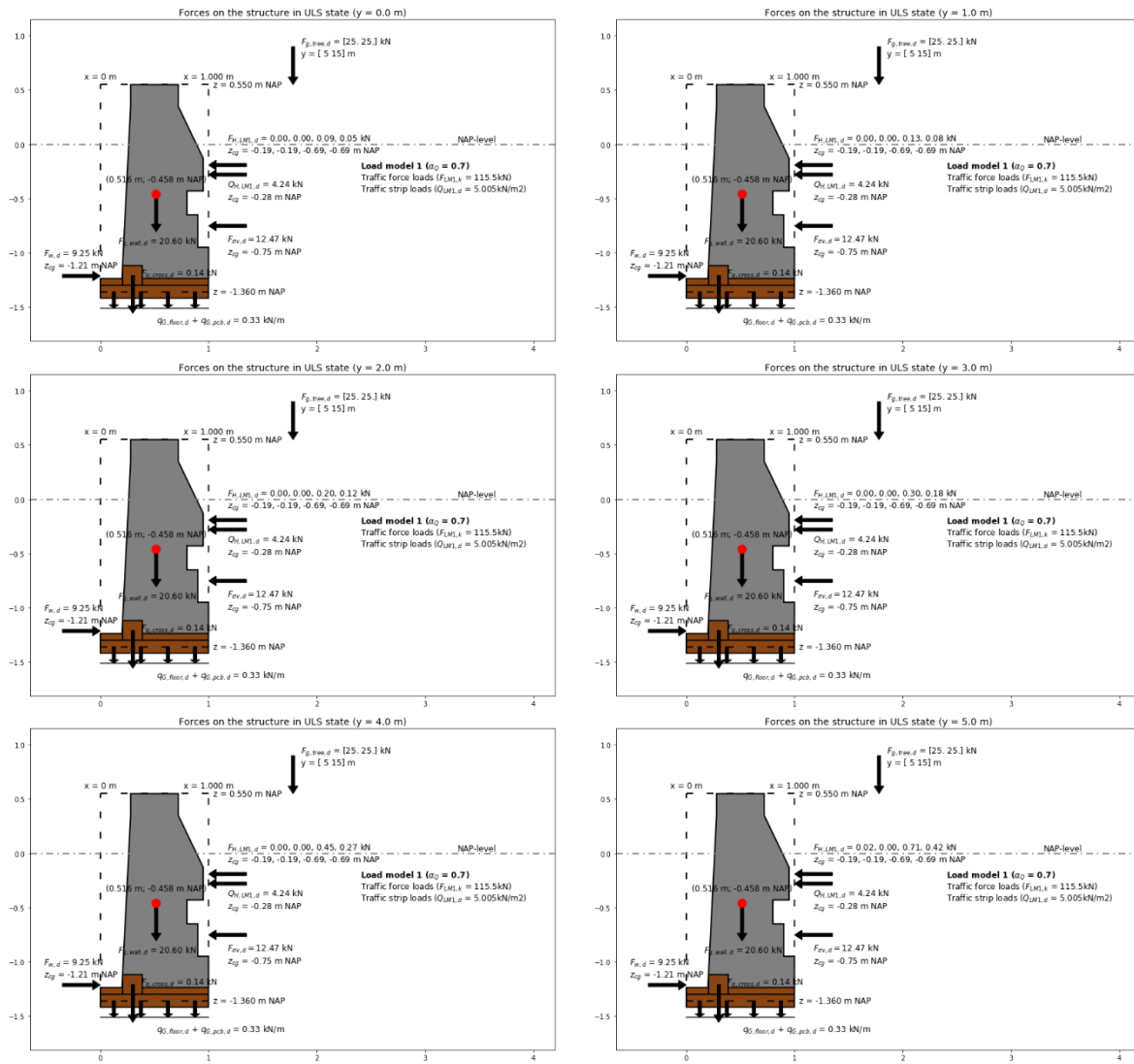
general soil information	
parameter	value
n_{probe} [-]	1
ξ_3 [-]	1.26
ξ_4 [-]	1.26
z_{gw} [m NAP]	-0.60
γ_{gw} [kN/m ³]	10.0

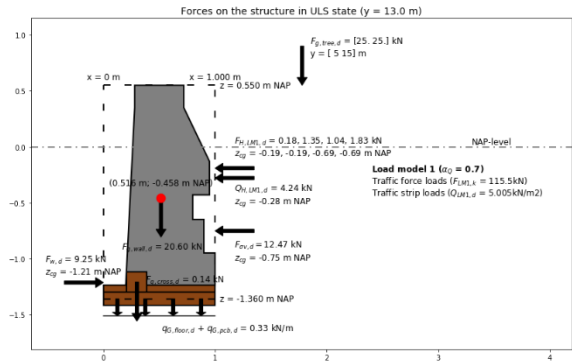
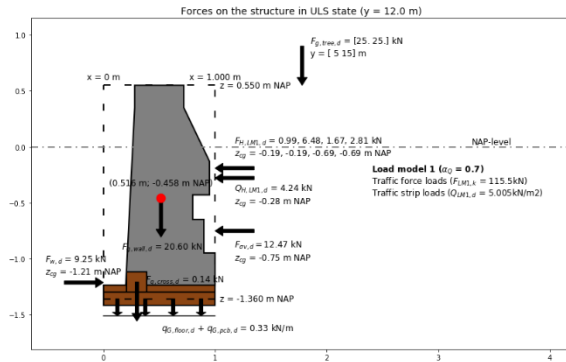
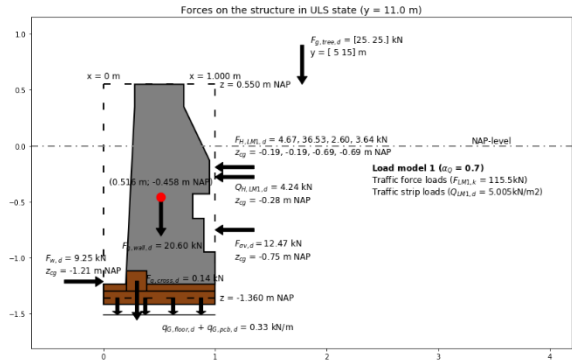
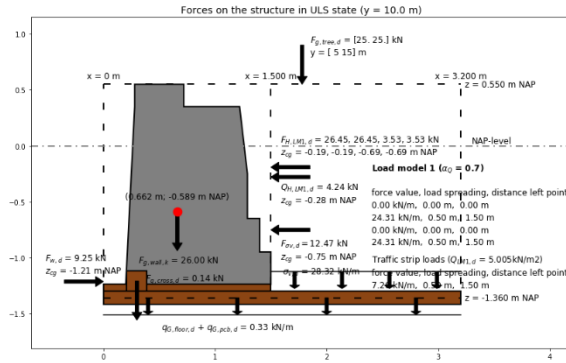
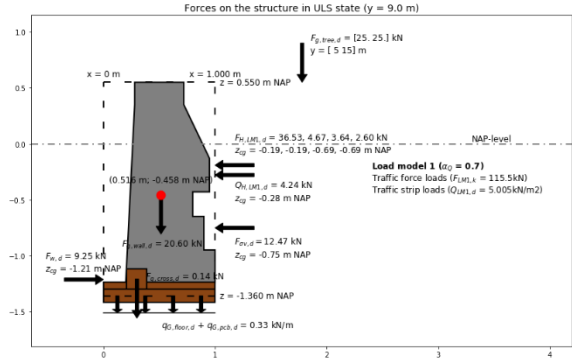
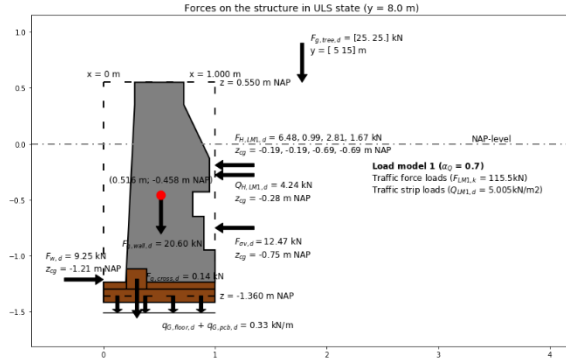
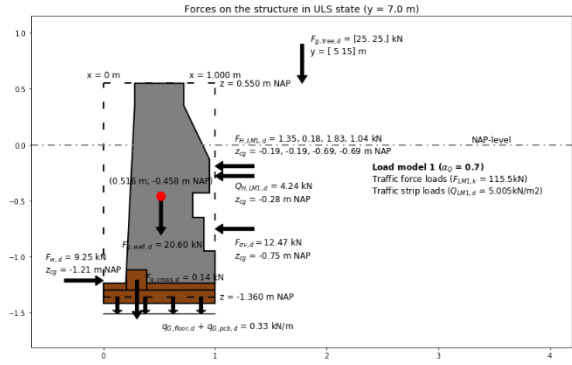
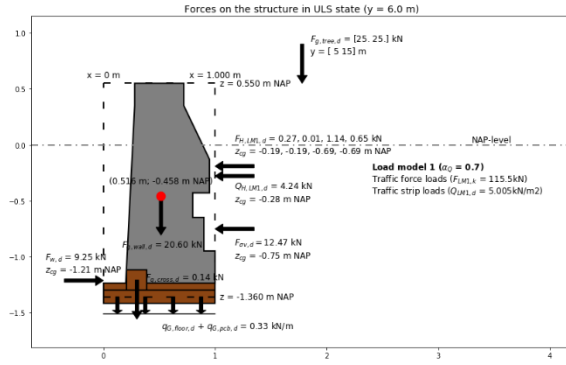
soil type classification					
NAP-level		$q_{\text{CPT,avg}}$ [MPa]	$f_{\text{CPT,avg}}$ [MPa]	$R_{\text{CPT,avg}}$ [%]	soil type
from	to				
+0.55	-2.00	0.5	0.035	7.00	peat, moderate
-2.00	-4.00	3.6	0.025	0.69	loam, slight sandy, dense
-4.00	-5.50	18.9	0.150	0.79	sand, clean, moderate
-5.50	-9.50	3.9	0.076	1.96	clay, slight sandy, dense
-9.50	-13.50	23.6	0.306	1.30	sand, clean, dense
-13.50	-16.00	5.0	0.148	2.99	clay, slight sandy, dense
-16.00	-18.50	18.3	0.218	1.19	sand, clean, moderate

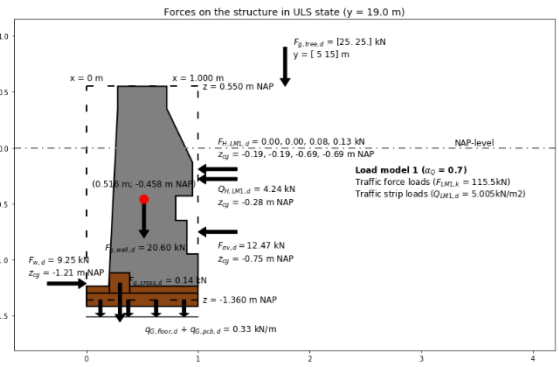
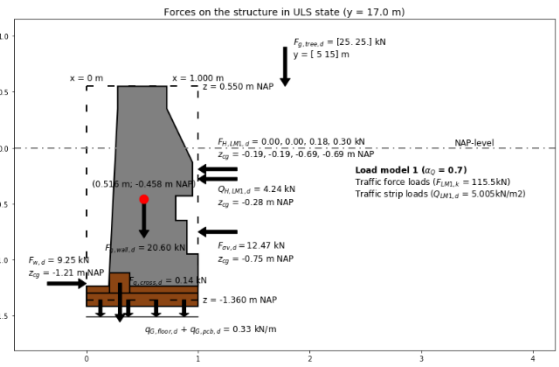
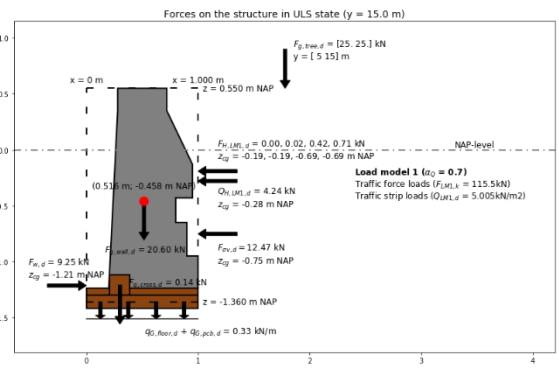
soil parameters						
NAP-level		γ_{dry} [kN/m ³]	γ_{sat} [kN/m ³]	ϕ' [°]	c' [kPa]	C_{α} [-]
from	to					
+0.55	-2.00	13.0	13.0	15.0	2.5	0.0153
-2.00	-4.00	22.0	22.0	35.0	2.5	0.0013
-4.00	-5.50	18.0	20.0	32.5	0	0
-5.50	-9.50	21.0	21.0	27.5	13.0	0.0031
-9.50	-13.50	20.0	22.0	40.0	0	0
-13.50	-16.00	21.0	21.0	27.5	13.0	0.0031
-16.00	-18.50	18.0	20.0	32.5	0	0

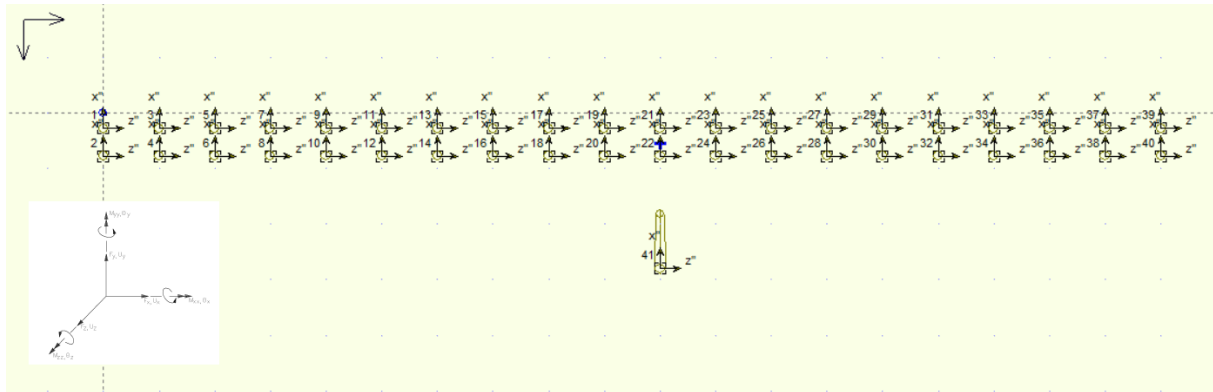
soil parameters							
zsoil [m NAP]		γ_{dry}	γ_{sat}	φ'	c'	C_α	E_{soil}
from	to	[kN/m ³]	[kN/m ³]	[°]	[kPa]	[-]	[MPa]
+0.55	-2.00	13.0	13.0	15.0	2.5	0.0153	1.0
-2.00	-4.00	22.0	22.0	35.0	2.5	0.0013	6.0
-4.00	-5.50	18.0	20.0	32.5	0	0	45.0
-5.50	-9.50	21.0	21.0	27.5	13.0	0.0031	8.0
-9.50	-13.50	20.0	22.0	40.0	0	0	85.0
-13.50	-16.00	21.0	21.0	27.5	13.0	0.0031	8.0
-16.00	-18.50	18.0	20.0	32.5	0	0	45.0

C.5.2 SUPERSTRUCTURE LOADS









horizontal pile displacement (main cross-section)						
pile no.	Z _{soil} [m NAP]		Z _{mid} [m NAP]	Z _{mid} [m]	v _{pile} [m]	figures
	from	to				
11	-1.83	-2.00	-1.92	-0.56	1.59×10 ⁻³	
	-2.00	-4.00	-3.00	-1.64	-3.95×10 ⁻⁴	
	-4.00	-5.50	-4.75	-3.39	1.90×10 ⁻⁵	
12	-1.42	-2.00	-1.71	-0.35	3.28×10 ⁻³	
	-2.00	-4.00	-3.00	-1.64	-3.95×10 ⁻⁴	
	-4.00	-5.50	-4.75	-3.39	1.90×10 ⁻⁵	

horizontal pile displacement (fortified cross-section)						
pile no.	Z _{soil} [m NAP]		Z _{mid} [m NAP]	Z _{mid} [m]	v _{pile} [m]	figures
	from	to				
21	-1.83	-2.00	-1.92	-0.56	1.69×10 ⁻³	
	-2.00	-4.00	-3.00	-1.64	-4.19×10 ⁻⁴	
	-4.00	-5.50	-4.75	-3.39	2.10×10 ⁻⁵	
22	-1.42	-2.00	-1.71	-0.35	3.48×10 ⁻³	
	-2.00	-4.00	-3.00	-1.64	-4.19×10 ⁻⁴	
	-4.00	-5.50	-4.75	-3.39	2.10×10 ⁻⁵	
41	-1.42	-2.00	-1.71	-0.35	3.06×10 ⁻³	
	-2.00	-4.00	-3.00	-1.64	-2.49×10 ⁻⁴	
	-4.00	-5.50	-4.75	-3.39	6.00×10 ⁻⁶	

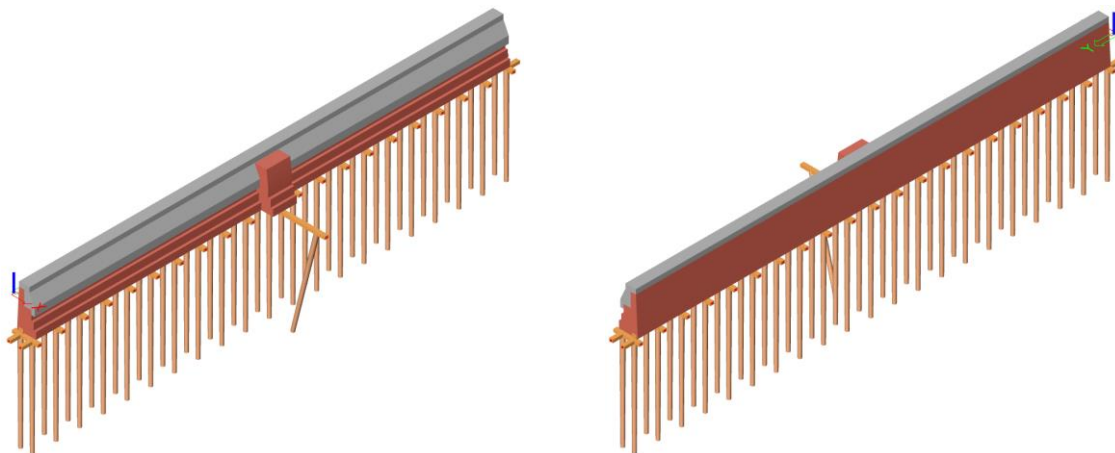
horizontal soil response (main cross-section)							
pile no.	Z _{soil} [m NAP]		soil type	α [-]	β [-]	k _s [kN/m ³]	p _{soil} [kN/m ²]
	from	to					
1	-1.83	-2.00	peat	1	3.0	7.23×10 ³	11.49
	-2.00	-4.00	loam	1/2	1.0	2.14×10 ⁴	8.47
	-4.00	-5.50	sand	1/3	0.7	8.53×10 ⁴	1.62
2	-1.42	-2.00	peat	1	3.0	7.23×10 ³	23.70
	-2.00	-4.00	loam	1/2	1.0	2.14×10 ⁴	8.47
	-4.00	-5.50	sand	1/3	0.7	8.53×10 ⁴	1.62

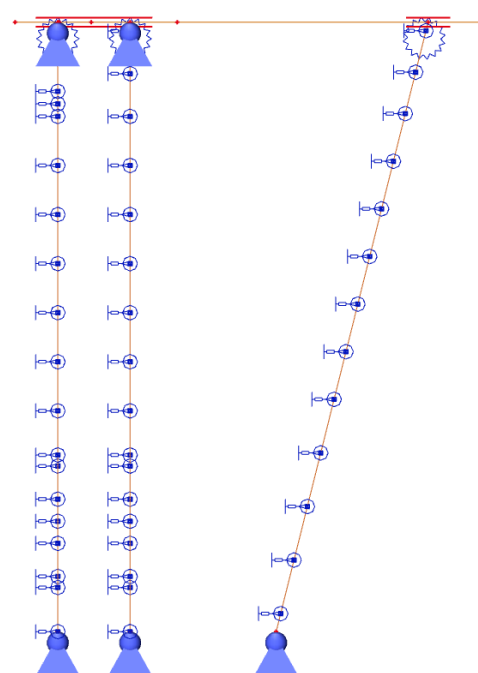
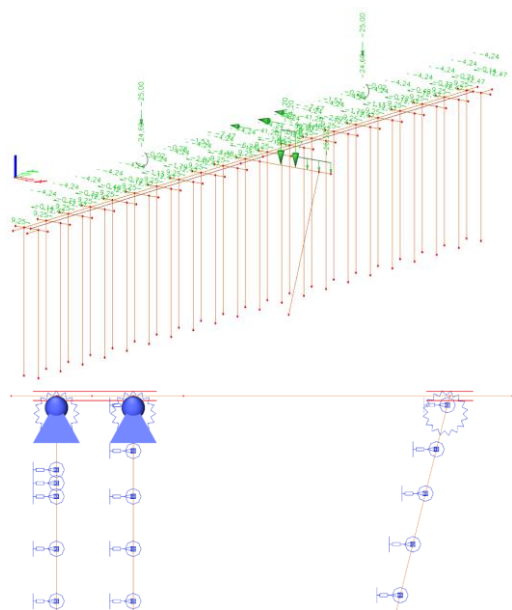
horizontal soil response (fortified cross-section)							
pile no.	z _{soil} [m NAP]		soil type	α [-]	β [-]	k _s [MN/m ³]	p _{soil} [MN/m ²]
	from	to					
1	-1.83	-2.00	peat	1	3.0	7.23×10 ³	12.21
	-2.00	-4.00	loam	1/2	1.0	2.14×10 ⁴	8.98
	-4.00	-5.50	sand	1/3	0.7	8.53×10 ⁴	1.71
2	-1.42	-2.00	peat	1	3.0	7.23×10 ³	25.15
	-2.00	-4.00	loam	1/2	1.0	2.14×10 ⁴	8.98
	-4.00	-5.50	sand	1/3	0.7	8.53×10 ⁴	1.79
fort	-1.42	-2.00	peat	1	3.0	7.23×10 ³	22.11
	-2.00	-4.00	loam	1/2	1.0	2.14×10 ⁴	5.34
	-4.00	-5.50	sand	1/3	0.7	8.53×10 ⁴	0.51

C.5.4 JOINT STIFFNESS

calculation joint stiffness	
parameter	value
H _{mor} [mm]	60.0
W _{notch} [mm]	18.0
a ₁ [mm]	81.0
a ₂ [mm]	20.0
a ₃ [mm]	20.0
k _{0,1} [N/mm]	1.97×10 ⁵
k _{90,1} [N/mm]	6.56×10 ³
k _{0,2} [N/mm]	4.40×10 ⁵
k _{90,2} [N/mm]	1.47×10 ⁴
k _{0,3} [N/mm]	4.40×10 ⁵
k _{90,3} [N/mm]	1.47×10 ⁴
k _{eq,1} [N/mm]	6.35×10 ³
k _{eq,2} [N/mm]	1.42×10 ⁴
k _{eq,3} [N/mm]	1.42×10 ⁴
k _r [MNm/rad]	0.05

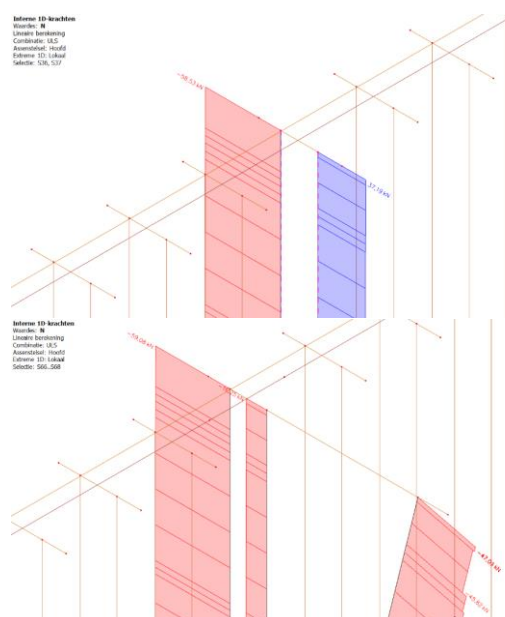
C.5.5 AXIAL PILE HEAD FORCES



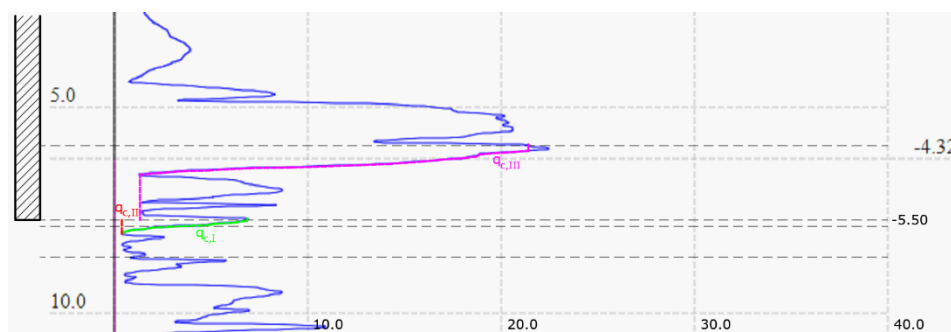


axial pile head forces (y = 5.00 m)	
pile row	$F_{\text{head},d}$ [kN]
1	-58.53
2	+37.19

axial pile head forces (y = 10.00 m)	
pile row	$F_{\text{head},d}$ [kN]
1	-59.08
2	-16.25
fort	-47.03



C.5.6 AXIAL PILE FORCES AND RESISTANCES



cone resistances	
parameter	value
$q_{CPT,I}$ [MPa]	3.5
$q_{CPT,II}$ [MPa]	0.5
$q_{CPT,III}$ [MPa]	5.5

maximum pile tip resistance (main cross-section)				
pile row	A_{tip} [mm ²]	$q_{b,max}$ [MPa]	$R_{b,max,k}$ [kN]	$R_{b,max,d}$ [kN]
1	1.59×10^4	2.63	41.74	25.02

maximum pile tip resistance (fortified cross-section)				
pile row	A_{tip} [mm ²]	$q_{b,max}$ [MPa]	$R_{b,max,k}$ [kN]	$R_{b,max,d}$ [kN]
1	1.59×10^4	2.63	41.74	25.02
2	1.59×10^4	2.63	41.74	25.02
3	1.59×10^4	2.63	41.74	25.02

maximum pile shaft resistance (main cross-section) ($z_{tp} = -4.00$ m NAP)							
pile row	ΔL [m]	$z_{\Delta L,avg}$ [m]	$d_{\Delta L,avg}$ [mm]	$C_{\Delta L,avg}$ [mm]	$q_{s,max}$ [MPa]	$R_{s,max,k}$ [kN]	$R_{s,max,d}$ [kN]
1	1.50	3.33	148.6	466.7	0.18	126.02	75.56

maximum pile shaft resistance (fortified cross-section) ($z_{tp} = -4.00$ m NAP)							
pile row	ΔL [m]	$z_{\Delta L,avg}$ [m]	$d_{\Delta L,avg}$ [mm]	$C_{\Delta L,avg}$ [mm]	$q_{s,max}$ [MPa]	$R_{s,max,k}$ [kN]	$R_{s,max,d}$ [kN]
1	1.50	3.33	148.6	466.7	0.18	126.02	75.56
2	1.50	3.33	148.6	466.7	0.18	126.02	75.56
3	1.50	3.33	148.6	466.7	0.18	126.02	75.56

negative skin friction (main cross-section) ($z_{tp} = -4.00$ m NAP)											
pile row	z_{mid} [m NAP]	t_i [m]	γ'_i [kN/m ³]	$z_{pile,mid}$ [m]	$C_{pile,mid}$ [m]	m_i [–]	$\sigma'_{m,i}$ [kN/m ²]	$\sigma_{nsf,i}$ [kN/m ²]	$F_{nsf,i}$ [kN]	$F_{nsf,k}$ [kN]	$F_{nsf,d}$ [kN]
1	–1.92	0.17	3.0	0.50	0.550	0.36	0.49	0.02	0.01	2.60	3.12
	–3.00	2.00	12.0	1.58	0.516	0.34	17.67	6.82	2.59		

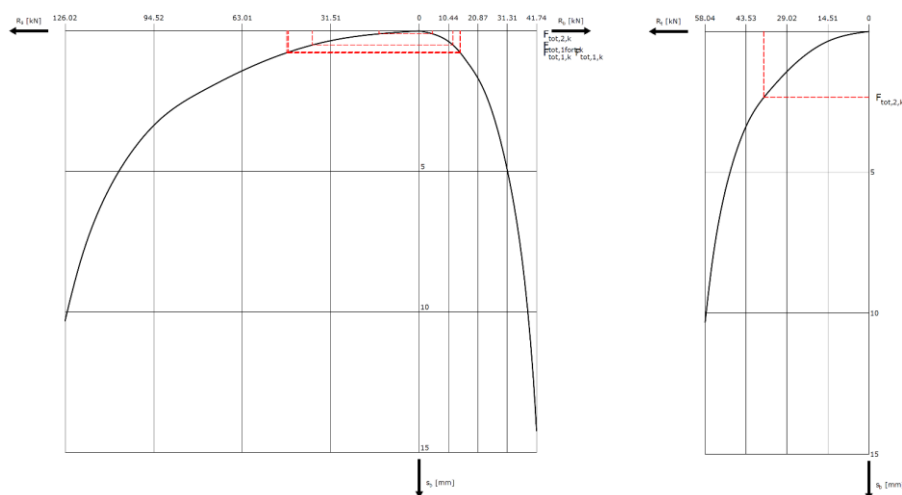
negative skin friction (fortified cross-section) ($z_{tp} = -4.00$ m NAP)											
pile row	z_{mid} [m NAP]	t_i [m]	γ'_i [kN/m ³]	$z_{pile,mid}$ [m]	$C_{pile,mid}$ [m]	m_i [–]	$\sigma'_{m,i}$ [kN/m ²]	$\sigma_{nsf,i}$ [kN/m ²]	$F_{nsf,i}$ [kN]	$F_{nsf,k}$ [kN]	$F_{nsf,d}$ [kN]
1	–1.92	0.17	3.0	0.50	0.550	0.36	0.49	0.02	0.01	2.60	3.12
	–3.00	2.00	12.0	1.58	0.516	0.34	17.67	6.82	2.59		
2	–1.71	0.58	3.0	0.29	0.556	0.37	1.57	0.17	0.07	2.86	3.43
	–3.00	2.00	12.0	1.58	0.516	0.34	18.21	7.35	2.79		
3	–1.71	0.58	3.0	0.29	0.556	0.37	1.61	0.13	0.08	3.02	3.62
	–3.00	2.00	12.0	1.58	0.516	0.34	19.71	5.90	3.54		

tensile resistance (main cross-section)										
pile row	z_{mid} [m NAP]	t_i [m]	$z_{pile,mid}$ [m]	$C_{pile,mid}$ [m]	$\alpha_{t,i}$ [–]	$q_{CPT,d,i}$ [MPa]	$q_{t,d,i}$ [MPa]	$R_{t,d,i}$ [kN]	$R_{t,d}$ [kN]	$R_{t,k}$ [kN]
2	–1.71	0.58	0.29	0.556	0.0035	0.18	6.21×10^{-4}	0.20	30.93	58.04
	–3.00	2.00	1.58	0.516	0.0035	1.28	4.48×10^{-3}	4.62		
	–4.75	1.50	3.33	0.467	0.0070	5.33	0.04	26.12		

C.5.7 PILE TIP SETTLEMENT AND FORCE

total pile head force (main cross-section)	
pile row	F_{tot} [kN]
1	-61.13
2	37.19

total pile head force (fortified cross-section)	
pile row	F_{tot} [kN]
1	-61.68
2	-19.11
fort	-50.05



pile settlement and rise (main cross-section)					
pile row	$R_{b,k}$ [kN]	$R_{s,k}$ [kN]	s_b [mm]	$R_{t,k}$ [kN]	s_{head} [mm]
1	14.4	46.7	0.8	—	—
2	—	—	—	37.2	2.3

pile settlement and rise (fortified cross-section)					
pile row	$R_{b,k}$ [kN]	$R_{s,k}$ [kN]	s_b [mm]	$R_{t,k}$ [kN]	s_{head} [mm]
1	14.6	47.1	0.8	—	—
2	4.7	14.4	0.1	—	—
fort	12.0	38.1	0.5	—	—

axial pile tip stiffness (main cross-section)	
pile row	k_{ax} [MN/m]
1	76.4
2	16.2

pile tip stiffness (fortified cross-section)	
pile row	k_{ax} [MN/m]
1	77.1
2	191.0
fort	100.2

C.5.8 NEUTRAL PLANE

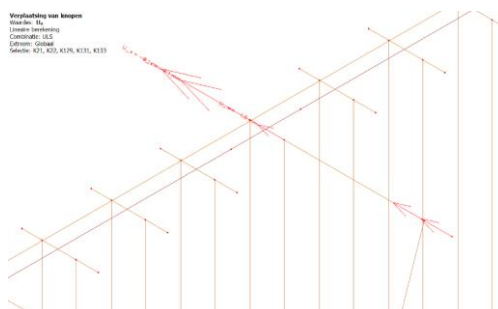
total soil settlement (main cross-section)				
pile row	Z_{top} [m NAP]	t_i [m]	$S_{soil,tot,i}$ [m]	$S_{soil,tot}$ [m]
1	-1.83	0.17	0.010	0.021
	-2.00	2.00	0.010	

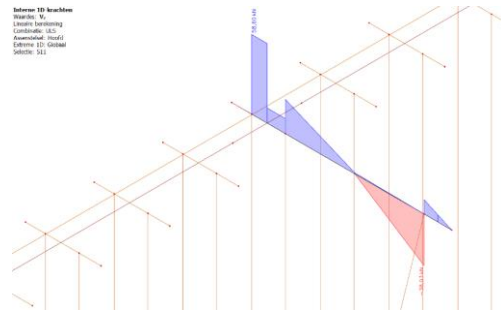
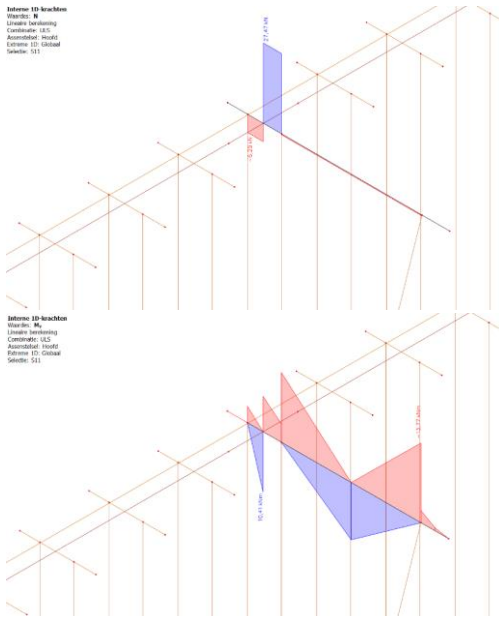
total soil settlement (fortified cross-section)				
pile row	Z_{top} [m NAP]	t_i [m]	$S_{soil,tot,i}$ [m]	$S_{soil,tot}$ [m]
1	-1.83	0.17	0.010	0.021
	-2.00	2.00	0.010	
2	-1.42	0.58	0.035	0.046
	-2.00	2.00	0.010	
fort	-1.42	0.58	0.035	0.046
	-2.00	2.00	0.010	

influence neutral plane (main cross-section)						
pile row	value	Z_{tp} [kN]	$R_{s,max,k}$ [kN]	$R_{s,max,d}$ [kN]	$F_{nsf,k}$ [kN]	$F_{nsf,d}$ [kN]
1	interaction	-3.65	133.46	80.01	1.87	2.24

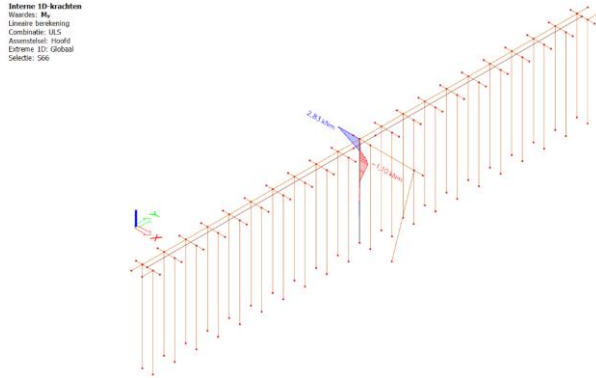
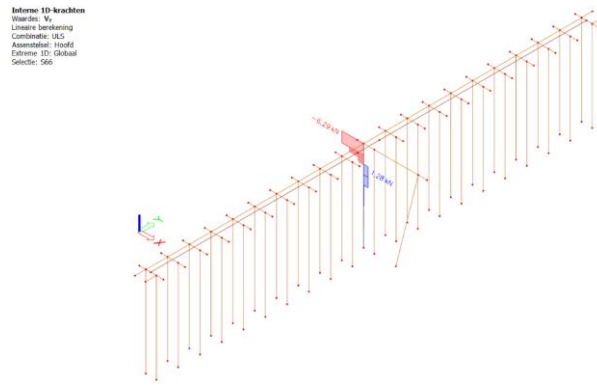
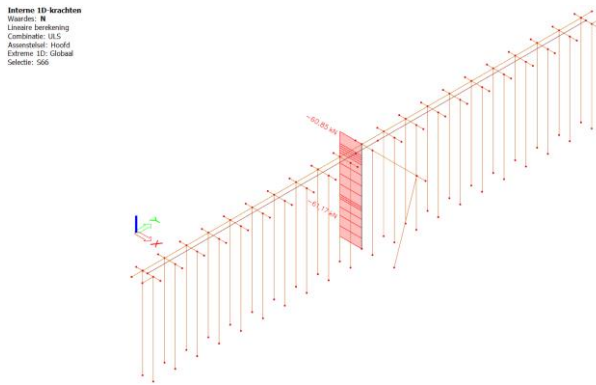
influence neutral plane (fortified cross-section)						
pile row	value	Z_{tp} [kN]	$R_{s,max,k}$ [kN]	$R_{s,max,d}$ [kN]	$F_{nsf,k}$ [kN]	$F_{nsf,d}$ [kN]
1	interaction	-3.64	133.68	80.14	1.85	2.22
2	interaction	-3.90	128.13	76.82	2.63	3.16
fort	interaction	-3.75	131.32	78.73	2.42	2.91

C.5.9 CALCULATION MODEL





extreme values (y = 10.00 m)				
parameter	minimum		maximum	
	value	pile row	value	pile row
$u_{x,int}$ [mm]	-4.1	1	-1.6	2
$u_{z,int}$ [mm]	-4.3	1	68.1	fort
N_{int} [kN]	-6.3	1-2	27.5	1-2
$V_{z,int}$ [kN]	-38.0	fort	58.6	1
$M_{y,int}$ [kNm]	-13.8	fort	10.4	1-2



extreme values in pile at first row (x = 0.29 m, y = 10.00 m)		
parameter	minimum value	maximum value
N_{int} [kN]	-61.2	-60.9
$V_{z,int}$ [kN]	-6.3	1.3
$M_{y,int}$ [kNm]	-1.1	2.8

C.5.10 STRUCTURAL DEFICIENCIES

changes in structural model		
modification	changing variable	adaptations
1	$p_m = 5 \text{ mm}$	$d_{head,1,2}$ (y = 0.00 m), ..., $d_{head,1,2}$ (y = 19.00 m): 180 mm → 160 mm
		$d_{tip,1,2}$ (y = 0.00 m), ..., $d_{tip,1,2}$ (y = 19.00 m): 142.3 mm → 127.3 mm
		$d_{head,fort}$ (y = 10.00 m): 180 mm → 160 mm
		$d_{tip,fort}$ (y = 10.00 m): 142.3 mm → 127.3 mm

2	$p_m = 5 \text{ mm}$	$d_{\text{head},1,2} (y = 10.00 \text{ m}): 180 \text{ mm} \rightarrow 160 \text{ mm}$
		$d_{\text{tip},1,2} (y = 10.00 \text{ m}): 142.3 \text{ mm} \rightarrow 127.3 \text{ mm}$
		$d_{\text{head},\text{fort}} (y = 10.00 \text{ m}): 180 \text{ mm} \rightarrow 160 \text{ mm}$
		$d_{\text{tip},\text{fort}} (y = 10.00 \text{ m}): 142.3 \text{ mm} \rightarrow 127.3 \text{ mm}$
3	$p_m = 5 \text{ mm}$	$d_{\text{head},1,2} (y = 0.00 \text{ m}), \dots, d_{\text{head},1,2} (y = 19.00 \text{ m}): 180 \text{ mm} \rightarrow 160 \text{ mm}$
		$d_{\text{tip},1,2} (y = 0.00 \text{ m}), \dots, d_{\text{tip},1,2} (y = 19.00 \text{ m}): 142.3 \text{ mm} \rightarrow 127.3 \text{ mm}$
4	$p_m = 15 \text{ mm}$	$d_{\text{head},1,2} (y = 0.00 \text{ m}), \dots, d_{\text{head},1,2} (y = 19.00 \text{ m}): 180 \text{ mm} \rightarrow 140 \text{ mm}$
		$d_{\text{tip},1,2} (y = 0.00 \text{ m}), \dots, d_{\text{tip},1,2} (y = 19.00 \text{ m}): 142.3 \text{ mm} \rightarrow 117.3 \text{ mm}$
		$d_{\text{head},\text{fort}} (y = 10.00 \text{ m}): 180 \text{ mm} \rightarrow 140 \text{ mm}$
		$d_{\text{tip},\text{fort}} (y = 10.00 \text{ m}): 142.9 \text{ mm} \rightarrow 117.9 \text{ mm}$
		$W_{\text{pcb}} (y = 0.00 \text{ m}), \dots, W_{\text{pcb}} (y = 19.00 \text{ m}): 160 \text{ mm} \rightarrow 150 \text{ mm}$
		$W_{\text{cross}} (x = 0.30 \text{ m}): 180 \text{ mm} \rightarrow 170 \text{ mm}$
5	$p_m = 15 \text{ mm}$	$d_{\text{head},1,2} (y = 10.00 \text{ m}): 180 \text{ mm} \rightarrow 140 \text{ mm}$
		$d_{\text{tip},1,2} (y = 10.00 \text{ m}): 142.3 \text{ mm} \rightarrow 117.3 \text{ mm}$
		$d_{\text{head},\text{fort}} (y = 10.00 \text{ m}): 180 \text{ mm} \rightarrow 140 \text{ mm}$
		$d_{\text{tip},\text{fort}} (y = 10.00 \text{ m}): 142.3 \text{ mm} \rightarrow 117.3 \text{ mm}$
		$W_{\text{pcb}} (y = 10.00 \text{ m}): 160 \text{ mm} \rightarrow 150 \text{ mm}$
		$W_{\text{cross}} (x = 0.30 \text{ m}): 180 \text{ mm} \rightarrow 170 \text{ mm}$
6	$p_m = 15 \text{ mm}$	$d_{\text{head},1,2} (y = 0.00 \text{ m}), \dots, d_{\text{head},1,2} (y = 19.00 \text{ m}): 180 \text{ mm} \rightarrow 140 \text{ mm}$
		$d_{\text{tip},1,2} (y = 0.00 \text{ m}), \dots, d_{\text{tip},1,2} (y = 19.00 \text{ m}): 142.3 \text{ mm} \rightarrow 117.3 \text{ mm}$
		$W_{\text{pcb}} (y = 0.00 \text{ m}), \dots, W_{\text{pcb}} (y = 19.00 \text{ m}): 160 \text{ mm} \rightarrow 150 \text{ mm}$
7	$p_m = 30 \text{ mm}$	$d_{\text{head},1,2} (y = 0.00 \text{ m}), \dots, d_{\text{head},1,2} (y = 19.00 \text{ m}): 180 \text{ mm} \rightarrow 110 \text{ mm}$
		$d_{\text{tip},1,2} (y = 0.00 \text{ m}), \dots, d_{\text{tip},1,2} (y = 19.00 \text{ m}): 142.3 \text{ mm} \rightarrow 102.3 \text{ mm}$
		$d_{\text{head},\text{fort}} (y = 10.00 \text{ m}): 180 \text{ mm} \rightarrow 110 \text{ mm}$
		$d_{\text{tip},\text{fort}} (y = 10.00 \text{ m}): 142.3 \text{ mm} \rightarrow 102.3 \text{ mm}$
		$W_{\text{pcb}} (y = 0.00 \text{ m}), \dots, W_{\text{pcb}} (y = 19.00 \text{ m}): 160 \text{ mm} \rightarrow 120 \text{ mm}$
		$W_{\text{cross}} (x = 0.30 \text{ m}): 180 \text{ mm} \rightarrow 140 \text{ mm}$
8	$p_m = 30 \text{ mm}$	$d_{\text{head},1,2} (y = 10.00 \text{ m}): 180 \text{ mm} \rightarrow 110 \text{ mm}$
		$d_{\text{tip},1,2} (y = 10.00 \text{ m}): 142.3 \text{ mm} \rightarrow 102.3 \text{ mm}$
		$d_{\text{head},\text{fort}} (y = 10.00 \text{ m}): 180 \text{ mm} \rightarrow 110 \text{ mm}$
		$d_{\text{tip},\text{fort}} (y = 10.00 \text{ m}): 142.3 \text{ mm} \rightarrow 102.3 \text{ mm}$
		$W_{\text{pcb}} (y = 10.00 \text{ m}): 160 \text{ mm} \rightarrow 120 \text{ mm}$
		$W_{\text{cross}} (y = 10.00 \text{ m}) = 180 \text{ mm} \rightarrow 140 \text{ mm}$
9	$p_m = 30 \text{ mm}$	$d_{\text{head},1,2} (y = 0.00 \text{ m}), \dots, d_{\text{head},1,2} (y = 19.00 \text{ m}): 180 \text{ mm} \rightarrow 110 \text{ mm}$
		$d_{\text{tip},1,2} (y = 0.00 \text{ m}), \dots, d_{\text{tip},1,2} (y = 19.00 \text{ m}): 142.3 \text{ mm} \rightarrow 102.3 \text{ mm}$
		$W_{\text{pcb}} (y = 0.00 \text{ m}), \dots, W_{\text{pcb}} (y = 19.00 \text{ m}): 160 \text{ mm} \rightarrow 120 \text{ mm}$
10	$e_y = 25 \text{ mm}$	$e_{y,\text{pcb}} (y = 10.00 \text{ m}): 0 \rightarrow 25 \text{ mm}$
11	$e_y = 50 \text{ mm}$	$e_{y,\text{pcb}} (y = 10.00 \text{ m}): 0 \rightarrow 50 \text{ mm}$
12	$e_y = 100 \text{ mm}$	$e_{y,\text{pcb}} (y = 10.00 \text{ m}): 0 \rightarrow 100 \text{ mm}$
13	$R_{c,\text{max}} = 0 \text{ kN},$ $R_{t,\text{max}} = 0 \text{ kN}$	$R_{c,\text{pile},1,d} (x = 0.29 \text{ m}, y = 10.00 \text{ m}): 100.58 \text{ kN} \rightarrow 0 \text{ kN}$
		$R_{c,\text{pile},2,d} (x = 0.78 \text{ m}, y = 10.00 \text{ m}): 100.58 \text{ kN} \rightarrow 0 \text{ kN}$
14	$R_{c,\text{max}} = 0 \text{ kN},$ $R_{t,\text{max}} = 0 \text{ kN}$	$R_{c,\text{pile},2,d} (x = 0.78 \text{ m}, y = 10.00 \text{ m}): 100.58 \text{ kN} \rightarrow 0 \text{ kN}$
		$R_{c,\text{pile},\text{fort}} (x = 2.80 \text{ m}, y = 10.00 \text{ m}): 100.58 \text{ kN} \rightarrow 0 \text{ kN}$
15	$S_b = 5 \text{ mm},$ $S_{\text{head}} = 5 \text{ mm}$	$k_{ax,1} (x = 0.29 \text{ m}, y = 10.00 \text{ m}) = 77.1 \text{ MN/m} \rightarrow 12.3 \text{ MN/m}$
		$k_{ax,2} (x = 0.78 \text{ m}, y = 10.00 \text{ m}) : 191.0 \text{ MN/m} \rightarrow 3.8 \text{ MN/m}$
		$k_{ax,\text{fort}} (x = 2.80 \text{ m}, y = 10.00 \text{ m}): 100.2 \text{ MN/m} \rightarrow 10.0 \text{ MN/m}$
16	$S_b = 5 \text{ mm},$ $S_{\text{head}} = 5 \text{ mm}$	$k_{ax,1} (x = 0.29 \text{ m}, y = 0.00 \text{ m}), \dots, k_{ax,1} (x = 0.29 \text{ m}, y = 9.00 \text{ m}): 76.4 \text{ MN/m} \rightarrow 12.2 \text{ MN/m}$
		$k_{ax,1} (x = 0.29 \text{ m}, y = 10.00 \text{ m}): 77.1 \text{ MN/m} \rightarrow 12.3 \text{ MN/m}$
		$k_{ax,1} (x = 0.29 \text{ m}, y = 11.00 \text{ m}), \dots, k_{ax,1} (x = 0.29 \text{ m}, y = 19.00 \text{ m}): 76.4 \text{ MN/m} \rightarrow 12.2 \text{ MN/m}$
		$k_{ax,2} (x = 0.78 \text{ m}, y = 0.00 \text{ m}), \dots, k_{ax,2} (x = 0.78 \text{ m}, y = 9.00 \text{ m}): 16.2 \text{ MN/m} \rightarrow 7.4 \text{ MN/m}$
		$k_{ax,2} (x = 0.78 \text{ m}, y = 10.00 \text{ m}): 191.0 \text{ MN/m} \rightarrow 3.8 \text{ MN/m}$
		$k_{ax,2} (x = 0.78 \text{ m}, y = 11.00 \text{ m}), \dots, k_{ax,2} (x = 0.78 \text{ m}, y = 19.00 \text{ m}): 16.2 \text{ MN/m} \rightarrow 7.4 \text{ MN/m}$
17		$k_{ax,1} (x = 0.29 \text{ m}, y = 10.00 \text{ m}): 77.1 \text{ MN/m} \rightarrow 6.2 \text{ MN/m}$

	S _b = 10 mm, S _{head} = 10 mm	k _{ax,2} (x = 0.78 m, y = 10.00 m): 191.0 MN/m → 1.9 MN/m k _{ax,fort} (x = 2.80 m, y = 10.00 m) = 100.2 MN/m → 5.0 MN/m
18	S _b = 10 mm, S _{head} = 10 mm	k _{ax,1} (x = 0.29 m, y = 0.00 m),..., k _{ax,1} (x = 0.29 m, y = 9.00 m): 76.4 MN/m → 6.1 MN/m k _{ax,1} (x = 0.29 m, y = 10.00 m): 77.1 MN/m → 6.2 MN/m k _{ax,1} (x = 0.29 m, y = 11.00 m),..., k _{ax,1} (x = 0.29 m, y = 19.00 m): 76.4 MN/m → 6.1 MN/m k _{ax,2} (x = 0.78 m, y = 0.00 m),..., k _{ax,2} (x = 0.78 m, y = 9.00 m): 16.2 MN/m → 3.7 MN/m k _{ax,2} (x = 0.78 m, y = 10.00 m): 191.0 MN/m → 1.9 MN/m k _{ax,2} (x = 0.78 m, y = 11.00 m),..., k _{ax,2} (x = 0.78 m, y = 19.00 m): 16.2 MN/m → 3.7 MN/m
19	S _b = 20 mm, S _{head} = 20 mm	k _{ax,1} (x = 0.29 m, y = 10.00 m): 77.1 MN/m → 3.1 MN/m k _{ax,2} (x = 0.78 m, y = 10.00 m): 191.0 MN/m → 1.0 MN/m k _{ax,fort} (x = 2.80 m, y = 10.00 m): 100.2 MN/m → 2.5 MN/m
20	S _b = 20 mm, S _{head} = 20 mm	k _{ax,1} (x = 0.29 m, y = 0.00 m),..., k _{ax,1} (x = 0.29 m, y = 9.00 m): 76.4 MN/m → 3.1 MN/m k _{ax,1} (x = 0.29 m, y = 10.00 m): 77.1 MN/m → 3.1 MN/m k _{ax,1} (x = 0.29 m, y = 11.00 m),..., k _{ax,1} (x = 0.29 m, y = 19.00 m): 76.4 MN/m → 3.1 MN/m k _{ax,2} (x = 0.78 m, y = 0.00 m),..., k _{ax,2} (x = 0.78 m, y = 9.00 m): 16.2 MN/m → 1.9 MN/m k _{ax,2} (x = 0.78 m, y = 10.00 m): 191.0 MN/m → 1.0 MN/m k _{ax,2} (x = 0.78 m, y = 11.00 m),..., k _{ax,2} (x = 0.78 m, y = 19.00 m): 16.2 MN/m → 1.9 MN/m

calculation results for pile cap beam (y = 10.00 m)										
mod.	u _{x,mod} [mm]		u _{z,mod} [mm]		N _{mod} [kN]		V _{z,mod} [kN]		M _{y,mod} [kNm]	
	min.	max.	min.	max.	min.	max.	min.	max.	min.	max.
1	-4,2	-1,5	-4,0	71,0	-6,0	28,5	-38,0	58,3	-13,7	10,4
2	-4,1	-1,5	-4,0	71,0	-5,8	28,1	-38,0	57,1	-13,7	10,2
3	-4,2	-1,5	-5,2	68,1	-6,0	28,8	-38,1	58,3	-13,8	10,4
4	-4,3	-1,3	-6,2	75,2	-5,8	29,6	-38,0	58,2	-13,7	10,4
5	-4,2	-1,2	-5,7	75,1	-5,3	28,6	-38,0	53,0	-13,7	9,9
6	-4,3	-1,2	-6,2	66,7	-5,8	30,3	-38,1	58,2	-13,9	10,4
7	-6,1	-0,2	-8,7	90,5	-5,8	32,1	-38,0	58,2	-13,7	10,4
8	-6,1	-0,1	-6,4	90,3	-5,1	30,0	-38,0	42,3	-13,7	9,9
9	-4,3	0,1	-8,7	60,4	-5,8	33,6	-38,2	58,2	-14,1	10,4
10	-4,1	-1,3	-4,3	68,2	-6,3	26,8	-38,0	58,5	-13,8	10,4
11	-4,2	-0,7	-4,3	68,6	-6,3	25,2	-38,0	58,3	-13,8	10,4
12	-4,4	0,5	-4,2	69,3	-6,3	21,2	-38,0	57,3	-13,8	10,2
13	-5,6	-3,0	-146,2	85,9	0,0	2,7	-40,9	25,6	-15,7	10,9
14	-6,1	-5,5	-81471,0	10,7	-6,7	0,0	0,0	80,0	-125,5	8,0
15	-4,2	-1,5	-8,2	63,2	-5,6	27,9	-38,1	53,2	-13,8	9,9
16	-4,3	-1,0	-8,3	68,3	-6,0	28,4	-38,1	57,7	-13,8	10,4
17	-4,2	-1,5	-13,7	57,7	-5,0	28,2	-38,1	47,9	-13,8	9,9
18	-4,5	-1,7	-12,9	68,5	-5,7	29,5	-38,1	56,4	-13,8	10,5
19	-4,4	-1,5	-24,7	46,7	-4,0	28,6	-38,1	39,9	-13,8	9,9
20	-4,9	-1,9	-21,4	68,5	-5,0	31,1	-38,1	53,8	-13,8	10,5

calculation results for pile in first pile row ($x = 0.29$ m, $y = 10.00$ m)						
mod.	N_{mod} [kN]		$V_{z,mod}$ [kN]		$M_{y,mod}$ [kNm]	
	min.	max.	min.	max.	min.	max.
1	-60,8	-60,6	-6,0	1,1	-0,9	2,8
2	-59,6	-59,4	-5,8	1,1	-0,9	2,7
3	-60,8	-60,6	-6,0	1,1	-0,9	2,8
4	-60,7	-60,5	-5,8	0,9	-0,7	2,7
5	-55,4	-55,2	-5,3	0,9	-0,6	2,5
6	-60,7	-60,5	-5,8	0,9	-0,7	2,7
7	-60,6	-60,4	-5,8	0,6	-0,5	2,7
8	-44,7	-44,5	-4,4	0,5	-0,4	2,0
9	-60,6	-60,4	-5,8	0,6	-0,4	2,7
10	-61,1	-60,8	-6,3	1,3	-1,1	2,8
11	-60,8	-60,5	-6,3	1,3	-1,1	2,8
12	-59,9	-59,5	-6,3	1,4	-1,2	2,7
13	-	-	-	-	-	-
14	-49,5	-49,2	-6,7	1,7	-1,4	2,6
15	-55,8	-55,4	-5,6	1,3	-1,1	2,3
16	-60,2	-59,9	-6,0	1,3	-1,1	2,6
17	-50,5	-50,2	-5,0	1,3	-1,1	1,9
18	-59,0	-58,7	-5,7	1,4	-1,2	2,3
19	-42,4	-42,1	-4,0	1,4	-1,1	1,2
20	-56,4	-56,0	-5,0	1,5	-1,3	1,7